

**Plant performance under changing temperatures:
functional characterization of ELF3 in *Arabidopsis
thaliana* and *Hordeum vulgare***

**Dissertation
zur Erlangung des
Doktorgrades der Naturwissenschaften (Dr. rer. nat.)**

der

Naturwissenschaftliche Fakultät III
Agrar- und Ernährungswissenschaften,
Geowissenschaften und Informatik

der Martin-Luther-Universität Halle-Wittenberg

vorgelegt von

Herrn M. Sc. Zihao Zhu

geb. am 12.11.1992 in Shanghai, China

Gutachter:

1. Prof. Dr. Marcel Quint
2. Prof. Dr. Salomé Prat

Verteidigung am 24.04.2023
Halle (Saale)

Table of contents

Table of contents	I
List of abbreviations	III
List of figures	V
List of tables	VI
1 Introduction.....	1
1.1 Plant performance under changing environment	1
1.2 The circadian clock anticipates cyclic environmental changes	2
1.3 Plant thermomorphogenesis signaling.....	4
1.4 <i>H. vulgare</i> as a model crop for adaptation to climate change	5
1.5 Natural variation for growth and developmental plasticity.....	7
1.6 Objectives.....	9
2 Materials and Methods	10
2.1 Plant material.....	10
2.1.1 <i>A. thaliana</i> lines	10
2.1.2 <i>H. vulgare</i> lines.....	10
2.2 Physiological assay	10
2.2.1 Seed sterilization and stratification	10
2.2.2 <i>A. thaliana</i> temperature assays	11
2.2.3 Growth assays under temperature cycles	11
2.2.4 <i>H. vulgare</i> temperature assay on plates	13
2.2.5 <i>H. vulgare</i> temperature assay in growth chambers	13
2.2.6 <i>H. vulgare</i> temperature assay in greenhouses	15
2.3 Molecular biology methods.....	16
2.3.1 DNA sequencing.....	16
2.3.2 Transcriptional analysis	17
2.4 Computational analysis.....	17
2.4.1 Phylogenetic analysis	17
2.4.2 Population genetic analysis	18
2.4.3 Growth curve modeling.....	18
2.4.4 Principal component analysis (PCA)	19
2.4.5 Pairwise correlation analysis	19
2.4.6 Statistical analysis and data visualization.....	19
3 Results I – Emergence and evolution of <i>ELF3</i> and its prion-like domain.....	21
3.1 Evolutionary origins of <i>ELF3/EEC</i> and PrD	21
3.2 PolyQ length contributes to PrD of <i>ELF3</i> in Brassicales.....	26
3.3 <i>ELF3</i> polyQ variation among Arabidopsis accessions	27
3.4 Evolution of Arabidopsis <i>ELF3</i> and polyQ	30
3.5 Association of polyQ variation and temperature responsive hypocotyl elongation.....	33
4 Results II – Arabidopsis <i>ELF3</i> controls temperature responsiveness of the circadian clock independently of the evening complex	37
4.1 <i>ELF3</i> and <i>GI</i> participate in complicated temperature-photoperiod crosstalk.....	37
4.2 <i>ELF3</i> and <i>GI</i> are not essential for temperature responsiveness under constant conditions	40
4.3 <i>ELF3</i> is required for clock-controlled physiological processes under temperature cycles	40

4.4	Neither <i>phyB</i> nor the EC is essential for <i>ELF3</i> -mediated rhythmic output under temperature cycles	44
4.5	<i>ELF3</i> is required for the oscillator's responsiveness to temperature cycles.....	46
4.6	<i>ELF3</i> is essential for precise gating of temperature signals.....	49
4.7	Functional <i>ELF3</i> is not required for temperature entrainment in <i>H. vulgare</i>	51
5	Results III – An exotic allele of barley <i>ELF3</i> contributes to developmental plasticity at elevated temperatures	53
5.1	<i>ELF3</i> is involved in barley thermomorphogenesis	53
5.2	<i>ELF3</i> sequence variation in HIF pairs.....	54
5.3	Elevated temperatures accelerate barley seedling establishment.....	55
5.4	An exotic <i>ELF3</i> allele affects barley temperature responsive growth and architecture.....	58
5.5	An exotic <i>ELF3</i> allele affects barley floral transition at elevated temperatures	62
5.6	An exotic <i>ELF3</i> allele stabilizes total grain weight at elevated temperatures.....	67
6	Discussion	73
6.1	Potential functions of <i>ELF3</i> polyQ and phase separation	73
6.2	<i>Arabidopsis ELF3</i> is an essential temperature Zeitnehmer	75
6.3	<i>Arabidopsis ELF3</i> can function independently of the EC.....	76
6.4	<i>ELF3</i> mediates crop domestication	77
6.5	<i>ELF3</i> is involved in barley thermomorphogenesis	78
6.6	Exotic barley <i>ELF3</i> alleles contribute to temperature responsive developmental plasticity.....	79
6.7	Early flowering is an adaptive response under climate change	81
7	Conclusions	83
8	Summary	84
9	References	85
	Appendix.....	96
	Appendix I.....	96
	Appendix II.....	101
	Appendix III.....	102
	Appendix IV	103
	Appendix V	110
	Appendix VI	114
	Acknowledgments.....	125
	Curriculum Vitae	126
	List of publications	126
	Declaration under Oath.....	127

List of abbreviations

3D	three-dimensional
ANOVA	analysis of variance
Arabidopsis	<i>Arabidopsis thaliana</i> (L.) Heynh.; <i>A. thaliana</i>
ATS	<i>A. thaliana</i> solution
barley	<i>Hordeum vulgare</i> L.; <i>H. vulgare</i>
BBX	B-box zinc finger protein
bHLH	basic helix-loop-helix
BLAST	Basic Local Alignment Search Tool
BM	BARLEY MADS-box
BR	brassinosteroids
CAA	cytosine-adenine-adenine
CCA1	CIRCADIAN CLOCK ASSOCIATED 1
CCR2	COLD, CIRCADIAN RHYTHM, AND RNA BINDING 2
cDNA	complementary DNA
CO	CONSTANS
CO ₂	carbon dioxide
Col-0	Columbia-0
COP1	CONSTITUTIVE PHOTOMORPHOGENIC 1
cv.	cultivar
DAS	days after sowing
DD	darkness
DNA	deoxyribonucleic acid
EAM	EARLY MATURITY
EC	evening complex
EEC	ESSENCE OF ELF3 CONSENSUS
ELF	EARLY FLOWERING
Fig.	Figure
FT	FLOWERING LOCUS T
G	threonine
GA	Gibberellic acid
GAPDH	glyceraldehyde 3-phosphate dehydrogenase
GI	GIGANTEA
HEB-25	Halle Exotic Barley-25
HIF	heterogenous inbred family
HSD	honestly significant difference
<i>Hsp</i>	<i>Hordeum vulgare</i> ssp. <i>Spontaneum</i>
IAA	indole-3-acetic acid
Indels	insertion-deletion mutations
Ka	nonsynonymous substitution rate
Ks	synonymous substitution rate
L3	third leaf
LD	long days
LED	light-emitting diodes
LHY	LATE ELONGATED HYPOCOTYL
LL	continuous light
LLPS	liquid-liquid phase separation
LLR	log-likelihood ratio

LUC	luciferase
LUX	LUX ARRHYTHMO
N	asparagine
NaClO	sodium hypochlorite
NAM	nested association mapping
NASC	Nottingham Arabidopsis Stock Centre
NIL	near isogenic line
OE	overexpression
PAR	photosynthetically active radiation
PCA	principal component analysis
PCH1	PHOTOPERIODIC CONTROL OF HYPOCOTYL1
PCL1	PHYTOCLOCK 1
PCR	polymerase chain reaction
phyA/B	phytochrome A/B
PIF4	PHYTOCHROME INTERACTING FACTOR 4
PLAAC	Prion-Like Amino Acid Composition
polyQ	polyglutamine
PP2A	PROTEIN 19 PHOSPHATASE2a subunit A3
Ppd-H1	PHOTOPERIOD H1
PrD	prion-like domain
PRR	PSEUDO-RESPONSE REGULATOR
QTL	quantitative trait locus
RAE	relative amplitude error
RIL	recombinant inbred line
RNA	ribonucleic acid
RT-qPCR	reverse transcription quantitative real-time PCR
RVE8	REVEILLE 8
scp	secure copy protocol
SD	short days
SEM	standard error of mean
SNP	single nucleotide polymorphism
SSH	public secure shell
STRING	Search Tool for the Retrieval of Interacting Genes/Proteins
SVP	SHORT VEGETATIVE PHASE
T0	coleoptile tiller
T1	first tiller
TGW	thousand grain weight
TIC	TIME FOR COFFEE
TIP41	INTERACTING PROTEIN OF 41 KDA
TOC1	TIMING OF CAB EXPRESSION 1
VRN	VERNALIZATION
W	tryptophan
w/v	weight/volume
Ws-2	Wassilewskija-2
XBAT	XB3 ORTHOLOG 5 IN ARABIDOPSIS THALIANA
YUC	YUCCA
ZT	Zeitgeber time

List of figures

Fig. 1-1 Plant anticipation, acclimation, and adaptation to changing environment.	1
Fig. 1-2 <i>A. thaliana</i> EARLY FLOWERING 3 as a key player in plant circadian clock and thermomorphogenesis.	3
Fig. 1-3 An overview of pathways controlling floral transition in <i>H. vulgare</i>	6
Fig. 1-4 <i>H. vulgare</i> HEB-25 population and HIF concept.	8
Fig. 2-1 Infrared imaging platform for circadian rhythmicity analysis.	12
Fig. 2-2 Image-based plant phenotyping for barley temperature assay in growth chambers.	14
Fig. 3-1 Phylogenetic tree of ELF3 and EEC.	23
Fig. 3-2 Arabidopsis ELF3 PrD and conserved regions of ELF3 and EEC.	25
Fig. 3-3 Phylogenetic tree and sequence alignment of Brassicales ELF3.	26
Fig. 3-4 Natural variation of ELF3 polyQ length in Arabidopsis accessions.	28
Fig. 3-5 Geographic distribution of ELF3 polyQ variation in Arabidopsis accessions.	29
Fig. 3-6 Population genetic signatures of Arabidopsis <i>ELF3</i>	31
Fig. 3-7 Genetic variation of <i>ELF3</i> in Arabidopsis accessions.	32
Fig. 3-8 Association of ELF3 polyQ variation with hypocotyl phenotypes.	34
Fig. 3-9 Visualization of potential polyQ-phenotype association.	35
Fig. 4-1 <i>ELF3</i> and <i>GI</i> are involved in temperature-photoperiod crosstalk.	38
Fig. 4-2 Temperature-photoperiod crosstalk at a higher temperature regime.	39
Fig. 4-3 Thermoresponsive growth is intact in continuous light.	40
Fig. 4-4 <i>ELF3</i> is required for rhythmic physiological processes under temperature cycles.	42
Fig. 4-5 Clock-controlled cotyledon movement entrained by different temperature cycles.	43
Fig. 4-6 <i>ELF3</i> -mediated rhythmic output is independent of <i>phyB</i> , <i>LUX</i> , and <i>ELF4</i>	45
Fig. 4-7 <i>ELF3</i> is required for the oscillator's responsiveness to temperature changes.	47
Fig. 4-8 The oscillator's responsiveness to temperature changes in darkness.	48
Fig. 4-9 <i>ELF3</i> is essential for circadian gating of temperature signals.	50
Fig. 4-10 <i>H. vulgare elf3</i> seedlings can be entrained by temperature cycles.	51
Fig. 5-1 <i>ELF3</i> is involved in the early temperature response of barley seedlings.	53
Fig. 5-2 Variations in <i>ELF3</i> sequence among HIF pairs.	55
Fig. 5-3 Elevated temperatures accelerate early growth and development of barley seedlings.	56
Fig. 5-4 Percentage of plants with coleoptile tillers.	58
Fig. 5-5 Effects of exotic <i>ELF3</i> alleles and elevated temperatures on barley growth and plant architecture.	59
Fig. 5-6 Effects of exotic <i>ELF3</i> alleles and elevated temperatures on barley tillering.	61
Fig. 5-7 Principal component analysis (PCA) of barley growth traits.	62
Fig. 5-8 Effects of elevated temperatures on barley leaf chlorophyll content.	63
Fig. 5-9 Effects of exotic <i>ELF3</i> alleles and elevated temperatures on barley floral transition.	64
Fig. 5-10 An exotic <i>ELF3</i> allele interacts with elevated temperatures to control meristem development and transcript levels of flowering genes.	66
Fig. 5-11 Growth and development phenotypes from temperature assay in greenhouses.	68
Fig. 5-12 Effects of exotic <i>ELF3</i> allele and elevated temperatures on barley spike parameters.	69

Fig. 5-13 Effects of exotic <i>ELF3</i> allele and elevated temperatures on barley yield related parameters.	70
Fig. 5-14 Correlation of temperature responses in selected traits.	71
Fig. 6-1 STRING-network for Arabidopsis <i>ELF3</i> and its interactors.	77
Appendix Fig. 1 Genomic setup of the used HIFs.	101

List of tables

Table 1 Gene homologues of the evening complex and <i>EEC</i> in various plant genomes. .	22
Table 2 List of <i>A. thaliana</i> accessions used in this study.	96
Table 3 List of primers used in this study.	102
Table 4 List of identified <i>ELF3</i> and <i>EEC</i> homologues in 274 plant genomes.	103
Table 5 Hypocotyl growth rate under temperature cycles in LL (related to Fig. 4-4B).	110
Table 6 Transcript levels of genes under temperature cycles in LL (related to Fig. 4-7). .	111
Table 7 Transcript levels of genes under temperature cycles in LL (normalized to <i>TIP41</i>).	112
Table 8 Transcript levels of genes under temperature cycles in DD (related to Fig. 4-8).	113
Table 9 Plant height during barley seedling establishment (related to Fig. 5-3A).	114
Table 10 Length and width of the first and second leaves (related to Fig. 5-3D).	115
Table 11 Plant height during barley growth and development (related to Fig. 5-5A).	116
Table 12 Top-view plant area during barley growth and development (related to Fig. 5-5B).	117
Table 13 Side-view plant area during barley growth and development (related to Fig. 5-5C).	118
Table 14 Plant volume during barley growth and development (related to Fig. 5-5D).	119
Table 15 Top-view convex hull area during barley growth and development (related to Fig. 5-5E).	120
Table 16 Side-view convex hull area during barley growth and development (related to Fig. 5-5F).	121
Table 17 Total tiller number during barley growth and development (related to Fig. 5-6).	122
Table 18 Chlorophyll content in the second leaf during barley growth and development (related to Fig. 5-8).	123
Table 19 Transcript levels of barley flowering genes during growth and development (related to Fig. 5-10B).	124

1 Introduction

1.1 Plant performance under changing environment

Like other organisms living on Earth, plants experience regular environmental changes with the rotation of the planet. These include light/dark and warm/cool cycles with a period of around 24 h, as well as seasonal changes in photoperiod and temperature. Plants have evolved an internal oscillator, known as circadian clock, that allows them to anticipate regular daily events and to adjust their internal cellular mechanisms accordingly (Thomas and Vince-Prue, 1996) (Fig. 1-1).

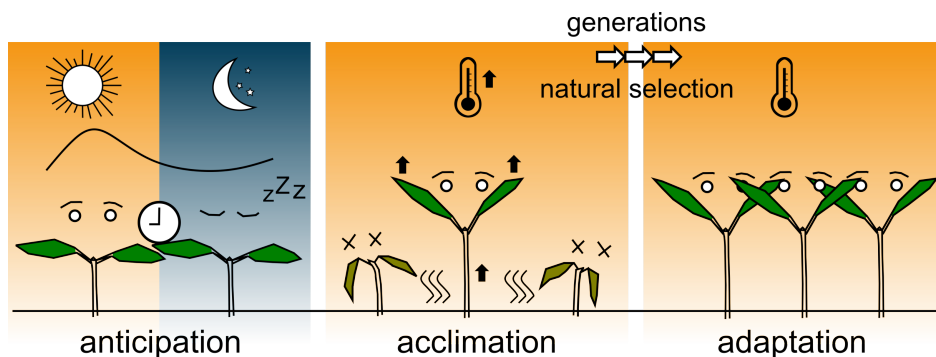


Fig. 1-1 Plant anticipation, acclimation, and adaptation to changing environment.

Hypocotyl elongation and leaf hyponasty response to high ambient temperature in *Arabidopsis thaliana* seedlings were used as examples.

With the proceedings of global climate change, extreme weather and climate events become more frequent and intense, including elevated atmospheric CO₂, droughts and flooding due to shifts in precipitation patterns, and extreme temperatures (Pörtner *et al.*, 2022). These unpredictable environmental changes, even moderate, can impact plant ecophysiology, spatial distribution, and productivity, threatening crop yield stability and food security (Leng and Huang, 2017). Meanwhile, individual plants are capable of temporarily adjusting their growth and development as a response to these changes, which is known as acclimation (Fig. 1-1). The term acclimation therefore applies to growth adjustments within the life cycle of a single or many plants. However, not all plant populations have the ability to acclimate. This ability can be achieved by natural selection when plant populations are exposed to the same changing environment over many generations. The ability to acclimate is therefore an evolutionary process which is called adaptation. Adaptation increases the fitness of a population in changing environments. Therefore, understanding how plants anticipate,

acclimate, and adapt to a changing environment is pivotal to keep the pace and mitigate the negative influence of climate changes.

1.2 The circadian clock anticipates cyclic environmental changes

As plants are more frequently encountering predictable environmental changes, circadian anticipation is the most general ability that contributes to plant performance. The circadian clock is an endogenous key network that utilizes external cues (known as *Zeitgeber*, time-giver), primarily light/dark and temperature cycles, as timing input to precisely generate internal biological rhythms. The oscillator components (known as *Zeitnehmer*, time-taker) receive the timing information from the *Zeitgeber* and help to reset and keep synchrony with the external environment. This *Zeitgeber-Zeitnehmer* communication is known as entrainment that sets the period and phase of the oscillator (Wang *et al.*, 2022). The period here indicates the necessary time for a completed cycle, whereas the phase is a specific time point (e.g., peak or valley positions) within a cycle, both determining the waveform of rhythmicity (McClung, 2006). Once correctly entrained, the rhythmicity generated by the oscillator can be sustained for several cycles, even in the absence of environmental cues (i.e., free-running conditions, such as constant light and temperature conditions). The ability of the circadian clock to anticipate cyclic environmental changes thereby confers fitness advantages to organisms (Xu *et al.*, 2022).

Knowledge of the plant circadian clock is mainly generated from studying the model plant *Arabidopsis thaliana* (*Arabidopsis*), with light as a primary *Zeitgeber*. In *Arabidopsis*, the central part of the circadian clock, the oscillator, is composed of multiple interconnected transcriptional-translational feedback loops (Huang and Nusinow, 2016; Nohales and Kay, 2016) (Fig. 1-2, left part). The morning loop contains two partially redundant MYB-like transcription factors CIRCADIAN CLOCK ASSOCIATED 1 (CCA1) and LATE ELONGATED HYPOCOTYL (LHY) which positively regulate the expression of *PSEUDO-RESPONSE REGULATOR 9* (*PRR9*) in the morning and *PRR7* in the afternoon (Farré *et al.*, 2005; Nakamichi *et al.*, 2010), while repressing two additional afternoon-phased genes, *PRR5* and *GIGANTEA* (*GI*) (Lu *et al.*, 2012; Kamioka *et al.*, 2016). *PRR9*, *PRR7*, and *PRR5* later repress the expression of *CCA1/LHY*, allowing the induction of evening-phased genes (Nakamichi *et al.*, 2010; Adams *et al.*, 2015). In the early evening, accumulation of TIMING OF CAB EXPRESSION 1 (*TOC1/PRR1*) represses *GI*, which in turn activates *TOC1* (Kim *et al.*, 2007). With the removal of repression and partially induced by another morning-

phased component REVEILLE 8 (RVE8), three evening-phased proteins EARLY FLOWERING 3 (ELF3), ELF4, and LUX ARRHYTHMO (LUX) accumulate and form a protein complex, named the evening complex (EC) (Hsu *et al.*, 2013). TOC1, GI, and the EC represent the evening loop (Fig. 1-2, left part). The EC directly represses the transcription of *PRR9*, *PRR7*, and *GI*, allowing CCA1 and LHY to accumulate before dawn (Nusinow *et al.*, 2011; Herrero *et al.*, 2012; Ezer *et al.*, 2017).

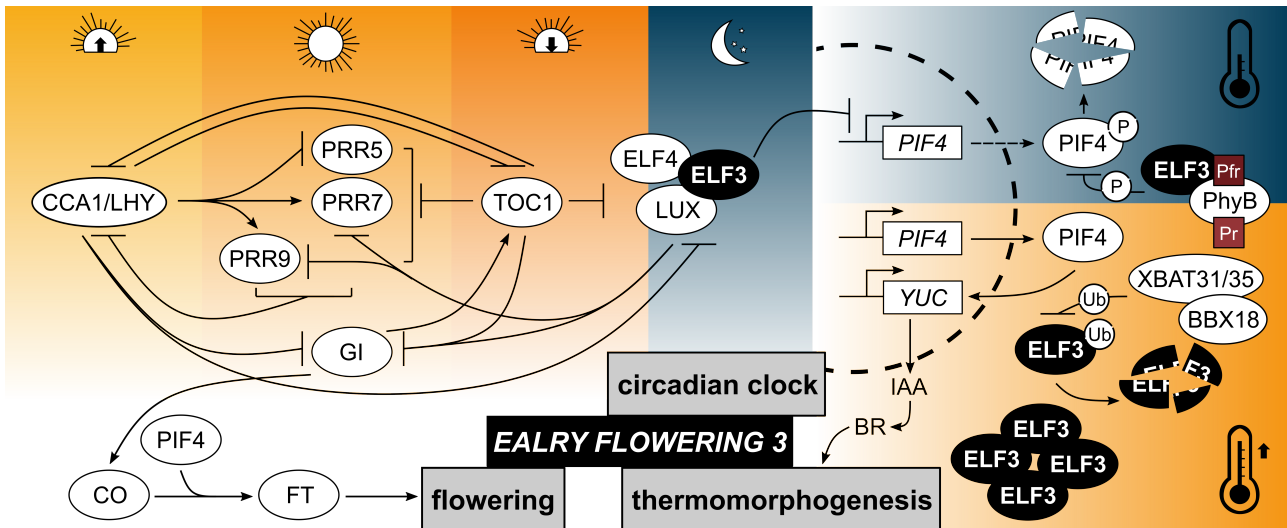


Fig. 1-2 A. *thaliana* EARLY FLOWERING 3 as a key player in plant circadian clock and thermomorphogenesis.

Left part: circadian clock morning loop is composed of CCA1 and LHY, which regulate PRRs and TOC1, whereas TOC1, GI, and the EC (ELF3/ELF4/LUX) form the evening loop. The connections between circadian clock oscillator components indicate transcriptional-translational regulation, with light/dark cycle as an example. For flowering control, ELF3 functions as a substrate adaptor for CONSTITUTIVE PHOTOMORPHOGENIC 1 (COP1) dependent degradation of GI, resulting in reduced expression of flowering-promoting genes *CONSTANS* (CO) and *FLOWERING LOCUS T* (FT) (Yu *et al.*, 2008). Right part: ELF3 is crucial for both temperature sensing and signaling. YUC, auxin biosynthesis genes; IAA, indole-3-acetic acid; BR, brassinosteroids; P, phosphorylation; Ub, Ubiquitination.

Although the transcriptional-translational feedback loops of identified integral components can explain circadian rhythmicity, the actual Zeitnehmer is still intriguing. Via potential interactions with photoreceptor phytochrome B (phyB), ELF3 and GI present one possible Zeitgeber-Zeitnehmer junction (Yeom *et al.*, 2014). Consistently, mutants of *ELF3* and *GI* display disrupted oscillator rhythmicity or periodicity under free-running conditions, as well as pleiotropic phenotypes such as elongated hypocotyls and altered flowering time (Hicks *et al.*, 1996; Park *et al.*, 1999; McWatters *et al.*, 2000) (Fig. 1-2). A recent study demonstrated that photoperiod-responsive growth and flowering time were lost in *elf3 gi*

double mutants, and thereby established these two genes as essential Zeitnehmers for clock entrainment to light signals (Anwer *et al.*, 2020).

Unlike the junction to the light Zeitgeber, the mechanism of clock entrainment to temperature cycles is still poorly understood (Avello *et al.*, 2019; Gil and Park, 2019). Based on the little that is known, *PRR7* and *PRR9* have conceivable roles for integrating temperature input to the oscillator, as *prr7 prr9* double mutants displayed arrhythmia depending on temperature regimes (Salomé and McClung, 2005; Salomé *et al.*, 2010). In addition, the EC has been proposed to repress the temperature input to the clock (Mizuno *et al.*, 2014). However, a previous finding suggested *ELF3* to not function as a temperature Zeitnehmer (Thines and Harmon, 2010).

1.3 Plant thermomorphogenesis signaling

While the circadian clock confers the ability to handle daily environmental fluctuations, plants still face challenges from unpredictable environments. As one of the most important aspects of climate change, global warming refers to the rise in ambient temperatures mainly due to increased concentration of greenhouse gases. Plants can acclimate rapidly to elevated temperatures with morphological and developmental adjustments, collectively termed thermomorphogenesis (Quint *et al.*, 2016). In *Arabidopsis*, thermomorphogenic seedling phenotypes include elongated hypocotyls and leaf hyponasty, which are known to avoid heat reflected from the ground and improve transpirational cooling capacity (Koini *et al.*, 2009; van Zanten *et al.*, 2009; Crawford *et al.*, 2012) (Fig. 1-1).

Changes in ambient temperatures can be perceived via multiple systems, with phyB as the first identified plant temperature sensor (Jung *et al.*, 2016; Legris *et al.*, 2016). Warm temperatures accelerate the dark/thermal reversion of phyB from its active Pfr form to its inactive Pr form (Delker *et al.*, 2017) (Fig. 1-2, right part). By stabilizing ELF3, the active Pfr form of phyB mediates degradation of the basic helix-loop-helix (bHLH) transcription factor PHYTOCHROME INTERACTING FACTOR 4 (PIF4) (Nieto *et al.*, 2015). As a central regulator of thermomorphogenesis signaling, PIF4 accumulates at warm temperatures and activates auxin biosynthesis genes, promoting cell elongation in petioles and hypocotyls, as well as thermonastic leaf movement (Franklin *et al.*, 2011; Park *et al.*, 2019) most likely in concert with brassinosteroid action (Ibañez *et al.*, 2018). On the other hand, PIF4 mediates thermal acceleration of flowering by activating *FT* (Kumar *et al.*, 2012).

In addition to phyB thermosensing, the prion-like domain (PrD) of ELF3 functions as a thermosensor, enabling the liquid-liquid phase separation (LLPS) of ELF3 from its dilute phase into liquid droplets (dense phase) at high temperatures (Jung *et al.*, 2020) (Fig. 1-2, right part). The aggregation of ELF3 in dense phase coordinates with its restricted mobilization to the nucleus (Ronald and Davis, 2021; Ronald *et al.*, 2022), and thereby relieves the transcriptional repression of *PIF4* (as a component of the EC) and potentially the direct interaction with PIF4 (Box *et al.*, 2015; Nieto *et al.*, 2015; Raschke *et al.*, 2015). In addition, B-box zinc finger protein 18 (BBX18) recruits the E3 ligase XB3 ORTHOLOG 5 IN ARABIDOPSIS THALIANA 31 (XBAT31) and XBAT35 to target ELF3 for degradation at high temperatures (Zhang *et al.*, 2021).

1.4 *H. vulgare* as a model crop for adaptation to climate change

With its multiple functions in the circadian clock and thermomorphogenesis, *ELF3* has been described as one of the key plasticity genes, conferring acclimation responses to changing environments (Blackman, 2017; Laitinen and Nikoloski, 2019). In the context of global climate change, expanding knowledge generated from Arabidopsis to crops and crop models is pivotal to achieve crop-level adaptations and yield stability (Challinor *et al.*, 2014). However, although *ELF3* homologues have been identified in multiple of crop species (Faure *et al.*, 2012; Zakhrebekova *et al.*, 2012; Ning *et al.*, 2015; Alvarez *et al.*, 2016; Lu *et al.*, 2017; Ridge *et al.*, 2017), their roles in crop acclimation and adaptation to changing temperatures are largely unknown.

Barley (*Hordeum vulgare*) as a globally cultivated robust crop, has emerged as a distinguished model for understanding crop adaptation to climate change (Dawson *et al.*, 2015; Harwood, 2019). The barley ortholog of Arabidopsis *ELF3*, *HvELF3* (also known as *EARLY MATURITY 8* or *Praematurum-a*), has conserved functions in flowering time regulation, which plays a critical role in barley adaptation/domestication to short growing seasons (Faure *et al.*, 2012; Zakhrebekova *et al.*, 2012). In addition, although the cycling of circadian genes tends to follow a different bimodal pattern and the predicted oscillator network needs to be validated, *HvELF3* is conserved as a core component also in the barley circadian clock (Müller *et al.*, 2020).

The current understanding of barley temperature responses is mainly restricted to its reproductive development, which is regulated by the circadian clock, photoperiod, and vernalization (Jacott and Boden, 2020) (Fig. 1-3). Loss of *ELF3* function facilitates the

expression of the photoperiod response gene *PHOTOPERIOD H1* (*Ppd-H1*), which corresponds to Arabidopsis *PRR37* (Turner *et al.*, 2005; Faure *et al.*, 2012). Up-regulation of *Ppd-H1* promotes the expression of *FT1*, a barley homologue of Arabidopsis *FT* (Campoli *et al.*, 2012). In addition, a potentially conserved barley *GI-CO1-FT1* pathway promotes *FT1* directly or via *Ppd-H1*, providing another connection to the circadian clock as *GI* is predicted to be repressed by barley *LUX1* (Müller *et al.*, 2020). Furthermore, in the vernalization pathway, *VERNALIZATION 1* (*VRN1*) and *VRN2* as key regulators activate or repress *FT1* (also known as *VRN3*) (Yan *et al.*, 2006; Trevaskis *et al.*, 2007). Florigen *FT1* translocates from leaves to the shoot apical meristem, associated with the expression of barley floral meristem identity genes *VRN1*, *BARLEY MADS-box 3* (*BM3*), and *BM8*, initiating inflorescence development (Trevaskis *et al.*, 2007; Li *et al.*, 2015). Cooperating with *FT1* in the acceleration of flowering, gibberellic acid (*GA*) biosynthesis is induced under long days, which is known to be related with *ELF3* function (Boden *et al.*, 2014).

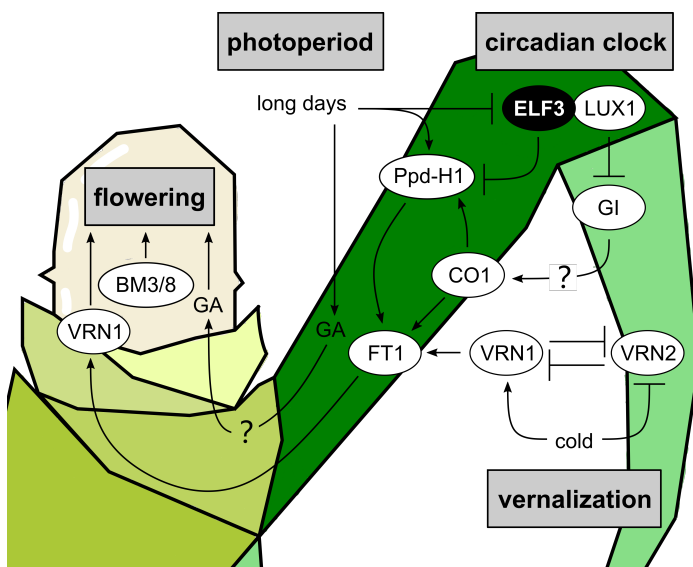


Fig. 1-3 An overview of pathways controlling floral transition in *H. vulgare*.

The connections with question marks are based on their functions in Arabidopsis, which have not been validated yet in barley.

The reproductive development of barley is generally accelerated in an *ELF3* loss-of-function background (Faure *et al.*, 2012; Zakhrebekova *et al.*, 2012). High ambient temperatures further induce the flowering in *elf3* mutants, however, with even reduced or invariable *FT1* levels, suggesting *FT1*-independent pathways (Hemming *et al.*, 2012; Ejaz and von Korff, 2017). In the circadian clock pathway, *ELF3* function is required for the temperature responsiveness of *GI* and *PRR* genes (Ford *et al.*, 2016; Müller *et al.*, 2020). In addition, acting downstream of *ELF3*, the effects of *Ppd-H1* in thermal acceleration of flowering depend on the allelic variation for *VRN1* (Ejaz and von Korff, 2017; Ochagavía *et al.*, 2021).

For example, *Ppd-H1* promotes floral development in the presence of a spring *VRN1* allele but not a winter *vrn1* allele, indicating the interaction with the vernalization pathway (Ejaz and von Korff, 2017). These findings suggest that the effects of temperature connect to all three major pathways in barley reproductive development, with ELF3 playing critical upstream roles.

1.5 Natural variation for growth and developmental plasticity

As our knowledge of barley *ELF3* was generated from induced mutants, it is necessary to have a confirmation in diverse genetic backgrounds for breeding applications. Domestication and breeding confer resilience to crops against adverse environments, however, such improvement meanwhile eliminates genetic diversity (Gasparini *et al.*, 2021). To improve growth and developmental plasticity ready for upcoming challenges, exploiting natural variation provides another approach that helps to identify new favorable alleles from wild relatives.

In Arabidopsis, recombinant inbred line (RIL) populations were generated using bi-parental crosses (natural accessions Bay-0 and Sha) or intercrossing of 19 accessions (MAGIC population) (Anwer *et al.*, 2014; Box *et al.*, 2015; Raschke *et al.*, 2015). Based on these populations, natural variation within *ELF3* was found to affect thermoresponsive growth, contributing to our understanding of its role in circadian clock and thermomorphogenesis. Besides single nucleotide polymorphisms (SNPs) in Arabidopsis *ELF3*, the temperature sensing PrD harbors natural variation of polyglutamine (polyQ) length caused by expanded cytosine-adenine-adenine (CAA) repeats. Similar to the aggregation of ELF3 responding to high temperatures (Jung *et al.*, 2020), in humans, the polyQ-extended proteins are known to aggregate in the degenerated neurons leading to so-called polyQ diseases (Fan *et al.*, 2014). This consistency suggests that the polyQ determines the thermosensing function of Arabidopsis ELF3-PrD. Variations in polyQ length have been investigated from more than one hundred natural accessions (Tajima *et al.*, 2007; Undurraga *et al.*, 2012). These studies reported significant correlations between polyQ length and circadian clock parameters, using natural or transgenic lines. However, the associations of polyQ length with temperature responsive phenotypes were not prominent (Press *et al.*, 2016). Thus, regarding temperature sensing and signaling, potential effects and evolutionary meaning of ELF3 polyQ variation are still unknown.

Barley germplasm consists of genetically diverse landraces and exotic accessions, and a large proportion of which is presumed to be adapted to various abiotic stresses (Newton *et al.*, 2011; Russell *et al.*, 2011). For instance, a spontaneous recessive *elf3* mutant was identified in barley landraces from the Qinghai-Tibetan Plateau, where low temperatures are the main restrictions for growth (Xia *et al.*, 2017). To examine potentially beneficial alleles from exotic progenitors in an elite background, the nested association mapping (NAM) population Halle Exotic Barley-25 (HEB-25) was generated by crossing 25 exotic barley accessions with the elite cultivar Barke (Maurer *et al.*, 2015) (Fig. 1-4A). Based on this population, *ELF3* was identified in a quantitative trait locus (QTL) region, responsible for various agronomic traits under different environments (Maurer *et al.*, 2016; Herzig *et al.*, 2018). To study the effects of exotic *ELF3* variants, heterogeneous inbred family (HIF) pairs were generated based on HEB-25 (Zahn *et al.*, 2022, Preprint) (Fig. 1-4B). In each HIF pair, two nearly isogenic sister lines differ only in the homozygous cultivated (elite) or exotic (wild) *ELF3* allele or region, allowing direct comparison. Recent field experiments revealed significant roles of exotic *ELF3* alleles in barley development and grain yield (Zahn *et al.*, 2022, Preprint), demonstrating that HIF pairs have suitable genetic backgrounds to study barley temperature responses.

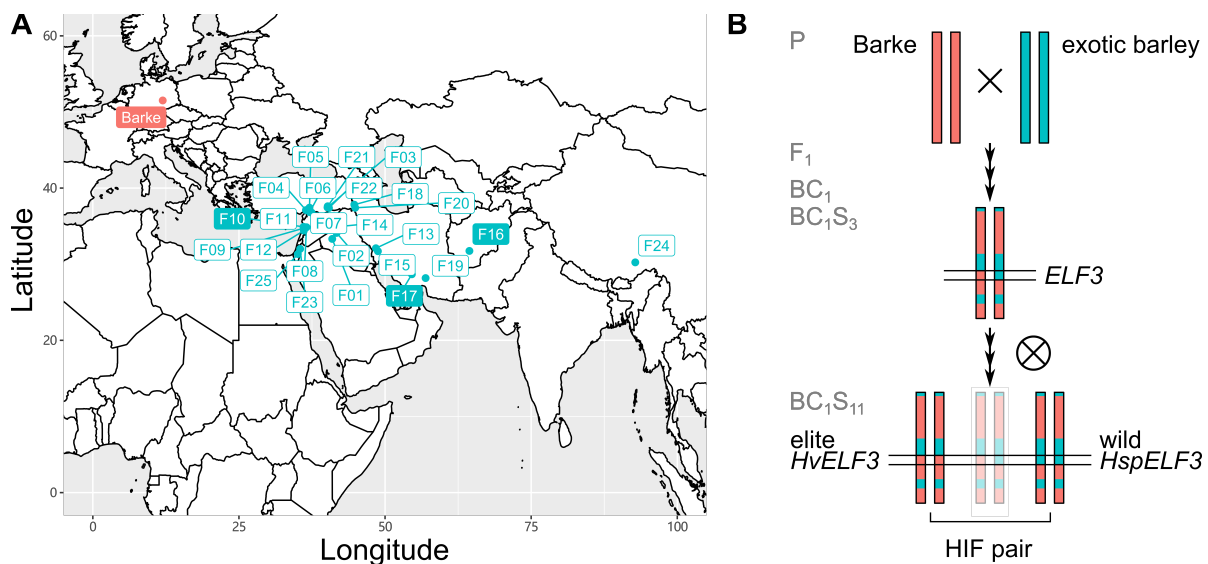


Fig. 1-4 *H. vulgare* HEB-25 population and HIF concept.

(A) Geographic origins of HEB-25 parental lines (Maurer *et al.*, 2015). Parental lines of HIF pairs used in this study are highlighted. (B) Generation of *ELF3* HIF pairs. *Hsp*, *Hordeum vulgare ssp. spontaneum*.

1.6 Objectives

The principal objective of this thesis is to functionally characterize *ELF3* as a determinant of plant performance under changing temperatures, from the eudicot model Arabidopsis to the monocot model crop barley. The work included the following aspects:

- I) Trace the evolutionary emergence of *ELF3*. Taking advantage of available plant genomes, this work intended to identify *ELF3* homologues across the plant kingdom, with the focus on PrD existence. In parallel, this work attempted to investigate natural variation of *ELF3* polyQ length among Arabidopsis accessions and its correlation with temperature responsive phenotypes.
- II) Determine the role of *ELF3* in circadian clock temperature entrainment in Arabidopsis seedlings. Infrared time-lapse imaging and genetic analyses allowed evaluation of oscillator rhythmicity under temperature cycles. The major focus was to understand how cyclic temperature signals are perceived by the oscillator, and whether *ELF3* acts as a temperature Zeitnehmer.
- III) Explore thermomorphogenesis and the potential role of *HvELF3* in barley. A combination of physiological assays, image-based phenotyping, and transcriptional analyses enabled characterizing growth, development, and yield-related responses to high temperatures in barley. In this process, using *elf3* loss-of-function alleles and HIF pairs generated from the HEB-25 population helped to evaluate the general function of *ELF3*, and specifically the function of exotic *ELF3* alleles.

2 Materials and Methods

2.1 Plant material

2.1.1 *A. thaliana* lines

All *A. thaliana* mutant lines used were in the Ws-2 (Wassilewskija-2) or the Columbia-0 (Col-0) background. The *elf3-4* (Hicks *et al.*, 1996; Zagotta *et al.*, 1996), *gi-158* and *elf3-4 gi-158* (Anwer *et al.*, 2020), *phyB-10* (Feldmann, 1991; Franklin *et al.*, 2003), and *pcl1-2* (Onai and Ishiura, 2005) null mutants were in the Ws-2 background. The *elf3-4 phyB-10* was generated by crossing. The *elf4-2*, *elf4-2 ELF3-OE*, and *elf3-1 ELF4-OE* mutants in the Col-0 background have likewise been described previously (Nusinow *et al.*, 2011; Box *et al.*, 2015; Jung *et al.*, 2020). Ws-2, *elf3-4*, *phyB-10*, and *elf3-4 phyB-10* additionally harbor a *CCR2:LUC* reporter construct, and Ws-2 and *pcl1-2* additionally harbor *GI:LUC*.

Natural accessions of *A. thaliana* obtained from Nottingham Arabidopsis Stock Centre (NASC) are listed in Appendix I.

2.1.2 *H. vulgare* lines

Three HIF pairs (10_190, 16_105, and 17_041) were selected from the barley NAM population HEB-25, with exotic barley accessions collected from Syria, Afghanistan, and Iran, respectively (Maurer *et al.*, 2015; Zahn *et al.*, 2022, Preprint) (Fig. 1-4). The genomic setup of these three HIF pairs was previously described and is visualized in Appendix II (Zahn *et al.*, 2022, Preprint). Bowman (elite cultivar), *elf3^{BW289}*, and *elf3^{BW290}* (*eam8.k* and *eam8.w* loss-of-function mutants BW289 and BW290 in Bowman background) were used as control and have been described previously (Faure *et al.*, 2012; Zakhrebekova *et al.*, 2012).

2.2 Physiological assay

2.2.1 Seed sterilization and stratification

A. thaliana seeds were surface sterilized by washing with 70% ethanol for 3 min, and with 4% NaClO (with 0.3% TritonX) for 8 min using an orbital shaker. Seeds were then rinsed with sterile water three times for 10 min each and stratified in sterile water for 3 d at 4°C in darkness. *H. vulgare* seeds used for sterile culture were likewise surface sterilized by washing with 4% NaClO for 30 min and cold stratified for 2 d at 4°C in darkness.

2.2.2 *A. thaliana* temperature assays

Sterilized seeds were allowed to germinate on solid *A. thaliana* solution (ATS) nutrient medium with 1% (w/v) sucrose (Lincoln *et al.*, 1990). Unless stated otherwise, seedlings were grown on vertically oriented plates placed in long days (LDs, 16 h light: 8 h dark) or short days (SDs, 8 h light: 16 h dark) with $90 \mu\text{mol m}^{-2}\text{s}^{-1}$ photosynthetically active radiation (PAR) using white fluorescent lamps (T5 4000K). Seedlings were grown at constant 16, 20, 22, or 28°C for 8 d. For temperature shift assays, seedlings grown at 20°C for 4 d were either shifted to 28°C or kept at 20°C for an additional 4 d. For assays in constant light (LL, $90 \mu\text{mol m}^{-2}\text{s}^{-1}$), seedlings were grown at constant 16, 22, or 28°C for 8 d. Seedlings were imaged and the length of hypocotyl was measured using the segmented line tool in ImageJ (<http://imagej.nih.gov/ij/>) or using RootDetection 0.1.2 (<http://www.labutils.de/rd.html>). Temperature response (%) was calculated as the ratio of each measured hypocotyl length at higher temperature (22°C or 28°C) relative to the median hypocotyl length at lower temperature (16°C or 20°C).

Temperature shift assays (20°C to 28°C) were used for screening of 253 *A. thaliana* accessions. The experiments were performed separately in nine sequential batches and Col-0 was included in each batch ($n=6-32$ depending on germination). To compare the data obtained among different batches, relative hypocotyl length was calculated by normalizing absolute value to the median hypocotyl length of Col-0 (Accession ID: 6909) at 20°C for each batch.

2.2.3 Growth assays under temperature cycles

2.2.3.1 Growth conditions

To unobstructedly visualize hypocotyl and cotyledons in air, seeds were sown on the agar ledge formed by removing part of the agar in square plates (Fig. 2-1, left part). After sowing, the redundant seeds were removed to ensure adequate seed-seed distance (around 5 mm), and small ditches were made next to each seed. Seeds were then relocated to the ditches so that the position of seeds and young seedlings were relatively fixed during the experiment. The plates were placed in constant light (LL, $30 \mu\text{mol m}^{-2}\text{s}^{-1}$) under specified temperature cycles (12 h 22°C: 12 h 16°C or 12 h 28°C: 12 h 22°C). For free-running conditions, seedlings were entrained by temperature cycles for 2 d after germination in LL and then on day 3 at Zeitgeber time (ZT) 00 (start of subjective warm period) seedlings were released into constant 22°C.

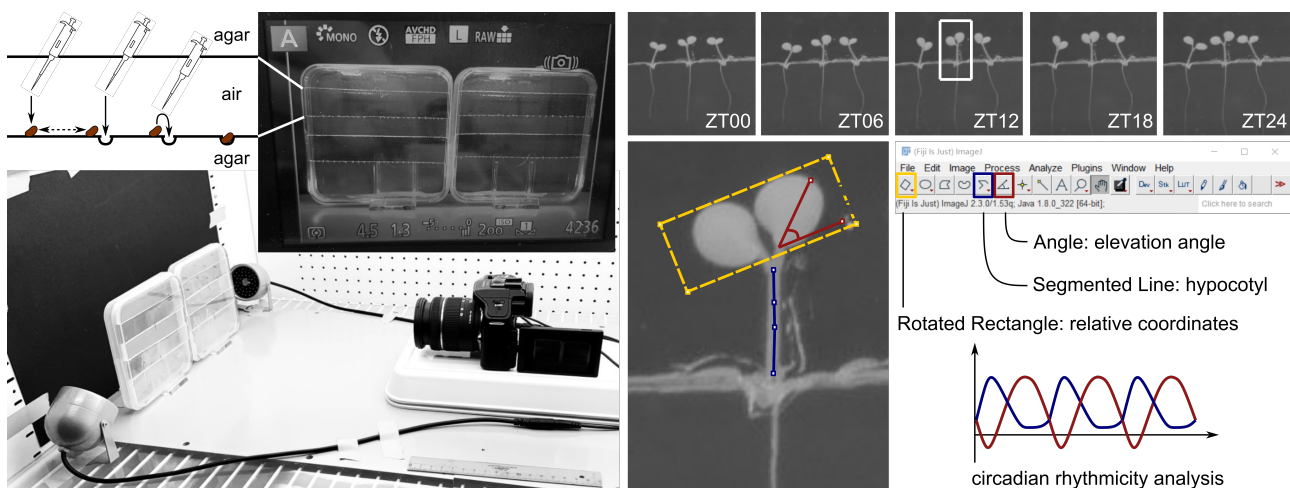


Fig. 2-1 Infrared imaging platform for circadian rhythmicity analysis.

Left part: Sowing step, camera screen with the view of plates and setting parameters, and the platform for imaging.

Right part: Images of the same *Ws-2* seedlings at various ZTs were shown as examples. The seedlings were under free-running conditions after temperature cycle entrainment.

2.2.3.2 Construction of infrared imaging platform

An infrared-based imaging system was constructed inside the growth chamber to monitor seedling phenotypes under cycling conditions (e.g., light/dark cycles and temperature cycles) with infrared illuminations (Fig. 2-1, left part). The camera (Panasonic G5, Kadoma, Osaka, Japan) was modified with infrared long pass 830 nm cut filters, which enabled imaging in darkness without disturbing seedling growth. The setting parameters of the camera were: lens H-PS14042, aperture f4.5, shutter speed 1.3", and ISO 200.

Imaging started at ZT00 on day 3 after germination. Photographs were taken every 60 min for 96 h. Interval timer shooting was achieved by using a remote controller (Rollei, Norderstedt, Germany).

2.2.3.3 Circadian rhythmicity analysis

Image stacks were imported as 'Image Sequence' in ImageJ (<http://imagej.nih.gov/ij/>), so that seedlings can be measured separately across different time points and minor changes between time points can be thereby detected (Fig. 2-1, right part). For cotyledon movement measurement, the angle between cotyledon position to its relative horizontal was defined as elevation angle, which was measured using the Angle tool. In case of non-straight seedling positions, relative coordinates were generated using the Rotated Rectangle tool,

to ensure both cotyledons having the same elevation angle. Hypocotyl length was measured using the Segmented Line tool, by slightly adjusting the control nodes between time points. The growth rate was calculated as absolute growth rate between two time points. The circadian parameters of cotyledon movement were determined using MFourFit method integrated in BioDare2 analysis platform (Zielinski *et al.*, 2014). The relative amplitude error (RAE) analysis was used to estimate the robustness of the circadian rhythm: RAE values range from 0 to 1, where 0 represents a robust rhythm, and 1 represents no rhythm.

2.2.4 *H. vulgare* temperature assay on plates

Sterilized Bowman and *elf3^{BW290}* seeds were sown on solid ATS nutrient medium with 1% (w/v) sucrose (Lincoln *et al.*, 1990). Vertically oriented plates were placed in darkness at 20°C to allow germination. After germination, plates were shifted to constant 28°C or were kept at constant 20°C, with LD (16 h light: 8 h dark) and light intensity of 90 $\mu\text{mol m}^{-2}\text{s}^{-1}$. The position of leaf tips was marked on the plate after germination and seedlings were imaged in two consecutive days at ZT08. The leaf length (from the marked position, $n=9-17$) was measured using RootDetection 0.1.2 (<http://www.labutils.de/rd.html>).

2.2.5 *H. vulgare* temperature assay in growth chambers

2.2.5.1 Growth conditions

Seeds of three HIF pairs (10_190, 16_105, and 17_041), Bowman, and *elf3^{BW290}* were directly sown in soil and placed in a growth chamber with day/night temperatures of 20°C/16°C, light intensity of 300 $\mu\text{mol m}^{-2}\text{s}^{-1}$ and LD (16 h light: 8 h dark). Five days after sowing (DAS), uniformly germinated seedlings ($n=11$) were either shifted to high ambient day/night temperatures (28°C/24°C, hereafter called 28°C treatment) or were kept at the 20°C/16°C temperature regime (hereafter called 20°C treatment). The position of plants in the growth chambers was randomly rotated twice per week.

2.2.5.2 Construction of image-based phenotyping platform

To non-destructively acquire barley growth and developmental phenotypes, an image-based phenotyping platform was constructed (Fig. 2-2A). A 1.2 m \times 1.2 m \times 1.8 m phenotyping frame was customized with a stand positioned in the middle of the frame to fix the position and direction of the plants during each imaging time point. The platform included

three Raspberry Pi 3 model B single-board microcomputers and three Raspberry Pi RGB camera modules (V2 8MP, Raspberry Pi foundation, Cambridge, England, UK), which enabled imaging from three directions: two side-views separated by 90° and a top-view. The illumination was provided by two light-emitting diodes (LED) lamps (4.6W, Philips, Eindhoven, Netherlands) from the top, and two LED light sets (10W, Neewer, Shenzhen, China) from the sides. The camera modules and light sets were positioned on the top of the frame or outside of it using tripods. The lens-pot distances were 1.25 m to the middle of the pot for side-views and 1.3 m to the top of the pot surface for top-view. To distinguish the plant parts from the surroundings, white foils (Colormatt-Hintergrund Super White, Studioexpress Vertriebs GmbH, Wiernsheim, Germany) were used as imaging background, blue cages (HNP Metalltechnik GmbH, Quedlinburg, Germany) were added to all pots, and blue meshes (Klartext Wunderlich Coating GmbH & Co. KG, Osterode am Harz, Germany) were used to cover the soil surface from 8 DAS.

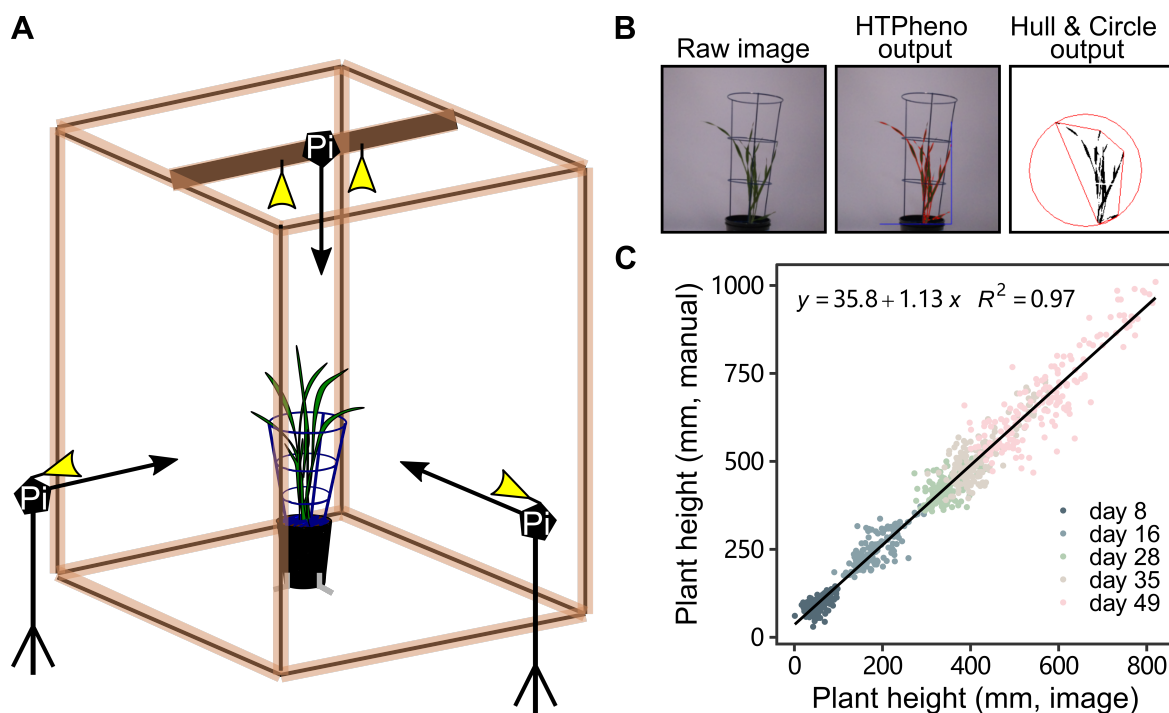


Fig. 2-2 Image-based plant phenotyping for barley temperature assay in growth chambers.

(A) Schematic representation of the phenotyping setup. Pi, a Raspberry Pi microcomputer and an RGB camera module with illumination. (B) Example of raw and output images from image analysis pipelines. (C) Correlation of plant height values obtained from image analysis (x axis) and from manual measurement (y axis). All values ($n=880$) obtained at 8, 16, 28, 35, and 49 DAS were used for analysis and plotting.

The operation protocol for simultaneously acquiring images from several directions was previously described (Tovar *et al.*, 2018). To use a Windows computer as a remote host, secure copy protocol (scp) was used to copy the public secure shell (SSH) key, and the rsync package was installed using Cygwin (<https://www.cygwin.com>) for proper synchronization of images.

2.2.5.3 Phenotyping

Plant height was manually measured daily between 5 and 14 DAS, from soil surface to the highest point of plants without straightening the plants. From 8 until 52 DAS, besides the manual measurement of plant height, total tiller number was counted, and each plant was imaged every two to four days. The images were analyzed with the HTPPheno pipeline (Hartmann *et al.*, 2011) for plant height (two side-views) and plant area (all three views) (Fig. 2-2B). The extracted values displayed a strong correlation with the manually measured values during the experiment (Fig. 2-2C), demonstrating the robustness of the imaging and image analysis pipelines.

Plant volume was calculated as the square root of the product of two side-view areas and the top-view area. For convex hull area, the plant silhouette images derived from the HTPPheno pipeline were further analyzed using the Hull and Circle plugin (Karperien, A., version 2.0a) in ImageJ (<http://imagej.nih.gov/ij/>).

The days until visible third leaf, coleoptile tiller, first tiller, flag leaf sheath opening, and heading (first visible awns) were daily scored. The chlorophyll content was measured using the SPAD-502Plus chlorophyll meter (Konica Minolta, Chiyoda City, Tokyo, Japan) every week from 16 until 52 DAS. The measurement took place around 3 cm from the leaf collar of the second leaf. For destructive measurement of leaf size, the first and second leaves of harvested plants ($n=5$) were imaged 16 DAS. The leaf length and width of the first and second leaves were measured using ImageJ (<http://imagej.nih.gov/ij/>). The measurement of leaf width took place at 2 cm from the leaf collar. All measurement and imaging were conducted between ZT03 and ZT06 on each measurement day.

2.2.6 *H. vulgare* temperature assay in greenhouses

Seeds of HIF pair 10_190 (hereafter called HIF pair 10), Bowman, and *elf3*^{BW290} were coated with Rubin TT (BASF, Ludwigshafen, Germany) to avoid fungal infections before being sown in soil. The experiment was conducted in the greenhouses at Julius Kühn-Institut

(Quedlinburg, Germany). Plants were grown under the 20°C treatment and LD (16 h light: 8 h dark, light intensity of 300 $\mu\text{mol m}^{-2}\text{s}^{-1}$). Plants ($n=12-15$) that reached BBCH-13 (Lancashire et al., 1991) were either shifted to the 28°C treatment or were kept under the 20°C treatment conditions.

The developmental stage was scored at 73 DAS. Plant height and total tiller number were scored at 118 DAS. At maturity (166 DAS for 28°C and 195 DAS for 20°C), the aerial part of the plants was harvested. From three randomly selected spikes of each plant, the length of the spike (excluding the awns) was measured, and the number of grains and florets per spike was determined. The average data for each plant was used for further analysis. Plant dry weight was measured after placing plant materials (aerial parts excluding the spikes) into a drying oven for 1 d at 60°C. The grains were threshed using an LD180 laboratory thresher (Wintersteiger, Ried im Innkreis, Austria). The number of grains per plant, grain area, thousand grain weight (TGW), and grain weight per plant were measured using MARViN ProLine seed analyzer (MARViTECH GmbH, Wittenburg, Germany).

2.3 Molecular biology methods

Primer sequences used for PCR, sequencing, and RT-qPCR are listed in Appendix III.

2.3.1 DNA sequencing

For *A. thaliana* ELF3 polyQ variation, *ELF3* coding sequences of 319 Arabidopsis accessions were obtained from 1001 genomes (Weigel and Mott, 2009). As these sequences contained a large proportion of unknown nucleotides in *ELF3* polyQ regions, polyQ variation of 115 accessions was correct with previously published dideoxy sequencing data (Tajima et al., 2007; Undurraga et al., 2012). In addition, the PrD regions were dideoxy sequenced and corrected in *ELF3* of the other 204 additional accessions. The PrD regions including polyQ were amplified using DreamTaq DNA polymerase (Thermo Fisher Scientific, Waltham, USA).

For *H. vulgare* HIF pairs, the entire *ELF3* genomic sequences was amplified using Ex Taq DNA Polymerase (Takara Bio, Kusatu, Shiga, Japan) and 1186 bp of promoter sequence upstream of the ELF3 start codon in HIF pair 10 was amplified using ALLin™ RPH Polymerase (highQu GmbH, Kraichtal, Germany).

The amplicons were purified using GeneJET Purification Kits (Thermo Fisher Scientific, Waltham, USA) and submitted to Eurofins Genomics (Ebersberg, Germany) for dideoxy sequencing.

2.3.2 Transcriptional analysis

For *A. thaliana* under temperature cycles, seedlings were entrained in LL ($90 \mu\text{mol m}^{-2}\text{s}^{-1}$) or darkness (DD), under 12 h 22°C: 12 h 16°C for 8 d. On day 9, starting from ZT00, the samples were harvested every 4 h. For the temperature gating assay, seedlings were entrained under temperature cycles (with LL) as described above for 8 d. On day 9, starting from ZT00, seedlings were either treated with a 4 h temperature pulse (28°C) at various ZTs, or were kept under the same conditions (no treatment) before samples were harvested at the specified time. For *H. vulgare* under temperature cycles, Bowman and *elf3*^{BW289} seedlings were entrained in LL ($90 \mu\text{mol m}^{-2}\text{s}^{-1}$), under 12 h 22°C: 12 h 16°C for 14 d. On day 15, starting from ZT00, the samples were harvested every 4 h.

For the *H. vulgare* temperature assay in growth chambers, leaf samples of HIF pair 10_190 (10_elite and 10_wild) were harvested at ZT08 at 5, 12, 19, 27, 33, and 40 DAS.

All experiments were performed using three biological replicates. Total RNA was extracted using the NucleoSpin RNA Plant Kit (Macherey-Nagel), cDNA was synthesized using the PrimeScript RT Reagent Kit (Perfect Real Time, Takara Bio), and quantitative real-time-PCR (qRT-PCR) was performed on an AriaMx Real-Time PCR System (Agilent) using Absolute Blue Low Rox Mix (Thermo Fisher Scientific). The relative expression values ($2^{\Delta\text{Ct}}$ values) were calculated using reference genes *PP2A* (AT1G13320) and *TIP41* (AT4G34270) for *A. thaliana*, and *HvACTIN* and *HvGAPDH* (Kikuchi *et al.*, 2012; Zakhrabekova *et al.*, 2012) for *H. vulgare*.

2.4 Computational analysis

2.4.1 Phylogenetic analysis

Copy number of ELF3, EEC, ELF4, and LUX in 42 plant species was obtained using HMMER (Finn *et al.*, 2011) and BLASTp (Altschul *et al.*, 1990) searches based on the Arabidopsis protein and coding sequences. ELF3 and EEC copies were classified using InterProScan (Jones *et al.*, 2014).

In addition, Arabidopsis ELF3 and EEC protein sequences were used to identify their homologous genes from available plant genomes in Phytozome v12.1, v13 (Goodstein *et al.*, 2012) and OneKP databases (Matasci *et al.*, 2014). In total, 434 sequences were obtained from 274 plant genomes (Appendix IV). Sequence alignment was performed using MUSCLE (Edgar, 2004) in AliView (Larsson, 2014).

Maximum likelihood phylogenetic analysis of the sequence alignment was performed using IQ-Tree (Nguyen *et al.*, 2015) with 10,000 replications of ultrafast bootstrap on the CIPRES Science Gateway (Miller *et al.*, 2012). The JTT+F+R10 model was selected as the best-fit amino acid substitution model according to Bayesian Information Criterion for the phylogenetic analysis of ELF3 in green plants. The JTT+R3 model was selected for the phylogenetic analysis of identified Brassicales ELF3. All identified ELF3 and EEC sequences were subjected to PLAAC (Lancaster *et al.*, 2014) to identify probable PrD regions with a default minimum domain length of 60. For each sequence, the COREscore and Log-likelihood ratio (LLR, without a hard cut-off compared to COREscore) were retrieved to represent prion-like properties.

For *A. thaliana* accessions, after removing the stop codon (as well as the sequence after a premature stop codon in one accession, ID: 9089), the corrected *ELF3* coding sequences from all 319 accessions were aligned and phylogenetic analysis was performed as described above. The MG+F3X4 model was selected as the best-fit codon model.

2.4.2 Population genetic analysis

Sequence polymorphism (π / π s), nucleotide diversity (π), and Tajima's D (Tajima, 1989) of *ELF3* were calculated among 319 Arabidopsis accessions, as well as sequence divergence (Ka/Ks) of *ELF3* between Arabidopsis and other Brassicaceae, using sliding window analyses (width: 30, step: 3) in DnaSP v6 (Rozas *et al.*, 2017). The *ELF3* sequences of nine Brassicaceae (*A. lyrata*, *A. halleri*, *B. oleracea var. capitata*, *B. stricta*, *C. hispanica*, *C. rubella*, *D. sophioides*, *E. salsugineum*, *T. arvense*) were used as an interspecific group for Ka/Ks analysis.

2.4.3 Growth curve modeling

For the *H. vulgare* temperature assay in growth chambers, growth curves were modeled for all traits which were obtained on successive days, as cubic splines in SAS PROC TRANSREG (SAS Institute, Inc., Cary, USA) with nknots set to 1. Based on the predicted

values the following parameters were derived for each line: maximum increase (difference between two consecutive days), day of maximum increase, maximum value, day of maximum value, end point value, and total area under the curve (based on the trapezoidal rule with trapezoids defined between each two consecutive days).

2.4.4 Principal component analysis (PCA)

PCA was performed with SAS PROC PRINCOMP (SAS Institute, Inc., Cary, USA) based on the arithmetic means of all obtained traits from *H. vulgare* temperature assay in growth chambers, or the derived growth curve modeling traits, for each line. Due to the different units and scales of the traits, the PCA was based on the correlation matrix.

2.4.5 Pairwise correlation analysis

For *H. vulgare* temperature assays in growth chambers and in greenhouses, pairwise correlation coefficients were determined for Bowman, *elf3*^{BW290}, and HIF pair 10_190 between all investigated traits obtained from both growth and development, and yield component experiments. As for PCA, correlations across all lines were based on arithmetic means, as well as the derived growth curve modeling traits. All Pearson correlation coefficients and their *P* values were computed using SAS PROC CORR (SAS Institute, Inc., Cary, USA).

2.4.6 Statistical analysis and data visualization

Unless stated otherwise, statistical analysis was performed in R (R Core Team, 2013) and data visualization was based on the ggplot2 package (Wickham *et al.*, 2016).

For the evolution of *ELF3*: sequence alignment was visualized in Jalview (Waterhouse *et al.*, 2009); phylogenetic trees were visualized and annotated in iTOL (Letunic and Bork, 2007); geographic distribution of *A. thaliana* accessions was mapped using the geodata (Hijmans *et al.*, 2022) and ggrepel (Slowikowski *et al.*, 2018) packages; distributions and Pearson correlations of polyQ length and phenotypic data were computed and visualized using the ggpubr (Kassambara, 2020) and plot3D (Soetaert, 2021) packages.

For *A. thaliana* physiological assays, hypocotyl length data were analyzed by two-way ANOVA, whereas growth rate, RAE, and RT-qPCR data were analyzed by one-way ANOVA and followed by Tukey's HSD *post hoc* test. The effect of the temperature pulse in the gating assay was analyzed by a two-sided Student's *t*-test using GraphPad QuickCalcs

(<http://graphpad.com/quickcalcs/>). Different cycling conditions were shaded in the plot using the package `ggpattern` (FC and Davis, 2022).

For *H. vulgare* physiological assays, significant differences between temperature treatments and genotypes were analyzed by two-way ANOVA followed by Tukey's HSD *post hoc* test. The genomic setup of HIF pairs was visualized using the `chromoMap` package (Anand and Rodriguez Lopez, 2022). The package `ggbeeswarm` (Clarke and Sherrill-Mix, 2017) was used for distribution of biological replicates in the boxplots, arranged without overlapping. Correlation between measured and extracted values was calculated and plotted using the `ggpmisc` package (Aphalo *et al.*, 2022). The results of PCA and pairwise correlation analysis were visualized using the `ggrepel` (Slowikowski *et al.*, 2018) and `corrplot` (Wei *et al.*, 2017) packages.

3 Results I – Emergence and evolution of *ELF3* and its prion-like domain

A recent study revealed that a prion-like domain (PrD) in Arabidopsis EARLY FLOWERING 3 (*ELF3*) functions as a thermosensor, which is required for the phase separation of *ELF3* in response to temperature changes (Jung *et al.*, 2020). However, as *ELF3* from the model grass *Brachypodium distachyon* lacks a PrD and temperature responsive aggregation, it is unknown whether and how the PrD is conserved in *ELF3* across the plant kingdom. This chapter aims to trace the evolutionary emergence of *ELF3* and its duplicate gene *ESSENCE OF ELF3 CONSENSUS (EEC)* with a focus on PrD existence. Furthermore, the length variation of polyglutamine (polyQ) within the *ELF3*-PrD was investigated among Arabidopsis natural accessions, as well as its correlation with temperature responsive hypocotyl elongation.

3.1 Evolutionary origins of *ELF3/EEC* and PrD

In the model plant Arabidopsis, the major functions of *ELF3* in circadian clock regulation require the evening complex (EC) with the involvement of *ELF4* and *LUX* (Nusinow *et al.*, 2011; Ezer *et al.*, 2017). Previous studies revealed *ELF3* homologue in the charophyte *Klebsormidium nitens*, whereas potential homologues of *ELF4* and *LUX* were identified even in chlorophytes like *Chlamydomonas reinhardtii* (Linde *et al.*, 2017). To obtain a general picture about the evolution of *ELF3* and its similar duplicate *EEC* across the plant kingdom, the copy number of the EC members *ELF3*, *ELF4*, and *LUX*, as well as *EEC* was determined in 42 plant species ranging from unicellular green algae to flowering plants (Table 1). An *ELF3* homologue was identified in the charophyte *Chara braunii*, confirming the origin of *ELF3* in charophyta. However, in contrast to previous reports (Linde *et al.*, 2017), no *ELF4* and only one *LUX* homologue was identified in *Chlamydomonas reinhardtii*, and four *ELF3* homologues were identified in *Physcomitrium patens* (Table 1). Interestingly, in contrast to the identification of the EC components back to the charophytes, the *EEC* homologues were only detected in the eudicots (Table 1). These data suggest that a duplication event in the last common ancestor of the eudicots gave rise to *EEC* in this lineage.

Table 1 Gene homologues of the evening complex and *EEC* in various plant genomes.

	Species	Orders	ELF3	EEC	ELF4	LUX
Chlorophyte	<i>Chlamydomonas reinhardtii</i>	Chlamydomonadales	0	0	0	1
	<i>Chara braunii</i>	Charales	1	0	1	1
	<i>Klebsormidium nitens</i>	Klebsormidiales	1	0	2	1
Charophyte	<i>Mesotaenium endlicherianum</i>	Zygnematales	1	0	2	1
	<i>Penium margaritaceum</i>	Desmidiaceae	1	0	4	1
	<i>Spirogloea muscicola</i>	Spirogloeeales	1	0	3	1
Bryophyte	<i>Physcomitrium patens</i>	Funariales	4	0	1	4
	<i>Marchantia polymorpha</i>	Marchantiales	1	0	1	1
Lycophyte	<i>Selaginella moellendorffii</i>	Selaginellales	2	0	4	1
Fern	<i>Ceratopteris richardii</i>	Polypodiales	4	0	8	6
Gymnosperm	<i>Ginkgo biloba</i>	Ginkgoales	3	0	2	1†
Angiosperm	<i>Amborella trichopoda</i>	Amborellales	1	0	2	1
	<i>Musa acuminata</i>	Zingiberales	4	0	5	3
	<i>Brachypodium distachyon</i>	Poales	1	0	3	1
Monocot	<i>Dioscorea cayenensis</i>	Dioscoreales	2*	0	2	1
	<i>Hordeum vulgare</i>	Poales	1	0	2	1
	<i>Oryza sativa</i>	Poales	2	0	3	1
	<i>Panicum hallii</i> var. <i>hallii</i>	Poales	2	0	3	1
	<i>Setaria italica</i>	Poales	2	0	2	1
	<i>Triticum aestivum</i>	Poales	1	0	6	3
	<i>Zea mays</i>	Poales	2	0	3	2
	<i>Beta vulgaris</i>	Caryophyllales	1	0	3	2
	<i>Daucus carota</i>	Apiales	1	0	4	3
	<i>Helianthus annuus</i>	Asterales	2	1	10	7
Eudicot	<i>Arabidopsis halleri</i>	Brassicales	1	1	5	2
	<i>Arabidopsis lyrata</i>	Brassicales	1	1	5	2
	<i>Arabidopsis thaliana</i>	Brassicales	1	1	5	2
	<i>Brassica oleracea</i>	Brassicales	2	3	13	2
	<i>Cucumis sativus</i>	Cucurbitales	1	1	3	2
	<i>Manihot esculenta</i>	Malpighiales	1	1	6	2
	<i>Glycine max</i>	Fabales	2	1	8	2
	<i>Lupinus angustifolius</i>	Fabales	2*	1*	7	2
	<i>Medicago truncatula</i>	Fabales	2	1	4	1
	<i>Phaseolus vulgaris</i>	Fabales	1	1	6	1
	<i>Vigna angularis</i>	Fabales	2*	1*	6	1
	<i>Gossypium raimondii</i>	Malvales	1	3	12	3
	<i>Theobroma cacao</i>	Malvales	1	1	4	1
	<i>Prunus persica</i>	Rosales	1	1	3	1
	<i>Populus trichocarpa</i>	Malpighiales	1	1	7	2
<i>Solanum lycopersicum</i>	Solanales	3	1	7	2	
<i>Solanum tuberosum</i>	Solanales	3	1	7	2	
<i>Vitis vinifera</i>	Vitales	1	1	4	1	

* In different species of the same genus

† Potential homologue

To trace the evolution and divergence of *ELF3* and *EEC* in more detail, the homologues of *ELF3* and *EEC* were identified from 274 plant genomes and the phylogenetic relationships among them were reconstructed. The sequences from similar angiosperm groups (e.g., basal angiosperms, monocots, eudicots, core eudicots) mostly clustered together in the phylogenetic tree (Fig. 3-1). As expected, *Arabidopsis* *ELF3* and *EEC* were separated into two different clades, with only core eudicot species included. In orders such as Buxales, Trochodendrales, Proteales, and Ranunculales, which are eudicots but not core eudicots, only *ELF3* homologues were detected and positioned in a clade with basal angiosperm and monocot *ELF3*s. Interestingly, this clade is more closely related to the *EEC* clade than to the *ELF3* clade from core eudicots. In addition, more genetic changes might have occurred in Brassicales and Saxifragales *EEC* as indicated by branch lengths (Fig. 3-1).

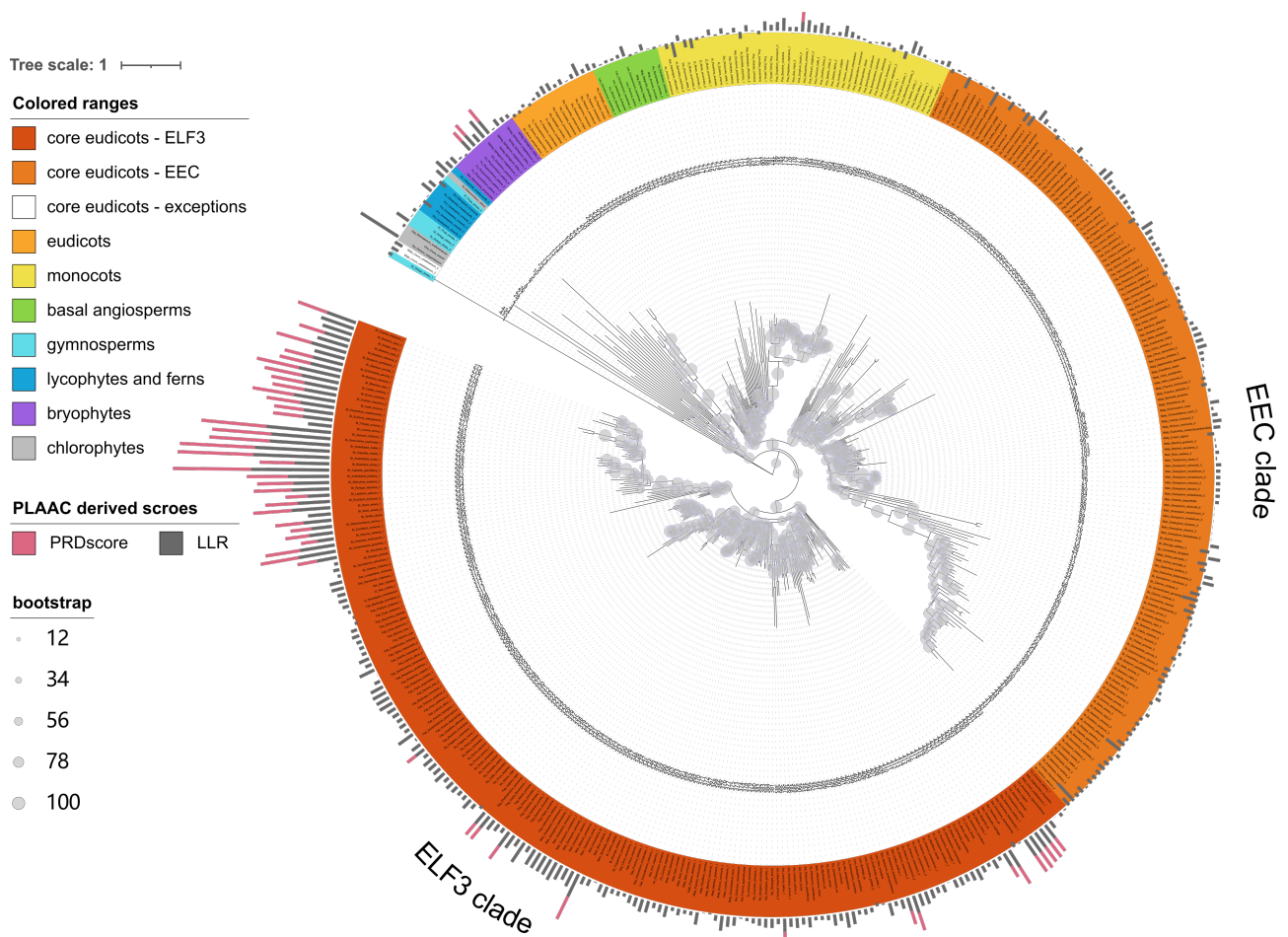


Fig. 3-1 Phylogenetic tree of *ELF3* and *EEC*.

The tree was constructed with the full-length protein sequences obtained from 274 plant genomes, using maximum likelihood IQ-Tree JTT+F+R10 model with 10,000 replications of ultrafast bootstrap (shown as circles). The *ELF3* and *EEC* clades are marked based on the position of *Arabidopsis* *ELF3* and *EEC*, respectively. The labels are colored according to

species group and clade. PLAAC derived scores are shown as stacked bar charts outside of the tree. Leaf names and scores are listed corresponding to the branch ID in Appendix IV.

Arabidopsis ELF3 is known to harbor a prion-like domain (PrD) which mediates the phase separation of ELF3 in response to temperature changes (Jung *et al.*, 2020). I next asked whether the PrD is conserved in identified ELF3/EEC homologues and analyzed all sequences using PLAAC and obtained COREscore and LLR: both scores indicate the probability to have prion subsequences with LLR not imposing a hard cutoff (Lancaster *et al.*, 2014). For instance, the PrD of *Arabidopsis* ELF3 was predicted to contain two subsequence regions and the overall COREscore and LLR are both 31.534 (Figs. 3-1, 3-2). When considering the hard cutoff, COREscore based PrD prediction mainly identified ELF3 sequences from core eudicots (Fig. 3-1). Besides that, ELF3 homologues in the moss *Physcomitrium patens* and *Sphagnum fallax*, as well as the monocot *Sorghum bicolor* were predicted to have a PrD with relatively low but positive COREscore. The highest scores were detected in Brassicales ELF3, with several species (*Capsella grandiflora*: 59.885, *Arabidopsis lyrata*: 58.268, *Capsella rubella*: 57.518, *Alyssum linifolium*: 49.964, *Arabidopsis halleri*: 46.358, *Descurainia sophioides*: 45.537, *Brassica rapa*: 32.622, and *Isatis tinctoria*: 32.092) displaying an even higher score than *Arabidopsis*, suggesting potentially conserved temperature sensing functions of PrD. Moreover, although four highly conserved regions were identified between ELF3 and EEC, the PrD region diverged between EEC and ELF3 of monocots compared to ELF3 in core eudicots. Notably, none of the sequences in the EEC clade was predicted to have a PrD (Figs. 3-1, 3-2). These data suggest the emergence of PrD in Brassicales ELF3.

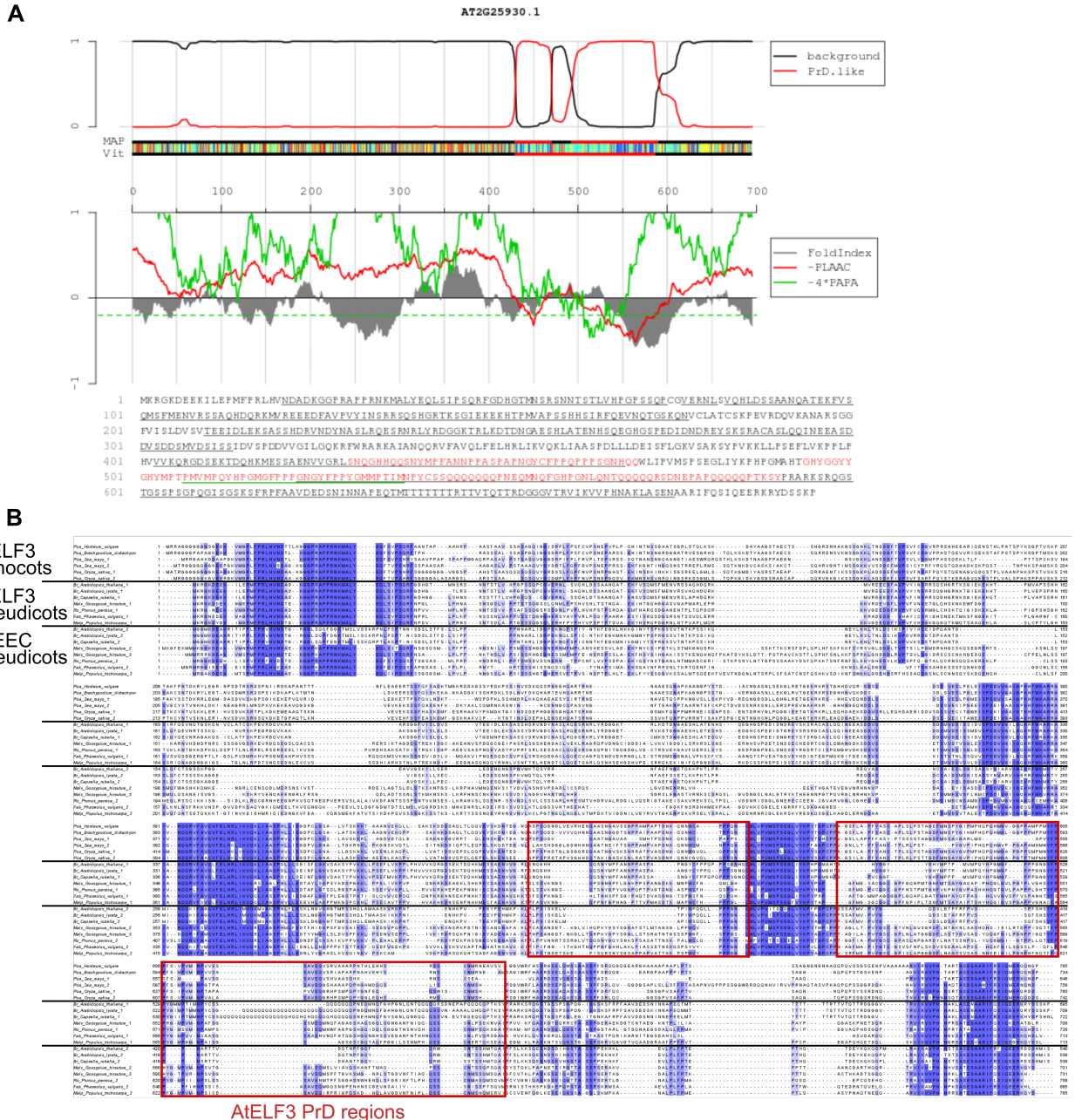


Fig. 3-2 Arabidopsis ELF3 PrD and conserved regions of ELF3 and EEC.

(A) PLAAC analysis of Arabidopsis ELF3 with a default minimum domain length of 60. (B) Multiple sequence alignment of ELF3/EEC homologues in monocots *Hordeum vulgare*, *Brachypodium distachyon*, *Zea mays*, *Oryza sativa*, and core eudicots *Arabidopsis thaliana*, *Arabidopsis lyrata*, *Capsella rubella*, *Gossypium hirsutum*, *Prunus persica*, *Phaselous vulgaris*, and *Populus trichocarpa*. Red rectangles indicate Arabidopsis ELF3 PrD regions as predicted in (A).

3.2 PolyQ length contributes to PrD of ELF3 in Brassicales

As the prediction of PrD was mainly restricted to ELF3 from Brassicales species, I investigated whether the potential PrDs of these species are conserved at the sequence level. I constructed a phylogenetic tree with identified Brassicales ELF3 only, separating different families (Fig. 3-3). As features of PrD (Harrison and Gerstein, 2003), we observed a considerable proportion of asparagine (N) and glutamine (Q) in the sequence alignment of part of predicted PrD regions (Fig. 3-3). Interestingly, Brassicaceae species displayed a polyglutamine (polyQ) stretch with different length, which was related to the PrD COREscore (Figs. 3-1, 3-3). For example, *Capsella grandiflora* with the highest COREscore (59.885) also displayed the longest polyQ stretch (33Q). It is important to note that the Arabidopsis accession used here was Col-0 with 7Q in the ELF3 polyQ stretch, whereas other species with longer polyQ all displayed a higher PrD COREscore compared to Arabidopsis. Since Arabidopsis accessions are known to vary in ELF3 polyQ length (Tajima *et al.*, 2007; Undurraga *et al.*, 2012), this might also be the case for the natural accessions in other Brassicales, which cannot be addressed in this phylogenetic tree. Nevertheless, these data suggest that ELF3 PrD is mainly contributed by polyQ length observed in the family Brassicaceae.

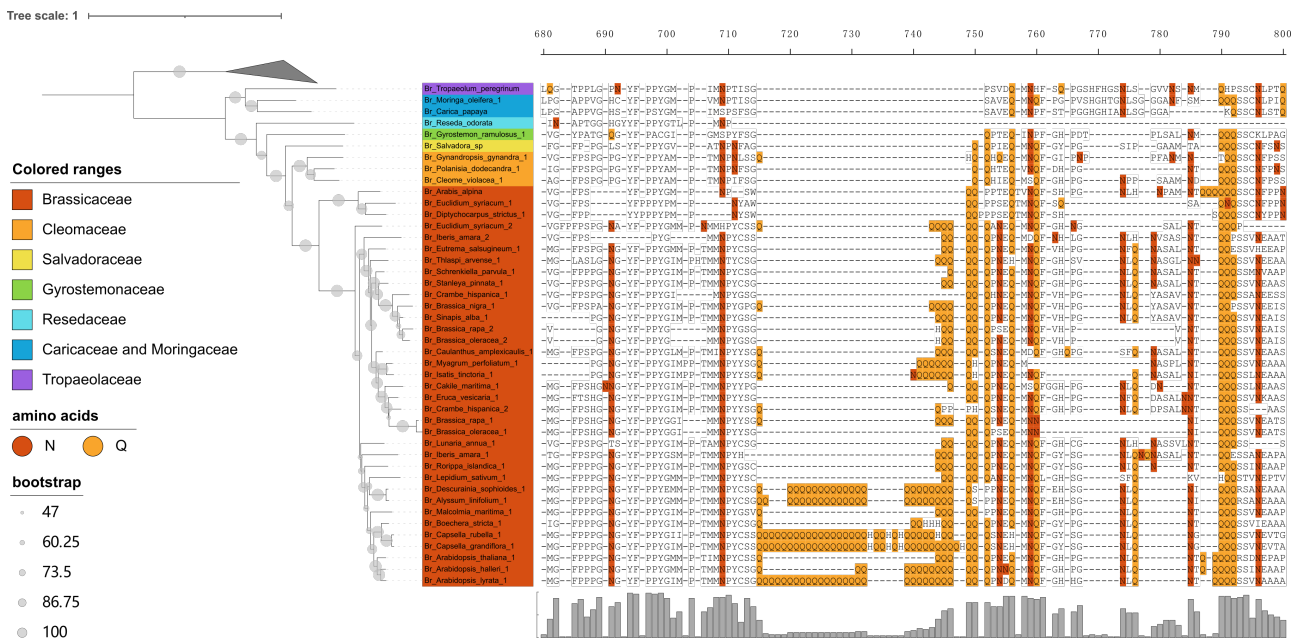


Fig. 3-3 Phylogenetic tree and sequence alignment of Brassicales ELF3.

The tree was constructed with the full-length protein sequences using maximum likelihood IQ-Tree JTT+R3 model with 10,000 replications of ultrafast bootstrap (shown as circles). Eight Poales species were used for rooting and collapsed. The labels are colored according

to the species family. The multiple sequence alignment represents polyQ regions in the PrD, with a frequency plot indicating sequence identity below the alignment. Amino acid asparagine (N) and glutamine (Q) are colored within the alignment.

3.3 ELF3 polyQ variation among Arabidopsis accessions

Although data are lacking from most Brassicaceae species, natural variation of ELF3 polyQ length has been investigated in several collections of Arabidopsis accessions (Tajima *et al.*, 2007; Undurraga *et al.*, 2012). The 1001 genomes provide polymorphism information in *ELF3*, whereas polyQ length cannot be identified due to unknown nucleotides in the region, probably caused by common problems of Illumina sequencing approaches in highly repetitive regions. Therefore, I first sequenced the corresponding *ELF3* region and corrected polyQ lengths in 204 Arabidopsis accessions from the 1001 genomes collection. Together with previously reported polyQ lengths in 115 accessions, PrD/polyQ sequence information in a total of 319 Arabidopsis accessions was obtained for further analyses (Tajima *et al.*, 2007; Undurraga *et al.*, 2012) (Fig. 3-4A).

Among the 319 Arabidopsis accessions, polyQ length in ELF3 displayed a normal distribution with 16Q being most frequent, although 15Q and 17Q were rather rare (Fig. 3-4B). The polyQ length ranged from 7Q to 29Q with a slightly skewed distribution towards <16Q. These data suggest that PrDs are conserved across Arabidopsis accessions, as it was originally discovered in Col-0 with the shortest polyQ length 7Q (Jung *et al.*, 2020).

To test whether the polyQ length is associated with geographic origin of the corresponding accessions, I plotted all obtained accessions on a map with the focus of Europe regions (where the most accessions were collected) (Fig. 3-4C). I could not detect special distribution patterns of ELF3 polyQ length, as the accessions collected from close sites can have varying polyQ length. For instance, the ELF3 polyQ length in accessions collected from south Sweden ranged from 9Q to 21Q. Two accessions with 26Q from Spain (ID: 9584) and Central Europe (ID: 7520) were both mixed with accessions with relatively short polyQ stretches in ELF3 (Fig. 3-4C). However, on a world map, several accessions with long polyQ stretches in ELF3 were detected in non-European regions (Fig. 3-5A). For example, all four accessions from Azerbaijan had 22-23Q (ID: 9069, 9070, 9089, and 9091), one accession carrying the longest polyQ was from Pakistan (29Q, ID: 8424), and one with 27Q was from Japan (ID: 7207) (Fig. 3-5A).

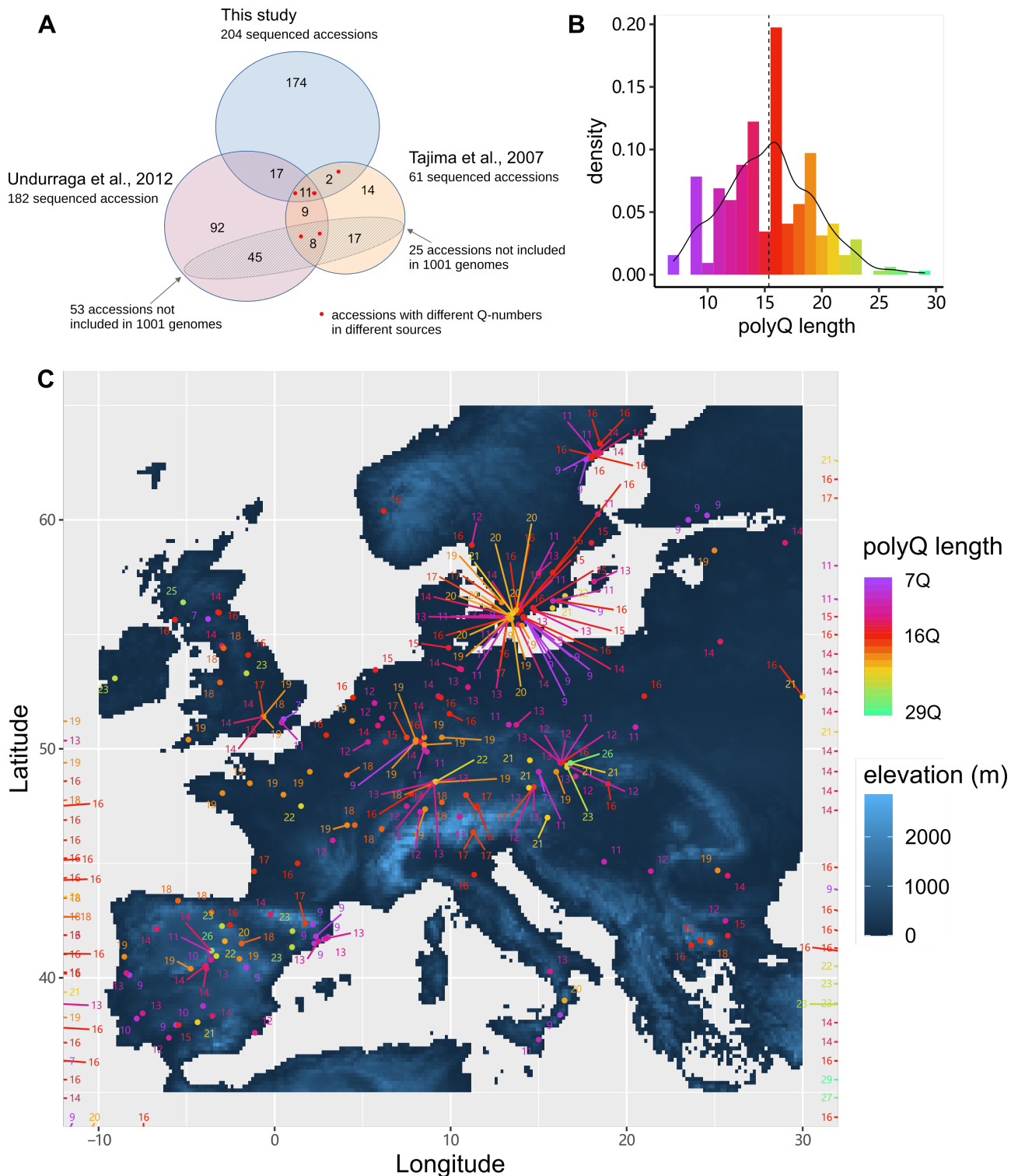


Fig. 3-4 Natural variation of ELF3 polyQ length in Arabidopsis accessions.

(A) An overview of Arabidopsis accessions with known ELF3 polyQ length. In total, 319 accessions included in the 1001 genomes collection were used in this study. (B) Density plot represents the distribution of ELF3 polyQ length from Arabidopsis accessions used in this study. The dashed line represents the mean polyQ length. (C) Geographic distribution of Arabidopsis accessions mapped with corresponding polyQ length and elevation information in Europe. The accession ID, name, and polyQ length are listed in Appendix I.

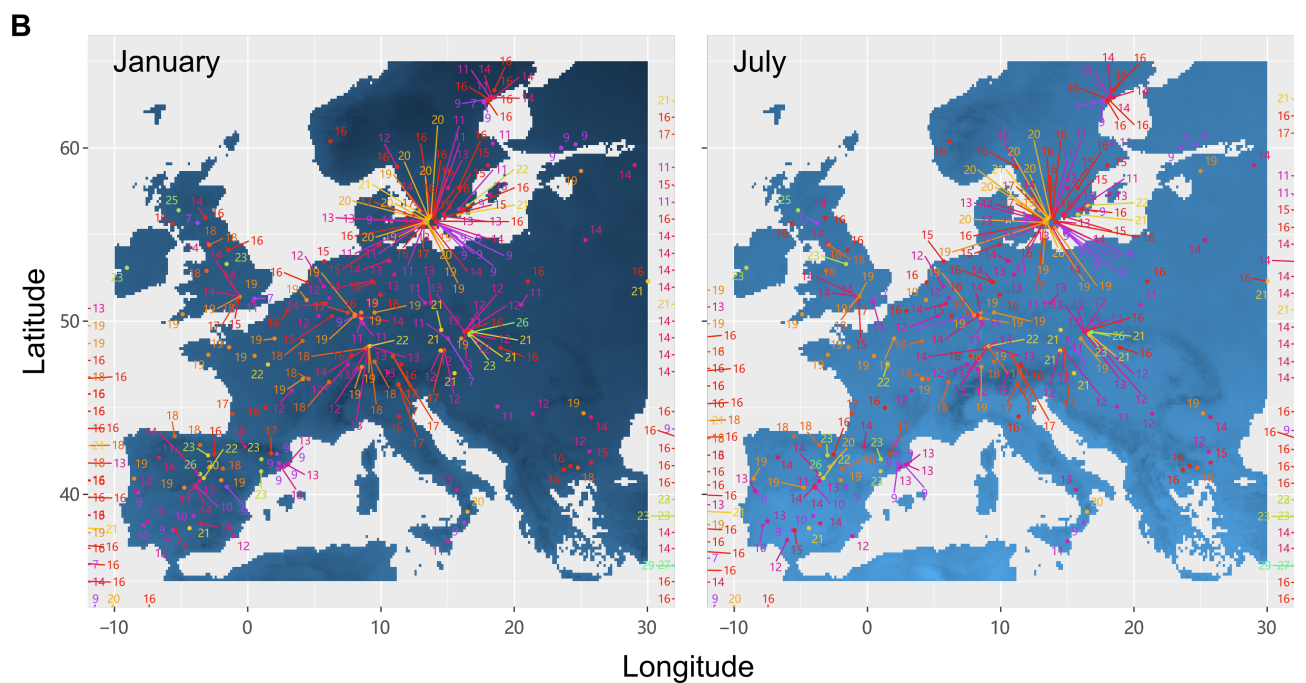
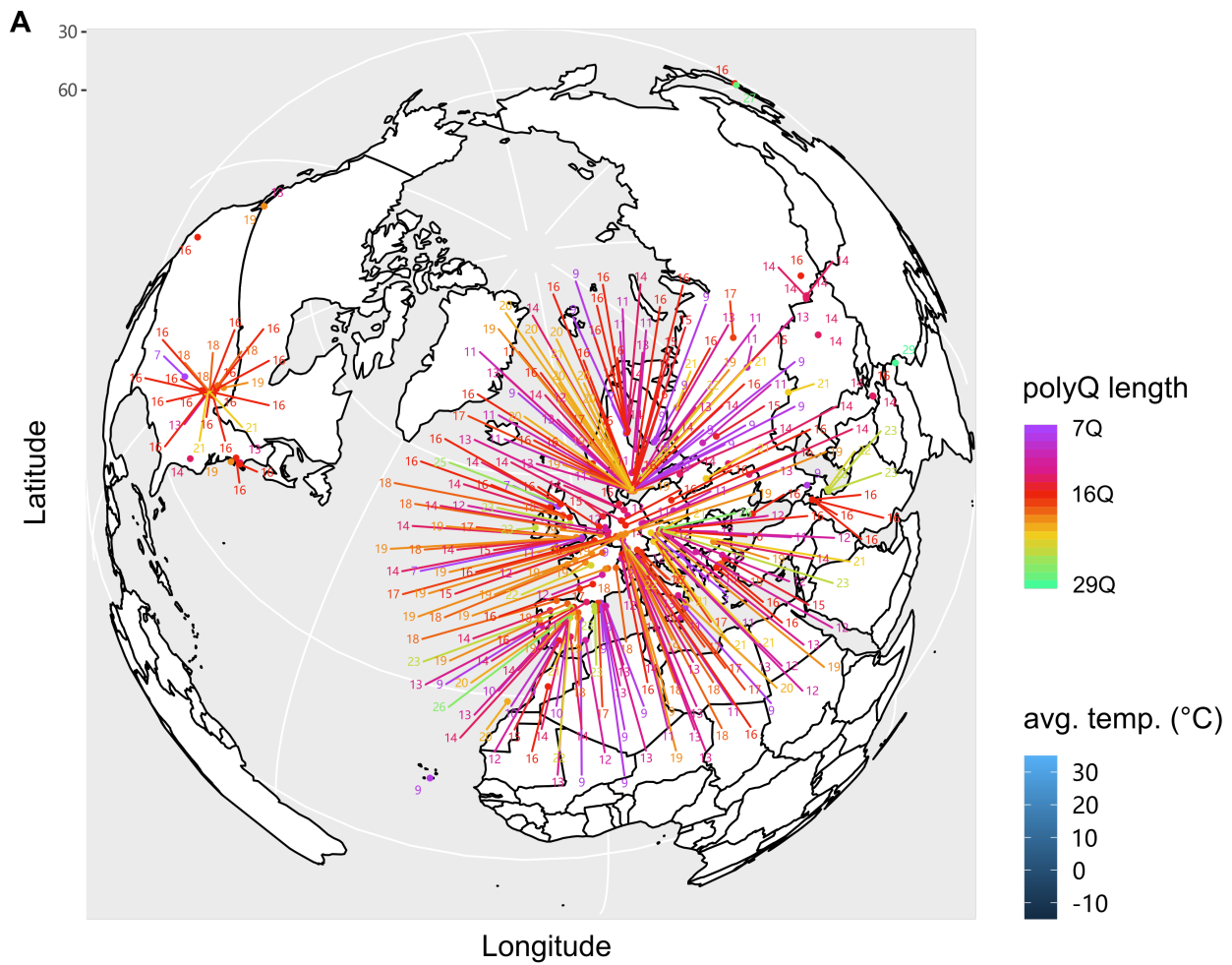


Fig. 3-5 Geographic distribution of ELF3 polyQ variation in *Arabidopsis* accessions.

(A) *Arabidopsis* accessions were plotted on a world map with corresponding polyQ length.
 (B) Association of ELF3 polyQ variation and average temperatures (historical climate data:

January and July, 1970-2000) in Europe. The accession ID, name, and polyQ length are listed in Appendix I.

In general, I could not detect potential associations of polyQ length with geographic or available climatic data of the local regions, for instance elevation (Fig. 3-4C) or average temperatures in January and July, respectively (Fig. 3-5B). On this basis, these data suggest that the polyQ variation in *ELF3* is not likely to be an evolutionary adaptation to different environments, which needs to be validated by quantitative analyses.

3.4 Evolution of Arabidopsis *ELF3* and polyQ

To further investigate whether polyQ variation confers any adaptive capabilities, I first tested whether Arabidopsis *ELF3* is under any directional selection pressure. I performed sliding window analyses for sequence polymorphism (π _a/ π _s) based on the full-length coding sequence of *ELF3* in 319 Arabidopsis accessions, as well as sequence divergence (Ka/Ks) analyses using nine Brassicaceae *ELF3* as an interspecific group. Across the coding region of *ELF3*, I observed few π _a/ π _s and Ka/Ks peaks (>1) with one Ka/Ks peak within the PrD region, indicating that these sites may be under positive selective pressure (Fig. 3-6A). The highest peak of both π _a/ π _s and Ka/Ks was detected at the same site. However, this could be explained by a relatively low synonymous substitution rate (Ks) at the site, as the overall nonsynonymous substitution rate (Ka) and nucleotide diversity (π) were very low in *ELF3* (Fig. 3-6A, B). The latter suggests that apart from the polyQ variation, *ELF3* is highly conserved among Arabidopsis accessions. And indeed, mostly null, or negative values of Tajima's D were detected across the coding region with an overall value of -2.45 ($P < 0.001$) (Fig. 3-6C). The negative Tajima's D indicates that Arabidopsis *ELF3* might have experienced a recent selective sweep.

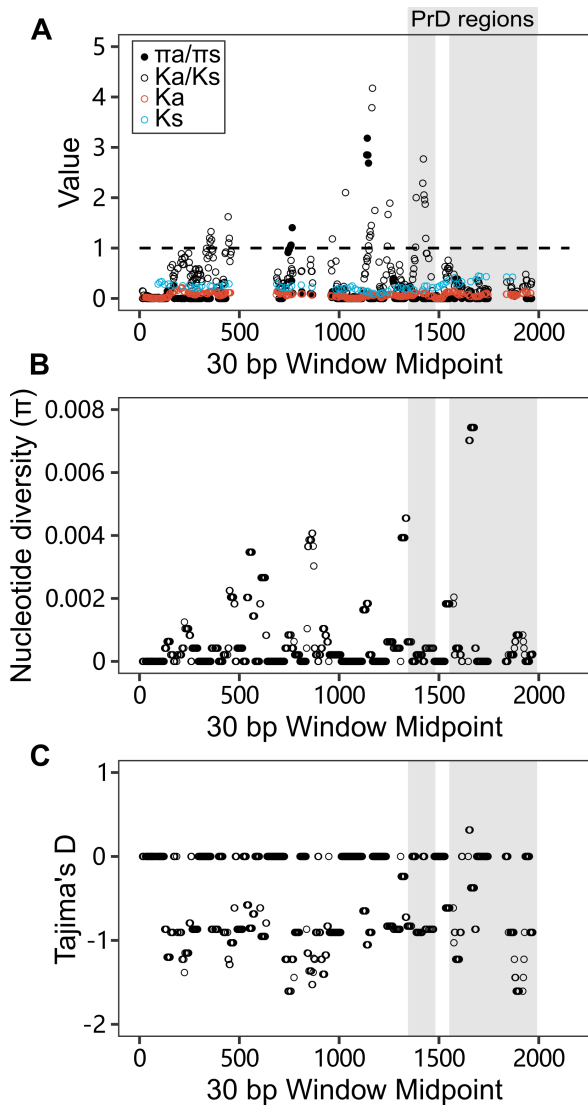


Fig. 3-6 Population genetic signatures of Arabidopsis *ELF3*.

(A-C) Sequence polymorphism and divergence (A), nucleotide diversity (B), and Tajima's D (C) of full-length *ELF3* were calculated from 319 Arabidopsis accessions using sliding window analyses (width: 30, step: 3). The *ELF3* sequences of nine Brassicaceae species (*A. lyrata*, *A. halleri*, *B. oleracea* var. *capitata*, *B. stricta*, *C. hispanica*, *C. rubella*, *D. sophioides*, *E. salsugineum*, *T. arvense*) were used as an interspecific group for Ka/Ks analysis. Shaded regions represent the predicted PrD, based on the sequence alignment using Arabidopsis *ELF3*.

Although only limited sequence variation was detected in *ELF3*, I next asked whether it is associated with polyQ variation. I constructed a phylogenetic tree with full-length coding sequence of *ELF3* from all 319 Arabidopsis accessions. After collapsing the identical sequences, I connected the leaves/nodes which displayed the same polyQ variation (Fig. 3-7). As connections largely crossed over the phylogenetic tree, the phylogeny of *ELF3* is not likely to be influenced by polyQ variation. These data suggest that even if polyQ variation might be of evolutionary relevance, it is not the driving force of *ELF3* evolution.

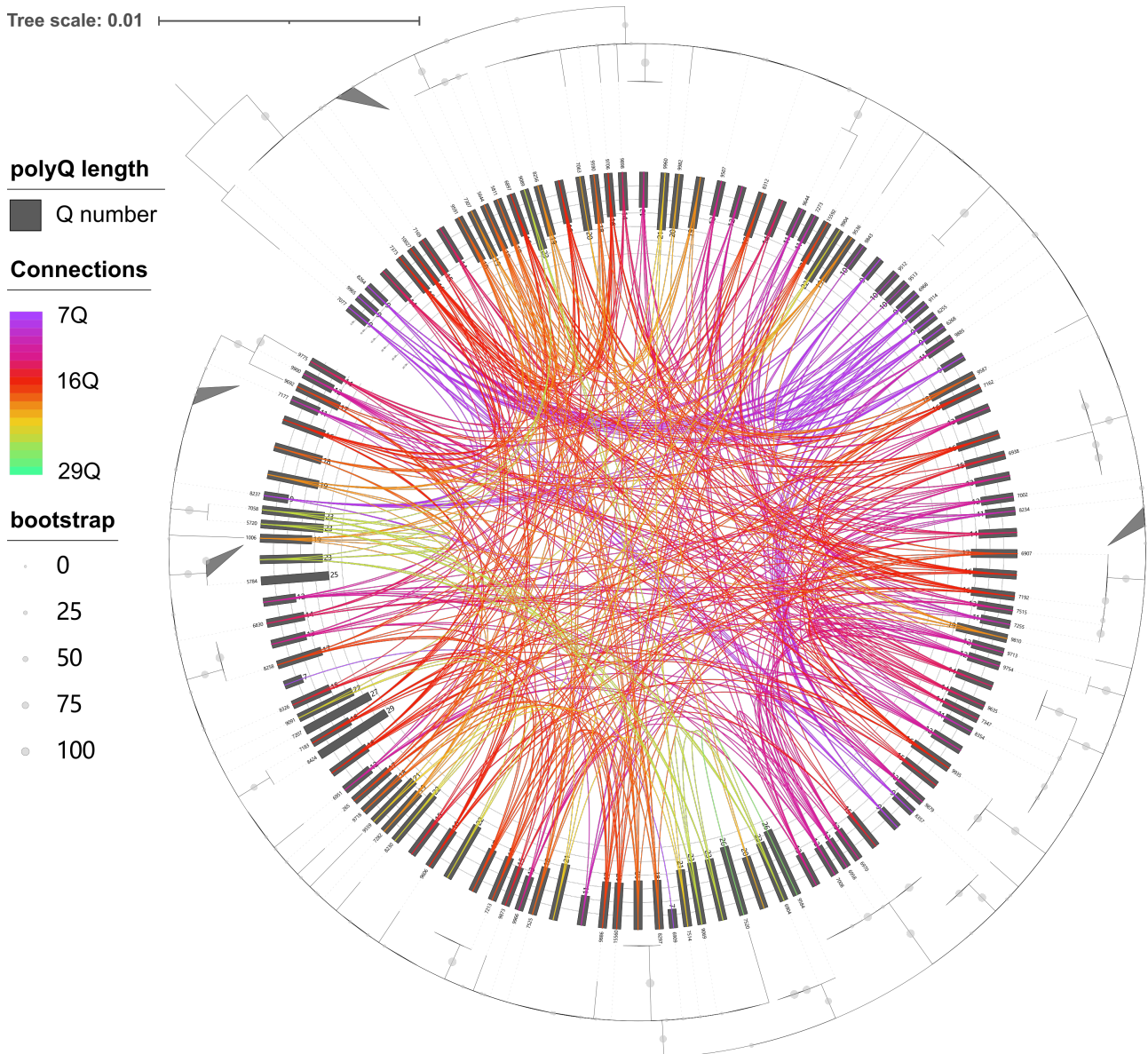


Fig. 3-7 Genetic variation of *ELF3* in Arabidopsis accessions.

The phylogenetic tree was constructed with the full-length coding sequences (without stop codon) obtained from 319 Arabidopsis accessions, using maximum likelihood IQ-Tree MGF3X4 model with 10,000 replications of ultrafast bootstrap (shown as circles). Identical sequences are collapsed and those with the same polyQ length are connected. The length of polyQ is shown as bar charts inside of the tree. The accession ID, name, and polyQ length are listed in Appendix I.

3.5 Association of polyQ variation and temperature responsive hypocotyl elongation

As a multifunctional protein, ELF3 plays prominent roles in circadian clock regulation and thermomorphogenesis. Previous studies reported significant correlation of ELF3 polyQ length with circadian rhythm parameters in natural *Arabidopsis* accessions (Tajima *et al.*, 2007) as well as transgenic lines (Undurraga *et al.*, 2012). However, such associations seemed to be more complicated or weaker regarding growth and developmental phenotypes at normal or elevated temperatures, which might depend on the genetic background of the transgenic lines (Undurraga *et al.*, 2012; Press *et al.*, 2016).

To further investigate potential associations between ELF3 polyQ variation and temperature responsive phenotypes in natural *Arabidopsis* accessions, growth assays were performed under normal (20°C) and elevated (28°C shift) temperatures. Hypocotyl length was measured as a classic phenotype to represent temperature responsiveness. For the growth assays, 253 accessions were selected as a subset of the previously described 319 accessions with similar distribution of polyQ variation (Figs. 3-4A, 3-8A). Relative hypocotyl length displayed more divergence after a temperature shift to 28°C compared to those kept at 20°C, however, no correlation was detected between polyQ length and relative hypocotyl length at either 20°C or 28°C (Fig. 3-8B). I then calculated the temperature response of hypocotyl elongation, and again no correlation with polyQ length was detected (Fig. 3-8C). Similarly, no association could be detected using a three-dimensional visualization of polyQ length, relative hypocotyl length at 20°C and 28°C (Figs. 3-8C, 3-9).

Therefore, these data suggest that ELF3 polyQ variation is not likely to be associated with temperature responsive hypocotyl elongation in natural *Arabidopsis* accessions. Consistently, previous reports using transgenic lines from two different genetic backgrounds could barely detect any associations of ELF3 polyQ length with temperature responsive phenotypes (Press *et al.*, 2016; Jung *et al.*, 2020). This indicates that the effects of polyQ length, if any, are not prominent and are very likely to be masked by the genetic backgrounds.

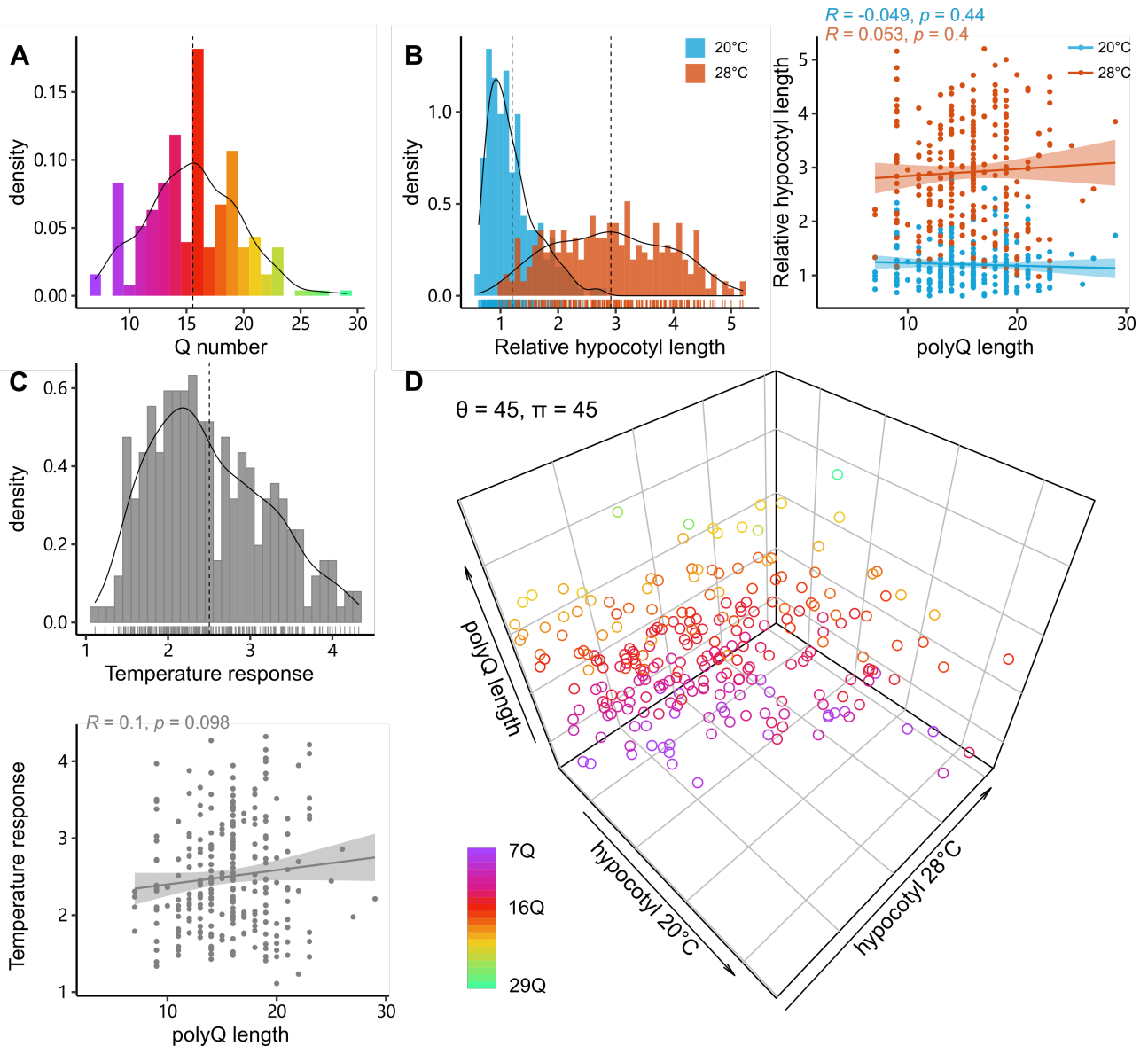


Fig. 3-8 Association of ELF3 polyQ variation with hypocotyl phenotypes.

(A) Distribution of polyQ length in 253 *Arabidopsis* accessions used for growth assays. (B, C) Distribution of relative hypocotyl length at 20°C or after a temperature shift to 28°C (B), temperature response (C), and their correlation with polyQ variation. Relative hypocotyl length represents the normalization of absolute hypocotyl length to median value of Col-0 at 20°C of each experiment. Vertical dashed lines in the density plots of (A) and (B) represent mean values. Arithmetic means of each accession shown as rugs below the distributions were used for distribution and Pearson correlation analysis. (D) Three-dimensional (3D) visualization of potential association among polyQ length, and relative hypocotyl length at 20°C and 28°C. θ and π represent the rotation angles of the 3D plot. The 3D plot can be visualized from four other directions in Fig. 3-9.

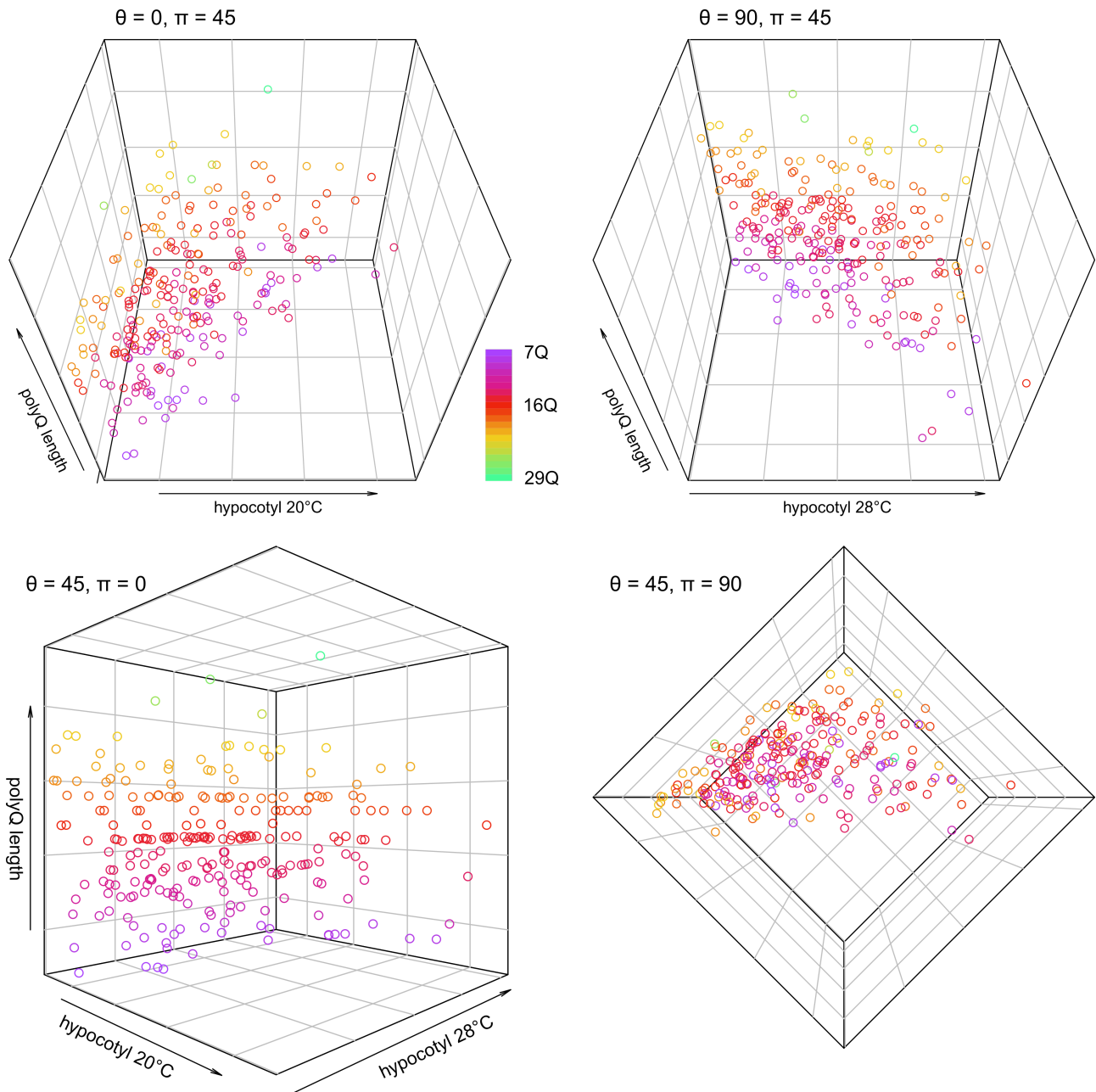


Fig. 3-9 Visualization of potential polyQ-phenotype association.

Four-direction 3D visualization of potential association among polyQ length and relative hypocotyl length at 20°C and 28°C. θ and π represent the rotation angles of the plot.

In conclusion, based on phylogenetic analyses using available plant genomes, the PrD emerged in Brassicales ELF3 (Fig. 3-1). Its functions in ELF3 temperature responsive aggregation are therefore not expected to be conserved in the other species. In addition, the ELF3 homologue EEC, whose function remains unknown, emerged as a duplication of ELF3 in core eudicots. Importantly, EEC lacks a predicted PrD (Figs. 3-1, 3-2). Sequence alignment of Brassicales ELF3 orthologues revealed that the PrD is mainly contributed by

long polyQ which is restricted to species in the Brassicaceae family (Fig. 3-3). The 1001 genomes collection provides a population of natural *Arabidopsis* accessions to study the potential evolution of *ELF3* and polyQ. Although extensive variation in polyQ length was observed in 319 accessions, it is independent of the sequence variation outside the PrD region in *ELF3* (Fig. 3-7). Population genomics suggest that, except for the polyQ stretch, *ELF3* coding sequence is highly conserved, probably under negative selection pressure (Fig. 3-6). Furthermore, I found no evidence that polyQ variation is associated with geographic or climatic conditions at the original collection sites of the corresponding *Arabidopsis* accessions, or temperature responsive hypocotyl length (Figs. 3-4, 3-5). Nevertheless, I cannot rule out the potential effects of few accessions with extreme polyQ length, as such effects might be masked in correlation analyses by the vast majority of accessions with moderate polyQ length in this study. It is worth further studying these accessions to understand the evolutionary meaning of polyQ variation.

4 Results II – Arabidopsis *ELF3* controls temperature responsiveness of the circadian clock independently of the evening complex¹

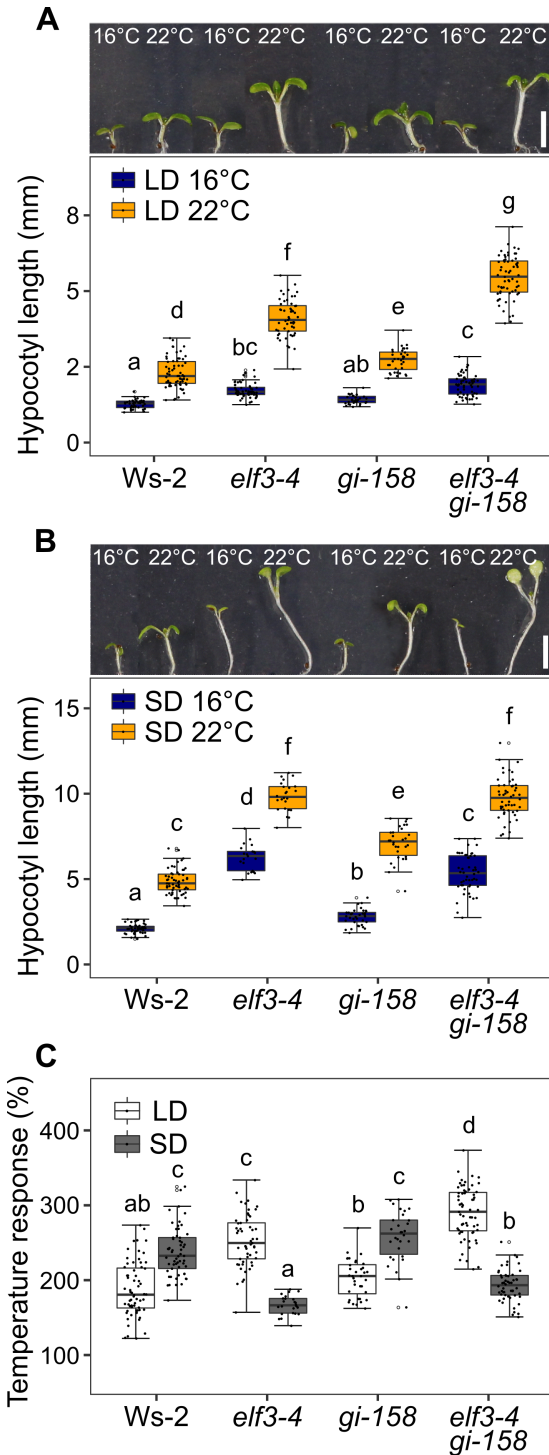
In Arabidopsis, *ELF3* is not only involved in thermomorphogenesis with its thermosensory PrD, but also functions as light Zeitnehmer together with *GIGANTEA* (*GI*). As outlined in the introduction, *ELF3* and *GI* together act as light Zeitnehmer, albeit at different times of day. However, regarding temperature entrainment of the oscillator, the role of *ELF3* and/or the entire evening complex (EC, *ELF3-ELF4-LUX*) remains intriguing. This chapter aims to understand how cyclic temperature signals are perceived by the oscillator, and whether *ELF3* acts as a temperature Zeitnehmer.

4.1 *ELF3* and *GI* participate in complicated temperature-photoperiod crosstalk

Temperature and light serve as two prominent entrainment cues of the circadian clock, both independently and collaboratively (Eckardt, 2005; Gil and Park, 2019). To assess whether light Zeitnehmers *ELF3* and *GI* concurrently control circadian temperature entrainment, I first estimated the extent of a possible temperature-photoperiod interconnection. Hypocotyl elongation was used as a classic phenotypic readout, which is known to be highly responsive to both temperature and photoperiod variations (Niwa *et al.*, 2009). Hypocotyl length was measured in *Ws-2*, the single mutants *elf3-4* and *gi-158*, and an *elf3-4 gi-158* double mutant grown in LD (Fig. 4-1A) or SD (Fig. 4-1B) conditions. To estimate temperature response under these photoperiods, the seedlings were grown at constant 16°C or 22°C. I observed greater hypocotyl elongation at higher temperature in all four genotypes under both photoperiods (Fig. 4-1A, B). However, the extent of the temperature response in LD or SD differed among them: *Ws-2* and *gi-158* were more responsive in SD than in LD, whereas *elf3-4* and *elf3-4 gi-158* displayed the opposite behavior (Fig. 4-1C).

¹ This chapter is adapted from **Zhu Z, Quint M, Anwer MU**. 2022. Arabidopsis EARLY FLOWERING 3 controls temperature responsiveness of the circadian clock independently of the evening complex. *Journal of Experimental Botany* **73**, 1049-1061.

Similar results were observed in seedlings grown under similar photoperiods, but at a higher temperature regime with constant 20°C or 28°C: only Ws-2 was less temperature responsive in both LD and SD, whereas all three mutants displayed the opposite results (Fig. 4-2A). Moreover, a similar response was detected in a temperature shift assay, where 4-day-old



seedlings were shifted from 20°C to 28°C or were kept at 20°C for an additional 4 d (Fig. 4-2B). Interestingly, the *elf3-4 gi-158* double mutant displayed an additive effect on hypocotyl length in LD, but not in SD or under constant 16°C. These results demonstrate that mutations in *ELF3* and/or *GI* affect temperature response, which is also strongly influenced by the photoperiod.

Together, this suggests that *ELF3* and *GI* are involved in a probably rather complicated temperature-photoperiod crosstalk.

Fig. 4-1 *ELF3* and *GI* are involved in temperature-photoperiod crosstalk.

(A, B) Representative images and hypocotyl length of 8-day-old *Arabidopsis* seedlings grown in long day (LD, 16 h light: 8 h dark, A) and short day photoperiods (SD, 8 h light: 16 h dark, B), at constant 16°C or 22°C. Scale bars=4 mm. (C) Temperature response of the measured hypocotyl length at 22°C relative to the median hypocotyl length at 16°C shown in (A) and (B). Boxes show medians and interquartile ranges. The whiskers extend to 1.5x interquartile ranges. Dots represent the values of individual seedlings. Different letters above the boxes indicate significant differences (two-way ANOVA and Tukey's HSD test, $P < 0.05$).

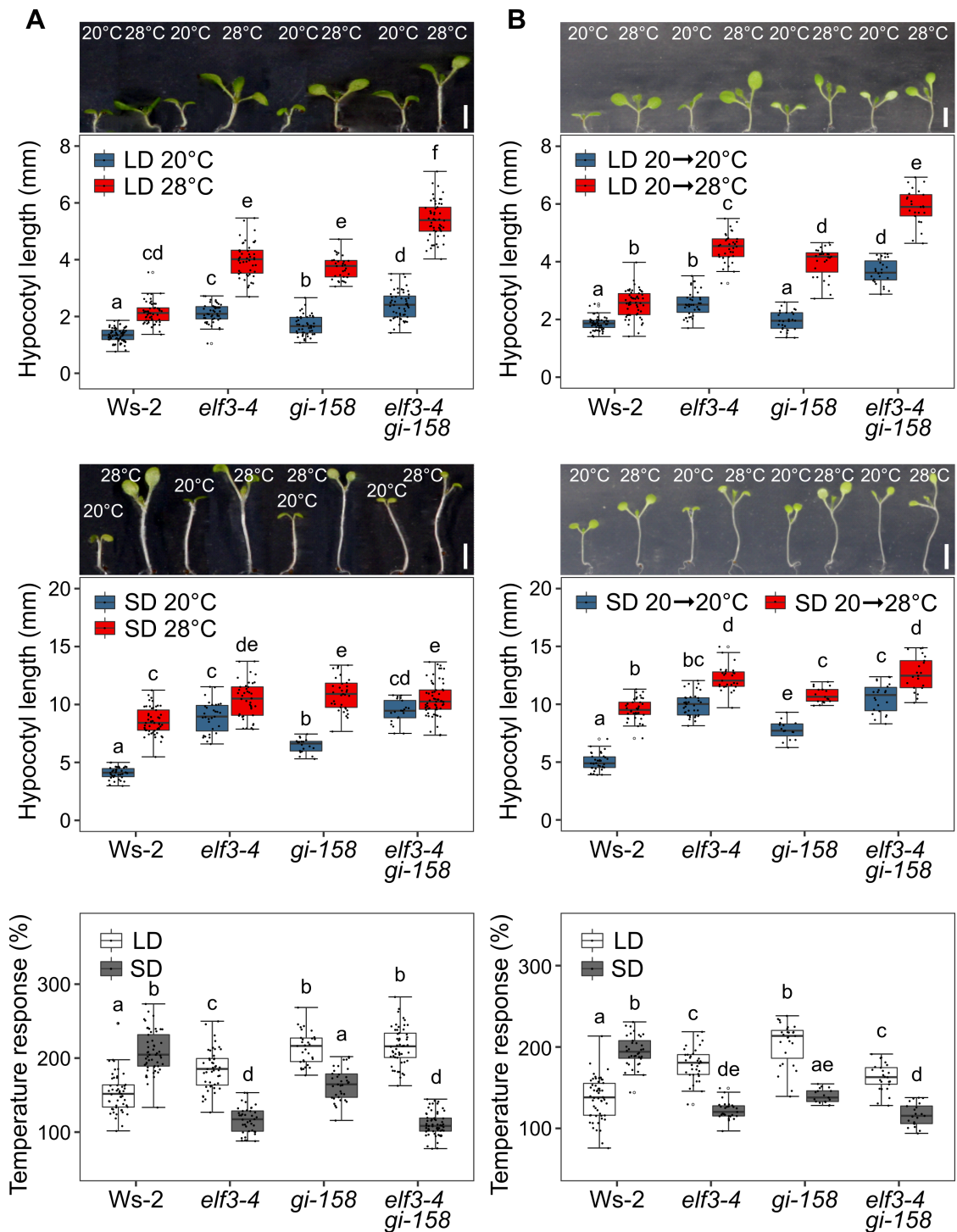


Fig. 4-2 Temperature-photoperiod crosstalk at a higher temperature regime.

(A, B) Representative images and hypocotyl length of 8-day-old *Arabidopsis* seedlings grown in long day (LD, 18 h light: 6 h dark) and short day photoperiods (SD, 6 h light: 18 h dark). Scale bars=4 mm. (A) Seedlings were grown at constant 20°C or 28°C. (B) Seedlings grown at 20°C for 4 d were shifted to 28°C or were kept at 20°C for additional 4 d. Boxes show medians and interquartile ranges. The whiskers extend to 1.5x interquartile ranges. Dots represent the values of individual seedlings. Different letters above the boxes indicate significant differences (two-way ANOVA and Tukey's HSD test, $P < 0.05$).

4.2 *ELF3* and *GI* are not essential for temperature responsiveness under constant conditions

Next, I sought to determine whether temperature responsive growth remains intact in the absence of photocycles, and whether *ELF3* and *GI* control temperature responsiveness under these non-cycling conditions. In continuous light (LL) conditions, I observed that *Ws-2* and *elf3-4* displayed the same hypocotyl length at 16°C and 28°C, whereas *elf3-4* showed a longer hypocotyl length than *Ws-2* at 22°C (Fig. 4-3). Similar temperature response patterns were detected in *gi-158* and *elf3-4 gi-158*, although they had longer hypocotyls at 22°C and 28°C than *Ws-2* and *elf3-4*, respectively. In contrast to the previous experiments (Figs. 4-1, 4-2), the temperature response among all four genotypes was relatively similar under non-cycling conditions (Fig. 4-3). As such, temperature response defects in *elf3* and *gi* mutants depend on the presence of photoperiods, while their temperature response remains intact in the absence of photoperiods (i.e., LL). These data indicate that although *ELF3* and *GI* play important roles in temperature-photoperiod crosstalk, they are not essential for temperature responsiveness under non-cycling conditions.

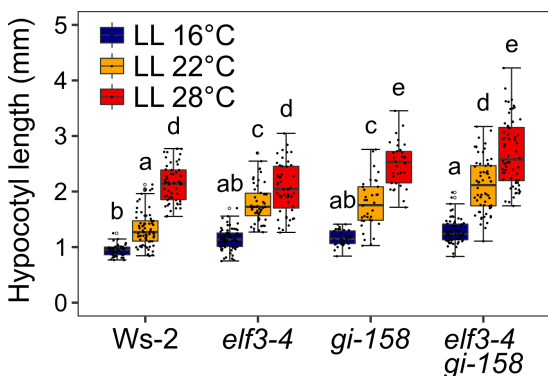


Fig. 4-3 Thermo-responsive growth is intact in continuous light.

Hypocotyl length of 8-day-old *Arabidopsis* seedlings grown in continuous light (LL) at constant 16°C, 22°C, or 28°C. Boxes show medians and interquartile ranges. The whiskers extend to 1.5x interquartile ranges. Dots represent the values of individual seedlings. Different letters above the boxes indicate significant differences (two-way ANOVA and Tukey's HSD test, $P < 0.05$).

4.3 *ELF3* is required for clock-controlled physiological processes under temperature cycles

Rhythmic patterns of several physiological processes such as growth and leaf movement are controlled by the circadian clock. Under diurnal conditions, circadian oscillators coordinate hypocotyl elongation with daily cyclic environmental changes such as photoperiod, resulting in maximum growth rate at dawn or early morning in SD and LD, respectively (Nozue *et al.*, 2007; Niwa *et al.*, 2009). This is largely processed by the light

Zeitnehmers *ELF3* and *GI*, which function to repress growth during the night and day times, respectively (Anwer *et al.*, 2020).

While the conclusions of the data shown so far apply to non-cycling temperature conditions, I next aimed to understand the role of *ELF3* and *GI* under cycling temperature conditions. To circumvent potential temperature-photoperiod crosstalk (Figs. 4-1, 4-2), I decided to design the experiments in the absence of photoperiod. It is important to note here that in darkness, *ELF3* is degraded, and *phyB* is absent in the nucleus (Liu *et al.*, 2001; Yu *et al.*, 2008). Ensuring both temperature sensors are functional, I used LL conditions with temperature cycles (12 h 22°C: 12 h 16°C) for entrainment. Growth rates of *Ws-2*, *elf3-4*, *gi-158*, and *elf3-4 gi-158* seedlings were measured every hour for 4 d (facilitated by the infrared imaging platform, Fig. 2-1).

Rhythmic growth patterns were detected in *Ws-2* and *gi-158* with maximum growth rates during mid to late stages (~ZT08) of the warm period (22°C) (Fig. 4-4A, B). In contrast, no clear growth peaks were detected in *elf3-4* and *elf3-4 gi-158*. The mutant *elf3-4* displayed a constant growth rate, which was lower than that of *Ws-2* during the warm period, but marginally higher during the cool period (16°C). Importantly, although *elf3-4 gi-158* seedlings displayed overall higher growth rates compared to *elf3-4*, no clear growth peaks were detected. These results indicate that rhythmic growth under temperature cycles requires *ELF3*, while *GI* most probably only plays a minor role.

Cotyledon movement is another classic physiological output being regulated by the circadian clock (Millar *et al.*, 1995). As expected for a functional clock, rhythmic cotyledon movement was detected in *Ws-2* and *gi-158*, with open and closed cotyledons during the warm and cool periods, respectively (Fig. 4-4A, C). This is in line with a previous report where similar patterns were observed in *Col-0* and *gi-2* seedlings entrained by 12 h 22°C: 12 h 12°C temperature cycles (Tseng *et al.*, 2004). However, in contrast to *Ws-2* and *gi-158*, the cotyledon movement was undetectable in *elf3-4* and *elf3-4 gi-158* seedlings under the same conditions, mirroring the growth rate data (Fig. 4-4A-C) and suggesting a dysfunctional clock. Based on the cotyledon movement data, relative amplitude error (RAE) analysis confirmed robust rhythms in *Ws-2* and *gi-158* (RAE ~0.5), whereas both *elf3-4* and *elf3-4 gi-158* were arrhythmic (RAE ~1.0) (Fig. 4-4D).

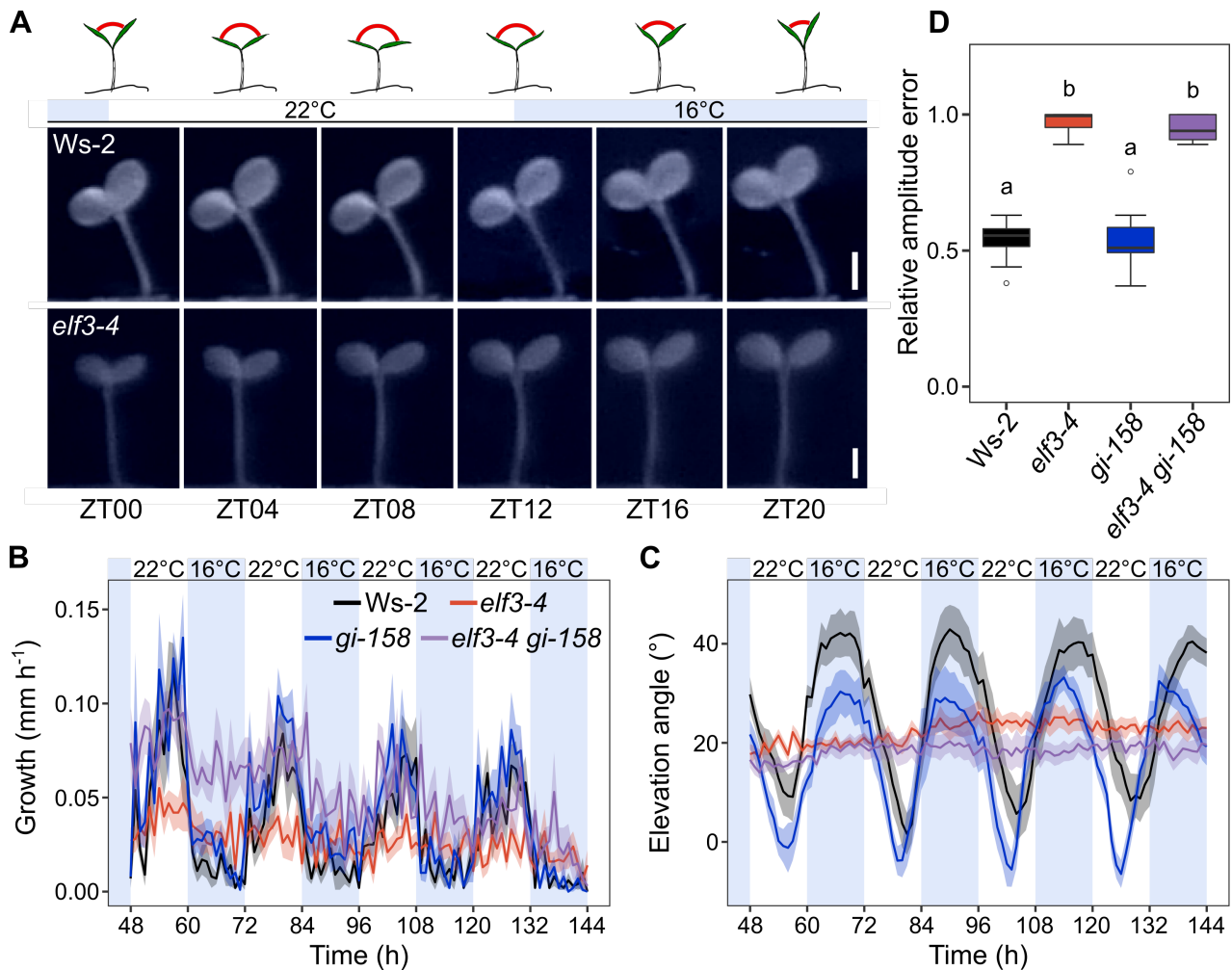


Fig. 4-4 *ELF3* is required for rhythmic physiological processes under temperature cycles.

(A) Representative images of 5-day-old *Ws-2* and *elf3-4* seedlings grown in LL under temperature cycles (12 h 22°C: 12 h 16°C). Non-shaded areas: 22°C; blue-shaded areas: 16°C. Scale bars=1 mm. Sketches above the images are shown for illustration purposes and represent the cotyledon movement of a hypothetical plant. The red arcs represent the hypothetical angles between two cotyledons. Hypocotyl growth rate (B) and cotyledon elevation angles (C) of *Arabidopsis* seedlings grown under temperature cycles as in (A). Lines represent the mean and ribbons indicate the standard error of mean (SEM) ($n=8$). (D) Relative amplitude error of cotyledon movement data shown in (C). Boxes show medians and interquartile ranges. The whiskers extend to 1.5x interquartile ranges. Dots represent the values of individual seedlings. Different letters above the boxes indicate significant differences (one-way ANOVA and Tukey's HSD test, $P<0.05$). Statistics of hypocotyl growth are in Appendix V.

To confirm that the observed cotyledon movement was driven by the circadian oscillator rather than the temperature variations, the seedlings entrained by temperature cycles for 2 d were transferred into free-running conditions (LL and constant 22°C). Robust rhythms were observed in *Ws-2* and *gi-158*, whereas both *elf3-4* and *elf3-4 gi-158* were arrhythmic in free-running conditions (Fig. 4-5A).

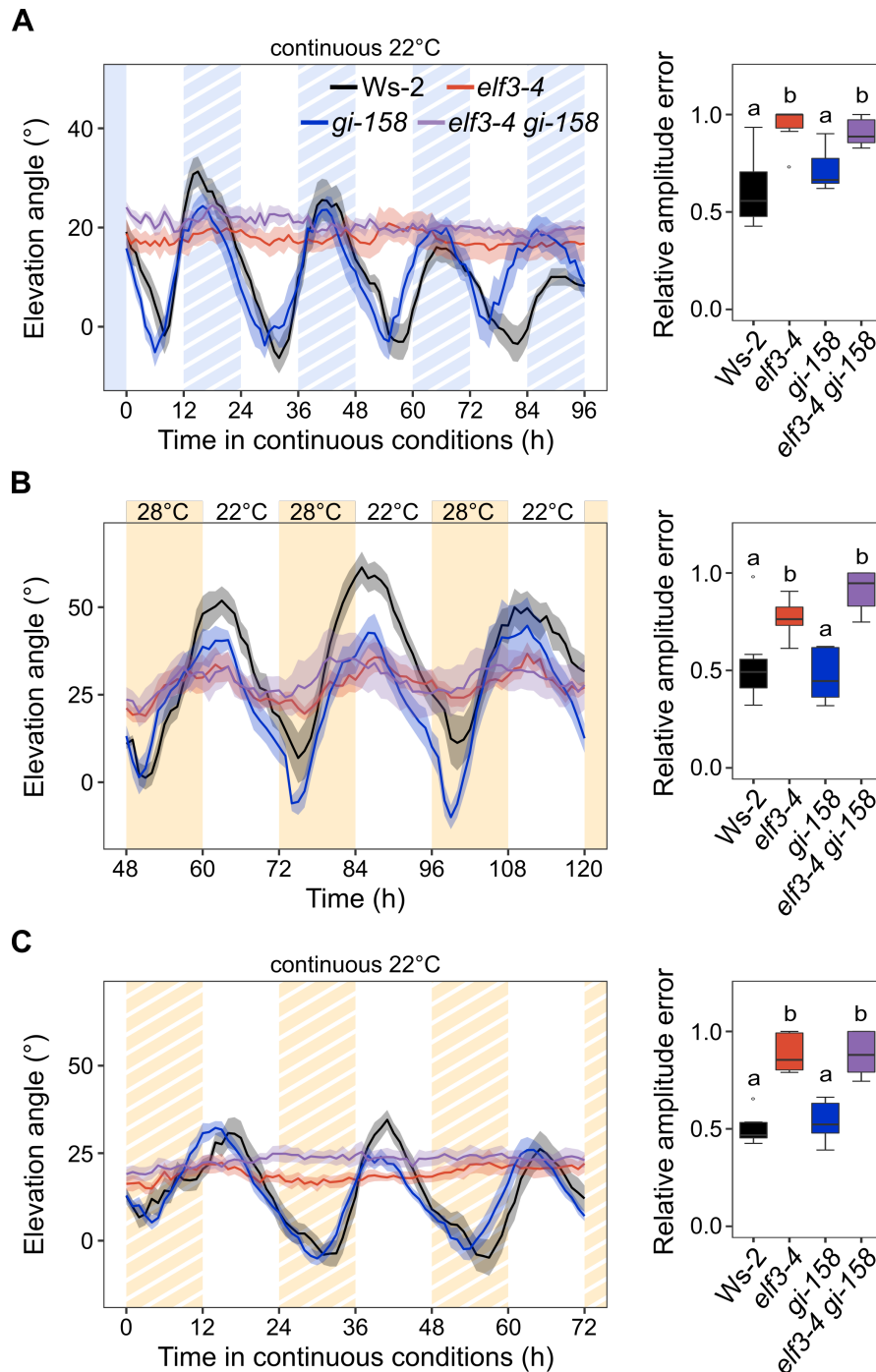


Fig. 4-5 Clock-controlled cotyledon movement entrained by different temperature cycles.

(A-C) Cotyledon elevation angle of *Arabidopsis* seedlings and the RAE of cotyledon movements. Seedlings were grown in LL under temperature cycles: 12 h 22°C: 12 h 16°C for (A) and 12 h 28°C: 12 h 22°C for (B) and (C). (A, C) On day 3 after germination, starting from ZT00, seedlings were released into constant conditions (constant 22°C). Non-shaded areas: 22°C; blue-striped areas: subjective 16°C; orange-shaded areas: 28°C; orange-striped areas: subjective 28°C. Lines represent the mean and ribbons indicate the SEM ($n=8$). Boxes show medians and interquartile ranges. The whiskers extend to 1.5x interquartile ranges. Dots represent the values of individual seedlings. Different letters above the boxes indicate significant differences (one-way ANOVA and Tukey's HSD test, $P<0.05$).

Previous studies reported that the rhythmicity in *prp7 prp9* double mutants was dependent on the temperature regime, with robust rhythms under 28°C: 22°C cycles but arrhythmia under 22°C: 12°C cycles (Salomé and McClung, 2005; Salomé *et al.*, 2010). To investigate whether this applies to the observed arrhythmia in *elf3-4* and *elf3-4 gi-158*, I monitored the cotyledon movement also under a comparable high temperature cycle regime (12 h 28°C: 12 h 22°C) and under free-running conditions (LL and constant 22°C) after entrainment. Consistent with the results from the low temperature cycle regime, robust rhythms were not detected in *elf3-4* or *elf3-4 gi-158*, as also evident from high RAE values (Fig. 4-5B, C).

Collectively, these data demonstrate that in contrast to clock-controlled rhythmic processes under photocycles (Anwer *et al.*, 2020), only *ELF3*, but not *GI*, is essential for clock-controlled rhythmic physiological processes under temperature cycles.

4.4 Neither *phyB* nor the EC is essential for *ELF3*-mediated rhythmic output under temperature cycles

As both *ELF3* and *phyB* function as temperature sensors (Jung *et al.*, 2016; Legris *et al.*, 2016; Jung *et al.*, 2020), the observed arrhythmia in *elf3* could be caused by (i) the absence of the thermosensory function of *ELF3* in response to temperature cycles, and/or by (ii) a defect in possible temperature signal transduction and integration via the functional *phyB-ELF3* interaction (Liu *et al.*, 2001; Ezer *et al.*, 2017). I next investigated the possible participation of *phyB* in circadian clock temperature entrainment, by using *phyB-10* and *elf3-4 phyB-10* seedlings grown under temperature cycles in LL. Similar to *Ws-2*, *phyB-10* loss-of-function mutants also displayed rhythmic cotyledon movement, whereas both *elf3-4* and *elf3-4 phyB-10* were arrhythmic (RAE ~1.0) (Fig. 4-6A). These results demonstrate that *phyB* is not necessary for rhythmic cotyledon movement under temperature cycles. Thus, in contrast to *phyB*, *ELF3* is essential to generate such clock-controlled output, suggesting that cyclic change in temperature is mainly relayed to the oscillator through *ELF3*.

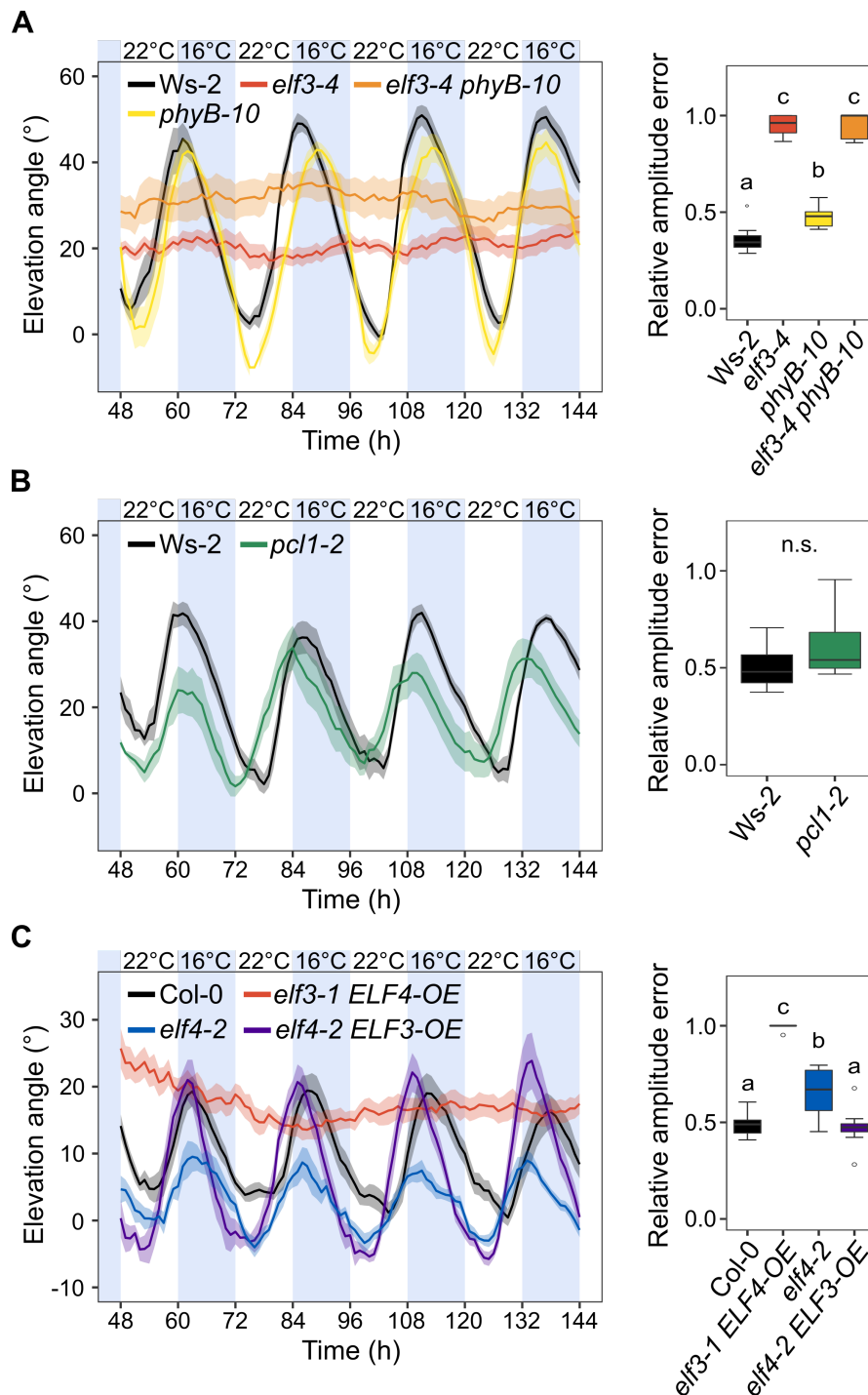


Fig. 4-6 *ELF3*-mediated rhythmic output is independent of *phyB*, *LUX*, and *ELF4*.

(A-C) Cotyledon elevation angle of *Arabidopsis* seedlings and the RAE of cotyledon movements. Seedlings were grown in LL under temperature cycles (12 h 22°C: 12 h 16°C). Non-shaded areas: 22°C; blue-shaded areas: 16°C. Lines represent the mean and ribbons indicate the SEM ($n=8$). Boxes show medians and interquartile ranges. The whiskers extend to 1.5x interquartile ranges. Dots represent the values of individual seedlings. Different letters above the boxes indicate significant differences (one-way ANOVA and Tukey's HSD test, $P<0.05$). n.s., not significant (two-sided Student's *t*-test).

The arrhythmia in *elf3* under temperature cycles could also be explained by a general clock dysfunction in LL (McWatters *et al.*, 2000; Herrero *et al.*, 2012). To exclude this possibility and to investigate the role of the EC in temperature entrainment, I tested whether the clock could be functionally entrained by temperature cycles in the absence of LUX or ELF4 – the other two components of the EC (Nusinow *et al.*, 2011; Ezer *et al.*, 2017). It is important to note here that loss-of-function of both *LUX* and *ELF4* display clock and developmental defects that resemble *elf3* null mutants, including arrhythmia in LL (McWatters *et al.*, 2000; Onai and Ishiura, 2005; Herrero *et al.*, 2012). However, I observed that unlike the arrhythmia in *elf3-4*, both *pcl1-2 (lux)* and *elf4-2* mutants, despite changes in phase and amplitude, displayed rhythmic cotyledon movement under temperature cycles (Fig. 4-6B, C). Interestingly, overexpression of *ELF3* in *elf4-2 (elf4-2 ELF3-OE)* could restore the amplitude decrease observed in the *elf4-2* single mutant, whereas *elf3-1 ELF4-OE* was still arrhythmic (RAE ~1.0) (Fig. 4-6C). These data demonstrate the important and specific role of *ELF3* in temperature entrainment of the circadian clock, which appears to be independent of an intact EC and possibly a functional oscillator.

4.5 *ELF3* is required for the oscillator's responsiveness to temperature cycles

As the arrhythmia in clock-controlled physiological processes under temperature cycles was specifically observed in the absence of *ELF3*, I hypothesized that this arrhythmia was a result of a dysfunctional oscillator that can no longer respond to changes in external temperature. To test this, I monitored the steady-state transcript levels of the key central oscillator genes *CCA1*, *LHY*, *PRR9*, *PRR7*, and *TOC1* under temperature cycles in LL. As expected for a functional oscillator, *Ws-2* and *gi-158* displayed rhythmic expression of these genes, although differences in the transcript level were occasionally detected (Fig. 4-7A-E). In *Ws-2* and *gi-158*, *CCA1* and *LHY* displayed peak transcript abundance at ZT00/24, *PRR9* at ZT04, *PRR7* at ZT08, and *TOC1* at ZT16 (*Ws-2*) or ZT12 (*gi-158*). In contrast, no rhythmic expression was detected in *elf3-4* and *elf3-4 gi-158*. In the absence of *ELF3*, almost no transcripts of *CCA1* and *LHY* can be detected, whereas *PRR9*, *PRR7*, and *TOC1* maintained high transcript levels without oscillations (Fig. 4-7A-E).

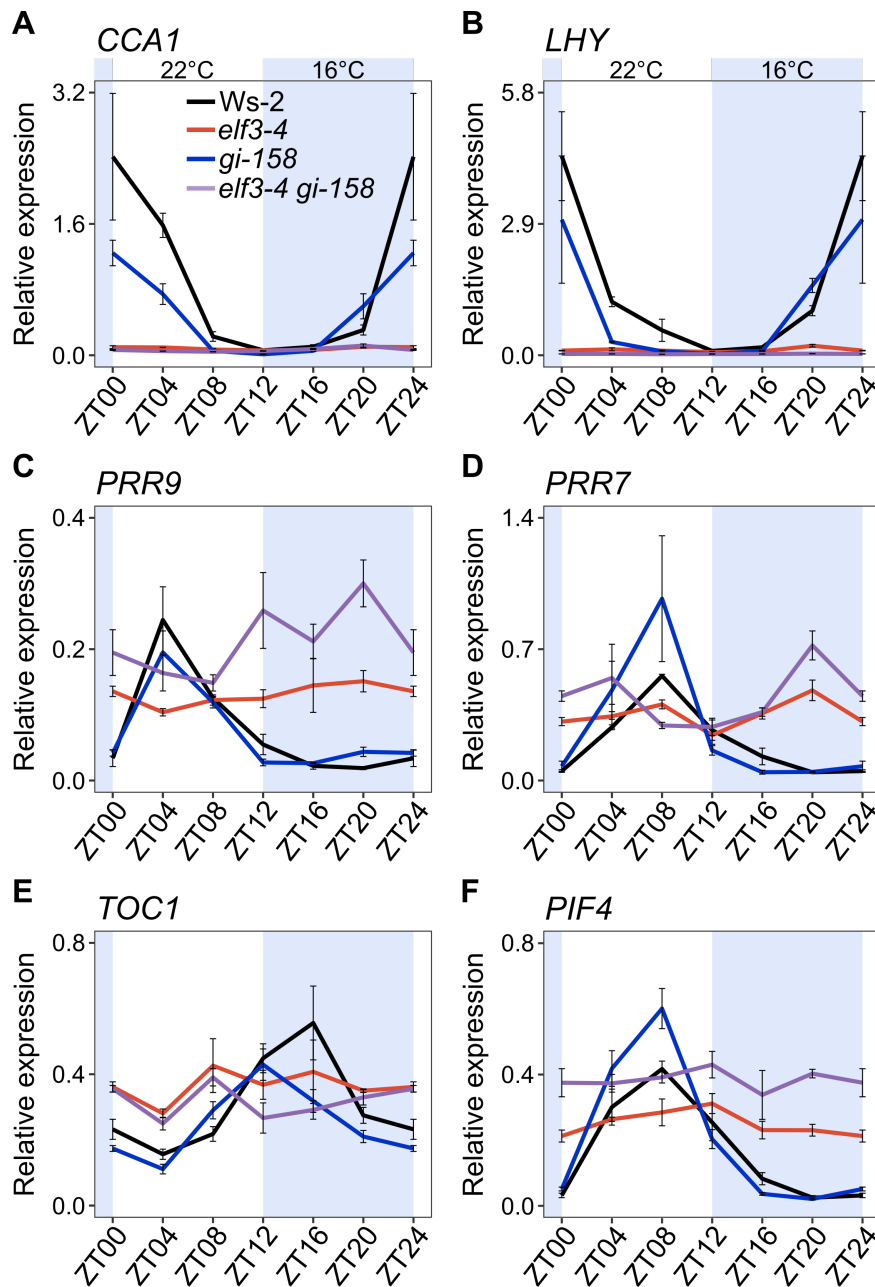


Fig. 4-7 *ELF3* is required for the oscillator's responsiveness to temperature changes.

Steady-state transcript levels of key clock oscillator genes *CCA1* (A), *LHY* (B), *PRR9* (C), *PRR7* (D), and *TOC1* (E), and the major growth promoter *PIF4* (F). Arabidopsis seedlings were harvested every 4 h after being entrained under temperature cycles (12 h 22°C: 12 h 16°C) for 8 d in LL. Non-shaded areas: 22°C; blue-shaded areas: 16°C. Expression levels were normalized to *PP2A*. Error bars indicate the SEM ($n=3$) of three biological replicates. Statistics and normalization to a second reference gene *TIP41* are in Appendix V.

Similar patterns of steady-state transcript level of these key clock genes were detected when plants were grown under the same temperature cycles in darkness (DD, Fig. 4-8A-E). The exceptions were that, in DD, *gi-158* displayed a temporarily slightly advanced peak of transcript abundance for *PRR7* at ZT04, slight peaks of *CCA1*, *LHY*, and *PRR9* expression

at ZT00/24 were detected in *elf3-4*, and no clear expression pattern of *TOC1* was detected in all four genotypes. These results indicate that *ELF3* is required to correctly set the phase of key central oscillator genes in response to cyclic temperatures.

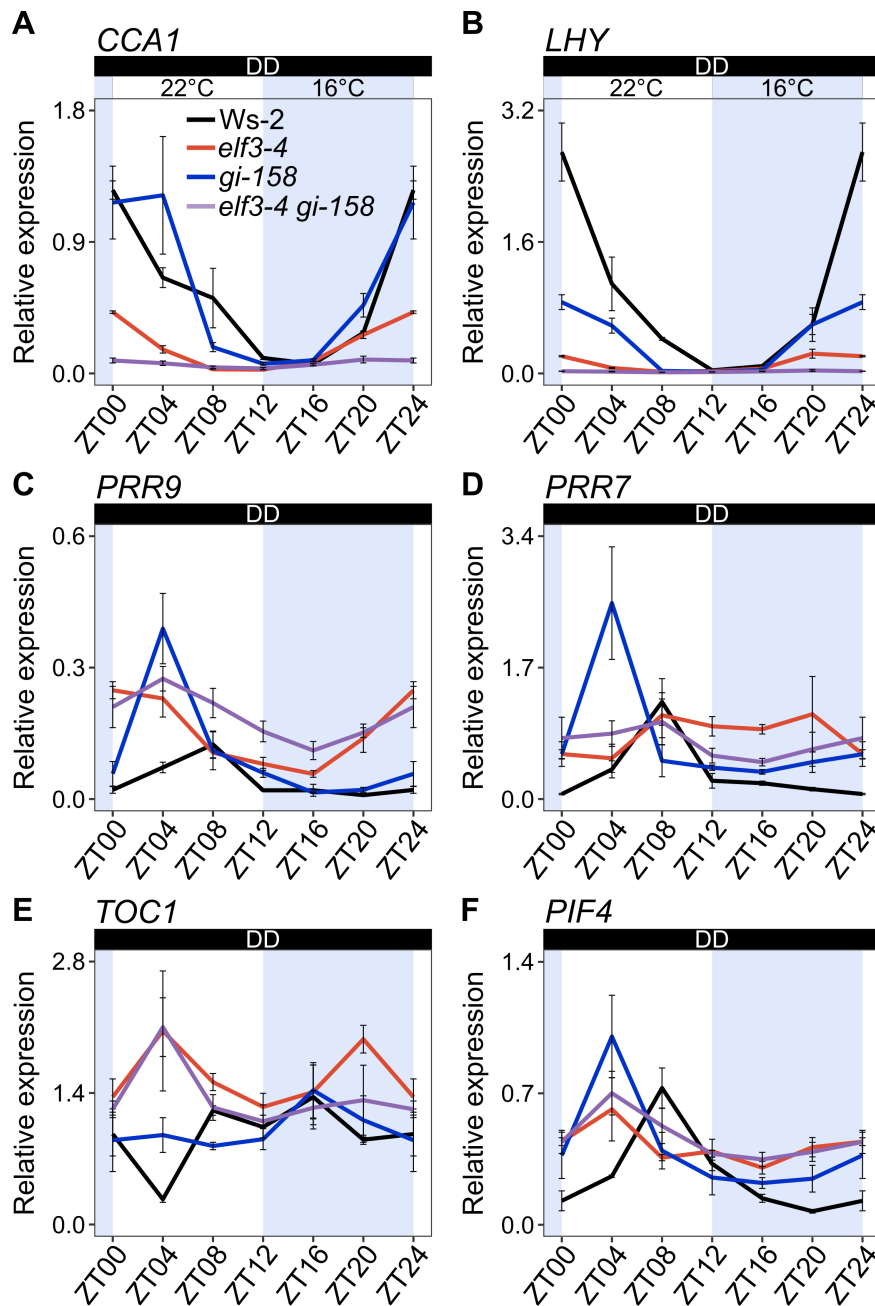


Fig. 4-8 The oscillator's responsiveness to temperature changes in darkness.

Steady-state transcript levels of key clock oscillator genes *CCA1* (A), *LHY* (B), *PRR9* (C), *PRR7* (D), and *TOC1* (E), and the major growth promoter *PIF4* (F). Arabidopsis seedlings were harvested every 4 h after being entrained under temperature cycles (12 h 22°C: 12 h 16°C) for 8 d in DD. Non-shaded areas: 22°C; blue-shaded areas: 16°C. Expression levels were normalized to *PP2A*. Error bars indicate the SEM ($n=3$) of three biological replicates. Statistics are in Appendix V.

Provided that the circadian clock regulates thermoresponsive growth by regulating the major growth promoter *PIF4* (Box *et al.*, 2015; Raschke *et al.*, 2015), I next monitored the steady-state transcript abundance of *PIF4* as a proxy to gauge the oscillator's ability to regulate its target genes under temperature cycles. I observed that, in *Ws-2* and *gi-158*, the transcript levels of *PIF4* specifically peaked during the warm period at ZT08 in LL, consistent with their rhythmic hypocotyl growth rate (Figs. 4-4B, 4-7F). In DD, *Ws-2* displayed the *PIF4* peak transcript abundance at the same time (ZT08) as in LL, whereas the peak was advanced to ZT04 in *gi-158* (Fig. 4-8F). Importantly, no clear peak of *PIF4* expression was detected in *elf3-4* and *elf3-4 gi-158*, mainly due to pronounced high transcript abundance during the cool period. Taken together, these data demonstrate that the oscillator's ability to properly respond to temperature input depends on functional *ELF3*.

4.6 *ELF3* is essential for precise gating of temperature signals

One hallmark property of the circadian clock is to regulate the oscillator's own sensitivity to environmental inputs in a time-of-day-dependent manner, termed as circadian gating. This ensures that the downstream processes maintain correct rhythms but are not influenced by untimely environmental inputs. For instance, a sudden change in light and temperature caused by cloud shading would not substantially affect the clock-controlled rhythmic processes.

To test the clock's gating ability in response to temperature, I monitored the steady-state transcript level of key clock-regulated temperature-responsive genes *PRR7*, *PRR9*, and *PIF4*. Seedlings entrained by temperature cycles were either treated with a 4 h temperature pulse (28°C pulse) at various ZTs or were kept under the same conditions (no treatment) before being harvested at the specified time points (Fig. 4-9). I found that in *Ws-2*, the temperature responsiveness of these genes was mainly restricted from late night to early morning (between ZT16 and ZT04) when the induction of *PRR7*, *PRR9*, and *PIF4* expression was detected (Fig. 4-9). In *gi-158*, the gates were opened slightly earlier, with induction of *PRR7* (ZT12-ZT24) and *PIF4* (ZT16-ZT24) observed. In contrast, the gating ability of the oscillator was severely compromised in *elf3-4* and *elf3-4 gi-158*. In the absence of *ELF3*, at some random time points, the response to the temperature pulse was opposite to that of the wild type, whereas no response was detected at the remaining time points. Hence, the transcript levels of *PRR7*, *PRR9*, and *PIF4* remained unchanged at the vast majority of time points. These data demonstrate that *ELF3* is not only essential to generate

robust rhythms under temperature cycles but is also pivotal to maintain the proper phase by gating the non-resetting temperature cues.

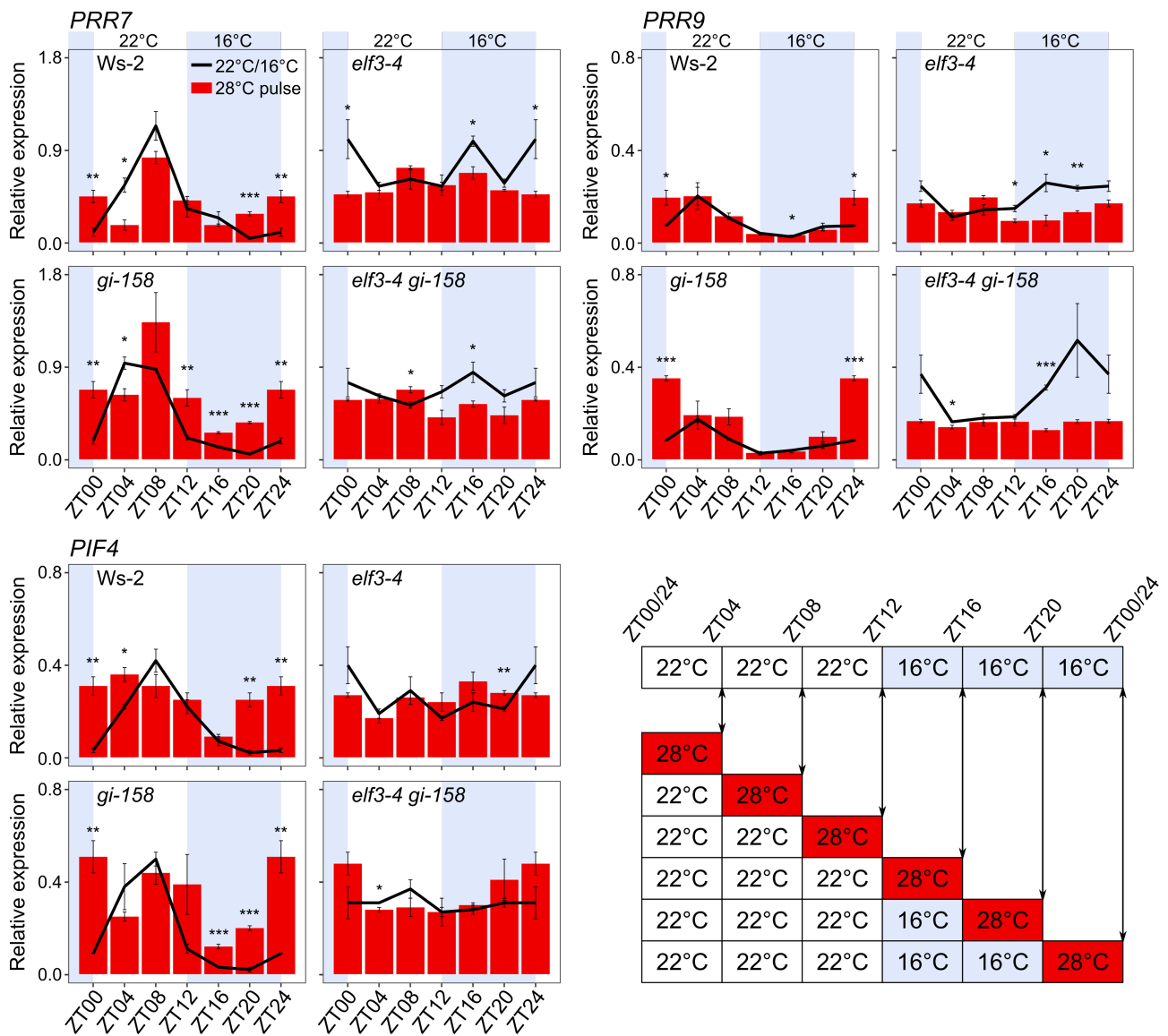


Fig. 4-9 *ELF3* is essential for circadian gating of temperature signals.

Effect of a 28°C temperature pulse at specified ZTs on the transcript levels of *PRR7*, *PRR9*, and *PIF4*. Arabidopsis seedlings were grown under temperature cycles (12 h 22°C: 12 h 16°C) for 8 d in LL. On day 9, seedlings were either treated with a temperature pulse (28°C pulse) for 4 h at indicated ZTs or were kept under the same conditions (no treatment, 22°C/16°C) before samples were harvested (as shown in the scheme). At the indicated ZTs, red bars represent transcript levels after treatment with a temperature pulse, whereas black lines represent transcript levels at the same time without treatment. Non-shaded areas: 22°C; blue-shaded areas: 16°C. Expression levels were normalized to *PP2A*. Error bars indicate the SEM ($n=3$) of three biological replicates. Asterisks above lines or bars indicate significant differences (* $P < 0.05$; ** $P < 0.01$; *** $P < 0.001$; two-sided Student's *t*-test).

4.7 Functional ELF3 is not required for temperature entrainment in *H. vulgare*

As the results so far demonstrate that *ELF3* controls circadian clock temperature entrainment in *Arabidopsis*, I next asked whether this role may be conserved across species. To test this, I chose the monocot model crop barley (*H. vulgare*), which diverged from the eudicot *Arabidopsis* lineage approx. 160 million years ago (<http://www.timetree.org>, Kumar *et al.*, 2017). I monitored the steady-state transcript abundance of barley circadian clock genes *HvCCA1*, *HvTOC1*, *HvPRR73*, and *HvGI* in cultivar Bowman and *elf3^{BW289}* (*elf3/eam8.k* loss-of-function mutant BW289 in Bowman background) seedlings entrained under the same temperature cycles in LL (Fig. 4-10).

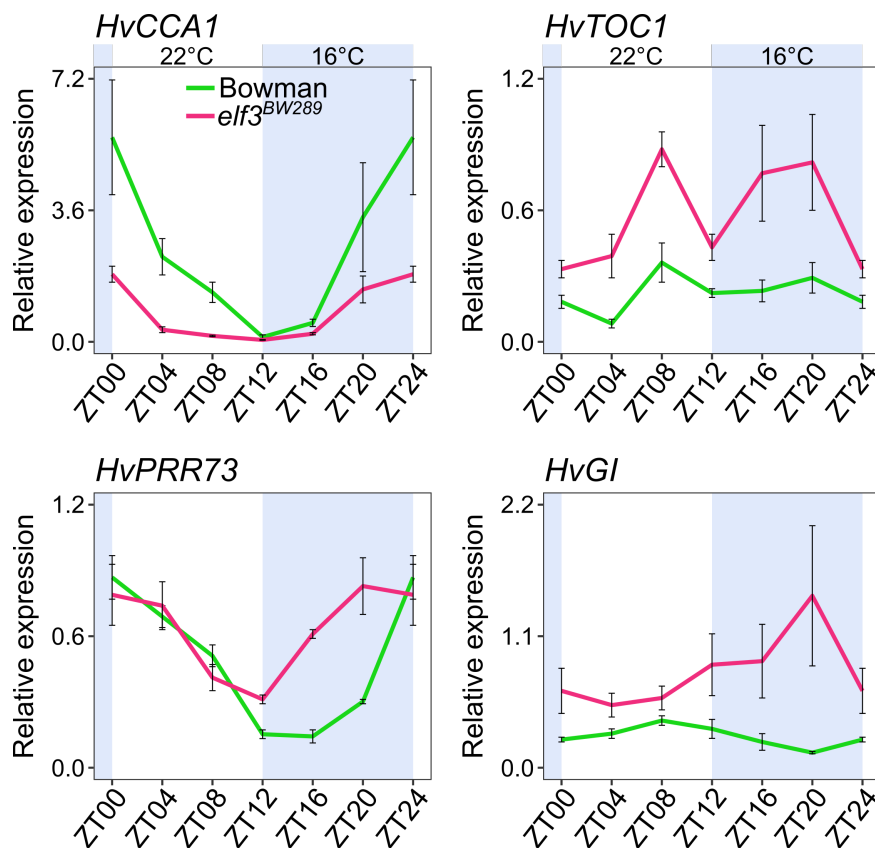


Fig. 4-10 *H. vulgare* *elf3* seedlings can be entrained by temperature cycles.

Steady-state transcript levels of barley clock genes *CCA1*, *TOC1*, *PRR73*, and *GI*. Bowman and *elf3^{BW289}* (*elf3/eam8.k* loss-of-function mutant BW289 in Bowman background) seedlings were harvested every 4 h after being entrained under temperature cycles (12 h 22°C: 12 h 16°C) for 14 d in LL. Non-shaded areas: 22°C; blue-shaded areas: 16°C. Expression levels were normalized to *HvACTIN*. Error bars indicate the SEM ($n=3$) of three biological replicates.

Barley clock genes displayed rhythmic expression patterns under temperature cycles in Bowman (Fig. 4-10). However, such rhythmic patterns were also maintained in *elf3^{BW289}*, although the amplitude was reduced in *HvCCA1* and *HvPRR73*, and the expression peak was shifted in *HvGI* (Fig. 4-10). These data show that the barley circadian oscillator was slightly disturbed in the absence of *ELF3* under temperature cycles. However, in contrast to Arabidopsis, functional *ELF3* is not a prerequisite for the oscillator's responsiveness to temperature changes in barley.

In conclusion, this chapter established Arabidopsis *ELF3* as an essential Zeitnehmer for temperature sensing of the circadian oscillator, which thereby coordinates the rhythmic control of temperature responsive physiological outputs.

5 Results III – An exotic allele of barley *ELF3* contributes to developmental plasticity at elevated temperatures²

For understanding crop acclimation and adaptation to changing temperatures, barley (*H. vulgare*) stands out as an excellent monocot model. As shown in the previous two chapters, the barley homologue of ELF3 lacking PrD is neither a potential thermosensor, nor a prerequisite for clock temperature entrainment. However, the importance of *HvELF3* in barley flowering time adaptation to short growing seasons is not negligible (Faure *et al.*, 2012; Zakhrebekova *et al.*, 2012). This chapter aims to understand the role of *HvELF3* in barley thermomorphogenesis, by using *elf3* loss-of-function alleles, as well as heterogeneous inbred family (HIF) pairs generated from the HEB-25 population.

5.1 *ELF3* is involved in barley thermomorphogenesis

I first performed a temperature assay on agar plates mimicking the standard growth conditions for Arabidopsis seedling assays. Leaf length was measured for the elite cultivar Bowman and *elf3*^{BW290} loss-of-function mutant seedlings grown in LD at 20°C or 28°C. In two consecutive days after germination, no difference in leaf length was observed between Bowman and *elf3*^{BW290} at 20°C. However, at 28°C *elf3*^{BW290} displayed longer leaves compared to Bowman (Fig. 5-1).

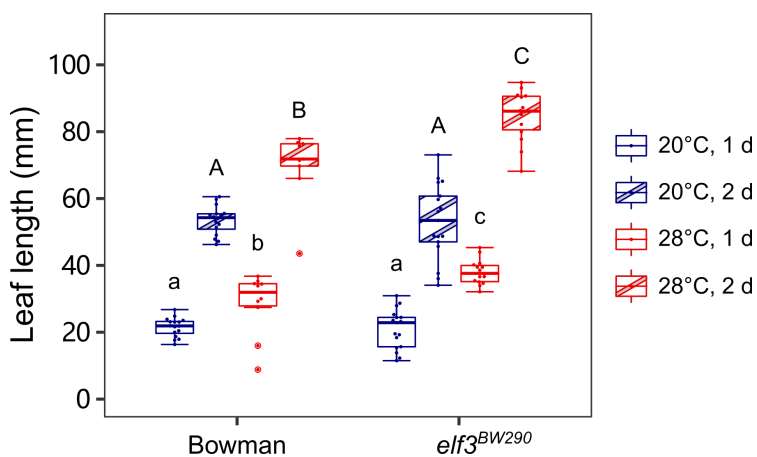


Fig. 5-1 *ELF3* is involved in the early temperature response of barley seedlings.

Bowman and *elf3*^{BW290} seedlings were grown at 20°C or 28°C in LD (16 h light/ 8 h dark). Boxes show medians and interquartile ranges. The whiskers extend to 1.5x interquartile ranges. Dots represent the values of individual plants ($n=9-17$).

Different letters above the boxes indicate significant differences (small and capital letters for the first and second days, respectively, two-way ANOVA and Tukey's HSD test, $P<0.05$).

² This chapter is adapted from **Zhu Z, Esche F, Babben S, Trenner J, Serfling A, Pillen K, Maurer A, Quint M.** 2023. An exotic allele of barley EARLY FLOWERING 3 contributes to developmental plasticity at elevated temperatures. *Journal of Experimental Botany*, doi: 10.1093/jxb/erac470.

These data suggest that *ELF3* is involved in the early temperature response of barley seedlings, being a repressor of elongation growth similar to the role of Arabidopsis *ELF3* (Box *et al.*, 2015; Raschke *et al.*, 2015).

5.2 *ELF3* sequence variation in HIF pairs

To further study the role of *ELF3* in barley temperature response, in addition to Bowman and *elf3^{BW290}*, three HIF pairs (10_190, 16_105, and 17_041) were selected from the barley NAM population HEB-25 (Maurer *et al.*, 2015) (Fig. 1-4A), which displayed differences for several developmental phenotypes between the HIF sister lines in previous field experiments (Zahn *et al.*, 2022, Preprint). Each HIF pair contains two near-isogenic lines (NILs), carrying either *HvELF3* (elite) from cultivar Barke or *HspELF3* (wild) from exotic barley accessions (Fig. 1-4B).

I first determined the full-length genomic sequence of *ELF3* in the three used HIF pairs and compared them to the previously sequenced parental lines (Zahn *et al.*, 2022, Preprint). A W669G substitution was detected in all three wild lines (Fig. 5-2). Furthermore, the 16_105_ *HspELF3* (hereafter called 16_wild) and 17_wild HIF pairs belong to the same haplotype carrying four additional non-synonymous single-nucleotide polymorphisms (SNPs) in *ELF3* compared to 10_wild (Fig. 5-2). In line with the previous observation using barley landraces from the Qinghai-Tibetan Plateau (Xia *et al.*, 2017), SNPs and insertion-deletion mutations (Indels) were identified especially in intron 2 of *ELF3* in 16_wild and 17_wild. However, the previously described alternative splicing mutation in intron 3 was not detected in these HIF lines (Xia *et al.*, 2017). In the previous field experiments, the strongest effects were found on shooting and head within HIF pair 10, which could be validated also in controlled environments (Zahn *et al.*, 2022, Preprint). Consistent with the phenotypes, differences in transcription levels were observed in *FT1* and *VRN1*, which are known to be regulated via *ELF3*, between 10_elite and 10_wild, without changes in *ELF3* transcript levels (Zahn *et al.*, 2022, Preprint). Structural modeling of translated *ELF3* protein variants predicted a potential influence of the W669G mutation (Fig. 5-2) on protein structure, which might be responsible for the observed phenotypic differences (Zahn *et al.*, 2022, Preprint). Hence, although the previous field and indoor experiments were not performed in a temperature context, using these phenotypically divergent HIF pairs promised to provide a suitable genetic background to study the role of exotic *ELF3* alleles in barley temperature response.

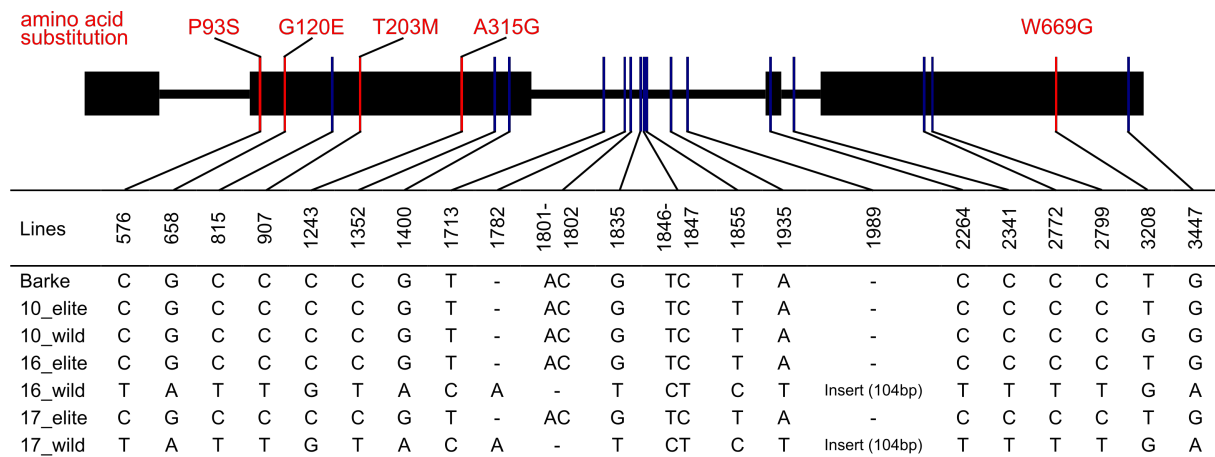


Fig. 5-2 Variations in *ELF3* sequence among HIF pairs.

Black rectangles (exons) and connecting lines (introns) represent the structure of barley *ELF3* (cv. Barke). Positions of the nonsynonymous single-nucleotide polymorphisms (SNPs) are shown as red vertical bars with corresponding amino acid substitutions shown above the scheme. The positions of the synonymous SNPs and the insertion-deletion mutations (Indels) in introns are shown as blue vertical bars. All mutations are listed in the table, using the Barke sequence as reference. The sequence of the 104-bp-insertion at position 1989 is: AGCAA ATGAAT GAATCT AACTC TAAAT ATGTCT ATATAC ATCGTA TGTAGT CCACTA GTGGAA TCTCTA GAAAGA CTTATA TTTAGG AACGGA GGGAGT AT.

In the following, I systematically analyzed the role of *ELF3* on temperature-sensitive development in general, and divided development into early seedling establishment, vegetative growth, and reproductive growth.

5.3 Elevated temperatures accelerate barley seedling establishment

To investigate the effect of *ELF3* and elevated temperatures on barley seedling establishment, the eight described genotypes were grown in LD with day/night temperatures of 20°C/16°C (20°C treatment) or 28°C/24°C (28°C treatment). At elevated temperatures, plant height was significantly increased in *elf3^{BW290}* from 6 days after sowing (DAS) on (Fig. 5-3A). This effect was also present in the corresponding cultivar Bowman, but much delayed (reliably from 13 to 14 DAS on). As observed in the temperature assay on plates (Fig. 5-1), the differences in plant height between Bowman and *elf3^{BW290}* were mostly observed at 28°C but not at 20°C (Fig. 5-3A). Hence, plant height is obviously a phenotype that is conditionally regulated by barley *ELF3* at elevated temperature during early vegetative growth. Similar results were obtained for HIF pair 10, with 10_wild showing a stronger temperature response compared to 10_elite (Fig. 5-3A), suggesting a genetic effect of the exotic barley allele on

plant height. In contrast, in HIF pairs 16 and 17, only temperature effects could be detected, but no allelic differences between the underlying *ELF3* variants.

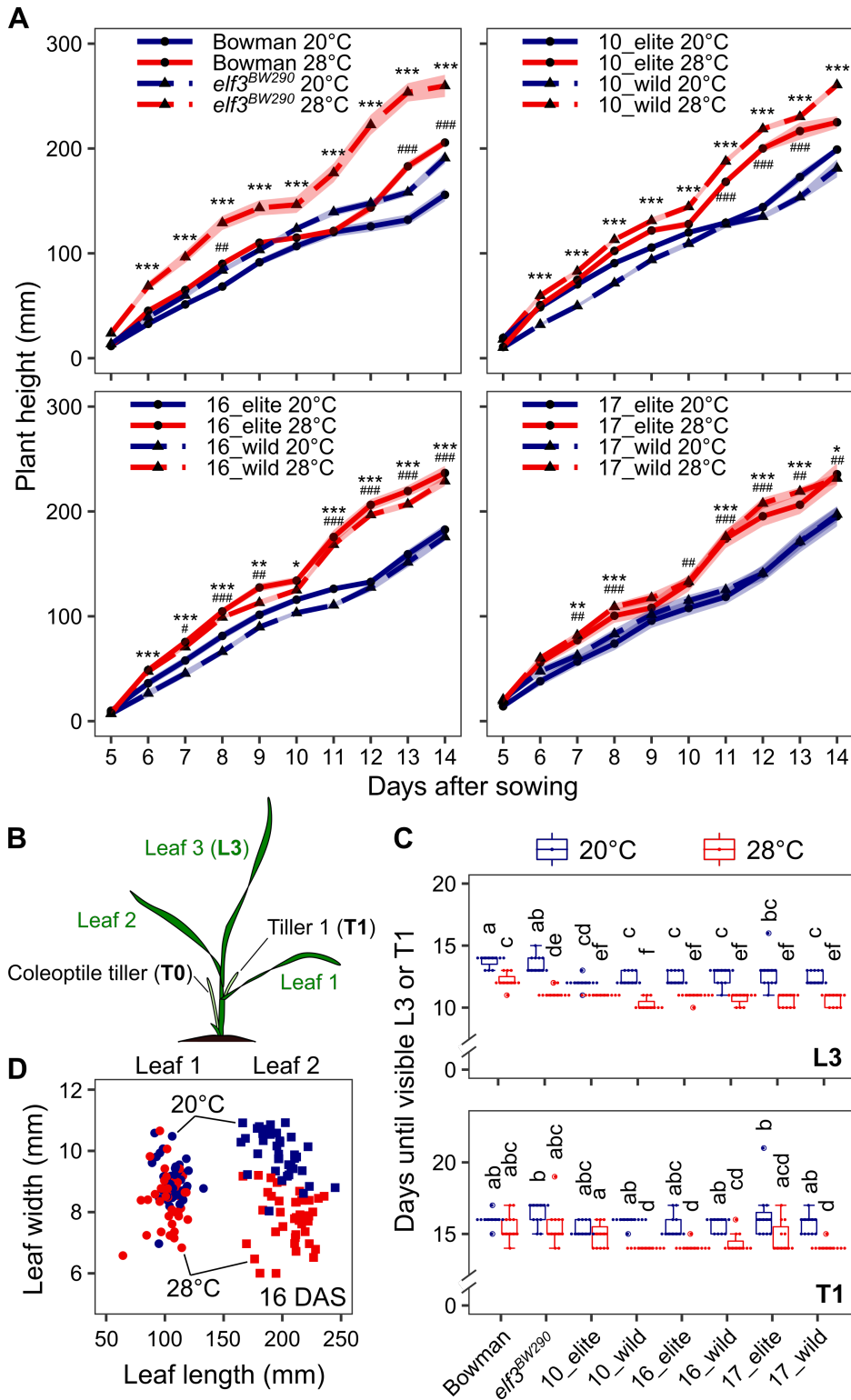


Fig. 5-3 Elevated temperatures accelerate early growth and development of barley seedlings.

Seedlings were grown in LD (16 h light/ 8 h dark) at day/night temperatures of 20/16°C (20°C). Five days after sowing (DAS), seedlings were shifted to 28/24°C (28°C) or were kept at 20°C. (A) Plant height was measured manually. Lines represent the mean and ribbons indicate the SEM ($n=11$). Hashtags (for Bowman and HIF elite lines with *HvELF3*) and asterisks (for *elf3^{BW290}* and HIF wild lines with *HspELF3*) indicate significant differences between two temperature treatments (# and *, $P<0.05$; ## and **, $P<0.01$; ### and ***, $P<0.001$; two-way ANOVA). (B) Schematic representation of a barley seedling in its three-leaf stage. (C) Days until visible third leaf (L3) and first tiller (T1). Boxes show medians and interquartile ranges. The whiskers extend to 1.5x interquartile ranges. Dots represent the values of individual plants. Different letters above the boxes indicate significant differences (two-way ANOVA and Tukey's HSD test, $P<0.05$). (D) Length and width of the first (circles) and second (squares) leaves ($n=5$) in all genotypes at 16 DAS. The genotypic effect and multiple comparisons are shown in Appendix VI.

Interestingly, I observed pauses of plant height increase in all genotypes during seedling establishment, most likely because plant height was first dominated by the length of the first leaf, before the second leaf took over (Fig. 5-3A, B). Notably, these pauses occurred earlier at elevated temperatures in almost all genotypes, indicating accelerated growth and development.

To test for accelerated development, the formation of the third leaf (L3) and the first tiller (T1) was scored during the experiment (Fig. 5-3B, C). Consistent with the results shown so far (Figs. 5-1, 5-3A), *elf3^{BW290}* displayed earlier L3 formation compared to Bowman at 28°C but not at 20°C (Fig. 5-3C). In contrast, the formation of the T1 in both Bowman and *elf3^{BW290}* was neither genotype nor temperature dependent. Except for the T1 formation in 10_elite, elevated temperatures generally accelerated the formation of the L3 and T1 in HIF pairs independently of *ELF3* alleles (Fig. 5-3C). Prior to the T1 formation, barley seedlings can develop coleoptile tillers (T0), which arise from below ground (Fig. 5-3B). Coleoptile tiller development was known to be related to seedling vigor in wheat (Liang and Richards, 1994; Fujita *et al.*, 2000), and can be suppressed by high ambient temperatures (Cannell, 1969). In confirmation of these reported observations, T0 formation was largely absent at 28°C, especially in Bowman and HIF pair 10 with no T0 at 18 DAS (Fig. 5-4). These results suggest less vigorous seedlings despite (or maybe rather because of) accelerated growth and development.

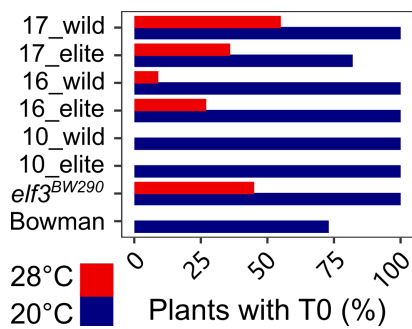


Fig. 5-4 Percentage of plants with coleoptile tillers.

Bowman, *elf3^{BW290}* and HIF pairs were grown in LD (16 h light/ 8 h dark) at day/night temperatures of 20/16°C (20°C). At 5 DAS, seedlings were shifted to 28/24°C (28°C) or were kept at 20°C. The formation of coleoptile tillers (T0) was scored at 18 DAS ($n=11$).

In addition to accelerated development, elevated temperatures also cause morphological changes, for example narrow leaves in wheat, reviewed by Lippmann *et al.* (2019). To test whether leaf shape was influenced by temperature, leaf length and width of the first and the second leaves were measured at 16 DAS. No difference in length or width was observed in the first leaf of each genotype, possibly due to its initiation before the start of the temperature treatments (Fig. 5-3D). However, significantly narrower second leaves were observed at 28°C regardless of the genotype, whereas leaf length did not differ, suggesting reduced leaf area as previously reported in wheat (Huang and Taylor, 1993; Lohraseb *et al.*, 2017).

Taken together, these results demonstrate that early seedling establishment is accelerated by elevated temperatures in barley, with *ELF3* alleles mainly affecting plant height.

5.4 An exotic *ELF3* allele affects barley temperature responsive growth and architecture

As significant effects of elevated temperatures were observed on multiple phenotypes during barley seedling establishment (Figs. 5-3, 5-4), I next asked whether the growth of barley plants would be further affected by prolonged high temperatures and whether *ELF3* alleles may differ in these responses. An image-based phenotyping platform was used to obtain phenotypic data in a non-destructive manner (Fig. 2-2).

Starting from 8 DAS, each plant was imaged every two to four days to obtain growth curves under 20°C or 28°C treatment. In confirmation of the above-described results (Fig. 5-3A), a similar effect of temperature on plant height was observed during the first two weeks of cultivation, lasting until around 30 DAS in all genotypes (Fig. 5-5A).

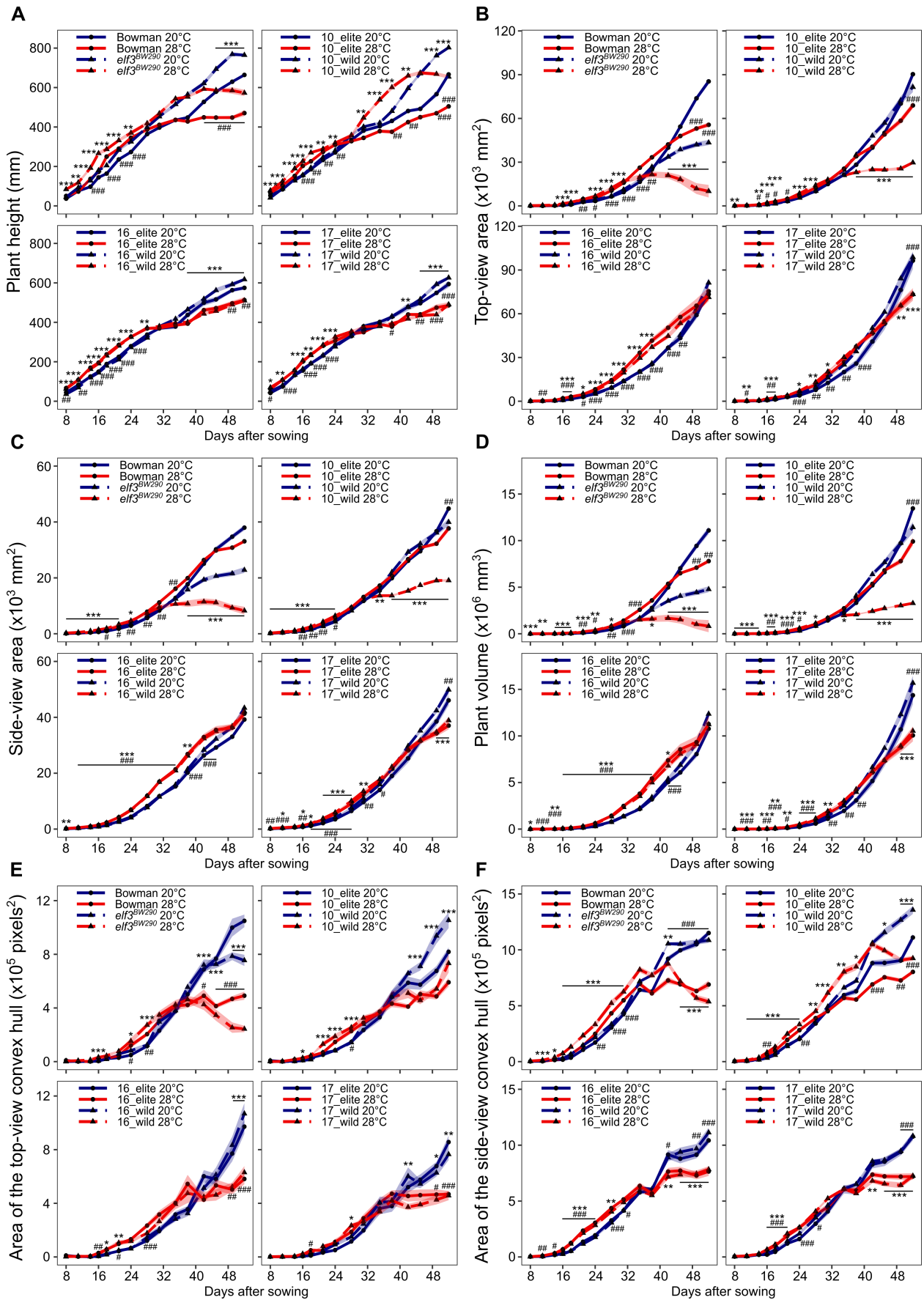


Fig. 5-5 Effects of exotic *ELF3* alleles and elevated temperatures on barley growth and plant architecture.

(A-F) Bowman, *elf3^{BW290}* and HIF pairs were grown in LD (16 h light/ 8 h dark) at day/night temperatures of 20/16°C (20°C). At 5 DAS, seedlings were shifted to 28/24°C (28°C) or were kept at 20°C. Plant height (A, average of two side-views) and plant area from top- (B) and side- (C, average of two side-views) views were obtained using the HTPPheno pipeline. Plant volume (D) was estimated using plant area data from top-view (B) and two side-views (C). Top- (E) and side- (F) view convex hull area was obtained using the Hull & Circle pipeline. Lines represent the mean and ribbons indicate SEM ($n=11$). Hashtags (for Bowman and HIF elite lines with *HvELF3*) and asterisks (for *elf3^{BW290}* and HIF wild lines with *HspELF3*) indicate significant differences between two temperature treatments (# and *, $P<0.05$; ## and **, $P<0.01$; ### and ***, $P<0.001$; two-way ANOVA). The genotypic effect and multiple comparisons are shown in Appendix VI.

However, after around 30 DAS, the positive effect of high temperature on plant height diminished and plants grown at 20°C were of similar size or even taller than those grown at 28°C. Although the time point when the 20°C grown plants surpassed the 28°C grown plants was genotype dependent, at 52 DAS, all genotypes displayed greater plant height at 20°C (Fig. 5-5A). These data are consistent with previously reported negative effects of high temperature on plant height at maturity (Abou-Elwafa and Amein, 2016). Considering the allelic effects of *ELF3*, both the *elf3^{BW290}* mutant and 10_wild allele surpassed their corresponding control lines (Bowman, 10_elite) after 31 and 38 DAS, respectively, under both temperature treatments (Fig. 5-5A). In contrast, in HIF pairs 16 and 17, the elite and exotic *ELF3* alleles did not differ remarkably in plant height, with mainly temperature effects observed.

Similar to plant height, reduced plant area was observed at elevated temperatures at 52 DAS, except for HIF pair 16 showing no temperature effect (Fig. 5-5B). Albeit greater in plant height, the plant area of *elf3^{BW290}* was smaller than Bowman from 45 DAS at 20°C and from 35 DAS at 28°C. However, the plant area of 10_elite and 10_wild plants did not differ at 20°C, but only at 28°C (Fig. 5-5B). In general, from 42 DAS, *elf3^{BW290}* and 10_wild at 28°C displayed lowest plant areas from both top- and side-views among all genotypes (Fig. 5-5B, C). As such, extended elongation growth seems to come at the cost of reduced leaf area for light interception and photosynthesis, which likely depends on *ELF3*. To represent plant biomass, the plant volume was estimated based on the plant areas of top- and two side-views, displaying similar trends as plant areas (Fig. 5-5D).

Interestingly, although the plant area was reduced in *elf3^{BW290}* and 10_wild at 28°C, relatively high convex hull areas were observed from both top- and side-views, especially in 10_wild (Fig. 5-5E, F). The convex hull area represents the smallest area enclosing the whole plant silhouette. Different to plant area, the convex hull area is mainly contributed by leaf length and bolting, representing the expansion of plants. Using both parameters (area and convex

hull area) allowed a more comprehensive description of plant architecture. These observations of reduced plant area but increased or stable convex hull area in *elf3^{BW290}* and 10_wild at 28°C could be a consequence of thinner leaves at 28°C (Fig. 5-3D). This conclusion is generally acceptable as the total tiller number at 52 DAS was not different (in *elf3^{BW290}*, HIF pair 10, 16_elite, and 17_elite) or even higher (in Bowman, 16_wild, and 17_wild) at 28°C (Fig. 5-6). The larger convex hull area is a proxy for a more openly structured habitus of the shoot. From work in *Arabidopsis*, it is known that such loose architectural adjustments promote ventilation and thereby facilitate evaporative leaf cooling at elevated temperatures (Crawford *et al.*, 2012).

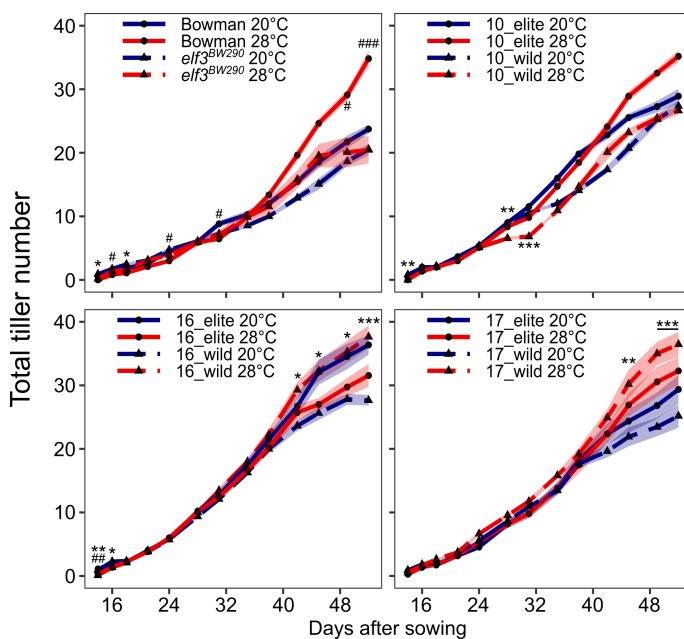


Fig. 5-6 Effects of exotic *ELF3* alleles and elevated temperatures on barley tillering.

Barley seedlings were grown in LD (16 h light/ 8 h dark) at day/night temperatures of 20/16°C (20°C). At 5 DAS, seedlings were shifted to 28/24°C (28°C) or were kept at 20°C. Lines represent the mean and ribbons indicate SEM ($n=11$). Hashtags (for Bowman and HIF elite lines with *HvELF3*) and asterisks (for *elf3^{BW290}* and HIF wild lines with *HspELF3*) indicate significant differences between two temperature treatments (# and *, $P<0.05$; ## and **, $P<0.01$; ### and ***, $P<0.001$; two-way ANOVA). Multiple comparisons are shown in Appendix VI.

To assess the overall phenotypic responses to elevated temperatures during vegetative growth and development, a principal component analysis (PCA) was carried out based on the arithmetic means of all obtained traits (Fig. 5-7A). The first two principal components (PC1 and PC2) accounted for 75.8% of the variance. PC1 separated samples by temperature treatment, whereas PC2 separated samples by genotype. While *elf3^{BW290}* displayed a clear divergence from other genotypes at both temperatures, this separation was observed in 10_wild only at 28°C (Fig. 5-7A). To avoid a potential bias in correlation caused by large amounts of non-significant data as part of the growth curve measured during early vegetative stage, an additional PCA was performed based on the growth curve modeling traits (Fig. 5-7B). Using these traits allowed to tone down the wealth of data and to focus on important time points (e.g., day of maximum increase, day of maximum value,

and end point) as well as general patterns of the growth curves (e.g., total area under the curve) instead of considering all measurement time points identically in the analysis. Again, clustering of *elf3*^{BW290} and 10_wild at 28°C was detected (Fig. 5-7B).

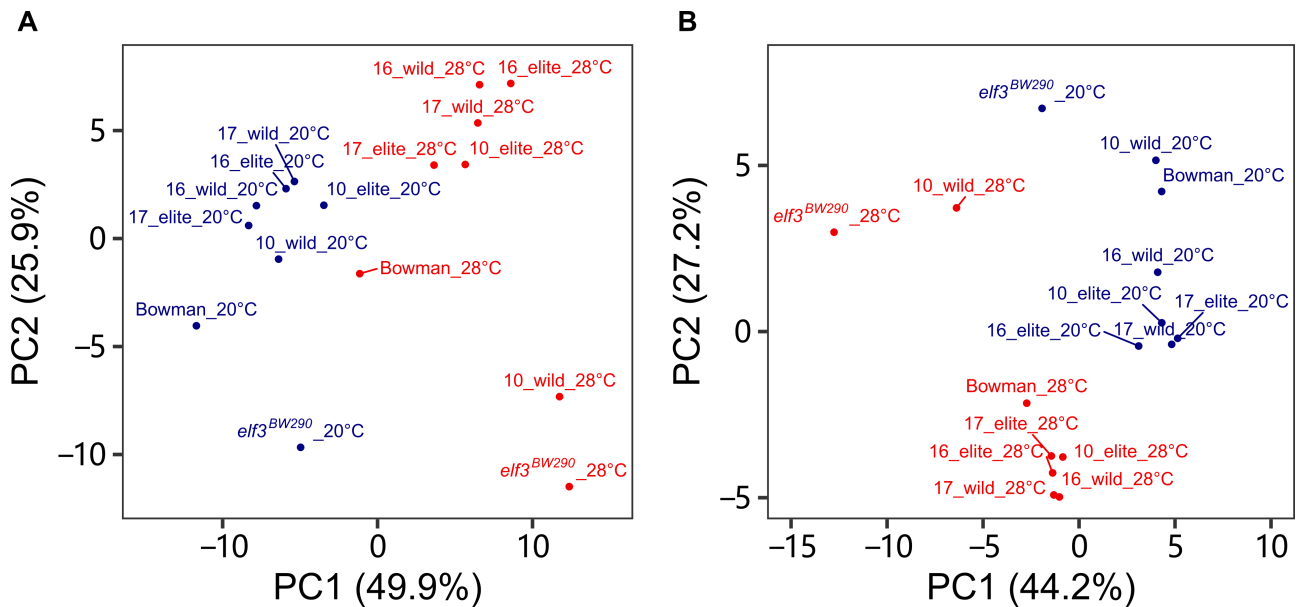


Fig. 5-7 Principal component analysis (PCA) of barley growth traits.

(A, B) PCA was based on the correlation matrix using the arithmetic means of all obtained traits (A), or the derived growth curve modeling traits (B) obtained from temperature assay in growth chambers.

Taken together, these data so far demonstrate that the Syrian *ELF3* allele in HIF pair 10 (10_wild) and *elf3*^{BW290} mutant tend to behave similarly during vegetative growth and development. It can therefore be concluded that *ELF3* in general but also naturally occurring genetic variation in wild barley populations contributes to architectural changes of shoot tissues at elevated temperatures.

5.5 An exotic *ELF3* allele affects barley floral transition at elevated temperatures

The plant life cycle can be divided into distinct phases from germination to senescence. The timing of transition from one phase to the next can be either accelerated or delayed by high temperatures, depending on plant species and temperature regimes, reviewed by Lippmann *et al.* (2019). Therefore, I asked whether exotic *ELF3* alleles are involved in regulating developmental timing of leaf senescence and flowering at elevated temperatures.

As chlorophyll degradation is one of the hallmarks of leaf senescence (Guo *et al.*, 2021), I monitored the chlorophyll content of the second leaf every week during the temperature assay in growth chambers (Fig. 5-8). As expected, all genotypes displayed earlier leaf senescence with reduced chlorophyll content at 28°C compared to 20°C. Independent of *ELF3*, earlier onset of leaf senescence was observed at both temperatures in HIF pairs 16 and 17, indicating an effect of the genetic background in these lines outside of the *ELF3* locus (Fig. 5-8). Consistent with previous reports from various species (Djanaguiraman and Prasad, 2010; Lobell *et al.*, 2012; Shirdelmoghanloo *et al.*, 2016), these data suggest premature leaf senescence at elevated temperatures in barley but argues against a role of *ELF3* in its regulation.

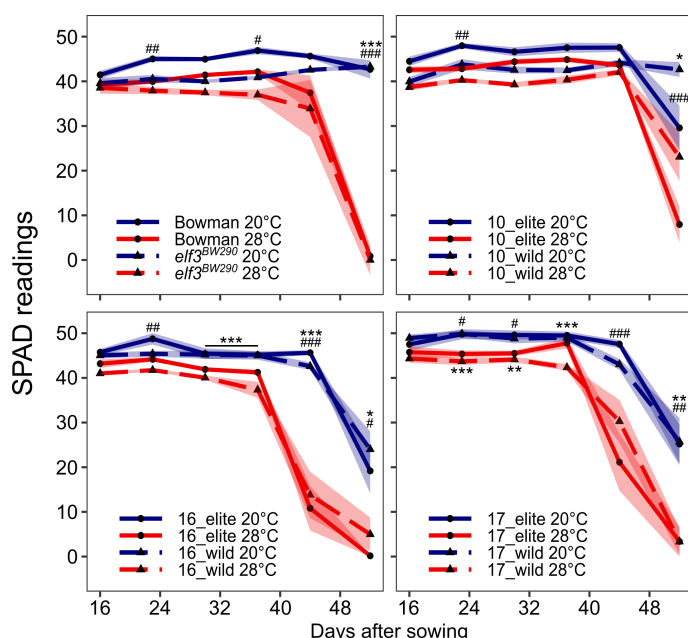


Fig. 5-8 Effects of elevated temperatures on barley leaf chlorophyll content.

Barley seedlings were grown in LD (16 h light/ 8 h dark) at day/night temperatures of 20/16°C (20°C). At 5 DAS, seedlings were shifted to 28/24°C (28°C) or were kept at 20°C. Lines represent the mean and ribbons indicate SEM ($n=11$). Hashtags (for Bowman and HIF elite lines with *HvELF3*) and asterisks (for *elf3^{BW290}* and HIF wild lines with *HspELF3*) indicate significant differences between two temperature treatments (# and *, $P<0.05$; ## and **, $P<0.01$; ### and ***, $P<0.001$; two-way ANOVA). Multiple comparisons are shown in Appendix VI.

Senescence of old leaves enables remobilization and retranslocation of nutrients to newly formed organs (e.g., sink leaves or seeds), and often correlates with the timing of flowering (Kim *et al.*, 2020). To test whether and how barley flowering time is affected by elevated temperatures and *ELF3* alleles, the days until flag leaf sheath opening (BBCH-47, Fig. 5-9A) (Lancashire *et al.*, 1991) and the days until heading as a proxy for flowering time (BBCH-49, Fig. 5-9B) were scored. In contrast to most *Arabidopsis* accessions (Ibañez *et al.*, 2017), but consistent with a previous report in barley (Ejaz and von Korff, 2017), Bowman displayed delayed flag leaf sheath opening and heading at high temperatures, whereas *elf3^{BW290}* displayed the opposite temperature effect (Fig. 5-9A, B). Although 10_elite plants did not finish flowering at both temperatures until the end of the experiment (62 DAS, data therefore

omitted from Fig. 5-9A, B), 10_wild plants flowered much earlier (Fig. 5-9A-C). Interestingly, the flowering time of 10_wild plants was further accelerated by elevated temperatures, displaying an even larger temperature response compared to *elf3^{BW290}* (Fig. 5-9A-C). The early flowering of *elf3^{BW290}* and 10_wild at 28°C indicates early bolting, which could partially explain previously observed architectural changes of these two lines (Figs. 5-5, 5-7). In addition, the flowering time of 17_wild was not temperature dependent (Fig. 5-9A, B), whereas HIF pair 16 and 17_elite did not start showing heading until the end of the experiment (data therefore omitted from Fig. 5-9A, B). Taken together, as in the vast majority of phenotypes the sister lines of HIF pair 10 differed, further analyses focused on these genotypes.

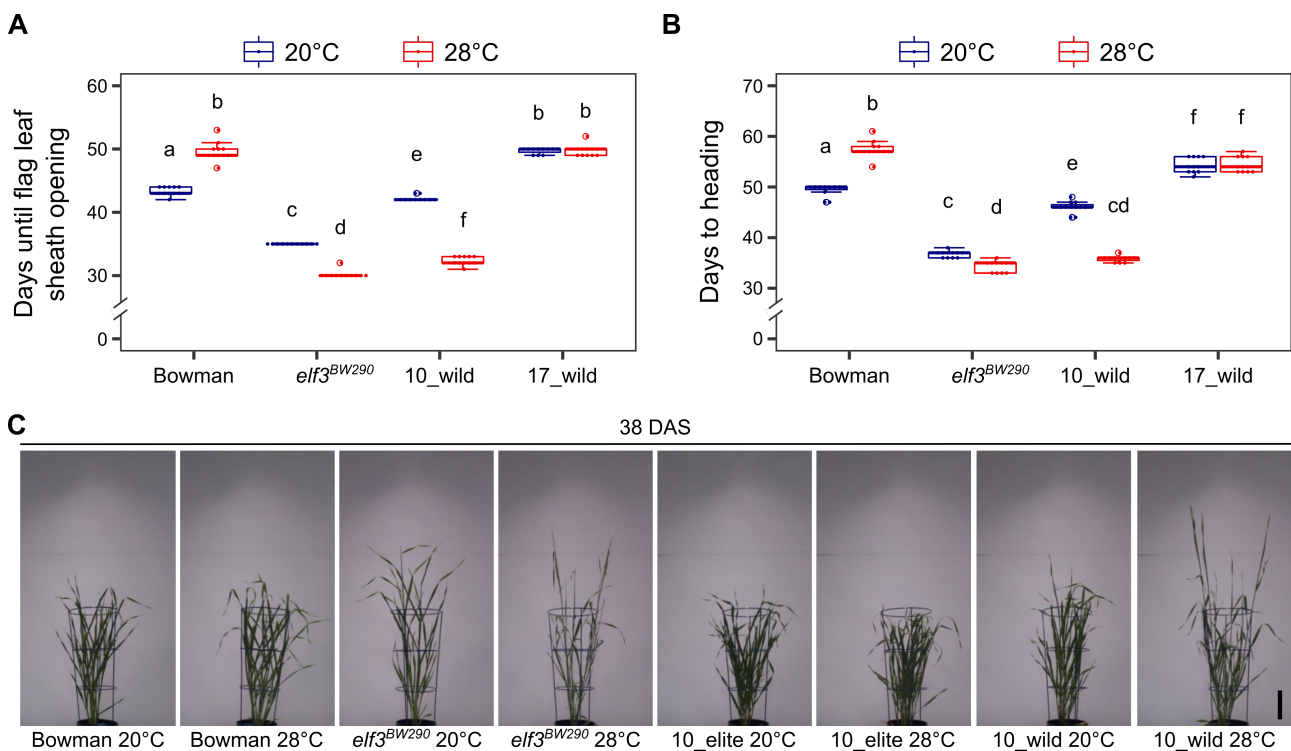


Fig. 5-9 Effects of exotic *ELF3* alleles and elevated temperatures on barley floral transition.

(A-C) Barley seedlings were grown in LD (16 h light/ 8 h dark) at day/night temperatures of 20/16°C (20°C). At 5 DAS, seedlings were shifted to 28/24°C (28°C) or were kept at 20°C. Days until flag leaf sheath opening (A) and heading (B) were scored in the lines showing visible awns before the end of the experiment. Boxes show medians and interquartile ranges. The whiskers extend to 1.5x interquartile ranges. Dots represent the values of individual plants. Different letters above the boxes indicate significant differences (two-way ANOVA and Tukey's HSD test, $P < 0.05$). (C) Representative images of Bowman, *elf3^{BW290}*, 10_elite, and 10_wild plants at 38 DAS. Scale bar = 10 cm.

To better understand the differences in the timing of floral transition between the elite and wild alleles of HIF pair 10, I first assessed the allelic effects on barley meristem development

and found that from 19 DAS, 10_wild plants displayed faster inflorescence development than 10_elite at both temperatures (Fig. 5-10A). In contrast to 10_elite, the meristem development of 10_wild was drastically accelerated by elevated temperatures, consistent with the flowering time results (Fig. 5-9).

Next, to substantiate these observations on the molecular and regulatory levels, the transcriptional behavior of barley floral regulator genes was investigated in leaf samples from the plants used for meristem dissection (Fig. 5-10B). With few exceptions, transcript levels of *Ppd-H1*, *FT1*, and *VRN1* remained largely unaltered by temperature or *ELF3* allele. The exceptions were: 10_elite at 28°C had reduced transcript levels of *Ppd-H1* (19 to 27 DAS) and *VRN1* (27 DAS) compared to 20°C; 20_wild at 28°C displayed reduced transcript levels of *Ppd-H1* and *FT1* at 40 DAS (Fig. 5-10B). As expected, during meristem development, transcript abundance of *BM3* and *BM8* increased in both lines and temperature conditions. However, the onset of *BM3* and *BM8* induction occurred already at 19 DAS in 10_wild at 28°C, which is earlier compared to 10_wild at 20°C and 10_elite (Fig. 5-10B). In line with the time points displaying morphological differences in shoot apical meristems (Fig. 5-10A), 10_wild plants displayed induced expression of *BM3* and *BM8* at 28°C between 19 to 33 DAS, when compared to 10_elite under the same conditions (for *BM3*), or 10_wild at 20°C (for *BM8*) (Fig. 5-10B). Importantly, across development, *ELF3* transcript levels hardly varied between both alleles in most time points. Moreover, ~1.2 kb of promoter sequence upstream of the *ELF3* start codon was identical between both alleles (Zahn *et al.*, 2022, Preprint). These data suggest that the observed phenotypes including the differences in transcript abundance of downstream genes are due to post-transcriptional differences between both alleles, possibly on the level of functional protein.

Together, flowering time data, floral meristem dissection and gene expression analyses demonstrate that the exotic *ELF3* allele in HIF pair 10 (10_wild) accelerates barley floral transition at elevated temperatures, putatively by promoting the transcript levels of floral regulators including *BM3* and *BM8* MADS-box genes.

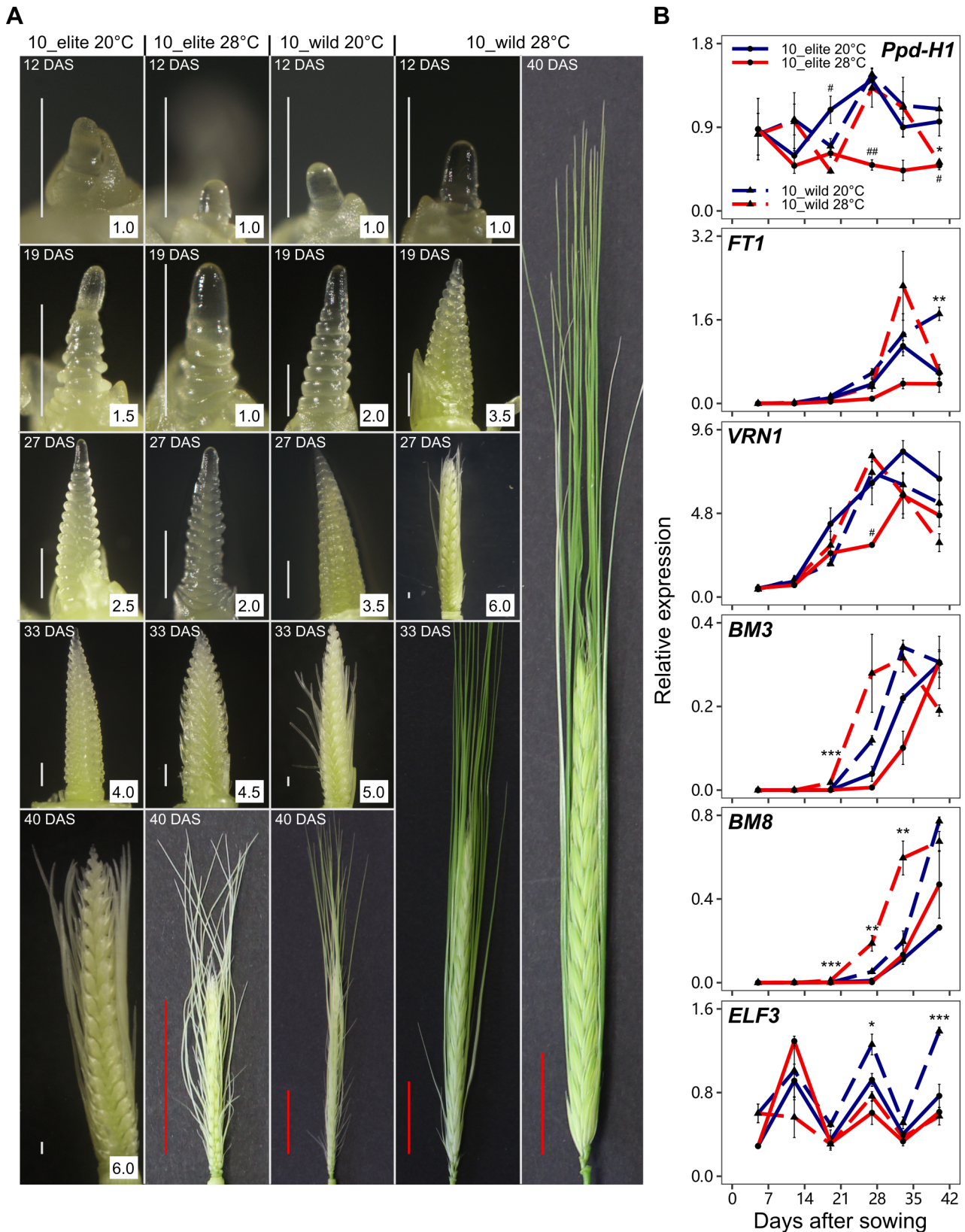


Fig. 5-10 An exotic *ELF3* allele interacts with elevated temperatures to control meristem development and transcript levels of flowering genes.

(A) Representative images of shoot apical meristem and inflorescence in 10_elite and 10_wild plants grown in LD (16 h light/ 8 h dark) at day/night temperatures of 20/16°C (20°C).

At 5 DAS, seedlings were shifted to 28/24°C (28°C) or were kept at 20°C. Three plants were harvested per genotype per temperature at 12, 19, 27, 33, and 40 DAS. Figures in white boxes indicate Waddington scale scores until 6.0. Scale bars, white = 500 µm; red = 2 cm. (B) Transcript levels of barley flowering genes. Leaf samples were harvested at ZT08 during meristem dissection at each time point in (A), as well as at 5 DAS before the start of temperature treatment. Expression levels were normalized to *HvACTIN* and *HvGAPDH*. Error bars indicate the SEM ($n=3$) of three biological replicates. Hashtags (for 10_elite) and asterisks (for 10_wild) indicate significant differences between two temperature treatments (# and *, $P<0.05$; ## and **, $P<0.01$; ### and ***, $P<0.001$; two-way ANOVA). Multiple comparisons are shown in Appendix VI.

5.6 An exotic *ELF3* allele stabilizes total grain weight at elevated temperatures

Under climate change scenarios, crop production and grain yield are predicted to be severely threatened by rising temperatures (Battisti and Naylor, 2009; Asseng *et al.*, 2015). With ambient temperature increased by 7 to 8°C, striking yield losses were observed in barley (Ejaz and von Korff, 2017; Ochagavía *et al.*, 2021). Interestingly, the early flowering mutant *elf3^{BW290}* was reported to maintain seed number at elevated temperatures (Ejaz and von Korff, 2017), thereby representing some sort of increased yield stability. Since (i) the exotic *ELF3* allele in HIF pair 10 (10_wild) behaved like *elf3^{BW290}* in many of the assays performed so far and (ii) to assess the effect of 10_wild on yield components at elevated temperatures, I performed a temperature assay in a greenhouse setting. In this assay, four genotypes (Bowman, *elf3^{BW290}*, and HIF pair 10) were grown in LD with day/night temperatures of 20°C/16°C (20°C treatment) or 28°C/24°C (28°C treatment). To avoid the effects of elevated temperatures on early seedling establishment (Figs. 5-3, 5-4), the temperature treatments started from the three-leaf stage (BBCH-13, 15 to 17 DAS) (Lancashire *et al.*, 1991).

I first examined whether the growth and developmental traits under greenhouse conditions were comparable to the results from the environmentally better controlled growth chamber experiments. Despite the expected generally delayed phase transition under greenhouse conditions, early heading was observed in *elf3^{BW290}* at both temperatures and in 10_wild at 28°C; all four genotypes displayed reduced plant height at elevated temperatures, 118 DAS (Fig. 5-11A, B). Total tiller number was not changed in Bowman but reduced in *elf3^{BW290}* at 28°C, 118 DAS, whereas both lines in HIF pair 10 had more tillers at 28°C than 20°C (Fig. 5-11C). Taken together, although the total tiller number data were different, the vast majority of phenotypes from the growth chambers were reproducible in the greenhouse (Figs. 5-6,

5-9, 5-11A-C). This suggested that documentation of yield related phenotypes in the greenhouse may as well provide reliable insight into the roles of *ELF3* and especially the exotic 10_wild allele.

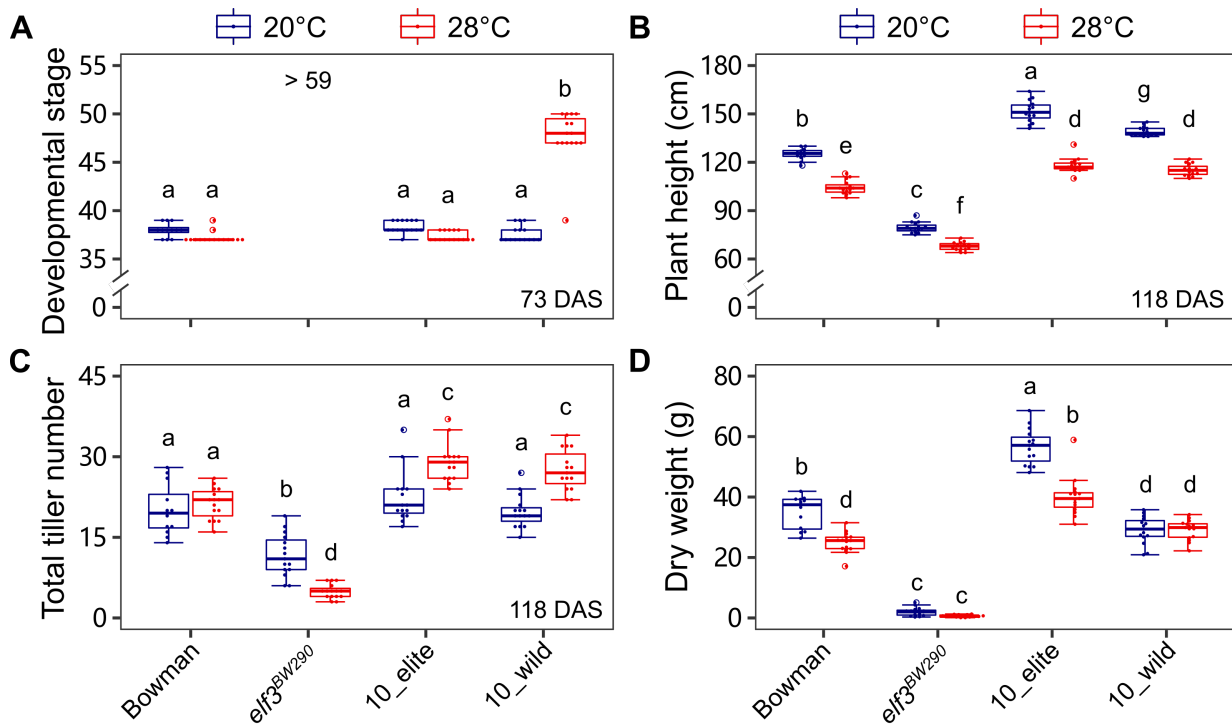


Fig. 5-11 Growth and development phenotypes from temperature assay in greenhouses.

(A-D) Barley seedlings were grown in greenhouse conditions with LD (16 h light/ 8 h dark) and day/night temperatures of 20/16°C (20°C). Plants that reached the three-leaf stage were shifted to 28/24°C (28°C) or were kept at 20°C. The developmental stage (A) was scored at 73 DAS, whereas plant height (B) and total tiller number (C) were scored at 118 DAS. The developmental stage of all *elf3*^{BW290} plants at both temperatures was at BBCH-59 or further at 73 DAS. At maturity, plant dry weight (aerial part, D) was scored. Boxes show medians and interquartile ranges. The whiskers extend to 1.5x interquartile ranges. Dots represent the values of individual plants ($n=12-15$). Different letters above or below the boxes indicate significant differences (two-way ANOVA and Tukey's HSD test, $P<0.05$).

I subsequently measured plant (shoot) dry weight, spike parameters (ear length and grains/florets per spike), and grain parameters (grain number, grain area, thousand grain weight, and grain weight per plant) at maturity. I found plant dry weight to be reduced in Bowman and 10_elite at 28°C, but it was not influenced by temperature in *elf3*^{BW290} and 10_wild (Fig. 5-11D). At both temperatures, plant dry weight was lower in *elf3*^{BW290} and 10_wild when compared to Bowman and 10_elite, respectively.

The ear length (excluding awns) of Bowman and *elf3*^{BW290} was not temperature dependent, with *elf3*^{BW290} having shorter ears than Bowman (Fig. 5-12A). Shorter ears were also

observed in 10_wild compared to 10_elite, but only at elevated temperatures. At 28°C, the number of grains and florets per spike was reduced in all genotypes except *elf3^{BW290}* (Fig. 5-12B, C). Such an *elf3^{BW290}* phenotype was consistent with the previous report by Ejaz and von Korff (2017). While *elf3^{BW290}* had less grains and florets per spike than Bowman under both temperatures, 10_wild only showed reduced numbers at 28°C compared to 10_elite (Fig. 5-12B, C). The ratio of grains and florets per spike was slightly reduced in HIF pair 10 at 28°C (Fig. 5-12D), indicating the negative effects of high temperature on floret fertility as previously reported for wheat (Prasad and Djanaguiraman, 2014).

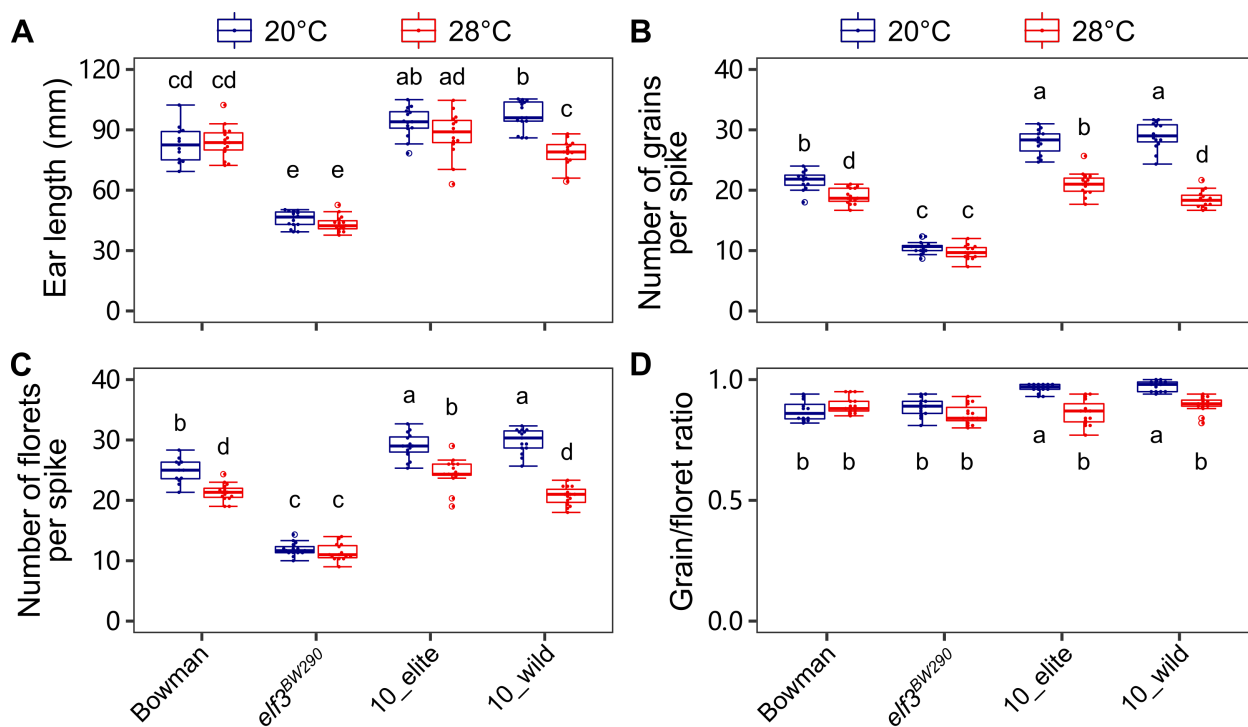


Fig. 5-12 Effects of exotic *ELF3* allele and elevated temperatures on barley spike parameters.

(A-D) Barley seedlings were grown in greenhouse conditions with LD (16 h light/ 8 h dark) and day/night temperatures of 20/16°C (20°C). Plants that reached the three-leaf stage were shifted to 28/24°C (28°C) or were kept at 20°C. At maturity, the spike parameters ear length (A), number of grains (B) and florets (C) per spike, and grain/floret ratio (D) were scored. Boxes show medians and interquartile ranges. The whiskers extend to 1.5x interquartile ranges. Dots represent the values of individual plants ($n=12-15$). Different letters above or below the boxes indicate significant differences (two-way ANOVA and Tukey's HSD test, $P < 0.05$).

The total grain number per plant displayed similar trends as the number of grains per spike, except that 10_wild had reduced total grain number at 20°C (Figs. 5-12B, 5-13A). The grain area was not affected by temperature in Bowman and *elf3^{BW290}*, with *elf3^{BW290}* having smaller

grain area compared to Bowman (Fig. 5-13B). In contrast, 10_elite and 10_wild displayed the same grain area which is reduced at 28°C.

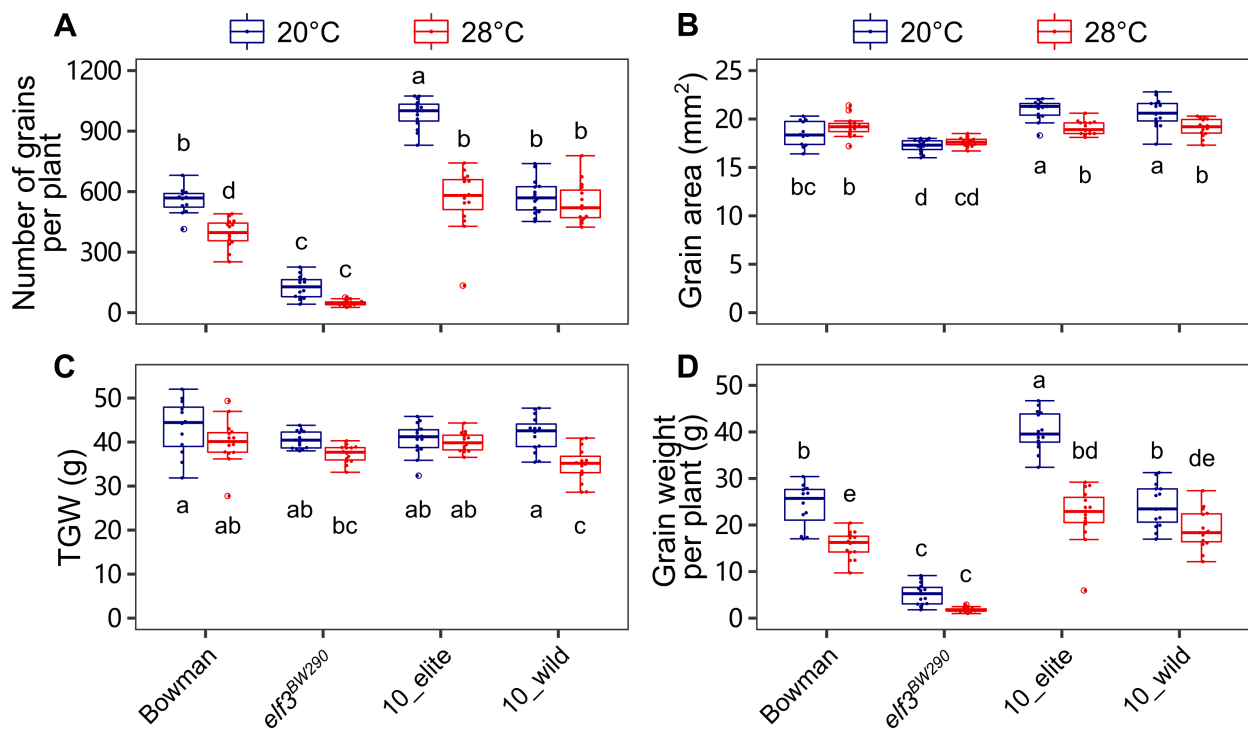


Fig. 5-13 Effects of exotic *ELF3* allele and elevated temperatures on barley yield related parameters.

(A-D) Barley seedlings were grown in greenhouse conditions with LD (16 h light/ 8 h dark) and day/night temperatures of 20/16°C (20°C). Plants that reached the three-leaf stage were shifted to 28/24°C (28°C) or were kept at 20°C. At maturity, number of grains per plant (A) grain area (B), thousand grain weight (C), and grain weight per plant (D) were scored. Boxes show medians and interquartile ranges. The whiskers extend to 1.5x interquartile ranges. Dots represent the values of individual plants ($n=12-15$). Different letters above or below the boxes indicate significant differences (two-way ANOVA and Tukey's HSD test, $P < 0.05$).

The thousand grain weight (TGW) was not affected by temperature in Bowman, *elf3^{BW290}* and 10_elite, whereas 10_wild had reduced TGW at 28°C (Fig. 5-13C). The reduction of TGW in 10_wild resulted in reduced grain weight per plant at 28°C, whereas the total grain weight of the other genotypes was mostly dependent on the number of grains per plant (Fig. 5-13A-D). Although the total grain weight was strikingly reduced in 10_wild at 20°C compared to 10_elite, it was not different at 28°C (Fig. 5-13D). These data suggest that the decrease in total grain weight caused by elevated temperatures is mainly due to reduced grain number, which is mitigated in HIF pair 10 with the exotic *ELF3* allele.

To understand whether these yield related parameters are linked to morphological and/or developmental traits, I analyzed putative correlations of temperature responses amongst

selected traits in Bowman, *elf3^{BW290}*, and HIF pair 10. As expected, high correlations can be observed among traits within similar growth and developmental stages (Fig. 5-14). During the early vegetative growth stage, temperature induced leaf and tiller formation correlated strongly with early plant architectural traits (e.g., convex hull area, area, and volume, 16 DAS). Similarly, temperature-induced reduction in total grain weight strongly correlated with grain number, plant dry weight, and late plant architectural traits (e.g., area and volume, 52 DAS, Fig. 5-14). Moreover, although the temperature response of TGW was not correlated with any other yield related trait, it correlated positively with the response of late plant architectural traits but negatively with the response of early architectural traits (Fig. 5-14). These correlation patterns indicate potential connections of traits in barley response to elevated temperature.

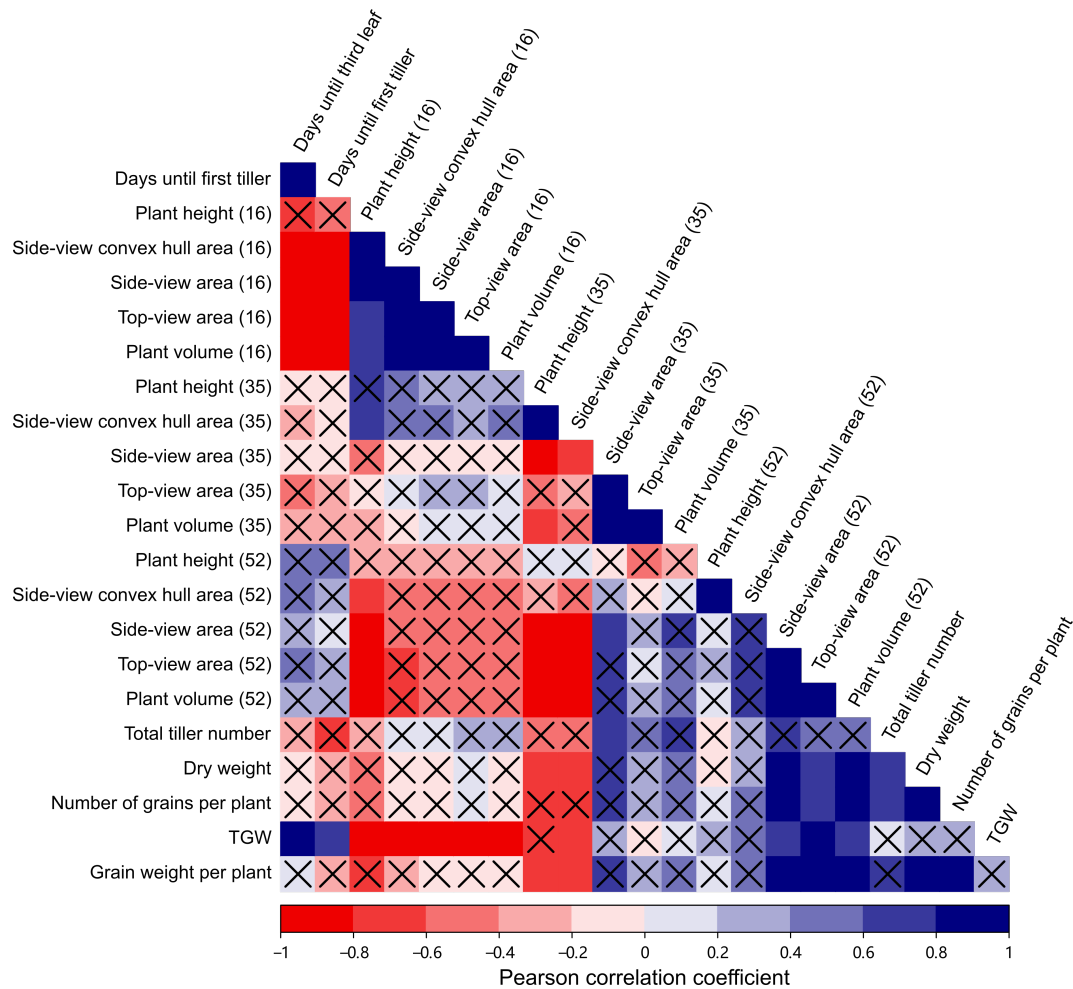


Fig. 5-14 Correlation of temperature responses in selected traits.

Pairwise correlation coefficients were determined for Bowman, *elf3^{BW290}*, and HIF pair 10 between selected growth, developmental, and yield related traits. Numbers in the bracket indicate DAS. Pearson correlation coefficients were tested for significance and only significant coefficients with $P < 0.05$ are not crossed.

In conclusion, these data demonstrate that an exotic barley *ELF3* allele from Syrian origin not only contributes to thermomorphogenic architectural adjustments, but also accelerates floral transition at elevated temperatures, potentially mitigating further yield loss by early flowering which prevents detrimental effects of high temperatures on grain development.

6 Discussion

In the context of global climate change, plant performance, especially yield performance, largely depends on the ability of plants to tackle cyclic light/temperature changes, as well as unpredictable environmental events. Therefore, characterizing the key players involved in plant anticipation, acclimation, and adaptation is a pivotal step to prevent potential yield losses. This work focused on the functions of *ELF3*, regarding plant performance under changing temperatures in *Arabidopsis* and barley.

6.1 Potential functions of *ELF3* polyQ and phase separation

Sensing changes in ambient temperature is the first step in plant thermomorphogenesis. Among the known plant temperature sensors reviewed by Hayes *et al.* (2021), the PrD in *Arabidopsis* *ELF3* mediates liquid-liquid phase separation (LLPS) of *ELF3* to form aggregates at elevated temperatures (Jung *et al.*, 2020). The *ELF3* PrD is featured by polyQ repeats, which vary in length among *Arabidopsis* accessions as investigated in this study (Figs. 3-2, 3-4). I found the probability of PrD existence to be related with the polyQ length in Brassicaceae family (Figs. 3-1, 3-3), whereas the shortest polyQ stretch with the length of 7Q was enough for PrD functions in *Arabidopsis* ecotype Col-0 (Jung *et al.*, 2020). However, the *ELF3* from non-Brassicales species rarely contained polyQ or a predicted PrD (Fig. 3-1). As replacing *Arabidopsis* *ELF3* with *Brachypodium distachyon* *ELF3* that lacks PrD abolished the temperature responsiveness (Jung *et al.*, 2020), these results suggest the temperature sensing ability of *ELF3* PrD is only applicable to a limited number of plant species.

To understand the evolutionary meaning and potential functions of polyQ variation, I next focused on natural *Arabidopsis* accessions. I found that apart from the polyQ variation, the coding sequence of *Arabidopsis* *ELF3* was highly conserved among accessions (Figs. 3-6, 3-7). In the geographic distribution of 319 sequenced *Arabidopsis* accessions, no significant pattern was observed between polyQ length and elevation (Fig. 3-4) or seasonal temperature variations (Fig. 3-5). As closely located accessions are expected to experience similar natural selection pressure, the observations in this study argue against the hypothesis that the polyQ variation is an evolutionary adaptation to varying latitudes or ambient temperatures (Wilkinson and Strader, 2020; Xu *et al.*, 2021).

Furthermore, no promising correlation between polyQ length and temperature responsive hypocotyl phenotypes was detected in the temperature assays using Arabidopsis accessions (Figs. 3-8, 3-9). This is consistent with previous reports using transgenic lines with different polyQ length in two different genetic backgrounds (Press *et al.*, 2016; Jung *et al.*, 2020). Therefore, it can be concluded that the temperature sensing functions of the ELF3 PrD mainly depend on the 'qualitative' existence of polyQ, rather than its 'quantitative' length. However, the potential effects of polyQ length (especially for extremely long polyQ repeats) on the aggregation properties under high temperatures cannot be ruled out. From a physical chemistry point of view, the aggregation properties of polyQ peptides depend on both polyQ length and temperature (Walters and Murphy, 2009; Böker and Paul, 2022). This means the longer the peptide is, the lower the transition temperature is required for its aggregation. For example, a polyQ peptide self-aggregates at a physiological temperature when its chain length is more than 25Q (Böker and Paul, 2022). Whether this also applies to the thermodynamics of ELF3 (which harbors polyQ peptide) needs to be investigated at a molecular level.

Interestingly, compared to temperature response, polyQ variation in ELF3 displayed more prominent correlations with circadian rhythm parameters. In natural Arabidopsis accessions, polyQ lengths were negatively correlated with circadian phase and period (Tajima *et al.*, 2007), whereas in transgenic lines, increase (23Q) or decrease (7Q and 10Q) in polyQ length resulted in higher RAE, compared to the most frequent polyQ length (16Q) (Undurraga *et al.*, 2012). These results suggest that the polyQ stretch (and PrD) mainly contributes to circadian clock functions, with temperature sensing being secondary. This hypothesis may also apply to *ELF3* itself, as the emergence and duplication of *ELF3* occurred much earlier with the other EC components, compared to the emergence of its PrD (Table 1; Fig. 3-1).

And indeed, temperature is just one of the aspects that affect LLPS behavior, reviewed by Xu *et al.* (2021). Besides environmental factors, LLPS also highly depends on the concentration and identities of macromolecules to form membraneless compartments. These compartments include cytoplasmic single-domain aggregations (e.g., purified ELF3 PrD at high temperatures) (Jung *et al.*, 2020), as well as nuclear bodies containing photoreceptors (so-called photobodies) or circadian clock components (Ronald and Davis, 2019). These LLPSs all seem to be related to cellular localization of proteins: in a light and temperature dependent manner, photoreceptor phyB reversibly accumulates as photobodies in the subnuclear compartments (Yamaguchi *et al.*, 1999; Hahm *et al.*, 2020;

Chen *et al.*, 2022); in a time-of-day dependent manner, circadian clock regulators such as ELF3, TOC1 (Wang *et al.*, 2010), ELF4 and GI (Herrero *et al.*, 2012; Kim *et al.*, 2013) (co)localize at nuclear bodies.

Interestingly, recent reports revealed that cellular localization of ELF3 is also responsive to light quality (Ronald *et al.*, 2022), in addition to high ambient temperatures (Ronald and Davis, 2021), further suggesting that the LLPS behavior of ELF3 may not be limited to temperature response. As ELF3 is known to interact with phyB, ELF4, and GI, future work is needed to understand whether and how ELF3 contributes to the LLPS behavior of other proteins and/or protein complexes under various stimuli.

6.2 Arabidopsis *ELF3* is an essential temperature Zeitnehmer

Although plant temperature sensors such as phyB and ELF3 have been identified, it remains unclear how temperature information is integrated in the circadian oscillator. A previous study proposed *ELF3* to be an essential component of the oscillator but dismissed its function as a temperature Zeitnehmer (Thines and Harmon, 2010). These conclusions were based on experiments performed on etiolated seedlings entrained by temperature cycles in darkness. However, under these conditions, (i) phyB is not photoactivated and is absent from the nucleus (Chen *et al.*, 2003); (ii) ELF3 degrades quickly as its accumulation is facilitated by interaction with phyB in light (Liu *et al.*, 2001; Yu *et al.*, 2008; Nieto *et al.*, 2015). As such, the non-responsiveness of the oscillator to temperature cycles could be partially attributed to the absence of both temperature sensors in darkness. On the other hand, a later study highlighted the importance of the EC in clock temperature sensing, based on experiments with different combinations of photoperiod and temperature (Mizuno *et al.*, 2014). However, under the applied experimental settings it was difficult to examine the exact role of *ELF3* in temperature entrainment, as *ELF3* functions as a light Zeitnehmer (Anwer *et al.*, 2020) and is involved in complicated photoperiod-temperature crosstalk (Figs. 4-1, 4-2). Therefore, whether *ELF3* functions as a temperature Zeitnehmer remained unclear.

Using temperature entrainment in continuous light eliminates these complications and provides the best possible condition to investigate the role of *ELF3* in the presence of phyB. Under these conditions, I found that the clock entrainment to temperature cycles requires functional *ELF3*. In *elf3* loss-of-function mutants, the oscillator components failed to properly respond to regular temperature changes (Fig. 4-7), or to sudden temperature pulses (Fig.

4-9). Consequently, clock-controlled physiological processes such as diurnal hypocotyl growth and cotyledon movement were arrhythmic under temperature cycles in *elf3* (Figs. 4-4, 4-5). Moreover, in confirmation of previous observations in etiolated seedlings (Thines and Harmon, 2010), *elf3* mutants failed to generate robust rhythms of key clock genes under temperature cycles in darkness (Fig. 4-8). Together, these data demonstrate that *ELF3* is an essential temperature Zeitnehmer for clock entrainment to temperature cycles.

Interestingly, another temperature sensor *phyB* was not responsible for sensing cyclic temperatures under conditions of this study, as *phyB* loss-of-function mutants displayed rhythmic cotyledon movement under temperature cycles (Fig. 4-6A). Although in this case the temperature sensing can be achieved by *ELF3* PrD, the role of *phyB* in clock-dependent thermomorphogenesis could not be eliminated as *elf3* mutants still displayed intact temperature response under non-cycling conditions (Fig. 4-3). Thus, regarding temperature sensing and signaling transduction, the functional divergence between *phyB* and *ELF3* needs to be further clarified.

6.3 Arabidopsis *ELF3* can function independently of the EC

The functions of Arabidopsis *ELF3* have long been associated with its recruitment of *ELF4* and *LUX* in forming the EC (Fig. 6-1), which acts as a core component of the circadian clock and a transcriptional repressor (Nusinow *et al.*, 2011; Chow *et al.*, 2012). In the EC, *LUX* is required for DNA binding (Onai and Ishiura, 2005), whereas *ELF4* modulates *ELF3* activity and stabilizes this binding property at high temperatures (Herrero *et al.*, 2012; Jung *et al.*, 2020; Silva *et al.*, 2020). However, in temperature entrainment experiments of this study, rhythmic cotyledon movements were detected in the loss-of-function mutants *pcl1* (*lux*) and *elf4* (Fig. 4-6B, C), suggesting that the temperature Zeitnehmer function of *ELF3* is independent of its interaction with *LUX* or *ELF4*.

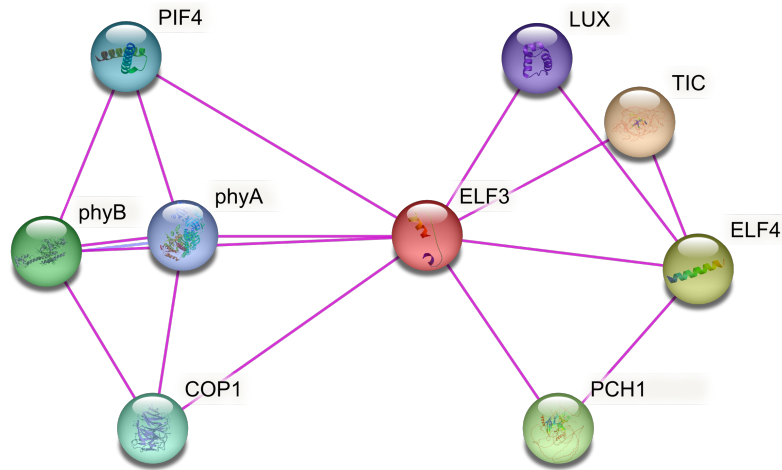


Fig. 6-1 STRING-network for Arabidopsis ELF3 and its interactors.

Arabidopsis ELF3 currently has eight experimentally determined interactors based on the STRING database (Szkarczyk *et al.*, 2021). The minimum interaction score was set as high confidence (0.700).

The EC-independent role of *ELF3* was also observed in ELF3-PIF4 interaction (Fig. 6-1), which prevents PIF4 from transcriptional activation of its target genes (Nieto *et al.*, 2015). This observation was based on the stabilization of ELF3 in light by phyB (Liu *et al.*, 2001), which likely competed with COP1-mediated ELF3 degradation (Yu *et al.*, 2008; Nieto *et al.*, 2022). Other circadian clock related interactors of ELF3 include TIME FOR COFFEE (TIC) (Hall *et al.*, 2003) and PHOTOPERIODIC CONTROL OF HYPOCOTYL1 (PCH1) (Huang *et al.*, 2016) (Fig. 6-1), as well as GI (Yu *et al.*, 2008), CCA1 and SHORT VEGETATIVE PHASE (SVP) (Yoshida *et al.*, 2009) (which were not detected by the STRING database in Fig. 6-1). Furthermore, regarding thermomorphogenesis, recent studies revealed the interactions of ELF3 with BBX18 and BBX23 (Ding *et al.*, 2018), by which BBX18 further recruits XBAT31 and XBAT35, mediating ELF3 degradation (Zhang *et al.*, 2021). As these interactions were (i) based on large and unspecific binding regions in ELF3, (ii) observed under various experimental conditions, and (iii) responsible for different functions of ELF3 in regulating circadian clock and ecophysiology, it is still unknown whether and how they are interconnected (e.g., competitive binding).

6.4 *ELF3* mediates crop domestication

Since it was identified (Hicks *et al.*, 1996), *ELF3* has been extensively studied in the model eudicot Arabidopsis, whereas understanding its functions in other plants especially crop species has just started. Our current knowledge highlights the conserved role of *ELF3* in

crop domestication: a process of plant selection for agriculturally favorable traits aimed for human requirements, rather than survival in natural and uncultivated environments (Chen *et al.*, 2015). Natural variation or loss-of-function in *ELF3* generally affects photoperiodic flowering in various species, including rice (Matsubara *et al.*, 2012; Saito *et al.*, 2012; Andrade *et al.*, 2022), barley (Faure *et al.*, 2012; Zakhrebekova *et al.*, 2012), wheat (Alvarez *et al.*, 2016), soybean (Lu *et al.*, 2017), chickpea (Ridge *et al.*, 2017), garden pea and lentil (Weller *et al.*, 2012). This allows the cultivation of LD crops under short growing seasons, and thereby extends spatial distribution.

As photoperiodic flowering is regulated by the circadian clock, the clock-related functions of *ELF3* are expected to be conserved. And indeed, the expression patterns of both flowering and clock related genes were altered in *ELF3* mutants in various species (Faure *et al.*, 2012; Saito *et al.*, 2012; Weller *et al.*, 2012; Andrade *et al.*, 2022). However, not all functions of *ELF3* were conserved across species. For example, a chickpea *elf3* mutant strongly affecting flowering time had no effect on rhythmic expression of clock genes (Ridge *et al.*, 2017). Similarly, in this study, barley *elf3^{BW289}* mutants showed only slightly altered expression levels of key clock genes and remained to be rhythmic under temperature cycles (Fig. 4-10). Therefore, functional divergence of *ELF3* among species needs to be further elucidated. Furthermore, natural variation of soybean *ELF3* (also known as *J*) displayed an extended vegetative phase, improving yield under SD conditions (Lu *et al.*, 2017). Together, these findings have already made *ELF3* an attractive breeding target in key crops, whereas exploring the regulatory mechanisms of *ELF3* under various environmental stimuli is still necessary for breeding applications.

6.5 *ELF3* is involved in barley thermomorphogenesis

Barley was one of the first crop species for which an *ELF3* homologue/orthologue was identified with strong effects on flowering time regulation (Faure *et al.*, 2012; Zakhrebekova *et al.*, 2012). In my thesis, barley was used as a monocot model, to explore the potential role of *ELF3* in crop thermomorphogenesis. Under elevated temperatures, barley lines displayed increased plant height (Figs. 5-1, 5-3A) and accelerated formation of leaves and tillers (Fig. 5-3C), which were coupled with reduced leaf width (Fig. 5-3D) and the absence of a coleoptile tiller (Fig. 5-4). These observations are consistent with previous reports in barley and wheat (Cannell, 1969; Huang and Taylor, 1993; Abou-Elwafa and Amein, 2016), even comparable to *Arabidopsis* thermomorphogenic phenotypes such as elongation of

hypocotyl and petioles (Quint *et al.*, 2016). Therefore, the general phenotypic responses to elevated temperatures during early vegetative development (thermomorphogenesis) seem to be largely conserved between monocots and eudicots.

During seedling establishment, the *elf3*^{BW290} mutant and the exotic allele 10_wild, which was derived from the HEB-25 mapping population (Maurer *et al.*, 2015), mainly interacted with temperature in controlling elongation growth (Figs. 5-1, 5-3A), again similar to *elf3* mutant phenotypes in *Arabidopsis* (Figs. 4-1, 4-2). However, the regulatory level of thermomorphogenesis in barley remains unclear, as (i) elongation of cereal leaves likely employs different mechanisms than those of eudicots (Fricke, 2002), and (ii) orthologous relationships of *PIF4*, the major thermomorphogenic regulator downstream of *Arabidopsis* *ELF3* (Box *et al.*, 2015; Raschke *et al.*, 2015), are not phylogenetically traceable between *Arabidopsis* and barley.

Upon prolonged exposure to elevated temperatures, plant height, area, and estimated biomass were reduced (Fig. 5-5). In combination with tillering (Fig. 5-6) and accelerated flowering (Fig. 5-9), these phenotypes collectively resulted in architectural changes in the *elf3*^{BW290} mutant and 10_wild (Figs. 5-5, 5-7, 5-9C). Such architectural acclimation can be characterized as well-distributed and distant plant organs (Fig. 5-9C), analogous to the open rosette structure in *Arabidopsis*, which improves leaf cooling and maintains photosynthetic efficiency at high temperatures (Crawford *et al.*, 2012). Interestingly, *elf3*^{BW290} displayed such architecture even at 20°C compared to Bowman (Figs. 5-5, 5-9C), similar to the constitutively thermoresponsive long hypocotyls and petioles in *Arabidopsis* *elf3* mutants at 16-22°C (Figs. 4-1, 4-2) (Jung *et al.*, 2020). These conserved architectural responses across species suggest that *ELF3* might play a similar role in thermomorphogenesis in *Arabidopsis* and cereals. As the cereal *ELF3* generally lacks the PrD (Fig. 3-1), it remains unclear whether temperature sensing functions are also conserved.

6.6 Exotic barley *ELF3* alleles contribute to temperature responsive developmental plasticity

As reproductive development is especially vulnerable to increasing temperature and ultimately accounts for plant yield performance, understanding the mechanisms of temperature responsive flowering contributes to crop adaptation to temperate climates (Fjellheim *et al.*, 2014). Although inflorescence development in barley is generally inhibited by elevated temperatures reviewed by Jacott and Boden (2020) and observed in Bowman,

floral transition was induced early by elevated temperatures in *elf3^{BW290}* and 10_wild (Figs. 5-9, 5-10). The observations of Bowman and *elf3^{BW290}* are highly consistent with a previous report using similar conditions (Ejaz and von Korff, 2017).

In contrast to the loss-of-function mutant *elf3^{BW290}* with truncated ELF3 protein (Zakhrabekova *et al.*, 2012), only a single amino acid substitution differentiates the two alleles of HIF pair 10 (W669G, Fig. 5-2). As transcript levels of *ELF3* between the two sister lines were mostly unchanged under diurnal conditions (Zahn *et al.*, 2022, Preprint) as well as at elevated temperatures (Fig. 5-10B), the W669G substitution may be responsible for functional differences on the protein level. And indeed, the W669G substitution was predicted to affect the secondary structure of ELF3 protein, putatively disturbing protein-protein interactions (Zahn *et al.*, 2022, Preprint).

Therefore, it is important to understand the functional divergence of different *ELF3* alleles in regulating its downstream genes. Under diurnal conditions, *elf3^{BW290}* promoted flowering by relieving the repression of *Ppd-H1* expression, whereas 10_wild induced the transcript levels of *FT1* and *VRN1* without influencing the levels of *Ppd-H1* (Ejaz and von Korff, 2017; Zahn *et al.*, 2022, Preprint). Surprisingly, no temperature effect was observed on the transcript levels of *Ppd-H1*, *FT1*, and *VRN1* during inflorescence development (Fig. 5-10). In contrast, associated with meristem development, the transcript levels of floral inducer MADS-box genes *BM3* and *BM8* were induced early by elevated temperatures exclusively in 10_wild (Fig. 5-10). As down-regulation of *BM3* and *BM8* was reported to be correlated with drought sensitive late flowering (Gol *et al.*, 2021), these observations suggest a convergent responsive pathway to naturally accompanying high temperature and drought. Considering the molecular connection between *ELF3* and *BM3/BM8*, gibberellic acid (GA) is a candidate mediator. It was reported that constitutive early flowering of barley *elf3* mutants is a result of induced GA biosynthesis, which can be blocked by the GA inhibitor paclobutrazol (Boden *et al.*, 2014). In addition, GA might act as an FT1-like mobile florigen (Fig. 1-3) (King and Evans, 2003). In Arabidopsis, GA biosynthesis is induced by high temperatures, and it has been suggested that bioactive GA contributes to thermomorphogenesis by delivering temperature signals from the root to the shoot via one of its precursors (Stavang *et al.*, 2009; Camut *et al.*, 2019). These results may provide insights for future research to study the role of GA in barley temperature response.

Surprisingly and in contrast to the above-described significant phenotypes of HIF pair 10, exotic *ELF3* alleles in HIF pairs 16 and 17 did not show a comparable temperature sensitivity (Figs. 5-5, 5-7), although they carried four more amino acid substitutions in addition to the

W669G replacement in *ELF3* (Fig. 5-2). This discrepancy suggests that the observations in HIF pair 10 rely on the genetic background apart from *ELF3*. And indeed, while HIF pair 10 carries the wild allele of *Ppd-H1*, HIF pairs 16 and 17 have the elite alleles; HIF pair 16 also has the wild allele of *VRN1*, whereas HIF pairs 10 and 17 contain the elite allele (Zahn *et al.*, 2022, Preprint). Thus, the wild *Ppd-H1* in HIF pair 10 is likely a prerequisite for the temperature phenotypes caused by exotic *ELF3*, although its expression did not differ (Figs. 5-9, 5-10). Moreover, the interesting temperature insensitive early flowering of 17_wild could result from the combination of exotic *ELF3* and elite *Ppd-H1* (Fig. 5-9A, B). Likewise, the overall late flowering of HIF pair 16 (did not show heading until the end of the experiment) can be explained by its specific wild *VRN1*. These hypotheses are supported by previous reports showing allelic effects of *Ppd-H1* and *VRN1* in barley temperature responsive flowering (Ejaz and von Korff, 2017; Ochagavía *et al.*, 2021). With varying developmental behaviors observed in exotic variants of *ELF3*, these data again emphasize the important upstream role of *ELF3* in barley floral transition at elevated temperatures. Nevertheless, the potential involvements of photoperiod and vernalization pathways, as well as other circadian clock components (Fig. 1-3) are worth investigating in greater detail.

6.7 Early flowering is an adaptive response under climate change

Besides the scientific interest in the regulatory mechanisms of flowering time, the goal of plant production under global climate change is to prevent yield loss. Generally, negative effects of elevated temperatures were observed on several yield related parameters in barley (Figs. 5-12, 5-13), consistent with previous reports (Dias and Lidon, 2009; Ejaz and von Korff, 2017; Ochagavía *et al.*, 2021). The total grain number was strongly affected by high temperatures in Bowman and 10_elite (Fig. 5-13A). In contrast, the reduction in grain number was not observed in *elf3^{BW290}* and 10_wild, resulting in stabilized total grain weight per plant (Fig. 5-13), which is potentially achieved by the nature of early flowering (Figs. 5-9, 5-10).

Early flowering or early maturing is generally coupled with yield loss, due to reduced leaf area and time available for photosynthetic assimilate production. However, it can also be a strategy of plants to avoid upcoming seasonal stressful conditions such as drought and heat in late spring or summer (Shavrukov *et al.*, 2017). Under global warming scenarios, various species display advanced flowering, and this trend is predicted to continue, indicating early flowering being an adaptive response (Parmesan and Yohe, 2003; Anderson *et al.*, 2012;

Zheng *et al.*, 2016; Büntgen *et al.*, 2022). Providing further evidence, the short life cycle of *elf3^{BW290}* and 10_wild at elevated temperatures was also characterized by open canopy architectures and stabilized total grain weight (Figs. 5-5, 5-9C, 5-13). With early flowering being an evolutionary heat (or drought) escape strategy under climate change (Franks *et al.*, 2007), *ELF3* therefore is a potentially important player contributing to this adaptive response. While the mechanistic consequences of allelic *ELF3* variants require extensive molecular studies, these findings encourage systematic exploitation of this genetic resource for breeding climate resilient crops.

7 Conclusions

This thesis characterized the functions of *ELF3* in Arabidopsis and barley, focusing on its role as a determinant of plant performance under changing temperatures. By identifying *ELF3* homologues and determining ELF3 PrD existence across the plant kingdom, this work traced the emergence of PrD to Brassicales species. Natural variation of ELF3 polyQ among Arabidopsis accessions was investigated, which is not correlated with geographic origins or temperature responsive phenotypes. Based on the infrared time-lapse imaging and genetic analyses under temperature cycles, Arabidopsis *ELF3* was revealed as an essential temperature Zeitnehmer independently of the evening complex. The role of *ELF3* in thermal responsive phenotypes of barley was investigated, using *elf3* loss-of-function alleles and HIF pairs generated from the HEB-25 population. An exotic allele of ELF3 was identified that contributes to plant architectural and developmental acclimation at high ambient temperatures.

8 Summary

Plants have evolved to anticipate and adjust their growth and development responding to environmental changes. To keep the pace of global climate change and to avoid yield loss, understanding the key regulators of plant performance is therefore imperative. This work characterized the functions of *EARLY FLOWERING 3* (*ELF3*) in plant responses to changing temperatures. The evolutionary emergence of *ELF3* temperature sensing prion-like domain (PrD) was traced to Brassicales species, while monocot crops generally lack such a domain in *ELF3*. Although PrDs are likely featured by polyglutamine (polyQ) repeats, the polyQ natural variation among *Arabidopsis thaliana* accessions was not associated with geographic origins or temperature responsive phenotypes. These findings indicate that rather than the length of polyQ, its presence alone is sufficient to contribute to phase separation properties that are potentially not limited to temperature sensing. Linked to its thermosensory functions, *Arabidopsis thaliana ELF3* was revealed as an essential temperature Zeitnehmer (time-taker) that coordinates rhythmic physiological outputs with temperature cycles. Importantly, this function is independent of an intact evening complex. Although these temperature related functions of *ELF3* were largely unknown in crop species, *ELF3* is an important flowering time regulator in crop domestication to short growing seasons. The thermomorphogenic functions of *ELF3* were further explored in barley, a monocot crop model. From a segregating mapping population, an exotic *ELF3* allele was identified playing significant roles in various levels of barley temperature response. Barley plants carrying this allele displayed architectural adjustment and accelerated floral transition at elevated temperatures, which consequently stabilized total grain weight. These results highlight *ELF3* as a determinant of plant performance under changing temperatures and provide insightful information for breeding applications.

9 References

- Abou-Elwafa SF, Amein KA.** 2016. Genetic diversity and potential high temperature tolerance in barley (*Hordeum vulgare*). *World Journal of Agricultural Research* **4**, 1-8.
- Adams S, Manfield I, Stockley P, Carré IA.** 2015. Revised Morning Loops of the *Arabidopsis* Circadian Clock Based on Analyses of Direct Regulatory Interactions. *PLoS One* **10**, e0143943.
- Altschul SF, Gish W, Miller W, Myers EW, Lipman DJ.** 1990. Basic local alignment search tool. *Journal of molecular biology* **215**, 403-410.
- Alvarez M, Tranquilli G, Lewis S, Kippes N, Dubcovsky J.** 2016. Genetic and physical mapping of the earliness per se locus *Eps-A m 1* in *Triticum monococcum* identifies EARLY FLOWERING 3 (ELF3) as a candidate gene. *Functional & Integrative Genomics* **16**, 365-382.
- Anand L, Rodriguez Lopez CM.** 2022. ChromoMap: an R package for interactive visualization of multi-omics data and annotation of chromosomes. *BMC bioinformatics* **23**, 1-9.
- Anderson JT, Inouye DW, McKinney AM, Colautti RI, Mitchell-Olds T.** 2012. Phenotypic plasticity and adaptive evolution contribute to advancing flowering phenology in response to climate change. *Proceedings of the Royal Society B: Biological Sciences* **279**, 3843-3852.
- Andrade L, Lu Y, Cordeiro A, Costa JM, Wigge PA, Saibo NJ, Jaeger KE.** 2022. The evening complex integrates photoperiod signals to control flowering in rice. *Proceedings of the National Academy of Sciences* **119**, e2122582119.
- Anwer MU, Boikoglou E, Herrero E, Hallstein M, Davis AM, James GV, Nagy F, Davis SJ.** 2014. Natural variation reveals that intracellular distribution of ELF3 protein is associated with function in the circadian clock. *eLife* **3**, e02206.
- Anwer MU, Davis A, Davis SJ, Quint M.** 2020. Photoperiod sensing of the circadian clock is controlled by EARLY FLOWERING 3 and GIGANTEA. *The Plant Journal* **101**, 1397-1410.
- Aphalo PJ, Slowikowski K, Mouksassi S.** 2022. Package 'ggpmisc'.
- Asseng S, Ewert F, Martre P, Rötter RP, Lobell DB, Cammarano D, Kimball BA, Ottman MJ, Wall G, White JW.** 2015. Rising temperatures reduce global wheat production. *Nature climate change* **5**, 143-147.
- Avello PA, Davis SJ, Ronald J, Pitchford JW.** 2019. Heat the Clock: Entrainment and Compensation in *Arabidopsis* Circadian Rhythms. *Journal of circadian rhythms* **17**, 5-5.
- Battisti DS, Naylor RL.** 2009. Historical warnings of future food insecurity with unprecedented seasonal heat. *Science* **323**, 240-244.
- Blackman BK.** 2017. Changing responses to changing seasons: natural variation in the plasticity of flowering time. *Plant Physiology* **173**, 16-26.
- Boden SA, Weiss D, Ross JJ, Davies NW, Trevaskis B, Chandler PM, Swain SM.** 2014. EARLY FLOWERING3 regulates flowering in spring barley by mediating gibberellin production and FLOWERING LOCUS T expression. *The Plant Cell* **26**, 1557-1569.
- Böker A, Paul W.** 2022. Thermodynamics and Conformations of Single Polyalanine, Polyserine, and Polyglutamine Chains within the PRIME20 Model. *The Journal of Physical Chemistry B* **126**, 7286-7297.
- Box Mathew S, Huang BE, Domijan M, Jaeger Katja E, Khattak Asif K, Yoo Seong J, Sedivy Emma L, Jones DM, Hearn Timothy J, Webb Alex AR, Grant A, Locke**

- James CW, Wigge Philip A.** 2015. ELF3 Controls Thermoresponsive Growth in Arabidopsis. *Current Biology* **25**.
- Büntgen U, Piermattei A, Krusic PJ, Esper J, Sparks T, Crivellaro A.** 2022. Plants in the UK flower a month earlier under recent warming. *Proceedings of the Royal Society B* **289**, 20212456.
- Campoli C, Shtaya M, Davis SJ, von Korff M.** 2012. Expression conservation within the circadian clock of a monocot: natural variation at barley Ppd-H1 affects circadian expression of flowering time genes, but not clock orthologs. *BMC Plant Biology* **12**, 1-15.
- Camut L, Regnault T, Sirlin-Josserand M, Sakvarelidze-Achard L, Carrera E, Zumsteg J, Heintz D, Leonhardt N, Lange MJP, Lange T.** 2019. Root-derived GA12 contributes to temperature-induced shoot growth in Arabidopsis. *Nature Plants* **5**, 1216-1221.
- Cannell R.** 1969. The tillering pattern in barley varieties: II. The effect of temperature, light intensity and daylength on the frequency of occurrence of the coleoptile node and second tillers in barley. *The Journal of Agricultural Science* **72**, 423-435.
- Challinor AJ, Watson J, Lobell DB, Howden S, Smith D, Chhetri N.** 2014. A meta-analysis of crop yield under climate change and adaptation. *Nature climate change* **4**, 287-291.
- Chen D, Lyu M, Kou X, Li J, Yang Z, Gao L, Li Y, Fan L-m, Shi H, Zhong S.** 2022. Integration of light and temperature sensing by liquid-liquid phase separation of phytochrome B. *Molecular cell* **82**, 3015-3029. e3016.
- Chen M, Schwab R, Chory J.** 2003. Characterization of the requirements for localization of phytochrome B to nuclear bodies. *Proceedings of the National Academy of Sciences* **100**, 14493-14498.
- Chen YH, Gols R, Benrey B.** 2015. Crop domestication and its impact on naturally selected trophic interactions. *Annu. Rev. Entomol* **60**, 35-58.
- Chow BY, Helfer A, Nusinow DA, Kay SA.** 2012. ELF3 recruitment to the PRR9 promoter requires other Evening Complex members in the Arabidopsis circadian clock. *Plant signaling & behavior* **7**, 170-173.
- Clarke E, Sherrill-Mix S.** 2017. Package 'ggbeeswarm'.
- Crawford AJ, McLachlan DH, Hetherington AM, Franklin KA.** 2012. High temperature exposure increases plant cooling capacity. *Current Biology* **22**, R396-R397.
- Dawson IK, Russell J, Powell W, Steffenson B, Thomas WT, Waugh R.** 2015. Barley: a translational model for adaptation to climate change. *New Phytologist* **206**, 913-931.
- Delker C, van Zanten M, Quint M.** 2017. Thermosensing enlightened. *Trends in Plant Science* **22**, 185-187.
- Dias A, Lidon F.** 2009. Evaluation of grain filling rate and duration in bread and durum wheat, under heat stress after anthesis. *Journal of Agronomy and Crop Science* **195**, 137-147.
- Ding L, Wang S, Song Z-T, Jiang Y, Han J-J, Lu S-J, Li L, Liu J-X.** 2018. Two B-box domain proteins, BBX18 and BBX23, interact with ELF3 and regulate thermomorphogenesis in Arabidopsis. *Cell Reports* **25**, 1718-1728. e1714.
- Djanaguiraman M, Prasad PV.** 2010. Ethylene production under high temperature stress causes premature leaf senescence in soybean. *Functional Plant Biology* **37**, 1071-1084.
- Eckardt NA.** 2005. Temperature entrainment of the Arabidopsis circadian clock. *The Plant Cell* **17**, 645-647.
- Edgar RC.** 2004. MUSCLE: multiple sequence alignment with high accuracy and high throughput. *Nucleic acids research* **32**, 1792-1797.
- Ejaz M, von Korff M.** 2017. The genetic control of reproductive development under high ambient temperature. *Plant Physiology* **173**, 294-306.

- Ezer D, Jung J-H, Lan H, Biswas S, Gregoire L, Box MS, Charoensawan V, Cortijo S, Lai X, Stöckle D, Zubieta C, Jaeger KE, Wigge PA.** 2017. The evening complex coordinates environmental and endogenous signals in Arabidopsis. *Nature Plants* **3**, 17087.
- Fan H-C, Ho L-I, Chi C-S, Chen S-J, Peng G-S, Chan T-M, Lin S-Z, Harn H-J.** 2014. Polyglutamine (PolyQ) diseases: genetics to treatments. *Cell transplantation* **23**, 441-458.
- Farré EM, Harmer SL, Harmon FG, Yanovsky MJ, Kay SA.** 2005. Overlapping and distinct roles of PRR7 and PRR9 in the Arabidopsis circadian clock. *Current Biology* **15**, 47-54.
- Faure S, Turner AS, Gruszka D, Christodoulou V, Davis SJ, von Korff M, Laurie DA.** 2012. Mutation at the circadian clock gene EARLY MATURITY 8 adapts domesticated barley (*Hordeum vulgare*) to short growing seasons. *Proceedings of the National Academy of Sciences* **109**, 8328-8333.
- FC M, Davis TL.** 2022. Package 'ggpattern'.
- Feldmann KA.** 1991. T - DNA insertion mutagenesis in Arabidopsis: mutational spectrum. *The Plant Journal* **1**, 71-82.
- Finn RD, Clements J, Eddy SR.** 2011. HMMER web server: interactive sequence similarity searching. *Nucleic acids research* **39**, W29-W37.
- Fjellheim S, Boden S, Trevaskis B.** 2014. The role of seasonal flowering responses in adaptation of grasses to temperate climates. *Frontiers in Plant Science* **5**, 431.
- Ford B, Deng W, Clausen J, Oliver S, Boden S, Hemming M, Trevaskis B.** 2016. Barley (*Hordeum vulgare*) circadian clock genes can respond rapidly to temperature in an EARLY FLOWERING 3-dependent manner. *Journal of Experimental Botany* **67**, 5517-5528.
- Franklin KA, Lee SH, Patel D, Kumar SV, Spartz AK, Gu C, Ye S, Yu P, Breen G, Cohen JD.** 2011. Phytochrome-interacting factor 4 (PIF4) regulates auxin biosynthesis at high temperature. *Proceedings of the National Academy of Sciences* **108**, 20231-20235.
- Franklin KA, Praekelt U, Stoddart WM, Billingham OE, Halliday KJ, Whitlam GC.** 2003. Phytochromes B, D, and E act redundantly to control multiple physiological responses in Arabidopsis. *Plant Physiology* **131**, 1340-1346.
- Franks SJ, Sim S, Weis AE.** 2007. Rapid evolution of flowering time by an annual plant in response to a climate fluctuation. *Proceedings of the National Academy of Sciences* **104**, 1278-1282.
- Fricke W.** 2002. Biophysical limitation of cell elongation in cereal leaves. *Annals of Botany* **90**, 157-167.
- Fujita R, Ueno K, Yamazaki K.** 2000. The development of coleoptile tillers in relation to seedling vigor in early-maturing varieties of spring type wheat. *Plant production science* **3**, 275-280.
- Gasparini K, dos Reis Moreira J, Peres LEP, Zsögön A.** 2021. De novo domestication of wild species to create crops with increased resilience and nutritional value. *Current Opinion in Plant Biology* **60**, 102006.
- Gil KE, Park CM.** 2019. Thermal adaptation and plasticity of the plant circadian clock. *New Phytologist* **221**, 1215-1229.
- Gol L, Haraldsson EB, von Korff M.** 2021. Ppd-H1 integrates drought stress signals to control spike development and flowering time in barley. *Journal of Experimental Botany* **72**, 122-136.
- Goodstein DM, Shu S, Howson R, Neupane R, Hayes RD, Fazo J, Mitros T, Dirks W, Hellsten U, Putnam N.** 2012. Phytozome: a comparative platform for green plant genomics. *Nucleic acids research* **40**, D1178-D1186.

- Guo Y, Ren G, Zhang K, Li Z, Miao Y, Guo H.** 2021. Leaf senescence: Progression, regulation, and application. *Molecular Horticulture* **1**, 1-25.
- Hahm J, Kim K, Qiu Y, Chen M.** 2020. Increasing ambient temperature progressively disassembles Arabidopsis phytochrome B from individual photobodies with distinct thermostabilities. *Nature communications* **11**, 1-14.
- Hall A, Bastow RM, Davis SJ, Hanano S, McWatters HG, Hibberd V, Doyle MR, Sung S, Halliday KJ, Amasino RM.** 2003. The TIME FOR COFFEE gene maintains the amplitude and timing of Arabidopsis circadian clocks. *The Plant Cell* **15**, 2719-2729.
- Harrison PM, Gerstein M.** 2003. A method to assess compositional bias in biological sequences and its application to prion-like glutamine/asparagine-rich domains in eukaryotic proteomes. *Genome Biology* **4**, 1-14.
- Hartmann A, Czauderna T, Hoffmann R, Stein N, Schreiber F.** 2011. HTPPheno: an image analysis pipeline for high-throughput plant phenotyping. *BMC bioinformatics* **12**, 1-9.
- Harwood WA.** 2019. An introduction to barley: the crop and the model. *Barley*: Springer, 1-5.
- Hayes S, Schachtschabel J, Mishkind M, Munnik T, Arisz SA.** 2021. Hot topic: Thermosensing in plants. *Plant, Cell & Environment* **44**, 2018-2033.
- Hemming MN, Walford SA, Fieg S, Dennis ES, Trevaskis B.** 2012. Identification of high-temperature-responsive genes in cereals. *Plant Physiology* **158**, 1439-1450.
- Herrero E, Kolmos E, Bujdoso N, Yuan Y, Wang M, Berns MC, Uhlworm H, Coupland G, Saini R, Jaskolski M, Webb A, Gonçalves J, Davis SJ.** 2012. EARLY FLOWERING4 Recruitment of EARLY FLOWERING3 in the Nucleus Sustains the Arabidopsis Circadian Clock. *The Plant Cell* **24**.
- Herzig P, Maurer A, Draba V, Sharma R, Draicchio F, Bull H, Milne L, Thomas WT, Flavell AJ, Pillen K.** 2018. Contrasting genetic regulation of plant development in wild barley grown in two European environments revealed by nested association mapping. *Journal of Experimental Botany* **69**, 1517-1531.
- Hicks KA, Millar AJ, Carre IA, Somers DE, Straume M, Meeks-Wagner DR, Kay SA.** 1996. Conditional circadian dysfunction of the Arabidopsis early-flowering 3 mutant. *Science* **274**, 790-792.
- Hijmans RJ, Ghosh A, Mandel AM.** 2022. Package 'geodata'.
- Hsu PY, Devisetty UK, Harmer SL.** 2013. Accurate timekeeping is controlled by a cycling activator in Arabidopsis. *eLife* **2**, e00473.
- Huang B, Taylor HM.** 1993. Morphological development and anatomical features of wheat seedlings as influenced by temperature and seeding depth. *Crop Science* **33**, 1269-1273.
- Huang H, Nusinow DA.** 2016. Into the Evening: Complex Interactions in the Arabidopsis Circadian Clock. *Trends in Genetics* **32**, 674-686.
- Huang H, Yoo CY, Bindbeutel R, Goldsworthy J, Tielking A, Alvarez S, Naldrett MJ, Evans BS, Chen M, Nusinow DA.** 2016. PCH1 integrates circadian and light-signaling pathways to control photoperiod-responsive growth in Arabidopsis. *eLife* **5**, e13292.
- Ibañez C, Delker C, Martinez C, Bürstenbinder K, Janitza P, Lippmann R, Ludwig W, Sun H, James GV, Klecker M.** 2018. Brassinosteroids dominate hormonal regulation of plant thermomorphogenesis via BZR1. *Current Biology* **28**, 303-310. e303.
- Ibañez C, Poeschl Y, Peterson T, Bellstädt J, Denk K, Gogol-Döring A, Quint M, Delker C.** 2017. Ambient temperature and genotype differentially affect developmental and phenotypic plasticity in Arabidopsis thaliana. *BMC Plant Biology* **17**, 1-14.
- Jacott CN, Boden SA.** 2020. Feeling the heat: developmental and molecular responses of wheat and barley to high ambient temperatures. *Journal of Experimental Botany* **71**, 5740-5751.

- Jones P, Binns D, Chang H-Y, Fraser M, Li W, McAnulla C, McWilliam H, Maslen J, Mitchell A, Nuka G.** 2014. InterProScan 5: genome-scale protein function classification. *Bioinformatics* **30**, 1236-1240.
- Jung J-H, Barbosa AD, Hutin S, Kumita JR, Gao M, Derwort D, Silva CS, Lai X, Pierre E, Geng F.** 2020. A prion-like domain in ELF3 functions as a thermosensor in *Arabidopsis*. *Nature* **585**, 256-260.
- Jung J-H, Domijan M, Klose C, Biswas S, Ezer D, Gao M, Khattak AK, Box MS, Charoensawan V, Cortijo S.** 2016. Phytochromes function as thermosensors in *Arabidopsis*. *Science* **354**, 886-889.
- Kamioka M, Takao S, Suzuki T, Taki K, Higashiyama T, Kinoshita T, Nakamichi N.** 2016. Direct Repression of Evening Genes by CIRCADIAN CLOCK-ASSOCIATED1 in the *Arabidopsis* Circadian Clock. *The Plant Cell* **28**, 696.
- Kassambara A.** 2020. Package 'ggpubr'. *R package version 0.1*, Vol. 6.
- Kikuchi R, Kawahigashi H, Oshima M, Ando T, Handa H.** 2012. The differential expression of HvCO9, a member of the CONSTANS-like gene family, contributes to the control of flowering under short-day conditions in barley. *Journal of Experimental Botany* **63**, 773-784.
- Kim C, Kim SJ, Jeong J, Park E, Oh E, Park Y-I, Lim PO, Choi G.** 2020. High ambient temperature accelerates leaf senescence via PHYTOCHROME-INTERACTING FACTOR 4 and 5 in *Arabidopsis*. *Molecules and cells* **43**, 645.
- Kim W-Y, Fujiwara S, Suh S-S, Kim J, Kim Y, Han L, David K, Putterill J, Nam HG, Somers DE.** 2007. ZEITLUPE is a circadian photoreceptor stabilized by GIGANTEA in blue light. *Nature* **449**, 356-360.
- Kim Y, Lim J, Yeom M, Kim H, Kim J, Wang L, Kim WY, Somers DE, Nam HG.** 2013. ELF4 regulates GIGANTEA chromatin access through subnuclear sequestration. *Cell Reports* **3**, 671-677.
- King RW, Evans LT.** 2003. Gibberellins and flowering of grasses and cereals: prizing open the lid of the "florigen" black box. *Annual Review of Plant Biology* **54**, 307.
- Koini MA, Alvey L, Allen T, Tilley CA, Harberd NP, Whitelam GC, Franklin KA.** 2009. High temperature-mediated adaptations in plant architecture require the bHLH transcription factor PIF4. *Current Biology* **19**, 408-413.
- Kumar S, Stecher G, Suleski M, Hedges SB.** 2017. TimeTree: a resource for timelines, timetrees, and divergence times. *Molecular biology and evolution* **34**, 1812-1819.
- Kumar SV, Lucyshyn D, Jaeger KE, Alós E, Alvey E, Harberd NP, Wigge PA.** 2012. Transcription factor PIF4 controls the thermosensory activation of flowering. *Nature* **484**, 242-245.
- Laitinen RA, Nikoloski Z.** 2019. Genetic basis of plasticity in plants. *Journal of Experimental Botany* **70**, 739-745.
- Lancashire PD, Bleiholder H, Boom TVD, Langelüddeke P, Stauss R, Weber E, Witzemberger A.** 1991. A uniform decimal code for growth stages of crops and weeds. *Annals of applied Biology* **119**, 561-601.
- Lancaster AK, Nutter-Upham A, Lindquist S, King OD.** 2014. PLAAC: a web and command-line application to identify proteins with prion-like amino acid composition. *Bioinformatics* **30**, 2501-2502.
- Larsson A.** 2014. AliView: a fast and lightweight alignment viewer and editor for large datasets. *Bioinformatics* **30**, 3276-3278.
- Legris M, Klose C, Burgie ES, Rojas CCR, Neme M, Hiltbrunner A, Wigge PA, Schäfer E, Vierstra RD, Casal JJ.** 2016. Phytochrome B integrates light and temperature signals in *Arabidopsis*. *Science* **354**, 897-900.

- Leng G, Huang M.** 2017. Crop yield response to climate change varies with crop spatial distribution pattern. *Scientific Reports* **7**, 1-10.
- Letunic I, Bork P.** 2007. Interactive Tree Of Life (iTOL): an online tool for phylogenetic tree display and annotation. *Bioinformatics* **23**, 127-128.
- Li C, Lin H, Dubcovsky J.** 2015. Factorial combinations of protein interactions generate a multiplicity of florigen activation complexes in wheat and barley. *The Plant Journal* **84**, 70-82.
- Liang Y, Richards R.** 1994. Coleoptile tiller development is associated with fast early vigour in wheat. *Euphytica* **80**, 119-124.
- Lincoln C, Britton JH, Estelle M.** 1990. Growth and development of the axr1 mutants of *Arabidopsis*. *The Plant Cell* **2**, 1071-1080.
- Linde AM, Eklund DM, Kubota A, Pederson ER, Holm K, Gyllenstrand N, Nishihama R, Cronberg N, Muranaka T, Oyama T.** 2017. Early evolution of the land plant circadian clock. *New Phytologist* **216**, 576-590.
- Lippmann R, Babben S, Menger A, Delker C, Quint M.** 2019. Development of wild and cultivated plants under global warming conditions. *Current Biology* **29**, R1326-R1338.
- Liu XL, Covington MF, Fankhauser C, Chory J, Wagner DR.** 2001. ELF3 encodes a circadian clock-regulated nuclear protein that functions in an *Arabidopsis* PHYB signal transduction pathway. *The Plant Cell* **13**, 1293-1304.
- Lobell DB, Sibley A, Ivan Ortiz-Monasterio J.** 2012. Extreme heat effects on wheat senescence in India. *Nature climate change* **2**, 186-189.
- Lohraseb I, Collins NC, Parent B.** 2017. Diverging temperature responses of CO₂ assimilation and plant development explain the overall effect of temperature on biomass accumulation in wheat leaves and grains. *AoB Plants* **9**, plw092.
- Lu S, Zhao X, Hu Y, Liu S, Nan H, Li X, Fang C, Cao D, Shi X, Kong L.** 2017. Natural variation at the soybean J locus improves adaptation to the tropics and enhances yield. *Nature genetics* **49**, 773-779.
- Lu SX, Webb CJ, Knowles SM, Kim SHJ, Wang Z, Tobin EM.** 2012. CCA1 and ELF3 Interact in the Control of Hypocotyl Length and Flowering Time in *Arabidopsis*. *Plant Physiology* **158**, 1079-1088.
- Matasci N, Hung L-H, Yan Z, Carpenter EJ, Wickett NJ, Mirarab S, Nguyen N, Warnow T, Ayyampalayam S, Barker M.** 2014. Data access for the 1,000 Plants (1KP) project. *Gigascience* **3**, 2047-2217X-2043-2017.
- Matsubara K, Ogiso-Tanaka E, Hori K, Ebana K, Ando T, Yano M.** 2012. Natural variation in Hd17, a homolog of *Arabidopsis* ELF3 that is involved in rice photoperiodic flowering. *Plant and Cell Physiology* **53**, 709-716.
- Maurer A, Draba V, Jiang Y, Schnaithmann F, Sharma R, Schumann E, Kilian B, Reif JC, Pillen K.** 2015. Modelling the genetic architecture of flowering time control in barley through nested association mapping. *BMC genomics* **16**, 1-12.
- Maurer A, Draba V, Pillen K.** 2016. Genomic dissection of plant development and its impact on thousand grain weight in barley through nested association mapping. *Journal of Experimental Botany* **67**, 2507-2518.
- McClung CR.** 2006. Plant circadian rhythms. *The Plant Cell* **18**, 792-803.
- McWatters HG, Bastow RM, Hall A, Millar AJ.** 2000. The ELF3 zeitnehmer regulates light signalling to the circadian clock. *Nature* **408**, 716-720.
- Millar AJ, Carre IA, Strayer CA, Chua N-H, Kay SA.** 1995. Circadian clock mutants in *Arabidopsis* identified by luciferase imaging. *Science* **267**, 1161-1163.
- Miller MA, Pfeiffer W, Schwartz T.** 2012. The CIPRES science gateway: enabling high-impact science for phylogenetics researchers with limited resources. *Proceedings of*

the 1st Conference of the Extreme Science and Engineering Discovery Environment: Bridging from the extreme to the campus and beyond, 1-8.

- Mizuno T, Nomoto Y, Oka H, Kitayama M, Takeuchi A, Tsubouchi M, Yamashino T.** 2014. Ambient Temperature Signal Feeds into the Circadian Clock Transcriptional Circuitry Through the EC Night-Time Repressor in *Arabidopsis thaliana*. *Plant and Cell Physiology* **55**, 958-976.
- Müller LM, Mombaerts L, Pankin A, Davis SJ, Webb AA, Goncalves J, von Korff M.** 2020. Differential effects of day/night cues and the circadian clock on the barley transcriptome. *Plant Physiology* **183**, 765-779.
- Nakamichi N, Kiba T, Henriques R, Mizuno T, Chua N-H, Sakakibara H.** 2010. PSEUDO-RESPONSE REGULATORS 9, 7, and 5 Are Transcriptional Repressors in the *Arabidopsis* Circadian Clock. *The Plant Cell* **22**, 594-605.
- Newton AC, Flavell AJ, George TS, Leat P, Mullholland B, Ramsay L, Revoredo-Giha C, Russell J, Steffenson BJ, Swanston JS.** 2011. Crops that feed the world 4. Barley: a resilient crop? Strengths and weaknesses in the context of food security. *Food security* **3**, 141-178.
- Nguyen L-T, Schmidt HA, Von Haeseler A, Minh BQ.** 2015. IQ-TREE: a fast and effective stochastic algorithm for estimating maximum-likelihood phylogenies. *Molecular biology and evolution* **32**, 268-274.
- Nieto C, Catalán P, Luengo LM, Legris M, López-Salmerón V, Davière JM, Casal JJ, Ares S, Prat S.** 2022. COP1 dynamics integrate conflicting seasonal light and thermal cues in the control of *Arabidopsis* elongation. *Science Advances* **8**, eabp8412.
- Nieto C, López-Salmerón V, Davière J-M, Prat S.** 2015. ELF3-PIF4 interaction regulates plant growth independently of the Evening Complex. *Current Biology* **25**, 187-193.
- Ning Y, Shi X, Wang R, Fan J, Park CH, Zhang C, Zhang T, Ouyang X, Li S, Wang G-L.** 2015. OsELF3-2, an ortholog of *Arabidopsis* ELF3, interacts with the E3 ligase APIP6 and negatively regulates immunity against *Magnaporthe oryzae* in rice. *Molecular Plant* **8**, 1679-1682.
- Niwa Y, Yamashino T, Mizuno T.** 2009. The circadian clock regulates the photoperiodic response of hypocotyl elongation through a coincidence mechanism in *Arabidopsis thaliana*. *Plant and Cell Physiology* **50**, 838-854.
- Nohales MA, Kay SA.** 2016. Molecular mechanisms at the core of the plant circadian oscillator. *Nature Structural & Molecular Biology* **23**, 1061-1069.
- Nozue K, Covington MF, Duek PD, Lorrain S, Fankhauser C, Harmer SL, Maloof JN.** 2007. Rhythmic growth explained by coincidence between internal and external cues. *Nature* **448**, 358-361.
- Nusinow DA, Helfer A, Hamilton EE, King JJ, Imaizumi T, Schultz TF, Farre EM, Kay SA.** 2011. The ELF4-ELF3-LUX complex links the circadian clock to diurnal control of hypocotyl growth. *Nature* **475**, 398-402.
- Ochagavía H, Kiss T, Karsai I, Casas AM, Igartua E.** 2021. Responses of Barley to High Ambient Temperature Are Modulated by Vernalization. *Frontiers in Plant Science* **12**.
- Onai K, Ishiura M.** 2005. PHYTOCLOCK 1 encoding a novel GARP protein essential for the *Arabidopsis* circadian clock. *Genes to Cells* **10**, 963-972.
- Park DH, Somers DE, Kim YS, Choy YH, Lim HK, Soh MS, Kim HJ, Kay SA, Nam HG.** 1999. Control of circadian rhythms and photoperiodic flowering by the *Arabidopsis* GIGANTEA gene. *Science* **285**, 1579-1582.
- Park Y-J, Lee H-J, Gil K-E, Kim JY, Lee J-H, Lee H, Cho H-T, Vu LD, De Smet I, Park C-M.** 2019. Developmental programming of thermonastic leaf movement. *Plant Physiology* **180**, 1185-1197.

- Parmesan C, Yohe G.** 2003. A globally coherent fingerprint of climate change impacts across natural systems. *Nature* **421**, 37-42.
- Pörtner HO, Roberts DC, Adams H, Adler C, Aldunce P, Ali E, Begum RA, Betts R, Kerr RB, Biesbroek R.** 2022. Climate change 2022: impacts, adaptation and vulnerability.
- Prasad PV, Djanaguiraman M.** 2014. Response of floret fertility and individual grain weight of wheat to high temperature stress: sensitive stages and thresholds for temperature and duration. *Functional Plant Biology* **41**, 1261-1269.
- Press MO, Lanctot A, Queitsch C.** 2016. ELF3 polyQ variation in *Arabidopsis thaliana* reveals PIF4-independent role in thermoresponsive flowering. *bioRxiv*, 038257.
- Quint M, Delker C, Franklin KA, Wigge PA, Halliday KJ, Zanten M.** 2016. Molecular and genetic control of plant thermomorphogenesis. *Nature Plants* **2**.
- R Core Team.** 2013. R: A language and environment for statistical computing.
- Raschke A, Ibanez C, Ullrich K, Anwer M, Becker S, Glockner A, Trenner J, Denk K, Saal B, Sun X, Ni M, Davis S, Delker C, Quint M.** 2015. Natural variants of ELF3 affect thermomorphogenesis by transcriptionally modulating PIF4-dependent auxin response genes. *BMC Plant Biology* **15**, 197.
- Ridge S, Deokar A, Lee R, Daba K, Macknight RC, Weller JL, Tar'an B.** 2017. The chickpea Early Flowering 1 (Efl1) locus is an ortholog of *Arabidopsis* ELF3. *Plant Physiology* **175**, 802-815.
- Ronald J, Davis SJ.** 2019. Focusing on the nuclear and subnuclear dynamics of light and circadian signalling. *Plant, Cell & Environment* **42**, 2871-2884.
- Ronald J, Davis SJ.** 2021. *Arabidopsis* ELF3 sub-nuclear localization responds to changes in ambient temperature. *Plant Physiology*.
- Ronald J, Su C, Wang L, Davis SJ.** 2022. Cellular localization of *Arabidopsis* EARLY FLOWERING3 is responsive to light quality. *Plant Physiology*.
- Rozas J, Ferrer-Mata A, Sánchez-DelBarrio JC, Guirao-Rico S, Librado P, Ramos-Onsins SE, Sánchez-Gracia A.** 2017. DnaSP 6: DNA sequence polymorphism analysis of large data sets. *Molecular biology and evolution* **34**, 3299-3302.
- Russell J, Dawson IK, Flavell AJ, Steffenson B, Weltzien E, Booth A, Ceccarelli S, Grando S, Waugh R.** 2011. Analysis of >1000 single nucleotide polymorphisms in geographically matched samples of landrace and wild barley indicates secondary contact and chromosome - level differences in diversity around domestication genes. *New Phytologist* **191**, 564-578.
- Saito H, Ogiso-Tanaka E, Okumoto Y, Yoshitake Y, Izumi H, Yokoo T, Matsubara K, Hori K, Yano M, Inoue H.** 2012. E7 encodes an ELF3-like protein and promotes rice flowering by negatively regulating the floral repressor gene *Ghd7* under both short-and long-day conditions. *Plant and Cell Physiology* **53**, 717-728.
- Salomé PA, McClung CR.** 2005. PSEUDO-RESPONSE REGULATOR 7 and 9 Are Partially Redundant Genes Essential for the Temperature Responsiveness of the *Arabidopsis* Circadian Clock. *The Plant Cell* **17**, 791-803.
- Salomé PA, Weigel D, McClung CR.** 2010. The role of the *Arabidopsis* morning loop components CCA1, LHY, PRR7, and PRR9 in temperature compensation. *The Plant Cell* **22**, 3650-3661.
- Shavrukov Y, Kurishbayev A, Jatayev S, Shvidchenko V, Zotova L, Koekemoer F, De Groot S, Soole K, Langridge P.** 2017. Early flowering as a drought escape mechanism in plants: how can it aid wheat production? *Frontiers in Plant Science* **8**, 1950.
- Shirdelmoghanloo H, Taylor JD, Lohraseb I, Rabie H, Brien C, Timmins A, Martin P, Mather DE, Emebiri L, Collins NC.** 2016. A QTL on the short arm of wheat (*Triticum*

- aestivum L.) chromosome 3B affects the stability of grain weight in plants exposed to a brief heat shock early in grain filling. *BMC Plant Biology* **16**, 1-15.
- Silva CS, Nayak A, Lai X, Hutin S, Hugouvieux V, Jung J-H, López-Vidriero I, Franco-Zorrilla JM, Panigrahi KC, Nanao MH.** 2020. Molecular mechanisms of Evening Complex activity in Arabidopsis. *Proceedings of the National Academy of Sciences* **117**, 6901-6909.
- Slowikowski K, Schep A, Hughes S, Lukauskas S, Irisson J-O, Kamvar ZN, Ryan T, Christophe D, Hiroaki Y, Gramme P.** 2018. Package 'ggrepel'. *Automatically position non-overlapping text labels with 'ggplot2*.
- Soetaert K.** 2021. Package 'plot3D'.
- Stavang JA, Gallego - Bartolomé J, Gómez MD, Yoshida S, Asami T, Olsen JE, García - Martínez JL, Alabadí D, Blázquez MA.** 2009. Hormonal regulation of temperature - induced growth in Arabidopsis. *The Plant Journal* **60**, 589-601.
- Szklarczyk D, Gable AL, Nastou KC, Lyon D, Kirsch R, Pyysalo S, Doncheva NT, Legeay M, Fang T, Bork P.** 2021. The STRING database in 2021: customizable protein-protein networks, and functional characterization of user-uploaded gene/measurement sets. *Nucleic acids research* **49**, D605-D612.
- Tajima F.** 1989. Statistical method for testing the neutral mutation hypothesis by DNA polymorphism. *Genetics* **123**, 585-595.
- Tajima T, Oda A, Nakagawa M, Kamada H, Mizoguchi T.** 2007. Natural variation of polyglutamine repeats of a circadian clock gene ELF3 in Arabidopsis. *Plant biotechnology* **24**, 237-240.
- Thines B, Harmon FG.** 2010. Ambient temperature response establishes ELF3 as a required component of the core Arabidopsis circadian clock. *Proceedings of the National Academy of Sciences* **107**, 3257-3262.
- Thomas B, Vince-Prue D.** 1996. *Photoperiodism in plants*: Elsevier.
- Tovar JC, Hoyer JS, Lin A, Tielking A, Callen ST, Elizabeth Castillo S, Miller M, Tessman M, Fahlgren N, Carrington JC.** 2018. Raspberry Pi-powered imaging for plant phenotyping. *Applications in Plant Sciences* **6**, e1031.
- Trevaskis B, Tadege M, Hemming MN, Peacock WJ, Dennis ES, Sheldon C.** 2007. Short vegetative phase-like MADS-box genes inhibit floral meristem identity in barley. *Plant Physiology* **143**, 225-235.
- Tseng T-S, Salomé PA, McClung CR, Olszewski NE.** 2004. SPINDLY and GIGANTEA interact and act in Arabidopsis thaliana pathways involved in light responses, flowering, and rhythms in cotyledon movements. *The Plant Cell* **16**, 1550-1563.
- Turner A, Beales J, Faure S, Dunford RP, Laurie DA.** 2005. The pseudo-response regulator Ppd-H1 provides adaptation to photoperiod in barley. *Science* **310**, 1031-1034.
- Undurraga SF, Press MO, Legendre M, Bujdoso N, Bale J, Wang H, Davis SJ, Verstrepen KJ, Queitsch C.** 2012. Background-dependent effects of polyglutamine variation in the Arabidopsis thaliana gene ELF3. *Proceedings of the National Academy of Sciences* **109**, 19363-19367.
- van Zanten M, Voesenek LA, Peeters AJ, Millenaar FF.** 2009. Hormone-and light-mediated regulation of heat-induced differential petiole growth in Arabidopsis. *Plant Physiology* **151**, 1446-1458.
- Walters RH, Murphy RM.** 2009. Examining polyglutamine peptide length: a connection between collapsed conformations and increased aggregation. *Journal of molecular biology* **393**, 978-992.
- Wang L, Fujiwara S, Somers DE.** 2010. PRR5 regulates phosphorylation, nuclear import and subnuclear localization of TOC1 in the Arabidopsis circadian clock. *The EMBO Journal* **29**, 1903-1915.

- Wang S, Steed G, Webb AA.** 2022. Circadian entrainment in Arabidopsis. *Plant Physiology* **190**, 981-993.
- Waterhouse AM, Procter JB, Martin DM, Clamp M, Barton GJ.** 2009. Jalview Version 2—a multiple sequence alignment editor and analysis workbench. *Bioinformatics* **25**, 1189-1191.
- Wei T, Simko V, Levy M, Xie Y, Jin Y, Zemla J.** 2017. Package 'corrplot'. *Statistician* **56**, e24.
- Weigel D, Mott R.** 2009. The 1001 genomes project for Arabidopsis thaliana. *Genome Biology* **10**, 1-5.
- Weller JL, Liew LC, Hecht VF, Rajandran V, Laurie RE, Ridge S, Wenden B, Vander Schoor JK, Jaminon O, Blassiau C.** 2012. A conserved molecular basis for photoperiod adaptation in two temperate legumes. *Proceedings of the National Academy of Sciences* **109**, 21158-21163.
- Wickham H, Chang W, Wickham MH.** 2016. Package 'ggplot2'. *Create elegant data visualisations using the grammar of graphics. Version, Vol. 2*, 1-189.
- Wilkinson EG, Strader LC.** 2020. A Prion-based thermosensor in plants. *Molecular cell* **80**, 181-182.
- Xia T, Zhang L, Xu J, Wang L, Liu B, Hao M, Chang X, Zhang T, Li S, Zhang H.** 2017. The alternative splicing of EAM8 contributes to early flowering and short-season adaptation in a landrace barley from the Qinghai-Tibetan Plateau. *Theoretical and applied genetics* **130**, 757-766.
- Xu X, Yuan L, Yang X, Zhang X, Wang L, Xie Q.** 2022. Circadian clock in plants: Linking timing to fitness. *Journal of integrative plant biology* **64**, 792-811.
- Xu X, Zheng C, Lu D, Song CP, Zhang L.** 2021. Phase separation in plants: New insights into cellular compartmentalization. *Journal of integrative plant biology* **63**, 1835-1855.
- Yamaguchi R, Nakamura M, Mochizuki N, Kay SA, Nagatani A.** 1999. Light-dependent translocation of a phytochrome B-GFP fusion protein to the nucleus in transgenic Arabidopsis. *The Journal of cell biology* **145**, 437-445.
- Yan L, Fu D, Li C, Blechl A, Tranquilli G, Bonafede M, Sanchez A, Valarik M, Yasuda S, Dubcovsky J.** 2006. The wheat and barley vernalization gene VRN3 is an orthologue of FT. *Proceedings of the National Academy of Sciences* **103**, 19581-19586.
- Yeom M, Kim H, Lim J, Shin A-Y, Hong S, Kim J-I, Nam HG.** 2014. How do phytochromes transmit the light quality information to the circadian clock in Arabidopsis? *Molecular Plant* **7**, 1701-1704.
- Yoshida R, Fekih R, Fujiwara S, Oda A, Miyata K, Tomozoe Y, Nakagawa M, Niinuma K, Hayashi K, Ezura H.** 2009. Possible role of EARLY FLOWERING 3 (ELF3) in clock - dependent floral regulation by SHORT VEGETATIVE PHASE (SVP) in Arabidopsis thaliana. *New Phytologist* **182**, 838-850.
- Yu J-W, Rubio V, Lee N-Y, Bai S, Lee S-Y, Kim S-S, Liu L, Zhang Y, Irigoyen ML, Sullivan JA.** 2008. COP1 and ELF3 control circadian function and photoperiodic flowering by regulating GI stability. *Molecular cell* **32**, 617-630.
- Zagotta MT, Hicks KA, Jacobs CI, Young JC, Hangarter RP, Meeks - Wagner DR.** 1996. The Arabidopsis ELF3 gene regulates vegetative photomorphogenesis and the photoperiodic induction of flowering. *The Plant Journal* **10**, 691-702.
- Zahn T, Zhu Z, Ritoff N, Krapf J, Junker A, Altmann T, Schmutzer T, Tueting C, Kastritis PL, Quint M, Pillen K, Maurer A.** 2022. Exotic alleles of EARLY FLOWERING 3 determine plant development and grain yield in barley. *bioRxiv*, 2022.2007.2015.500212. [Preprint]
- Zakhrabekova S, Gough SP, Braumann I, Müller AH, Lundqvist J, Ahmann K, Dockter C, Matyszcak I, Kurowska M, Druka A.** 2012. Induced mutations in circadian clock

regulator Mat-a facilitated short-season adaptation and range extension in cultivated barley. *Proceedings of the National Academy of Sciences* **109**, 4326-4331.

Zhang LL, Shao YJ, Ding L, Wang MJ, Davis SJ, Liu JX. 2021. XBAT31 regulates thermoresponsive hypocotyl growth through mediating degradation of the thermosensor ELF3 in *Arabidopsis*. *Science Advances* **7**, eabf4427.

Zheng B, Chenu K, Chapman SC. 2016. Velocity of temperature and flowering time in wheat—assisting breeders to keep pace with climate change. *Global Change Biology* **22**, 921-933.

Zhu Z, Quint M, Anwer MU. 2022. *Arabidopsis* EARLY FLOWERING 3 controls temperature responsiveness of the circadian clock independently of the evening complex. *Journal of Experimental Botany* **73**, 1049-1061.

Zhu Z, Esche F, Babben S, Trenner J, Serfling A, Pillen K, Maurer A, Quint M. 2023. An exotic allele of barley EARLY FLOWERING 3 contributes to developmental plasticity at elevated temperatures. *Journal of Experimental Botany*, doi: 10.1093/jxb/erac470.

Zielinski T, Moore AM, Troup E, Halliday KJ, Millar AJ. 2014. Strengths and limitations of period estimation methods for circadian data. *PLoS One* **9**, e96462.

Appendix

Appendix I

Table 2 List of *A. thaliana* accessions used in this study.

ID*	Stock N.	Name	PolyQ length	Sequencing [†]	Phenotyping
265	WT_1369	PYL-6	17	yes	yes
350	WT_1480	TOU-A1-88	19	yes	
430	WT_0830	Gr-1	21	yes	yes
484	WT_1637	BRR23	16	yes	yes
628	WT_1643	LI-OF-061	19	yes	yes
915	WT_1254	LIN S-5	13	yes	
1006	WT_1494	Ale-Stenar-77-31	19	yes	yes
1061	WT_0993	Broesarp-11-135	14	yes	
1652	WT_1656	DuckLkSP40	16	yes	yes
1684	WT_1658	Haz-10	16	yes	yes
1741	WT_1660	KBS-Mac-74	16	yes	yes
1793	WT_1663	L-R-5	16	yes	yes
1797	WT_1664	L-R-10	16	yes	yes
2141	WT_1678	MSGA-61	16	yes	yes
2159	WT_1679	Paw-13	16	yes	yes
2166	WT_1680	Paw-20	16	yes	yes
2171	WT_1342	Paw-26	16	yes	yes
2191	WT_1681	Pent-7	16	yes	yes
2276	WT_1409	SLSP-31	18	yes	yes
4840	WT_1689	UKSW06-240	19	yes	yes
5104	WT_1534	UKSE06-252	7	yes	yes
5353	WT_1529	UKNW06-003	14	yes	yes
5644	WT_1532	UKNW06-481	18	yes	yes
5651	WT_1693	UKNW06-488	18	yes	yes
5720	WT_1520	Cal-2	23	yes	yes
5768	WT_1525	UKID63	16	yes	yes
5784	WT_1764	Ty-1	25	yes	yes
5811	WT_1518	UKID107	18	yes	yes
5837	WT_0797	Bor-1	13		yes
5921	WT_1067	DraIV 3-7	12	yes	
6009	WT_1072	Eden-1	11		
6016	WT_1080	Eds-1	14		
6039	WT_1169	Hovdala-2	16		
6040	WT_1196	Kni-1	19		
6042	WT_1258	Lom1-1	11		
6043	WT_1772	Loev-1	16		
6046	WT_1728	Loev-5	16	yes	yes
6064	WT_1324	Nyl-2	14		
6074	WT_1330	oer-1	9	yes	yes
6077	WT_1500	Rev-3	20	yes	yes
6086	WT_1736	Sr:3	16	yes	yes
6088	NA	Stu1-1	16		
6091	WT_1502	T1010	19	yes	yes
6094	WT_1433	T1040	11	yes	yes
6097	WT_1737	T1070	17	yes	yes
6101	WT_1503	T1120	11	yes	yes
6102	WT_1739	T1130	13	yes	yes
6104	WT_1740	T1160	20	yes	yes
6105	WT_1741	T450	13	yes	yes
6109	WT_1436	T510	11	yes	yes
6119	WT_1504	T620	11	yes	yes
6123	WT_1505	T680	14	yes	yes
6125	WT_1442	T710	20	yes	yes
6126	WT_1743	T720	17	yes	yes
6131	WT_1744	T780	20	yes	yes
6142	WT_1445	T900	20	yes	yes
6145	WT_1749	T930	20	yes	yes
6149	WT_1446	T970	14	yes	yes

ID*	Stock N.	Name	PolyQ length	Sequencing†	Phenotyping
6150	WT_1751	T980	21	yes	yes
6151	WT_1752	T990	16	yes	yes
6166	WT_1753	TAA 17	9	yes	yes
6180	WT_1453	TaeL 07	7	yes	yes
6194	WT_1755	TDr-8	13	yes	yes
6242	WT_1757	Tomegap-2	16	yes	yes
6243	WT_1479	Tottarp-2	16	yes	yes
6244	WT_1758	TRae 01	14	yes	yes
6255	WT_1513	TV-7	9	yes	yes
6268	WT_1763	TV-22	9	yes	yes
6276	WT_1512	TV-30	9	yes	yes
6390	WT_1515	Udul 3-36	21	yes	yes
6396	WT_1516	Udul 4-9	12	yes	yes
6814	WT_1702	KNO-15	16	yes	yes
6830	WT_1215	Kz-13	14		
6897	WT_0780	Ag-0	16		yes
6898	WT_0784	An-1	19		yes
6900	WT_0978	Bil-5	16		
6901	WT_0979	Bil-7	16		
6903	WT_0798	Bor-4	13		yes
6904	WT_0799	Br-0	23		yes
6907	WT_1028	CIBC-17	17		
6908	WT_1604	CIBC-5	19		yes
6909	WT_1034	Col-0	7	yes	yes
6911	WT_1042	Cvi-0	9	yes	yes
6913	WT_1073	Eden-2	11		
6915	WT_0816	Ei-2	15		yes
6919	WT_0826	Ga-0	9		yes
6920	WT_1123	Got-22	16		
6922	WT_0832	Gu-0	19		yes
6923	WT_1172	HR-10	14		
6924	WT_0836	HR-5	19		yes
6926	WT_0845	Kin-0	19	yes	yes
6929	WT_0847	Kondara	14		yes
6931	WT_0850	Kz-9	14		yes
6932	WT_1239	Ler-1	17		
6933	WT_1257	LL-0	13		
6938	WT_0862	Ms-0	15		yes
6940	WT_0864	Mz-0	14		yes
6943	WT_1315	NFA-10	18		yes
6944	WT_1617	NFA-8	14		yes
6945	WT_0868	Nok-3	16		yes
6951	WT_0880	Pu2-23	12		yes
6956	WT_0881	Pu2-7	16		yes
6957	WT_1365	Pu2-8	11		yes
6958	WT_0883	Ra-0	12	yes	yes
6959	WT_1379	Rennes-1	19	yes	yes
6961	WT_0892	Se-0	14		yes
6963	WT_1621	Sorbo	14		yes
6966	WT_1417	Sq-1	14	yes	yes
6967	WT_0898	Sq-8	15		yes
6968	WT_0904	Tamm-2	9		yes
6969	WT_1455	Tamm-27	9		yes
6970	WT_0908	Ts-1	13		yes
6971	WT_1484	Ts-5	13	yes	yes
6973	WT_1548	UII2-3	15	yes	yes
6974	NA	UII2-5	11		
6975	WT_0911	Uod-1	12		yes
6976	WT_1550	Uod-7	21		yes
6979	WT_0918	Wei-0	12		
6981	WT_1622	Ws-2	16		
6982	WT_0921	Wt-5	14		
6984	WT_0924	Zdr-1	13		
6990	WT_1722	Amel-1	15	yes	yes
6992	WT_0785	Ang-0	12		yes
7002	WT_0789	Baa-1	12	yes	yes

ID*	Stock N.	Name	PolyQ length	Sequencing†	Phenotyping
7003	WT_1598	Bs-1	12		yes
7008	WT_0792	Benk-1	12	yes	yes
7025	WT_0794	Bl-1	16		yes
7036	WT_1599	Bu-0	19	yes	yes
7058	WT_0998	Bur-0	23	yes	yes
7063	NA	Can-0	20		
7067	WT_1040	Ct-1	11		
7077	WT_0807	Co-1	9		yes
7081	WT_1605	Co	13	yes	yes
7094	WT_1044	Da-0	11		
7103	WT_0814	Dra-0	12		yes
7106	WT_1607	Dr-0	13		yes
7111	WT_1077	Edi-0	16	yes	
7126	WT_0821	Es-0	9	yes	yes
7127	WT_0822	Est	19		yes
7143	WT_0828	Gel-1	14	yes	yes
7161	WT_0827	Gd-1	14		yes
7162	WT_0837	Hs-0	16		yes
7169	WT_0834	Hh-0	15	yes	yes
7177	WT_0840	Jm-0	11		yes
7183	WT_1703	Kas-1	16	yes	
7192	WT_0844	Kil-0	16	yes	yes
7202	WT_0842	Kb-0	19	yes	yes
7207	WT_0849	Kyoto	27	yes	yes
7208	WT_0852	Lan-0	7		yes
7213	WT_1238	Ler-0	17	yes	yes
7217	WT_0856	Lm-2	19	yes	yes
7223	WT_0854	Li-2:1	16	yes	yes
7236	WT_0855	Litva	14	yes	yes
7255	WT_0859	Mh-0	11		yes
7258	WT_0870	Nw-0	14	yes	yes
7268	WT_0869	Np-0	13		yes
7273	WT_1317	No-0	11		yes
7282	WT_0873	Or-0	19	yes	yes
7288	WT_1335	Oy-0	16	yes	yes
7296	WT_1348	Petergof	14		
7298	WT_0876	Pi-0	13	yes	yes
7305	WT_1619	Pt-0	13	yes	yes
7306	WT_0879	Pog-0	19		yes
7307	WT_1358	Pn-0	19	yes	yes
7322	WT_1386	Rsch-4	11	yes	yes
7323	WT_0891	Rubezhnoe-1	14		yes
7327	WT_1404	Sf-1	9		yes
7344	WT_0895	Sg-1	18	yes	yes
7347	WT_0899	Stw-0	14		yes
7349	WT_0902	Ta-0	21	yes	yes
7373	WT_1485	Tsu-0	16		yes
7383	WT_0913	Van-0	13		
7394	WT_0916	Wa-1	16		
7396	WT_1578	Ws-0.2	21	yes	yes
7413	WT_1577	Wil-2	14		yes
7416	WT_0922	Yo-0	16		
7418	WT_1595	Zu-1	19	yes	yes
7461	WT_1136	H55	7		
7471	WT_0886	RLD-1	19		yes
7475	WT_1706	KEN	16		yes
7477	WT_1574	WAR	16	yes	yes
7514	WT_0890	RRS-7	21		yes
7515	WT_0889	RRS-10	13		yes
7516	NA	Var2-1	9		
7517	NA	Var2-6	9		
7520	WT_0857	Lp2-2	26		yes
7521	WT_1260	Lp2-6	21		
7525	WT_1384	Rmx-A180	18	yes	yes
7529	WT_1707	627RMX-1MN4	18	yes	yes
7530	WT_1708	627RMX-1MN5	18	yes	yes

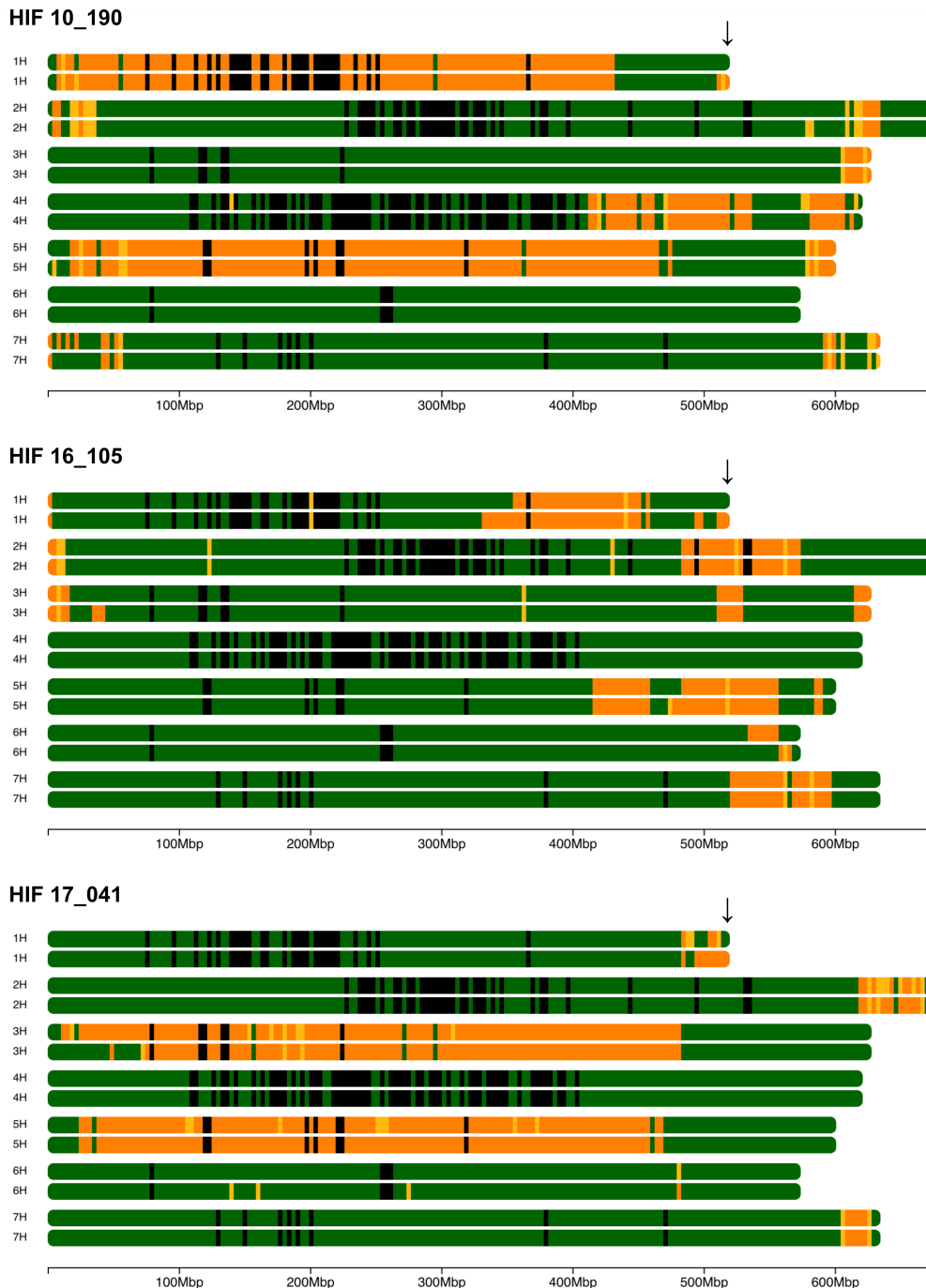
ID*	Stock N.	Name	PolyQ length	Sequencing [†]	Phenotyping
7917	WT_1359	PNA3.10	21	yes	yes
8214	WT_1609	Gy-0	19		yes
8222	NA	Lis-2	13		
8227	WT_1471	THoe 03	9	yes	yes
8230	WT_0940	Algutsum	22		
8233	WT_1047	Dem-4	16		
8234	WT_1135	Gul1-2	11		
8235	WT_1157	Hod	12		
8237	WT_1190	Kaevlinge-1	9		
8238	WT_1193	Kent	11		
8241	WT_1252	Liarum	16		
8242	WT_1253	Lilloe-1	21		
8246	WT_1313	NC-6	14		
8247	WT_1395	San-2	20	yes	yes
8249	WT_1767	Vimmerby	16	yes	yes
8256	WT_0954	Ba1-2	19		
8258	WT_0955	Ba4-1	17		
8264	WT_0795	Bla-1	9		yes
8283	WT_1059	Dra3-1	16		
8290	WT_1086	En-1	11		
8297	WT_1115	Ge-0	18		
8306	WT_1168	Hov4-1	16		
8311	WT_1610	In-0	16		yes
8312	WT_1611	Is-0	17		yes
8326	WT_1255	Lis-1	15		
8334	WT_1263	Lu-1	13		
8343	WT_0865	Na-1	22		yes
8351	WT_1333	Ost-0	11		yes
8354	WT_0875	Per-1	11		yes
8357	WT_0877	Pla-0	9		yes
8365	WT_1371	Rak-2	19	yes	yes
8366	WT_0885	Rd-0	19		yes
8369	WT_1733	Rev-1	19	yes	yes
8376	WT_1396	Sanna-2	16		yes
8386	WT_1418	Sr:5	12	yes	yes
8387	WT_1420	St-0	15	yes	yes
8424	WT_1612	Kas-2	29	yes	yes
8427	WT_1509	UII2-13	16	yes	yes
8699	WT_1716	328PNA062	16	yes	yes
9069	WT_1579	Xan-5	23	yes	yes
9070	WT_1580	Xan-6	23	yes	yes
9089	WT_1311	Nar-3	23	yes	yes
9091	WT_1312	Nar-5	22	yes	yes
9114	WT_1228	Lag2-7	9	yes	yes
9128	WT_1581	Yeg-2	16	yes	yes
9130	WT_1582	Yeg-4	16	yes	yes
9133	WT_1584	Yeg-7	16	yes	yes
9134	WT_1585	Yeg-8	16	yes	yes
9298	WT_1078	Edi-1	14	yes	
9343	WT_1606	Dju-1	13	yes	yes
9370	WT_1718	EkS 3	13	yes	yes
9437	WT_1732	Puk-2	15	yes	yes
9476	WT_1557	VarA 1	9	yes	yes
9481	WT_1769	Yst-1	14	yes	yes
9507	WT_1031	IP-Coa-0	13	yes	
9512	WT_1566	IP-Vid-1	10	yes	yes
9513	WT_0930	IP-Adc-5	10	yes	yes
9536	WT_1037	IP-Cor-0	19	yes	
9540	WT_1084	IP-Elb-0	9	yes	yes
9559	WT_1304	IP-Mon-5	21	yes	yes
9564	WT_1318	IP-Nog-17	9	yes	yes
9568	WT_1338	IP-Pan-0	14	yes	yes
9577	WT_1382	IP-Ria-0	9	yes	yes
9578	WT_1391	IP-Sac-0	14	yes	yes
9584	WT_1429	IP-Stp-0	26	yes	yes
9587	WT_1457	IP-Tdc-0	18	yes	yes

ID*	Stock N.	Name	PolyQ length	Sequencing [†]	Phenotyping
9589	WT_1476	IP-Tor-1	20	yes	yes
9590	WT_1759	IP-Trs-0	18	yes	yes
9591	WT_1553	IP-Vad-0	18	yes	yes
9593	WT_1561	IP-Vaz-0	23	yes	yes
9594	WT_1562	IP-Vdm-0	23	yes	yes
9597	WT_1567	IP-Vig-1	16	yes	yes
9602	WT_1572	IP-Vpa-1	14	yes	yes
9606	WT_0933	Aitba-1	16	yes	
9622	WT_1724	Bijisk-4	16	yes	yes
9635	WT_1319	Nosov-1	14	yes	yes
9636	WT_1320	Noveg-1	14	yes	yes
9637	WT_1729	Noveg-2	14	yes	yes
9642	WT_1374	Rakit-3	14	yes	yes
9644	WT_1596	Zupan-1	11	yes	yes
9692	WT_1017	Castelfed-3-208	17	yes	
9706	WT_1055	Dospa-1	16	yes	
9713	WT_1421	Stara-1	12	yes	yes
9714	WT_1127	Grivo-1	15	yes	yes
9718	WT_1411	Smolj-1	18	yes	yes
9723	WT_1408	Slavi-2	16	yes	yes
9733	WT_0971	Bela-2	16	yes	
9736	WT_1467	Teiu-2	19	yes	yes
9754	WT_1419	Sredn-1	12	yes	yes
9768	WT_1389	Ru4-16	22	yes	yes
9775	WT_0974	Berg-1	14	yes	yes
9783	WT_1491	Tu-PK-7	13	yes	yes
9794	WT_1486	Tu-B1-2	18	yes	yes
9804	WT_1326	Obe1-15	18	yes	yes
9806	WT_1387	Ru-2	13	yes	yes
9810	WT_1489	Tu-KS-7	19	yes	yes
9811	WT_1490	Tu-NK-12	13	yes	yes
9816	WT_1493	Tu-WH	13	yes	yes
9825	WT_0983	IP-Boa-0	14	yes	yes
9837	WT_1036	IP-Con-0	9	yes	
9843	WT_1085	IP-Elp-0	10	yes	
9873	WT_1314	IP-Ndc-0	15	yes	yes
9876	WT_1336	IP-Pad-0	23	yes	yes
9878	WT_1345	IP-Pee-0	13	yes	yes
9879	WT_1347	IP-Per-0	12	yes	yes
9885	WT_1362	IP-Prd-0	11	yes	yes
9886	WT_1363	IP-Pru-0	17	yes	yes
9887	WT_1367	IP-Pun-0	19	yes	yes
9898	WT_1414	IP-Som-0	14	yes	yes
9900	WT_1483	IP-Tri-0	12	yes	yes
9904	WT_1558	IP-Vas-0	22	yes	yes
9912	WT_1726	CIRY-13	18	yes	yes
9926	WT_1482	TRE-1	18	yes	yes
9935	WT_1723	BAU-15	16	yes	yes
9941	WT_0765	Fei-0	19		yes
9960	WT_0737	Kidr-1	21	yes	yes
9965	WT_0725	Mammo-2	9	yes	yes
9966	WT_0723	Monte-1	13	yes	yes
9973	WT_0716	Mitterberg-1-181	17	yes	yes
9982	WT_0729	Apost-1	20	yes	yes
10004	WT_0734	Bolin-1	14	yes	yes
10006	WT_0754	Kastel-1	16	yes	yes
10027	WT_1632	Uk-6	16	yes	yes
14312	WT_1623	Kos-1	21	yes	yes
14318	WT_1629	Shu-1	16	yes	yes
15560	WT_1631	Valm	17	yes	yes
15591	WT_1633	OOE1-1	12	yes	yes
15592	WT_1634	OOE3-1	17	yes	yes
15593	WT_1770	OOE3-2	12	yes	yes

* Accession ID based on the 1001 genomes collection

† 'yes' means it was sequenced and/or phenotyped in this thesis

Appendix II



Appendix Fig. 1 Genomic setup of the used HIFs.

Comparison of two sister lines (upper chromosomes, elite line; lower chromosomes, wild line) in each HIF pair based on the genotype data generated from the Infinium iSelect 50k SNP chip (Zahn *et al.*, 2022, Preprint). Black regions were not covered in genotyping. Green and orange parts represent homozygous elite and wild regions, respectively, whereas yellow parts represent heterozygous loci. The arrows indicate the *ELF3* locus on chromosome 1H. The additional seven major flowering time genes exhibited the same fixed homozygous alleles between sister lines in all three HIF pairs. Window scaling was based on length proportion and 200 windows were created for the longest chromosome.

Appendix III

Table 3 List of primers used in this study.

Stock N.	Primer name	Sequence (5' - 3')	Purpose
3270	ELF3_PRD_F	ACAAAGGGGTGACTCGGAGA	PCR/sequencing
3271	ELF3_PRD_R	GTCACTCCTCCCCATCTCT	PCR/sequencing
1235	HvELF3_F1	CCGAGTGAGTGAGTGAGTGA	PCR/sequencing
1238	HvELF3_R6	AGCATACTCTGAAGCGCTAATTG	PCR/sequencing
1236	HvELF3_F4	AGTGAGTGAGTGAGCATGGC	sequencing
1239	HvELF3_F5	TAGTTCACACGGCAGAGACA	sequencing
1249	HvELF3_F6	TCCATCATTTTGCGTGCCTT	sequencing
1250	HvELF3_F7	GTTGTGCGGTGCTATTGGTCC	sequencing
1240	HvELF3_R7	TTGTTGTGCGGTAGGAGCAGG	sequencing
3964	pHvELF3_F1	GGAGCAACTTTTGAACACATGC	PCR/sequencing
3965	pHvELF3_R1	CTTGAGGGTGGTGTGCGTTGA	PCR/sequencing
3966	pHvELF3_F2	GCCCATTTTGCGTCGAAAGT	PCR/sequencing
3967	pHvELF3_R2	GCATGCCGGATTTATTTCGACC	PCR/sequencing
708	PP2A_F	TATCGGATGACGATTCTTCGTGCAG	qRT-PCR ref
707	PP2A_R	GCTTGGTCGACTATCGGAATGAGAG	qRT-PCR ref
1604	TIP41_F	GTGAAAACCTGTTGGAGAGAAGCAA	qRT-PCR ref
1603	TIP41_R	TCAACTGGATACCCTTTTCGCA	qRT-PCR ref
289	CCA1_F	TCTGTGTCTGACGAGGGTCAATT	qRT-PCR
288	CCA1_R	ACTTTGCGGCAATACCTCTCTGG	qRT-PCR
287	LHY_F	CAACAGCAACAACAATGCAACTAC	qRT-PCR
286	LHY_R	AGAGAGCCTGAAACGCTATACGA	qRT-PCR
291	TOC1_F	ATCTTCGCAGAATCCCTGTGATA	qRT-PCR
290	TOC1_R	GCACCTAGCTTCAAGCACTTTACA	qRT-PCR
279	PRR9_F	GCACAGAGAAACCAAAGGAA	qRT-PCR
278	PRR9_R	CTTTCACTCGAGGACGTTGT	qRT-PCR
285	ELF3_F	GATGCCACCATAATGACC	qRT-PCR
284	ELF3_R	TTGCTCGCGGATAAGACTTT	qRT-PCR
277	PRR7_F	TGAAAGTTGGAAAAGGACCA	qRT-PCR
276	PRR7_R	GTTCCACGTGCATTAGCTCT	qRT-PCR
1805	PIF4_F	ATCATCTCCGACCGGTTTGC	qRT-PCR
1806	PIF4_R	AGTGCTACCAACCTAGTG	qRT-PCR
1257	HvACTIN_F	GCCGTGCTTTCCCTCTATG	qRT-PCR ref
1258	HvACTIN_R	GCTTCTCCTTGATGTCCCTTA	qRT-PCR ref
1253	HvGAPDH_F	GTGAGGCTGGTGTGATTACG	qRT-PCR ref
1254	HvGAPDH_R	TGGTGCAGCTAGCATTGAGAC	qRT-PCR ref
2209	HvCCA1_F	CGACAAGACACAGCAAGCAT	qRT-PCR
2210	HvCCA1_R	CTTCATCTTGCTCCCCTCTG	qRT-PCR
2211	HvTOC1_F	TCCAGGGACGTTGAGTTGGTT	qRT-PCR
2212	HvTOC1_R	TTTTGAGCGGTTGGGGGTTG	qRT-PCR
2215	HvPRR73_F	GCAACATTTCCGGGAAGCTG	qRT-PCR
2216	HvPRR73_R	TGCCATTTGAGCCCTGCTTT	qRT-PCR
2213	HvGI_F	AGGCGAAATGGTAATGTTGC	qRT-PCR
2214	HvGI_R	CAGACATCTGCGTTTCAGGA	qRT-PCR
2223	Ppd-H1_F	GATGGATTCAAAGGCAAGGA	qRT-PCR
2224	Ppd-H1_R	GAACAATTGGCTCCTCCAAA	qRT-PCR
1408	VRN1_F	TAACCCCATGGAGGGGAGAG	qRT-PCR
1409	VRN1_R	GCCCAGGTGGAAAGGAAACT	qRT-PCR
1406	FT1_F	GCCGTCTACTTCAACTGCCA	qRT-PCR
1407	FT1_R	GTGAGCGGTGAGTAGGTCAA	qRT-PCR
1418	BM3_F	TGCTTCCACTTAGGCCATATCA	qRT-PCR
1419	BM3_R	GGAGTCGTATGAGGCTGTGCG	qRT-PCR
1416	BM8_F	GAAGTGGTGGAGAGGCAGAA	qRT-PCR
1417	BM8_R	ATGAGCTAGTCTGGGCTTGG	qRT-PCR
1255	HvELF3_F	CCTACCGACAACAAGCAGAA	qRT-PCR
1256	HvELF3_R	CATGAATCCCCAGCTGTAG	qRT-PCR

Appendix IV

Table 4 List of identified *ELF3* and *EEC* homologues in 274 plant genomes.

Branch ID	Leaf name	LLR*	CORE score	Original name	Source [†]
219	Ac_Acorus_americanus	-0.373	0	Acora.01G093700.1.p	Phytozome
211	Al_Posidonia_australis	4.428	0	BYQM_scaffold_2000764	OneKP
209	Al_Spirodela_polyrhiza_1	-5.258	0	Spipo14G0012700	Phytozome
217	Al_Spirodela_polyrhiza_2	-11.702	0	Spipo21G0028200	Phytozome
210	Al_Zostera_marina	-1	0	Zosma3g01990.1	Phytozome
222	Am_Amborella_trichopoda	2.151	0	evm_scaffold00036.83	Phytozome
391	Ap_Daucus_carota	8.556	0	DCAR_000777	Phytozome
392	Ap_Mydocarpus_sp	3.761	0	AJFN_scaffold_2101285	OneKP
393	Ap_Pittosporum_resiniferum	2.743	0	SALZ_scaffold_2015578	OneKP
397	Aq_Ilex_paraguariensis	9.823	0	SXML_scaffold_2017329	OneKP
396	Aq_Ilex_vomitorea	11.641	0	ASMV_scaffold_2109631	OneKP
218	Asp_Asparagus_officinalis_1	-4.139	0	evm.model.AsparagusV1_01.2112	Phytozome
174	Asp_Asparagus_officinalis_2	4.749	0	evm.model.AsparagusV1_05.2084	Phytozome
172	Asp_Drakaea_elastica	-1.113	0	XZME_scaffold_2000911	OneKP
171	Asp_Goodyera_pubescens	3.49	0	VTUS_scaffold_2009034	OneKP
387	Ast_Helianthus_annuus_1	6.375	0	HanXRQChr02g0047961	Phytozome
385	Ast_Helianthus_annuus_2	4.142	0	HanXRQChr17g0539091	Phytozome
163	Ast_Helianthus_annuus_3	1.911	0	HanXRQChr05g0139911	Phytozome
386	Ast_Lactuca_sativa_1	10.024	10.024	Lsat_1_v5_gn_3_25981.1	Phytozome
388	Ast_Lactuca_sativa_2	7.469	0	Lsat_1_v5_gn_6_7561.1	Phytozome
389	Ast_Phelline_lucida	5.153	0	AUIP_scaffold_2029906	OneKP
390	Ast_Platycodon_grandiflorus	7.735	0	IHPC_scaffold_2000327	OneKP
223	Au_Illicium_floridanum	0.868	0	VZCI_scaffold_2013687	OneKP
421	Be_Aextoxicon_punctatum	7.334	0	QUTB_scaffold_2017709	OneKP
160	Bo_Heliotropium_greggii	2.293	0	ABEH_scaffold_2016792	OneKP
161	Bo_Heliotropium_mendocinum	1.789	0	MZOB_scaffold_2058736	OneKP
77	Br_Akania_lucens	6.698	0	HYZL_scaffold_2142848	OneKP
255	Br_Alyssum_linifolium_1	49.964	49.964	Alyli.0086s0016.1.p	Phytozome
47	Br_Alyssum_linifolium_2	-4.38	0	Alyli.0032s0261.1.p	Phytozome
257	Br_Arabidopsis_halleri_1	46.358	46.358	Araha.14473s0003.1	Phytozome
45	Br_Arabidopsis_halleri_2	-4.531	0	Araha.25327s0001.1	Phytozome
259	Br_Arabidopsis_lyrata_1	58.268	58.268	AL4G18010.t1	Phytozome
44	Br_Arabidopsis_lyrata_2	-1.131	0	AL3G35380.t1	Phytozome
262	Br_Arabidopsis_thaliana_1	31.534	31.534	AT2G25930.1	Phytozome
41	Br_Arabidopsis_thaliana_2	-3.481	0	AT3G21320.1	Phytozome
285	Br_Arabis_alpina	21.631	21.631	TZWR_scaffold_2004755	OneKP
260	Br_Boechnera_stricta_1	26.649	26.649	Bostr.26326s0056.1	Phytozome
49	Br_Boechnera_stricta_2	-4.38	0	Bostr.19424s0520.1	Phytozome
276	Br_Brassica_nigra_1	26.42	0	IPWB_scaffold_2086871	OneKP
59	Br_Brassica_nigra_2	2.095	0	IPWB_scaffold_2016265	OneKP
266	Br_Brassica_oleracea_1	24.423	24.225	Bol045737	Phytozome
279	Br_Brassica_oleracea_2	24.426	0	Bol026498	Phytozome
56	Br_Brassica_oleracea_3	2.949	0	Bol026618	Phytozome
69	Br_Brassica_oleracea_4	1.664	0	Bol038369	Phytozome
38	Br_Brassica_oleracea_5	-1.907	0	Bol018791	Phytozome
267	Br_Brassica_rapa_1	32.622	32.622	Brara.I04408.1	Phytozome
278	Br_Brassica_rapa_2	20.276	20.276	Brara.D01576.1	Phytozome
57	Br_Brassica_rapa_3	0.287	0	Brara.C03827.1	Phytozome
70	Br_Brassica_rapa_4	-2.667	0	Brara.E02076.1	Phytozome
39	Br_Brassica_rapa_5	-4.357	0	Brara.A02777.1	Phytozome
268	Br_Cakile_maritima_1	28.992	28.992	Camar.4838s0002.1.p	Phytozome
67	Br_Cakile_maritima_2	-3.044	0	Camar.0343s0018.1.p	Phytozome
261	Br_Capsella_grandiflora_1	59.885	59.885	Cagra.25895s0001.1	Phytozome
50	Br_Capsella_grandiflora_2	-3.787	0	Cagra.1757s0023.1	Phytozome
258	Br_Capsella_rubella_1	57.518	57.518	Carubv10022728m	Phytozome
46	Br_Capsella_rubella_2	-3.787	0	Carubv10013409m	Phytozome
345	Br_Carica_papaya	0.606	0	evm.model.supercontig_78.11	Phytozome
272	Br_Caulanthus_amplexicaulis_1	26.168	26.168	Caamp.0008s0143.1.p	Phytozome
60	Br_Caulanthus_amplexicaulis_2	-5.067	0	Caamp.1039s1307.1.p	Phytozome
250	Br_Cleome_violacea_1	12.66	12.66	Clevi.0008s0742.1.p	Phytozome
246	Br_Cleome_violacea_2	2.435	0	Clevi.0032s0147.1.p	Phytozome

Branch ID	Leaf name	LLR*	CORE score	Original name	Source†
33	Br_Cleome_violacea_3	-5.389	0	Clevi.0041s0079.1.p	Phytozome
31	Br_Cleome_violacea_4	-7.503	0	Clevi.0041s0083.1.p	Phytozome
36	Br_Cochlearia_officinalis	-13.934	0	CSUV_scaffold_2017998	OneKP
35	Br_Corynandra_viscosa	-8.22	0	UPZX_scaffold_2004150	OneKP
275	Br_Crambe_hispanica_1	23.548	23.548	Crahi.0581s0023.1.p	Phytozome
270	Br_Crambe_hispanica_2	24.821	24.821	Crahi.0693s0003.1.p	Phytozome
55	Br_Crambe_hispanica_3	4.115	0	Crahi.0068s0027.1.p	Phytozome
68	Br_Crambe_hispanica_4	-2.611	0	Crahi.0437s0023.1.p	Phytozome
256	Br_Descurainia_sophioides_1	45.537	45.537	Desop.0027s0043.1.p	Phytozome
48	Br_Descurainia_sophioides_2	-6.067	0	Desop.0097s0103.1.p	Phytozome
286	Br_Diptychocarpus_strictus_1	16.025	16.025	Distr.0001s0039.1.p	Phytozome
64	Br_Diptychocarpus_strictus_2	-5.326	0	Distr.0033s0025.1.p	Phytozome
43	Br_Draba_oligosperma	-17.711	0	LAPO_scaffold_2110461	OneKP
269	Br_Eruca_vesicaria_1	25.84	25.84	Eruve.0086s0018.1.p	Phytozome
66	Br_Eruca_vesicaria_2	2.251	0	Eruve.6574s0001.1.p	Phytozome
284	Br_Euclidium_syriacum_1	18.346	18.346	Eusyr.0003s0426.1.p	Phytozome
253	Br_Euclidium_syriacum_2	24.947	24.693	Eusyr.0134s0253.1.p	Phytozome
37	Br_Euclidium_syriacum_3	-6.517	0	Eusyr.0017s0291.1.p	Phytozome
281	Br_Eutrema_salsugineum_1	22.857	22.857	Thhalv10001926m	Phytozome
53	Br_Eutrema_salsugineum_2	-3.326	0	Thhalv10020453m	Phytozome
249	Br_Gynandropsis_gynandra_1	29.192	29.192	MBQU_scaffold_2008466	OneKP
32	Br_Gynandropsis_gynandra_2	-12.482	0	MBQU_scaffold_2009842	OneKP
287	Br_Gyrostemon_ramosus_1	4.72	0	UAXP_scaffold_2011631	OneKP
72	Br_Gyrostemon_ramosus_2	-3.484	0	UAXP_scaffold_2017306	OneKP
283	Br_Iberis_amara_1	29.595	29.595	lbeam.1921s0011.1.p	Phytozome
252	Br_Iberis_amara_2	17.516	0	lbeam.3422s0005.1.p	Phytozome
52	Br_Iberis_amara_3	-2.715	0	lbeam.3284s0005.1.p	Phytozome
271	Br_Isatis_tinctoria_1	32.092	32.092	Isati.0505s0007.1.p	Phytozome
61	Br_Isatis_tinctoria_2	-3.282	0	Isati.0644s0022.1.p	Phytozome
254	Br_Lepidium_sativum_1	16.937	16.937	Lesat.0012s0041.1.p	Phytozome
42	Br_Lepidium_sativum_2	-7.046	0	Lesat.0024s0264.1.p	Phytozome
75	Br_Limnanthes_douglasii	9.337	0	CRNC_scaffold_2042295	OneKP
265	Br_Lunaria_annua_1	18.304	0	Luann.0747s0002.1.p	Phytozome
71	Br_Lunaria_annua_2	1.354	0	Luann.0007s0252.1.p	Phytozome
263	Br_Malcolmia_maritima_1	27.59	27.59	Mamar.0033s0092.1.p	Phytozome
40	Br_Malcolmia_maritima_2	-5.591	0	Mamar.0029s0981.1.p	Phytozome
346	Br_Moringa_oleifera_1	6.367	0	CZPV_scaffold_2006628	OneKP
76	Br_Moringa_oleifera_2	-7.309	0	CZPV_scaffold_2051291	OneKP
273	Br_Myagrum_perfoliatum_1	27.741	27.741	Myper.0026s0027.1.p	Phytozome
62	Br_Myagrum_perfoliatum_2	-5.61	0	Myper.0028s0672.1.p	Phytozome
251	Br_Polanisia_dodecandra_1	26.869	26.869	QSKP_scaffold_2009050	OneKP
34	Br_Polanisia_dodecandra_2	-4.087	0	QSKP_scaffold_2009380	OneKP
247	Br_Reseda_odorata	3.014	0	SWPE_scaffold_2062214	OneKP
264	Br_Rorippa_islandica_1	28.979	28.979	Roisl.0082s0517.1.p	Phytozome
51	Br_Rorippa_islandica_2	2.957	0	Roisl.0115s0477.1.p	Phytozome
248	Br_Salvadora_sp	15.32	15.32	RTTY_scaffold_2003647	OneKP
280	Br_Schrenkiella_parvula_1	23.649	22.433	Sp4g05820.1	Phytozome
65	Br_Schrenkiella_parvula_2	1.012	0	Sp3g19380.1	Phytozome
277	Br_Sinapis_alba_1	23.533	0	VMNH_scaffold_2015996	OneKP
58	Br_Sinapis_alba_2	-2.57	0	VMNH_scaffold_2086691	OneKP
274	Br_Stanleya_pinnata_1	23.827	0	Stapi.0477s0007.1.p	Phytozome
54	Br_Stanleya_pinnata_2	-2.741	0	Stapi.3359s0003.1.p	Phytozome
282	Br_Thlaspi_arvense_1	22.936	22.936	Thlar.0125s0039.1.p	Phytozome
63	Br_Thlaspi_arvense_2	-3.702	0	Thlar.0048s0138.1.p	Phytozome
344	Br_Tropaeolum_peregrinum	8.484	0	MYZV_scaffold_2059453	OneKP
245	Bu_Buxus sempervirens_1	-2.463	0	IWMW_scaffold_2002385	OneKP
244	Bu_Buxus sempervirens_2	-2.492	0	IWMW_scaffold_2090445	OneKP
427	Ca_Amaranthus_hypochondriacus	6.345	0	AHYPO_008224-RA	Phytozome
428	Ca_Beta_vulgaris	12.526	12.526	EL10Ac2g03948.1	Phytozome
429	Ca_Chenopodium_quinoa	13.705	13.705	AUR62009205-RA	Phytozome
430	Ca_Spinacia_oleracea	13.439	13.439	Spov3_chr4.03819	Phytozome
3	Cha_Chara_braunii	-0.022	0	Cbraunii_ELF3	other
168	Co_Caiophora_chuquitensis	0.69	0	VTLJ_scaffold_2070922	OneKP
420	Co_Cornus_florida	3.14	0	BFJL_scaffold_2007482	OneKP
418	Co_Hydrangea_quercifolia	9.371	0	ZETY_scaffold_2002616	OneKP

Branch ID	Leaf name	LLR*	CORE score	Original name	Source†
419	Co_Nyssa_ogeche	5.258	0	VUSY_scaffold_2027802	OneKP
433	Cu_Cucumis_sativus_1	0.909	0	Cucsa.395270.1	Phytosome
123	Cu_Cucumis_sativus_2	5.011	0	Cucsa.360760.1	Phytosome
4	De_Penium_margaritaceum	33.88	0	Pmargaritaceum_ELF3	other
16	Dic_Ceratodon_purpureus	7.332	0	CepurGG1.9G105700.1.p	Phytosome
422	Dil_Dillenia_indica_1	3.095	0	EHNF_scaffold_2000714	OneKP
170	Dil_Dillenia_indica_2	-3.157	0	EHNF_scaffold_2011941	OneKP
173	Dio_Dioscorea_alata_1	4.025	0	Dioal.2252s0007.1.p	Phytosome
212	Dio_Dioscorea_alata_2	4.375	0	Dioal.2934s0036.1.p	Phytosome
395	Dip_Symphoricarpos_sp	5.666	0	CAQZ_scaffold_2007129	OneKP
164	Er_Ardisia_humilis	-9.336	0	ODDO_scaffold_2105263	OneKP
415	Er_Fouquieria_macdougallii_1	6.646	0	YSRZ_scaffold_2092112	OneKP
165	Er_Fouquieria_macdougallii_2	-0.285	0	YSRZ_scaffold_2020919	OneKP
417	Er_Maesa_lanceolata	7.238	0	DTOA_scaffold_2095414	OneKP
413	Er_Manilkara_zapota	0.26	0	BEFC_scaffold_2018766	OneKP
416	Er_Rhododendron_tomentosum	5.663	0	WXVX_scaffold_2017785	OneKP
414	Er_Synsepalum_dulcificum_1	6.333	0	WRPP_scaffold_2006528	OneKP
167	Er_Synsepalum_dulcificum_2	0.238	0	WRPP_scaffold_2008141	OneKP
166	Er_Ternstroemia_gymnanthera	-1.567	0	NGRR_scaffold_2023483	OneKP
319	Fab_Acacia_argyrophylla	7.992	0	ZCDJ_scaffold_2016863	OneKP
304	Fab_Arachis_hypogaea_1	13.408	0	arahy.Tifrunner.gnm1.ann1.14SSB6.1	Phytosome
317	Fab_Arachis_hypogaea_2	12.403	0	arahy.Tifrunner.gnm1.ann1.K5TY51.1	Phytosome
321	Fab_Bauhinia_tomentosa	4.086	0	JETM_scaffold_2003748	OneKP
314	Fab_Cicer_arietinum_1	-2.311	0	Ca_01620	Phytosome
295	Fab_Cicer_arietinum_2	5.523	0	Ca_09197	Phytosome
131	Fab_Cicer_arietinum_3	9.459	0	Ca_10118	Phytosome
307	Fab_Codariocalyx_motorius	8.216	0	SUAK_scaffold_2042167	OneKP
320	Fab_Copaifera_officinalis	8.233	8.076	RKLL_scaffold_2013837	OneKP
308	Fab_Glycine_max_1	3.832	0	Glyma.04G050200.1	Phytosome
298	Fab_Glycine_max_2	7.18	0	Glyma.17G231600.1	Phytosome
134	Fab_Glycine_max_3	3.074	0	Glyma.08G197500.1	Phytosome
309	Fab_Glycine_soja	3.832	0	FPLR_scaffold_2024074	OneKP
313	Fab_Glycyrrhiza_glabra	5.826	0	PEZP_scaffold_2008368	OneKP
312	Fab_Glycyrrhiza_lepidota	4.736	0	JTQQ_scaffold_2005272	OneKP
305	Fab_Gompholobium_polymorphum	1.146	0	VLNB_scaffold_2003784	OneKP
311	Fab_Lotus_japonicus_1	4.1	0	Lj1g0009532.1	Phytosome
139	Fab_Lotus_japonicus_2	-1.494	0	Lj3g0013066.1	Phytosome
303	Fab_Lupinus_albus_1	4.25	0	Lalb_Chr22g0355951	Phytosome
306	Fab_Lupinus_albus_2	-0.094	0	Lalb_Chr23g0267721	Phytosome
130	Fab_Lupinus_albus_3	-5.606	0	Lalb_Chr25g0280491	Phytosome
296	Fab_Medicago_truncatula_1	5.546	0	Medtr1g016920.1	Phytosome
315	Fab_Medicago_truncatula_2	2.124	0	Medtr3g103970.1	Phytosome
132	Fab_Medicago_truncatula_3	3.787	0	Medtr8g015480.1	Phytosome
301	Fab_Phaseolus_acutifolius_1	10.42	0	Phacu.CVR.001G033200.1	Phytosome
138	Fab_Phaseolus_acutifolius_2	2.607	0	Phacu.CVR.010G170000.1	Phytosome
300	Fab_Phaseolus_lunatus_1	10.893	0	PI01G0000037300.1.v1	Phytosome
136	Fab_Phaseolus_lunatus_2	2.607	0	PI10G0000335200.1.v1	Phytosome
302	Fab_Phaseolus_vulgaris_1	11.373	0	Phvul.001G032900.1	Phytosome
137	Fab_Phaseolus_vulgaris_2	2.607	0	Phvul.010G142900.7	Phytosome
316	Fab_Trifolium_pratense_1	-1.436	0	Tp57577_TGAC_v2_mRNA26220	Phytosome
297	Fab_Trifolium_pratense_2	4.64	0	Tp57577_TGAC_v2_mRNA13433	Phytosome
133	Fab_Trifolium_pratense_3	5.806	0	Tp57577_TGAC_v2_mRNA9055	Phytosome
299	Fab_Vigna_unguiculata_1	11.059	0	Vigun08g035200.1.p	Phytosome
310	Fab_Vigna_unguiculata_2	5.237	0	Vigun09g227400.1.p	Phytosome
135	Fab_Vigna_unguiculata_3	3.766	0	Vigun10g177000.1.p	Phytosome
318	Fab_Xanthocercis_zambesiaca	4.609	0	ZSSR_scaffold_2025321	OneKP
339	Fag_Alnus_serrulata_1	4.252	0	LWDA_scaffold_2002989	OneKP
140	Fag_Alnus_serrulata_2	0.077	0	LWDA_scaffold_2001528	OneKP
338	Fag_Betula_pendula	6.167	0	CWZU_scaffold_2047095	OneKP
335	Fag_Carya_illinoensis_1	8.763	0	Caril.16G031500.1.p	Phytosome
141	Fag_Carya_illinoensis_2	8.693	0	Caril.01G224800.1.p	Phytosome
143	Fag_Castanea_crenata	-1.43	0	NHUA_scaffold_2004876	OneKP
342	Fag_Castanea_dentata_1	13.383	11.983	Caden.01G011300.1.p	Phytosome
144	Fag_Castanea_dentata_2	0.844	0	Caden.05G056000.1.p	Phytosome
343	Fag_Castanea_pumila_1	11.382	0	UZWG_scaffold_2013481	OneKP

Branch ID	Leaf name	LLR*	CORE score	Original name	Source†
145	Fag_Castanea_pumila_2	0.844	0	UZWG_scaffold_2006913	OneKP
340	Fag_Fagus_sylvatica	17.561	0	SVVG_scaffold_2073660	OneKP
336	Fag_Juglans_nigra	11.044	11.044	DXQW_scaffold_2063283	OneKP
334	Fag_Lophozonia_obliqua_1	5.209	0	TJLC_scaffold_2013402	OneKP
146	Fag_Lophozonia_obliqua_2	4.989	0	TJLC_scaffold_2000518	OneKP
142	Fag_Morella_cerifera	6.522	0	INSP_scaffold_2003628	OneKP
341	Fag_Quercus_shumardii	6.339	0	HENI_scaffold_2011763	OneKP
15	Fu_Physcomitrium_patens_1	1.381	0	Pp3c1_12790V3.1	Phytozome
18	Fu_Physcomitrium_patens_2	9.158	9.158	Pp3c11_14750V3.1	Phytozome
14	Fu_Physcomitrium_patens_3	-1.19	0	Pp3c7_10610V3.1	Phytozome
17	Fu_Physcomitrium_patens_4	10.678	10.678	Pp3c7_10630V3.1	Phytozome
405	Gen_Apocynum_androsaemifolium	3.577	0	JCLQ_scaffold_2046858	OneKP
404	Gen_Coffea_arabica_1	10.574	10.574	evm.model.Scaffold_597.214	Phytozome
155	Gen_Coffea_arabica_2	-7.319	0	evm.model.Scaffold_352.280	Phytozome
406	Gen_Holarrhena_pubescens	7.206	0	JGYZ_scaffold_2047241	OneKP
379	Ger_Francoa_appendiculata	0.764	0	HDWF_scaffold_2006203	OneKP
378	Ger_Geranium_carolinianum	6.528	0	VKGP_scaffold_2014390	OneKP
1	Gi_Ginkgo_biloba_1	-3.292	0	Gb_05973	other
27	Gi_Ginkgo_biloba_2	0.459	0	Gb_02475	other
28	Gi_Ginkgo_biloba_3	11.027	0	Gb_27015	other
398	Ic_Pyrenacantha_malvifolia	3.23	0	QZZU_scaffold_2009667	OneKP
13	Kl_Klebsormidium_nitens	12.047	0	Klebsormidium_nitens_ELF3	other
401	Lam_Buddleja_sp	3.577	0	GRFT_scaffold_2016732	OneKP
399	Lam_Erythranthe_guttata_1	-1.054	0	Migut.E01551.1	Phytozome
402	Lam_Erythranthe_guttata_2	-2.914	0	Migut.A00160.1	Phytozome
162	Lam_Erythranthe_guttata_3	-11.816	0	Migut.I00992.1	Phytozome
403	Lam_Olea_europaea	9.884	0	TORX_scaffold_2011390	OneKP
400	Lam_Schlegelia_parasitica	4.313	0	GAKQ_scaffold_2018921	OneKP
228	Lau_Cinnamomum_kanehirae_1	8.111	0	CKAN_00080000	Phytozome
227	Lau_Cinnamomum_kanehirae_2	1.774	0	CKAN_00191600	Phytozome
230	Lau_Cinnamomum_kanehirae_3	3.659	0	CKAN_01147800	Phytozome
229	Lau_Peumus_boldus	2.785	0	KRJP_scaffold_2014506	OneKP
224	Mag_Annona_muricata	4.793	0	YZRI_scaffold_2000887	OneKP
225	Mag_Magnolia_grandiflora	-0.664	0	WBOD_scaffold_2005290	OneKP
226	Mag_Myristica_fragrans	-1.432	0	OBPL_scaffold_2009542	OneKP
108	Malp_Bischofia_javanica	2.028	0	VNMY_scaffold_2017888	OneKP
374	Malp_Chrysobalanus_icaco_1	7.824	0	ZBVT_scaffold_2012782	OneKP
106	Malp_Chrysobalanus_icaco_2	1.763	0	ZBVT_scaffold_2063962	OneKP
101	Malp_Croton_tiglium	-5.256	0	VVPY_scaffold_2064728	OneKP
104	Malp_Erythroxylum_coca	6.93	0	RPPC_scaffold_2073745	OneKP
99	Malp_Euphorbia_mesembryanthemifolia	5.173	0	LSLA_scaffold_2057717	OneKP
373	Malp_Licania_michauxii_1	11.341	0	HBUQ_scaffold_2004829	OneKP
105	Malp_Licania_michauxii_2	4.262	0	HBUQ_scaffold_2008544	OneKP
431	Malp_Linum_usitatissimum_1	0.122	0	Lus10007459	Phytozome
434	Malp_Linum_usitatissimum_2	-6.683	0	Lus10006857	Phytozome
435	Malp_Linum_usitatissimum_3	-5.882	0	Lus10037599	Phytozome
94	Malp_Malesherbia_fasciculata	3.485	0	COAQ_scaffold_2010793	OneKP
376	Malp_Manihot_esculenta_1	-0.284	0	Manes.16G077200.1	Phytozome
102	Malp_Manihot_esculenta_2	1.062	0	Manes.04G136600.1	Phytozome
377	Malp_Manihot_grahamii_1	-1.162	0	XNLP_scaffold_2017807	OneKP
103	Malp_Manihot_grahamii_2	0.611	0	XNLP_scaffold_2007743	OneKP
74	Malp_Ochna_serrulata_1	-7.242	0	CKDK_scaffold_2093907	OneKP
73	Malp_Ochna_serrulata_2	-4.567	0	CKDK_scaffold_2024476	OneKP
366	Malp_Passiflora_caerulea	9.443	0	SIZE_scaffold_2013559	OneKP
93	Malp_Passiflora_edulis	2.53	0	EZZT_scaffold_2008682	OneKP
107	Malp_Phyllanthus_sp	0.113	0	YGAT_scaffold_2006934	OneKP
367	Malp_Populus_deltoides_1	2.871	0	Podel.06G246600.1.p	Phytozome
96	Malp_Populus_deltoides_2	-4.345	0	Podel.03G048200.1.p	Phytozome
368	Malp_Populus_trichocarpa_1	3.123	0	Potri.006G233800.1	Phytozome
97	Malp_Populus_trichocarpa_2	-3.066	0	Potri.003G045000.1	Phytozome
375	Malp_Ricinus_communis_1	4.274	0	29794.m003359	Phytozome
100	Malp_Ricinus_communis_2	6.649	0	30146.m003441	Phytozome
369	Malp_Salix_dasyclados	6.089	0	IEPQ_scaffold_2006985	OneKP
371	Malp_Salix_erioccephala	2.712	0	GLVK_scaffold_2015191	OneKP
372	Malp_Salix_purpurea_1	5.041	0	SapurV1A.3017s0030.1	Phytozome

Branch ID	Leaf name	LLR*	CORE score	Original name	Source†
95	Malp_Salix_purpurea_2	-0.628	0	SapurV1A.1320s0030.1	Phytozome
370	Malp_Salix_viminalis	8.592	0	KKDQ_scaffold_2024203	OneKP
98	Malp_Viola_canadensis	0.907	0	NJLF_scaffold_2011630	OneKP
349	Malv_Bixa_orellana_1	6.173	0	KPTE_scaffold_2009852	OneKP
92	Malv_Bixa_orellana_2	2.744	0	KPTE_scaffold_2011441	OneKP
432	Malv_Edgeworthia_chrysantha	2.88	0	AWJM_scaffold_2017163	OneKP
354	Malv_Gossypium_barbadense_1	13.335	0	Gobar.A07G024900.1.p	Phytozome
80	Malv_Gossypium_barbadense_2	3.27	0	Gobar.A09G084400.1.p	Phytozome
88	Malv_Gossypium_barbadense_3	-0.212	0	Gobar.D05G137700.1.p	Phytozome
350	Malv_Gossypium_darwinii_1	12.053	0	Godar.D07G025000.1.p	Phytozome
81	Malv_Gossypium_darwinii_2	3.27	0	Godar.A09G102700.1.p	Phytozome
89	Malv_Gossypium_darwinii_3	-0.212	0	Godar.D05G144000.1.p	Phytozome
355	Malv_Gossypium_hirsutum_1	13.335	0	Gohir.1Z072500.1.p	Phytozome
79	Malv_Gossypium_hirsutum_2	3.27	0	Gohir.A09G080800.1.p	Phytozome
87	Malv_Gossypium_hirsutum_3	-0.212	0	Gohir.D05G134900.1.p	Phytozome
352	Malv_Gossypium_mustelinum_1	13.335	0	Gomus.A07G024200.1.p	Phytozome
83	Malv_Gossypium_mustelinum_2	3.27	0	Gomus.A09G087900.1.p	Phytozome
90	Malv_Gossypium_mustelinum_3	-0.212	0	Gomus.D05G143100.1.p	Phytozome
353	Malv_Gossypium_tomentosum_1	13.335	0	Gotom.A07G024400.1.p	Phytozome
82	Malv_Gossypium_tomentosum_2	3.27	0	Gotom.A09G098300.1.p	Phytozome
86	Malv_Gossypium_tomentosum_3	-0.212	0	Gotom.D05G145400.1.p	Phytozome
351	Malv_Gossypium_raitmondii_1	15.088	0	Gorai.001G024000.1	Phytozome
109	Malv_Gossypium_raitmondii_2	-0.768	0	Gorai.003G060800.1	Phytozome
78	Malv_Gossypium_raitmondii_3	4.037	0	Gorai.006G096400.1	Phytozome
85	Malv_Gossypium_raitmondii_4	-0.212	0	Gorai.009G138600.1	Phytozome
356	Malv_Hibiscus_cannabinus	9.587	0	OLXF_scaffold_2014757	OneKP
84	Malv_Hoheria_angustifolia	2.866	0	ZSAB_scaffold_2036792	OneKP
347	Malv_Muntingia_calabura	5.291	0	ATFX_scaffold_2046240	OneKP
348	Malv_Schizolaena_sp	19.081	19.081	WMUK_scaffold_2000766	OneKP
357	Malv_Theobroma_cacao_1	12.755	0	Thecc1EG037249t1	Phytozome
91	Malv_Theobroma_cacao_2	1.03	0	Thecc1EG028963t1	Phytozome
394	Malv_Wikstroemia_indica	3.012	0	QJXB_scaffold_2000421	OneKP
11	Mar_Marchantia_polymorpha	6.259	0	Mapoly0014s0139.1	Phytozome
382	My_Corymbia_citriodora_1	3.829	0	Cocit.F0677.1.p	Phytozome
149	My_Corymbia_citriodora_2	0.614	0	Cocit.F2489.1.p	Phytozome
384	My_Eucalyptus_grandis_1	6.712	0	Eucgr.C02997.1	Phytozome
150	My_Eucalyptus_grandis_2	-3.7	0	Eucgr.F03094.1	Phytozome
147	My_Oenothera_berlandieri	-0.807	0	EQYT_scaffold_2010727	OneKP
148	My_Oenothera_suffulta	0.102	0	JKNQ_scaffold_2008905	OneKP
383	My_Syzygium_micranthum	5.413	0	NEBM_scaffold_2013272	OneKP
381	My_Tetrazygia_bicolor	7.021	0	SWGX_scaffold_2006915	OneKP
220	Ny_Nymphaea_colorata_1	-1.499	0	Nycol.A02041.1.p	Phytozome
221	Ny_Nymphaea_colorata_2	-0.43	0	Nycol.F00558.1.p	Phytozome
122	Ox_Cephalotus_follicularis	-3.922	0	YZVJ_scaffold_2010285	OneKP
365	Ox_Cunonia_capensis	4.163	0	TIUZ_scaffold_2007112	OneKP
364	Ox_Elaeocarpus_sylvestris	8.992	0	THHD_scaffold_2009392	OneKP
26	Pi_Thuja_plicata_1	2.53	0	Thupl.29377949s0003.1.p	Phytozome
25	Pi_Thuja_plicata_2	7.332	0	Thupl.29380725s0010.1.p	Phytozome
175	Poa_Ananas_comosus	0.492	0	Aco005852.1	Phytozome
200	Poa_Brachypodium_distachyon	2.661	0	Bradi2g14290.1	Phytozome
201	Poa_Brachypodium_hybridum	2.225	0	Brahy.D02G0200100.1.p	Phytozome
203	Poa_Brachypodium_mexicanum	1.256	0	Brame.03PG298400.1.p	Phytozome
199	Poa_Brachypodium_stacei	-1.373	0	Brast08G002600.1	Phytozome
202	Poa_Brachypodium_sylvaticum	0.681	0	Brasy1G332900.1.p	Phytozome
185	Poa_Eleusine_coracana	9.799	0	ELECO.r07.1AG0021330.1	Phytozome
207	Poa_Hordeum_vulgare	8.521	0	HORVU1Hr1G094980.1	Phytozome
208	Poa_Joinvillea_ascendens	-2.572	0	Joasc.09G167600.1.p	Phytozome
177	Poa_Miscanthus_sinensis_1	9.101	0	Misin05G173100.1.p	Phytozome
191	Poa_Miscanthus_sinensis_2	7.289	0	Misin16G260800.1.p	Phytozome
189	Poa_Oropetium_thomaeum_1	-3.217	0	Oropetium_20150105_04072A	Phytozome
186	Poa_Oropetium_thomaeum_2	6.586	0	Oropetium_20150105_23950A	Phytozome
188	Poa_Oryza_sativa_1	7.122	0	LOC_Os06g05060.1	Phytozome
187	Poa_Oryza_sativa_2	4.465	0	LOC_Os01g38530.1	Phytozome
198	Poa_Panicum_hallii_1	2.73	0	Pahal.C01693.1	Phytozome
180	Poa_Panicum_hallii_2	8.052	0	Pahal.H01171.1	Phytozome

Branch ID	Leaf name	LLR*	CORE score	Original name	Source†
197	Poa_Panicum_virgatum_1	4.549	0	Pavir.J05026.1	Phytozome
181	Poa_Panicum_virgatum_2	5.856	0	Pavir.Ea01714.1	Phytozome
179	Poa_Paspalum_vaginatum_1	3.039	0	Pavag03G158100.1.p	Phytozome
193	Poa_Paspalum_vaginatum_2	3.616	0	Pavag09G259600.1.p	Phytozome
194	Poa_Setaria_italica_1	0.234	0	Seita.3G121000.1	Phytozome
182	Poa_Setaria_italica_2	2.893	0	Seita.5G204600.1	Phytozome
195	Poa_Setaria_viridis_1	2.118	0	Sevir.3G123200.1	Phytozome
183	Poa_Setaria_viridis_2	1.548	0	Sevir.5G206400.1	Phytozome
192	Poa_Sorghum_bicolor_1	9.728	0	Sobic.009G257300.1	Phytozome
178	Poa_Sorghum_bicolor_2	7.568	7.568	Sobic.003G191700.1	Phytozome
204	Poa_Thinopyrum_intermedium	2.623	0	Thint.03G0586000.1.p	Phytozome
205	Poa_Triticum_aestivum	4.536	0	Traes_1AL_52C5531A4.1	Phytozome
196	Poa_Urochloa_fusca_1	1.605	0	Urofu.3G150900.1.p	Phytozome
184	Poa_Urochloa_fusca_2	6.492	0	Urofu.5G292000.1.p	Phytozome
190	Poa_Zea_mays_1	-6.01	0	Zm00008a026555_T01	Phytozome
176	Poa_Zea_mays_2	3.352	0	Zm00008a014437_T01	Phytozome
7	Pol_Ceratopteris_richardii_1	-7.733	0	Ceric.02G084100.1.p	Phytozome
5	Pol_Ceratopteris_richardii_2	9.303	0	Ceric.03G010400.1.p	Phytozome
6	Pol_Ceratopteris_richardii_3	-0.499	0	Ceric.08G069300.1.p	Phytozome
8	Pol_Ceratopteris_richardii_4	-0.468	0	Ceric.14G010200.1.p	Phytozome
241	Pr_Meliosma_cuneifolia	1.903	0	AALA_scaffold_2014849	OneKP
242	Pr_Platanus_occidentalis	-2.051	0	VQFW_scaffold_2009679	OneKP
232	Ra_Aquilegia_coerulea_1	4.37	0	Aqcoe7G417000.1	Phytozome
231	Ra_Aquilegia_coerulea_2	5.394	0	Aqcoe7G142600.1	Phytozome
239	Ra_Argemone_mexicana	0.579	0	CCHG_scaffold_2063783	OneKP
234	Ra_Capnoides_sempervirens	2.671	0	AUGV_scaffold_2013471	OneKP
240	Ra_Chelidonium_majus	4.231	0	XMVD_scaffold_2053225	OneKP
235	Ra_Corydalis_linstowiana	6.197	0	ZGQD_scaffold_2013982	OneKP
233	Ra_Hypecoum_procumbens	6.617	0	NMGG_scaffold_2065255	OneKP
238	Ra_Papaver_bracteatum	10.145	0	ZSNV_scaffold_2025678	OneKP
237	Ra_Papaver_rhoeas	3.289	0	IORZ_scaffold_2027685	OneKP
236	Ra_Papaver_somniferum	3.681	0	SUFP_scaffold_2027421	OneKP
323	Ro_Cannabis_sativa	4.12	0	DGNP_scaffold_2005108	OneKP
324	Ro_Celtis_occidentalis	8.468	0	KYAD_scaffold_2008995	OneKP
333	Ro_Dryas_octopetala	5.669	0	SQCF_scaffold_2000931	OneKP
127	Ro_Elaeagnus_pungens	4.241	0	RBYC_scaffold_2017609	OneKP
325	Ro_Ficus_religiosa	4.399	0	EDHN_scaffold_2010547	OneKP
329	Ro_Fragaria vesca_1	7.24	0	mrna02656.1-v1.0-hybrid	Phytozome
125	Ro_Fragaria vesca_2	2.533	0	mrna22895.1-v1.0-hybrid	Phytozome
328	Ro_Fragaria_x_ananassa_1	8.147	0	maker-Fvb2-4-226.65	Phytozome
124	Ro_Fragaria_x_ananassa_2	2.533	0	maker-Fvb6-1-133.36	Phytozome
128	Ro_Frangula_caroliniana	3.445	0	WVEF_scaffold_2057738	OneKP
322	Ro_Humulus_lupulus	4.085	0	AQGE_scaffold_2008477	OneKP
331	Ro_Kerria_japonica	4.518	0	TJQY_scaffold_2009698	OneKP
330	Ro_Malus_domestica	9.319	0	MDP0000129641	Phytozome
326	Ro_Morus_nigra	-2.6	0	XVJB_scaffold_2000580	OneKP
332	Ro_Prunus_persica_1	6.704	0	Prupe.1G416000.1	Phytozome
126	Ro_Prunus_persica_2	3.564	0	Prupe.3G054300.1	Phytozome
327	Ro_Rosa_palustris	6.607	0	IANR_scaffold_2013640	OneKP
129	Ro_Ziziphus_jujuba	3.032	0	ZHEE_scaffold_2043480	OneKP
425	San_Daenikera_sp	-4.541	0	BSEY_scaffold_2085931	OneKP
426	San_Exocarpos_cupressiformis	-0.808	0	XGFU_scaffold_2013721	OneKP
361	Sap_Acer_negundo_1	9.815	0	VFFP_scaffold_2005559	OneKP
120	Sap_Acer_negundo_2	3.16	0	VFFP_scaffold_2007973	OneKP
113	Sap_Ailanthus_altissima	-0.739	0	QICX_scaffold_2038041	OneKP
362	Sap_Anacardium_occidentale_1	5.959	0	Anaoc.0019s0253.1.p	Phytozome
110	Sap_Anacardium_occidentale_2	-2.798	0	Anaoc.0914s0004.1.p	Phytozome
117	Sap_Azadirachta_indica	4.735	0	UVDC_scaffold_2042648	OneKP
359	Sap_Citrus_clementina_1	3.718	0	Ciclev10007592m	Phytozome
115	Sap_Citrus_clementina_2	6.085	0	Ciclev10024969m	Phytozome
360	Sap_Citrus_sinensis_1	3.718	0	orange1.1g004928m	Phytozome
116	Sap_Citrus_sinensis_2	6.085	0	orange1.1g004483m	Phytozome
119	Sap_Kirkia_wilmsii	-3.289	0	BCAA_scaffold_2073197	OneKP
121	Sap_Litchi_chinensis	0.193	0	WAXR_scaffold_2000314	OneKP
118	Sap_Melia_azedarach	3.007	0	VCCF_scaffold_2010620	OneKP

Branch ID	Leaf name	LLR*	CORE score	Original name	Source†
337	Sap_Phellodendron_amurense	11.044	11.044	PGKL_scaffold_2074628	OneKP
358	Sap_Poncirus_trifoliata_1	2.464	0	Ptrif.0001s0468.1.p	Phytozome
114	Sap_Poncirus_trifoliata_2	7.175	0	Ptrif.0007s0826.1.p	Phytozome
112	Sap_Quassia_amara	-2.882	0	IKFD_scaffold_2008453	OneKP
363	Sap_Toxicodendron_radicans_1	7.153	0	YUOM_scaffold_2012634	OneKP
111	Sap_Toxicodendron_radicans_2	1.377	0	YUOM_scaffold_2008412	OneKP
151	Sax_Astilbe_chinensis	2.439	0	CKKR_scaffold_2063203	OneKP
423	Sax_Bergenia_sp	11.044	9.833	CIAC_scaffold_2027267	OneKP
153	Sax_Cercidiphyllum_japonicum	4.16	0	NUZN_scaffold_2001312	OneKP
290	Sax_Hamamelis_virginiana_1	9.638	0	YHXT_scaffold_2010362	OneKP
154	Sax_Hamamelis_virginiana_2	8.866	0	YHXT_scaffold_2011928	OneKP
288	Sax_Itea_virginica	6.302	0	UWFU_scaffold_2004878	OneKP
293	Sax_Kalanchoe_fedtschenkoi_1	14.679	14.679	Kaladp0039s0732.1	Phytozome
29	Sax_Kalanchoe_fedtschenkoi_2	8.615	0	Kaladp0092s0181.1	Phytozome
294	Sax_Kalanchoe_laxiflora_1	14.679	14.679	Kalax.0540s0009.1	Phytozome
30	Sax_Kalanchoe_laxiflora_2	6.627	0	Kalax.1678s0001.1	Phytozome
289	Sax_Loropetalum_chinense	9.843	0	HQRJ_scaffold_2024346	OneKP
424	Sax_Oresitrophe_rupifraga	15.118	14.861	UHBY_scaffold_2030188	OneKP
152	Sax_Pectiantia_pentandra	1.092	0	DAYQ_scaffold_2058037	OneKP
10	Se_Selaginella_moellendorffii_1	6.305	0	411196	Phytozome
12	Se_Selaginella_moellendorffii_2	6.481	0	415241	Phytozome
158	So_Ipomoea_nil	-2.256	0	NHAG_scaffold_2051016	OneKP
159	So_Ipomoea_purpurea	1.272	0	SDXI_scaffold_2016990	OneKP
412	So_Solanum_lycopersicum_1	6.085	0	Solyc08g065870.2.1	Phytozome
408	So_Solanum_lycopersicum_2	9.606	0	Solyc12g095900.1.1	Phytozome
410	So_Solanum_lycopersicum_3	7.095	0	Solyc11g070100.1.1	Phytozome
157	So_Solanum_lycopersicum_4	-8.102	0	Solyc06g062480.2.1	Phytozome
411	So_Solanum_tuberosum_1	4.65	0	PGSC0003DMT400035914	Phytozome
407	So_Solanum_tuberosum_2	13.836	13.836	PGSC0003DMT400075345	Phytozome
409	So_Solanum_tuberosum_3	9.803	0	PGSC0003DMT400065601	Phytozome
156	So_Solanum_tuberosum_4	-8.645	0	PGSC0003DMT400012338	Phytozome
21	Sphag_Sphagnum_fallax_1	5.92	0	Sphfalx0084s0050.1	Phytozome
19	Sphag_Sphagnum_fallax_2	3.142	0	Sphfalx0299s0004.1	Phytozome
23	Sphag_Sphagnum_fallax_3	12.032	11.574	Sphfalx0004s0165.1	Phytozome
24	Sphag_Sphagnum_magellanicum_1	16.26	0	Sphmag10G060500.1.p	Phytozome
22	Sphag_Sphagnum_magellanicum_2	0.869	0	Sphmag11G082000.1.p	Phytozome
20	Sphag_Sphagnum_magellanicum_3	3.988	0	Sphmag04G092400.1.p	Phytozome
9	Spi_Spirogloea_muscicola	-6.514	0	Smuscicola_ELF3	other
243	Tr_Trochodendron_aralioides	2.412	0	SWOH_scaffold_2004856	OneKP
292	Vi_Tetrastigma_voinierianum	5.056	0	SZPD_scaffold_2011653	OneKP
291	Vi_Vitis_vinifera_1	6.756	0	GSVIVT01035337001	Phytozome
169	Vi_Vitis_vinifera_2	1.417	0	GSVIVT01016905001	Phytozome
213	Zi_Musa_acuminata_1	-1.007	0	GSMUA_Achr1T05150_001	Phytozome
214	Zi_Musa_acuminata_2	-2.244	0	GSMUA_Achr5T09620_001	Phytozome
215	Zi_Musa_acuminata_3	-7.679	0	GSMUA_Achr1T14390_001	Phytozome
216	Zi_Musa_acuminata_4	-6.123	0	GSMUA_Achr2T08490_001	Phytozome
380	Zy_Krameria_lanceolata	2.279	0	ZHMB_scaffold_2016475	OneKP
2	Zyg_Mesotaenium_endlicherianum	1.983	0	Mendlicheranium_ELF3	other

* For each sequence, the Log-likelihood ratio (LLR) and COREscore were retrieved using PLAAC (<http://plaac.wi.mit.edu>, Lancaster *et al.*, 2014) to represent prion-like properties

† Gene homologues were identified from available plant genomes in Phytozome v12.1, v13 (<https://phytozome-next.jgi.doe.gov>, Goodstein *et al.*, 2012) and OneKP (<http://www.onekp.com>, Matasci *et al.*, 2014) databases

Appendix V

Table 5 Hypocotyl growth rate under temperature cycles in LL (related to Fig. 4-4B).

Time (h)/ZT*	48/ZT00	52/ZT04	56/ZT08	60/ZT12	64/ZT16	68/ZT20	72/ZT24	
Genotype	Growth (mm h ⁻¹) ± SEM (n=8)							P
Ws-2	0.0075 ±	0.0533 ±	0.0996 ±	0.0584 ±	0.0164 ±	0.0100 ±	0.0042 ±	0.004
	0.0056 a [†]	0.0250 ab	0.0353 b	0.0199 ab	0.0092 a	0.0071 a	0.0034 a	
<i>elf3-4</i>	0.0273 ±	0.0448 ±	0.0469 ±	0.0432 ±	0.0258 ±	0.0244 ±	0.0278 ±	0.299
	0.0070	0.0113	0.0071	0.0113	0.0058	0.0074	0.0114	
<i>gi-158</i>	0.0082 ±	0.0795 ±	0.0746 ±	0.0533 ±	0.0318 ±	0.0126 ±	0.0264 ±	0.002
	0.0065 a	0.0125 c	0.0192 bc	0.0178 abc	0.0078 abc	0.0072 ab	0.0206 abc	
<i>elf3-4</i>	0.0788 ±	0.0858 ±	0.0971 ±	0.0806 ±	0.0595 ±	0.0476 ±	0.0656 ±	0.300
<i>gi-158</i>	0.0202	0.0148	0.0112	0.0150	0.0111	0.0144	0.0174	
	72/ZT00	76/ZT04	80/ZT08	84/ZT12	88/ZT16	92/ZT20	96/ZT24	
Ws-2	0.0042 ±	0.0361 ±	0.0836 ±	0.0410 ±	0.0095 ±	0.0128 ±	0.0019 ±	0.003
	0.0034 a	0.0138 ab	0.0187 b	0.0208 ab	0.0055 a	0.0128 a	0.0011 a	
<i>elf3-4</i>	0.0278 ±	0.0239 ±	0.0258 ±	0.0150 ±	0.0364 ±	0.0382 ±	0.0205 ±	0.649
	0.0114	0.0086	0.0081	0.0064	0.0144	0.0108	0.0073	
<i>gi-158</i>	0.0264 ±	0.0589 ±	0.0941 ±	0.0540 ±	0.0309 ±	0.0196 ±	0.0062 ±	0.002
	0.0206 a	0.0199 ab	0.0100 b	0.0162 ab	0.0123 a	0.0098 a	0.047 a	
<i>elf3-4</i>	0.0656 ±	0.0641 ±	0.0756 ±	0.0725 ±	0.0529 ±	0.0575 ±	0.0296 ±	0.399
<i>gi-158</i>	0.0174	0.0115	0.0145	0.0183	0.0163	0.0129	0.0127	
	96/ZT00	100/ZT04	104/ZT08	108/ZT12	112/ZT16	116/ZT20	120/ZT24	
Ws-2	0.0019 ±	0.0408 ±	0.0405 ±	0.0711 ±	0.0049 ±	0.0058 ±	0.0239 ±	0.001
	0.0011 a	0.0121 ab	0.0120 ab	0.0231 b	0.0043 a	0.0056 a	0.0131 ab	
<i>elf3-4</i>	0.0205 ±	0.0314 ±	0.0276 ±	0.0255 ±	0.0425 ±	0.0168 ±	0.0108 ±	0.193
	0.0073	0.0119	0.0070	0.0064	0.0125	0.0064	0.0035	
<i>gi-158</i>	0.0062 ±	0.0461 ±	0.0535 ±	0.0530 ±	0.0155 ±	0.0223 ±	0.0164 ±	0.024
	0.0047	0.0117	0.0190	0.0149	0.0073	0.0098	0.0113	
<i>elf3-4</i>	0.0296 ±	0.0804 ±	0.0776 ±	0.0401 ±	0.0530 ±	0.0356 ±	0.0211 ±	0.017
<i>gi-158</i>	0.0127 ab	0.0102 b	0.0216 ab	0.0079	0.0147 ab	0.0129 ab	0.0107 a	
	120/ZT00	124/ZT04	128/ZT08	132/ZT12	136/ZT16	140/ZT20	144/ZT24	
Ws-2	0.0239 ±	0.0296 ±	0.0668 ±	0.0366 ±	0.0019 ±	0.0064 ±	0.0009 ±	0.000
	0.0131 a	0.0154 ab	0.0116 b	0.0078 ab	0.0013 a	0.0039 a	0.0005 a	
<i>elf3-4</i>	0.0108 ±	0.0295 ±	0.0334 ±	0.0172 ±	0.0162 ±	0.0204 ±	0.0142 ±	0.458
	0.0035	0.0120	0.0105	0.0059	0.0056	0.0090	0.0090	
<i>gi-158</i>	0.0164 ±	0.0534 ±	0.0861 ±	0.0335 ±	0.0076 ±	0.0000 ±	0.0000 ±	0.000
	0.0113 ab	0.0124 bc	0.0219 c	0.0119 ab	0.0050 ab	0.0000 a	0.0000 a	
<i>elf3-4</i>	0.0211 ±	0.0394 ±	0.0428 ±	0.0193 ±	0.0268 ±	0.0257 ±	0.0032 ±	0.104
<i>gi-158</i>	0.0107	0.0109	0.0125	0.0070	0.0088	0.0112	0.0032	

* Seedlings were grown under 12 h 22°C: 12 h 16°C temperature cycles in LL. Indicated time points (every 4 h) were selected for statistics.

† Different letters indicate significant differences in growth rate within indicated time points per genotype per day (one-way ANOVA and Tukey's HSD test). The value with the highest mean is considered as a peak (shown in bold) that is significantly higher than the values of more than three other time points.

Table 6 Transcript levels of genes under temperature cycles in LL (related to Fig. 4-7).

ZT*	ZT00/24	ZT04	ZT08	ZT12	ZT16	ZT20	P
Genotype	CCA1 relative expression \pm SEM (n=3)						P
Ws-2	2.2428 \pm 0.7727 a[†]	1.5875 \pm 0.1476 ab	0.2306 \pm 0.0583 b	0.0621 \pm 0.0174 b	0.1062 \pm 0.0244 b	0.3102 \pm 0.0613 b	0.001
elf3-4	0.1007 \pm 0.0175	0.0976 \pm 0.0016	0.0719 \pm 0.0139	0.0610 \pm 0.0051	0.0677 \pm 0.0063	0.1059 \pm 0.0165	0.064
gi-158	1.2499 \pm 0.1559 a	0.7480 \pm 0.1260 b	0.0544 \pm 0.0090 c	0.0133 \pm 0.0013 c	0.0565 \pm 0.0098 c	0.5993 \pm 0.1529 b	0.000
elf3-4 gi-158	0.0667 \pm 0.0070 a	0.0528 \pm 0.0008 a	0.0449 \pm 0.0023 a	0.0542 \pm 0.0034 a	0.0780 \pm 0.0062 ab	0.1194 \pm 0.0202 b	0.001
	LHY relative expression \pm SEM (n=3)						
Ws-2	4.4052 \pm 0.9873 a	1.1700 \pm 0.1084 b	0.5359 \pm 0.2465 b	0.0787 \pm 0.0286 b	0.1578 \pm 0.0230 b	0.9713 \pm 0.1112 b	0.000
elf3-4	0.0854 \pm 0.0059 a	0.1132 \pm 0.0343 ab	0.0840 \pm 0.0175 a	0.0521 \pm 0.0139 a	0.0700 \pm 0.0029 a	0.1930 \pm 0.0287 b	0.003
gi-158	2.9962 \pm 1.4138 a	0.2764 \pm 0.0165 ab	0.0689 \pm 0.0215 b	0.0083 \pm 0.0000 b	0.0746 \pm 0.0132 b	1.5321 \pm 0.1575 ab	0.017
elf3-4 gi-158	0.0110 \pm 0.0004 ab	0.0116 \pm 0.0017 ab	0.0040 \pm 0.0004 b	0.0088 \pm 0.0040 ab	0.0090 \pm 0.0004 ab	0.0169 \pm 0.0012 a	0.002
	PRR9 relative expression \pm SEM (n=3)						
Ws-2	0.0328 \pm 0.0126 ab	0.2447 \pm 0.0509 c	0.1253 \pm 0.0025 b	0.0539 \pm 0.0156 ab	0.0212 \pm 0.0051 ab	0.0177 \pm 0.0022 a	0.000
elf3-4	0.1354 \pm 0.0079	0.1033 \pm 0.0056	0.1221 \pm 0.0079	0.1241 \pm 0.0137	0.1445 \pm 0.0414	0.1509 \pm 0.0163	0.665
gi-158	0.0410 \pm 0.0049 a	0.1950 \pm 0.0329 c	0.1186 \pm 0.0087 b	0.0264 \pm 0.0051 a	0.0253 \pm 0.0008 a	0.0427 \pm 0.0071 a	0.000
elf3-4 gi-158	0.1948 \pm 0.0350	0.1635 \pm 0.0275	0.1483 \pm 0.0124	0.2593 \pm 0.0581	0.2118 \pm 0.0265	0.3008 \pm 0.0359	0.066
	PRR7 relative expression \pm SEM (n=3)						
Ws-2	0.0463 \pm 0.0070 ab	0.2812 \pm 0.0129 c	0.5575 \pm 0.0078 d	0.2657 \pm 0.0544 c	0.1247 \pm 0.0446 b	0.0398 \pm 0.0060 a	0.000
elf3-4	0.3115 \pm 0.0218 ab	0.3402 \pm 0.0641 ab	0.4039 \pm 0.0239 ab	0.2385 \pm 0.0488 a	0.3555 \pm 0.0302 ab	0.4791 \pm 0.0552 b	0.034
gi-158	0.0721 \pm 0.0275 a	0.4797 \pm 0.1555 ab	0.9709 \pm 0.3374 b	0.1570 \pm 0.0254 a	0.0402 \pm 0.0104 a	0.0418 \pm 0.0038 a	0.001
elf3-4 gi-158	0.4483 \pm 0.0280 ab	0.5457 \pm 0.1809 ab	0.2909 \pm 0.0169 a	0.2832 \pm 0.0463 a	0.3623 \pm 0.0222 ab	0.7201 \pm 0.0777 b	0.023
	TOC1 relative expression \pm SEM (n=3)						
Ws-2	0.2311 \pm 0.0307 ab	0.1547 \pm 0.0156 a	0.2169 \pm 0.0225 ab	0.4489 \pm 0.0443 bc	0.5571 \pm 0.1131 c	0.2739 \pm 0.0244 ab	0.001
elf3-4	0.3609 \pm 0.0158	0.2800 \pm 0.0134	0.4263 \pm 0.0825	0.3676 \pm 0.0445	0.4075 \pm 0.0973	0.3496 \pm 0.0056	0.675
gi-158	0.1724 \pm 0.0089 ab	0.1092 \pm 0.0148 a	0.2894 \pm 0.0263 bc	0.4294 \pm 0.0481 d	0.3179 \pm 0.0350 cd	0.2090 \pm 0.0186 abc	0.000
elf3-4 gi-158	0.3555 \pm 0.0100 ab	0.2486 \pm 0.0194 a	0.3904 \pm 0.0263 b	0.2658 \pm 0.0463 ab	0.2906 \pm 0.0285 ab	0.3292 \pm 0.0236 ab	0.027
	PIF4 relative expression \pm SEM (n=3)						
Ws-2	0.0286 \pm 0.0068 a	0.2991 \pm 0.0551 b	0.4161 \pm 0.0241 b	0.2523 \pm 0.0563 b	0.0797 \pm 0.0186 a	0.0217 \pm 0.0062 a	0.000
elf3-4	0.2105 \pm 0.0184	0.2620 \pm 0.0064	0.2830 \pm 0.0411	0.3101 \pm 0.0306	0.2288 \pm 0.0269	0.2284 \pm 0.0180	0.129
gi-158	0.0482 \pm 0.0059 ab	0.4175 \pm 0.0546 c	0.6012 \pm 0.0616 d	0.2010 \pm 0.0291 b	0.0333 \pm 0.0041 ab	0.0177 \pm 0.0028 a	0.000
elf3-4 gi-158	0.3739 \pm 0.0430	0.3722 \pm 0.0271	0.3904 \pm 0.0172	0.4293 \pm 0.0407	0.3366 \pm 0.0750	0.4019 \pm 0.0131	0.734

* Seedlings were grown under 12 h 22°C: 12 h 16°C temperature cycles in LL for 8 d. On day 9, starting from ZT00, samples were harvested every 4 h. Expression levels were normalized to *PP2A*.

† Different letters indicate significant differences in expression level within indicated time points per genotype (one-way ANOVA and Tukey's HSD test). The value with the highest mean is considered as a peak (shown in bold) that is significantly higher than the values of more than three other time points.

Table 7 Transcript levels of genes under temperature cycles in LL (normalized to *TIP41*).

ZT*	ZT00/24	ZT04	ZT08	ZT12	ZT16	ZT20	
Genotype	CCA1 relative expression \pm SEM (n=3)						P
Ws-2	1.8204 \pm 0.3081 a[†]	1.0539 \pm 0.3406 ab	0.4563 \pm 0.0545 b	0.1533 \pm 0.0523 b	0.1828 \pm 0.0425 b	0.6715 \pm 0.1905 b	0.001
<i>elf3-4</i>	0.1544 \pm 0.0160	0.4005 \pm 0.1180	0.2252 \pm 0.0435	0.1761 \pm 0.0250	0.3459 \pm 0.0512	0.3706 \pm 0.0444	0.047
<i>gi-158</i>	3.6910 \pm 1.0694 a	0.8647 \pm 0.1871 b	0.1978 \pm 0.0979 b	0.0506 \pm 0.0155 b	0.2105 \pm 0.0102 b	3.5906 \pm 0.8222 a	0.001
<i>elf3-4 gi-158</i>	0.3236 \pm 0.2081	0.3118 \pm 0.0301	0.1671 \pm 0.0253	0.1737 \pm 0.0484	0.2614 \pm 0.0234	0.3754 \pm 0.0898	0.602
	LHY relative expression \pm SEM (n=3)						
Ws-2	5.5182 \pm 0.4642 a	1.6866 \pm 0.4339 bc	0.4443 \pm 0.1154 c	0.1723 \pm 0.0553 c	0.1909 \pm 0.0039 c	2.7373 \pm 0.9278 b	0.000
<i>elf3-4</i>	0.2253 \pm 0.0179 a	0.2880 \pm 0.0512 ab	0.1318 \pm 0.0105 a	0.1870 \pm 0.0049 a	0.1745 \pm 0.0646 a	0.6756 \pm 0.0426 b	0.000
<i>gi-158</i>	5.7996 \pm 1.9007 a	0.4666 \pm 0.0521 b	0.1378 \pm 0.0399 b	0.0539 \pm 0.0177 b	0.1884 \pm 0.0413 b	5.0783 \pm 0.8279 a	0.001
<i>elf3-4 gi-158</i>	0.1837 \pm 0.0948	0.0285 \pm 0.0030	0.1087 \pm 0.0499	0.0219 \pm 0.0046	0.0264 \pm 0.0033	0.0737 \pm 0.0292	0.144
	PRR9 relative expression \pm SEM (n=3)						
Ws-2	0.1181 \pm 0.0108 ab	0.4720 \pm 0.1328 a	0.3977 \pm 0.0628 ab	0.1741 \pm 0.0408 ab	0.0667 \pm 0.0344 b	0.2005 \pm 0.0994 ab	0.015
<i>elf3-4</i>	0.2159 \pm 0.0223 a	0.3668 \pm 0.0531 ab	0.3456 \pm 0.0512 ab	0.3704 \pm 0.0351 ab	0.4035 \pm 0.1402 ab	0.8881 \pm 0.2794 b	0.049
<i>gi-158</i>	0.0933 \pm 0.0305 a	0.2545 \pm 0.0356 ab	0.4211 \pm 0.0302 b	0.1587 \pm 0.0294 a	0.0794 \pm 0.0154 a	0.1984 \pm 0.0658 a	0.000
<i>elf3-4 gi-158</i>	0.4237 \pm 0.1602 a	0.4796 \pm 0.0690 a	0.4946 \pm 0.0901 a	0.4888 \pm 0.0391 a	1.1621 \pm 0.1250 b	1.1386 \pm 0.2096 b	0.002
	PRR7 relative expression \pm SEM (n=3)						
Ws-2	0.0712 \pm 0.0043 a	0.2783 \pm 0.0626 ab	1.3103 \pm 0.1355 c	0.6801 \pm 0.2406 b	0.2799 \pm 0.0879 ab	0.1411 \pm 0.0229 ab	0.000
<i>elf3-4</i>	0.4797 \pm 0.0452	1.1963 \pm 0.4317	0.8720 \pm 0.1553	1.1204 \pm 0.1508	1.2500 \pm 0.4953	1.7892 \pm 0.1962	0.123
<i>gi-158</i>	0.1445 \pm 0.0269 a	2.3501 \pm 0.2075 c	2.3331 \pm 0.3763 c	1.0363 \pm 0.0930 b	0.1998 \pm 0.0537 ab	0.2070 \pm 0.0149 ab	0.000
<i>elf3-4 gi-158</i>	1.4909 \pm 0.3774	2.1698 \pm 0.2511	2.2135 \pm 0.4283	1.8657 \pm 0.3856	2.1383 \pm 0.3451	2.4344 \pm 0.2268	0.497
	TOC1 relative expression \pm SEM (n=3)						
Ws-2	0.4939 \pm 0.0302 a	0.7581 \pm 0.1264 a	0.6684 \pm 0.1217 a	1.6722 \pm 0.1997 b	0.5627 \pm 0.0281 a	0.5940 \pm 0.0219 a	0.000
<i>elf3-4</i>	1.1617 \pm 0.1302	1.3364 \pm 0.2924	1.7945 \pm 0.3527	1.3964 \pm 0.1759	1.2212 \pm 0.3362	1.6132 \pm 0.0961	0.499
<i>gi-158</i>	0.4691 \pm 0.1156 a	1.4310 \pm 0.1604 ab	1.7915 \pm 0.6708 ab	1.9640 \pm 0.1714 b	0.9478 \pm 0.1259 ab	1.0811 \pm 0.0861 ab	0.036
<i>elf3-4 gi-158</i>	0.8808 \pm 0.1422	1.3757 \pm 0.2116	1.3460 \pm 0.4821	0.9150 \pm 0.1944	1.5050 \pm 0.2669	1.5736 \pm 0.4146	0.502
	PIF4 relative expression \pm SEM (n=3)						
Ws-2	0.1074 \pm 0.0035 a	0.6061 \pm 0.0802 bc	1.1929 \pm 0.1364 d	0.7713 \pm 0.1799 cd	0.2091 \pm 0.0205 ab	0.0796 \pm 0.0155 a	0.000
<i>elf3-4</i>	0.6111 \pm 0.0582 a	1.1694 \pm 0.2737 ab	0.7410 \pm 0.0395 ab	1.0251 \pm 0.0963 ab	1.3850 \pm 0.2228 b	1.0126 \pm 0.1178 ab	0.049
<i>gi-158</i>	0.2251 \pm 0.0915 ab	1.5621 \pm 0.2260 c	2.4750 \pm 0.1535 d	0.7262 \pm 0.1269 b	0.0580 \pm 0.0549 a	0.0905 \pm 0.0155 a	0.000
<i>elf3-4 gi-158</i>	1.0559 \pm 0.2557 a	1.9220 \pm 0.1204 ab	1.6899 \pm 0.3049 ab	1.6970 \pm 0.2294 ab	2.3498 \pm 0.1983 ab	2.4644 \pm 0.4898 b	0.049

* Seedlings were grown under 12 h 22°C: 12 h 16°C temperature cycles in LL for 8 d. On day 9, starting from ZT00, samples were harvested every 4 h. Expression levels were normalized to *TIP41* (AT4G34270).

† Different letters indicate significant differences in expression level within indicated time points per genotype (one-way ANOVA and Tukey's HSD test). The value with the highest mean is considered as a peak (shown in bold) that is significantly higher than the values of more than three other time points.

Table 8 Transcript levels of genes under temperature cycles in DD (related to Fig. 4-8).

ZT*	ZT00/24	ZT04	ZT08	ZT12	ZT16	ZT20	
Genotype	CCA1 relative expression ± SEM (n=3)						P
Ws-2	1.2574 ± 0.0631 a [†]	0.6539 ± 0.0682 b	0.5135 ± 0.2051 bc	0.1004 ± 0.0104 cd	0.0592 ± 0.0026 d	0.2736 ± 0.0133 bcd	0.000
elf3-4	0.4167 ± 0.0084 a	0.1595 ± 0.0253 c	0.0223 ± 0.0011 d	0.0200 ± 0.0037 d	0.0786 ± 0.0040 d	0.2598 ± 0.0245 b	0.000
gi-158	1.1713 ± 0.2508 a	1.2214 ± 0.4053 a	0.1751 ± 0.0312 b	0.0608 ± 0.0099 b	0.0850 ± 0.0102 b	0.4639 ± 0.0815 ab	0.002
elf3-4 gi-158	0.0832 ± 0.0171	0.0643 ± 0.0156	0.0359 ± 0.0088	0.0287 ± 0.0071	0.0538 ± 0.0073	0.0899 ± 0.0232	0.064
	LHY relative expression ± SEM (n=3)						
Ws-2	2.7008 ± 0.3554 a	1.0864 ± 0.3283 b	0.4135 ± 0.0173 bc	0.0277 ± 0.0092 c	0.0789 ± 0.0117 c	0.5893 ± 0.1235 bc	0.000
elf3-4	0.2001 ± 0.0077 a	0.0569 ± 0.0066 b	0.0086 ± 0.0017 b	0.0189 ± 0.0126 b	0.0489 ± 0.0054 b	0.2315 ± 0.0544 a	0.000
gi-158	0.8628 ± 0.0902 a	0.5746 ± 0.0916 a	0.0203 ± 0.0038 b	0.0104 ± 0.0003 b	0.0309 ± 0.0103 b	0.5875 ± 0.2054 a	0.000
elf3-4 gi-158	0.0165 ± 0.0021	0.0112 ± 0.0029	0.0032 ± 0.0004	0.0067 ± 0.0019	0.0145 ± 0.0038	0.0259 ± 0.0118	0.076
	PRR9 relative expression ± SEM (n=3)						
Ws-2	0.0191 ± 0.0077 a	0.0707 ± 0.0121 ab	0.1235 ± 0.0307 b	0.0182 ± 0.0008 a	0.0182 ± 0.0138 a	0.0071 ± 0.0010 a	0.000
elf3-4	0.2480 ± 0.0196 a	0.2290 ± 0.0426 a	0.1046 ± 0.0130 b	0.0788 ± 0.0150 b	0.0557 ± 0.0076 b	0.1378 ± 0.0325 a	0.000
gi-158	0.0561 ± 0.0283 a	0.3896 ± 0.0808 b	0.1089 ± 0.0435 a	0.0583 ± 0.0104 a	0.0131 ± 0.0014 a	0.0192 ± 0.0056 a	0.000
elf3-4 gi-158	0.2095 ± 0.0474 ab	0.2745 ± 0.0283 a	0.2187 ± 0.0337 ab	0.1534 ± 0.0238 ab	0.1096 ± 0.0209 b	0.1508 ± 0.0110 ab	0.018
	PRR7 relative expression ± SEM (n=3)						
Ws-2	0.0544 ± 0.0095 a	0.3754 ± 0.1112 a	1.2529 ± 0.3027 b	0.2273 ± 0.0957 a	0.1954 ± 0.0275 a	0.1178 ± 0.0230 a	0.000
elf3-4	0.5748 ± 0.1601	0.5198 ± 0.1831	1.0803 ± 0.2927	0.9360 ± 0.1266	0.8973 ± 0.0615	1.0932 ± 0.4919	0.509
gi-158	0.5732 ± 0.0575 a	2.5391 ± 0.7324 b	0.4870 ± 0.2074 a	0.3980 ± 0.0340 a	0.3433 ± 0.0298 a	0.4701 ± 0.1349 a	0.002
elf3-4 gi-158	0.7825 ± 0.2720	0.8412 ± 0.1663	0.9947 ± 0.2969	0.5547 ± 0.0958	0.4696 ± 0.0492	0.6372 ± 0.2218	0.510
	TOC1 relative expression ± SEM (n=3)						
Ws-2	0.9602 ± 0.2345 ab	0.2613 ± 0.0329 a	1.2131 ± 0.0514 b	1.0353 ± 0.1270 ab	1.3578 ± 0.3430 b	0.8997 ± 0.0282 ab	0.016
elf3-4	1.3573 ± 0.1940	2.0654 ± 0.6431	1.5174 ± 0.0916	1.2508 ± 0.1465	1.4111 ± 0.2885	1.9775 ± 0.1485	0.369
gi-158	0.8942 ± 0.3355	0.9496 ± 0.1865	0.8324 ± 0.0399	0.9055 ± 0.1122	1.4289 ± 0.2970	1.1089 ± 0.2600	0.499
elf3-4 gi-158	1.2253 ± 0.0890	2.1064 ± 0.3141	1.2452 ± 0.1378	1.0964 ± 0.1763	1.2418 ± 0.1816	1.3230 ± 0.3751	0.095
	PIF4 relative expression ± SEM (n=3)						
Ws-2	0.1223 ± 0.0534 ab	0.2543 ± 0.0069 ab	0.7268 ± 0.1074 c	0.3206 ± 0.0366 b	0.1358 ± 0.0214 ab	0.0663 ± 0.0098 a	0.000
elf3-4	0.4393 ± 0.0211	0.6128 ± 0.1697	0.3535 ± 0.0163	0.3875 ± 0.0648	0.2996 ± 0.0338	0.4095 ± 0.0518	0.180
gi-158	0.3660 ± 0.1239 a	1.0029 ± 0.2212 b	0.3912 ± 0.0980 a	0.2473 ± 0.0929 a	0.2179 ± 0.0288 a	0.2410 ± 0.0717 a	0.005
elf3-4 gi-158	0.4381 ± 0.0620 ab	0.6993 ± 0.1169 b	0.5234 ± 0.0944 ab	0.3746 ± 0.0183 ab	0.3442 ± 0.0380 b	0.3846 ± 0.0509 ab	0.036

* Seedlings were grown under 12 h 22°C: 12 h 16°C temperature cycles in DD for 8 d. On day 9, starting from ZT00, samples were harvested every 4 h. Expression levels were normalized to *PP2A*.

† Different letters indicate significant differences in expression level within indicated time points per genotype (one-way ANOVA and Tukey's HSD test). The value with the highest mean is considered as a peak (shown in bold) that is significantly higher than the values of more than three other time points.

Appendix VI

Table 9 Plant height during barley seedling establishment (related to Fig. 5-3A).

Genotype	Temp	Plant height (mm) ± SEM (n=11)											
		5 DAS	6 DAS	7 DAS	8 DAS	9 DAS	10 DAS	11 DAS	12 DAS	13 DAS	14 DAS	P	
Bowman	20°C	11.91 ± 1.50abcd†	32.73 ± 1.32ef ***	51.27 ± 2.07fg ***	68.36 ± 1.84gh ***	91.45 ± 3.16fg ***							
	28°C	11.64 ± 0.94abcd	45.18 ± 1.28ace ***	65.00 ± 0.99bcef ***	90.00 ± 1.29bcde ***	110.09 ± 2.17abdef ***							
BW290	20°C	13.55 ± 2.40abcde	39.09 ± 2.73cef ***	59.82 ± 2.94cefg ***	83.82 ± 2.72cdeh ***	103.36 ± 2.72adefg ***							
	28°C	23.73 ± 3.32e	68.64 ± 3.77d ***	96.45 ± 3.34d ***	129.00 ± 3.03f ***	143.36 ± 3.02h **							
10_elite	20°C	19.36 ± 1.72bce	48.64 ± 2.20abc ***	70.36 ± 1.56abce ***	90.64 ± 1.42bcde ***	105.55 ± 1.47adefg ***							
	28°C	10.73 ± 1.60abcd	50.64 ± 1.84abc ***	74.73 ± 1.35abc ***	102.36 ± 1.67ab ***	121.82 ± 2.76abc ***							
10_wild	20°C	10.18 ± 0.89abd	32.00 ± 1.59ef ***	49.82 ± 1.80fg ***	71.55 ± 2.00gh ***	93.82 ± 2.67efg ***							
	28°C	18.00 ± 2.88bcde	59.64 ± 2.66abd ***	82.73 ± 2.65ad ***	113.00 ± 2.37af ***	131.09 ± 3.01ch ***							
16_elite	20°C	9.82 ± 2.49abd	36.18 ± 3.77cef ***	57.82 ± 3.89efg ***	81.27 ± 3.78efg ***	101.45 ± 3.51defg ***							
	28°C	8.00 ± 1.14ad	48.73 ± 2.74abc ***	75.45 ± 2.83ab ***	104.64 ± 3.42ab ***	127.45 ± 3.76bch ***							
16_wild	20°C	7.00 ± 2.39a	26.45 ± 3.45f ***	45.45 ± 3.41g ***	66.27 ± 2.97g ***	89.73 ± 2.40g ***							
	28°C	7.27 ± 1.04a	47.36 ± 1.55abc ***	70.64 ± 1.38abce ***	99.00 ± 1.66abcd ***	112.91 ± 2.83abcde ***							
17_elite	20°C	14.18 ± 2.17abcde	38.00 ± 4.30cef ***	56.82 ± 4.74efg **	73.91 ± 6.28efg *	95.82 ± 6.94efg *							
	28°C	18.45 ± 2.05bce	55.82 ± 4.15abd ***	77.18 ± 5.62ab **	100.55 ± 6.68abc *	108.09 ± 7.21abdefg0.452							
17_wild	20°C	20.64 ± 2.87ce	47.55 ± 4.16abc ***	62.64 ± 4.56bcef *	83.18 ± 4.77degh **	101.55 ± 5.62defg *							
	28°C	19.27 ± 2.07bce	60.09 ± 2.92bd ***	81.82 ± 3.02ad ***	109.00 ± 3.16a ***	117.55 ± 4.84abcd 0.155							
Time		10 DAS	11 DAS	12 DAS	13 DAS	14 DAS							
Bowman	20°C	106.91 ± 3.71ef **	120.27 ± 4.56bc *	125.73 ± 5.06c	0.432132.00 ± 5.04f	0.390	155.82 ± 6.15g **						
	28°C	115.00 ± 2.09cdef	0.113121.36 ± 2.99bc	0.097143.73 ± 4.59c	***	183.00 ± 4.62bc	***	205.64 ± 3.57abc					
BW290	20°C	123.55 ± 2.83cde	***	139.45 ± 3.77c **	147.91 ± 3.58c	0.119158.27 ± 3.67cef	0.057	190.91 ± 5.43f					
	28°C	146.36 ± 2.84b	0.478176.73 ± 6.84a	***	222.55 ± 7.90b	***	253.55 ± 6.78d	**	259.73 ± 7.14de				0.537
10_elite	20°C	119.91 ± 1.17cdef	***	129.18 ± 1.49bc ***	144.09 ± 3.54c	***	172.73 ± 4.94ce	***	199.00 ± 2.92bcf				
	28°C	127.91 ± 3.27abcd	0.170168.18 ± 3.35a	***	200.09 ± 3.54ab	***	216.64 ± 8.28a	0.081	225.00 ± 5.80abc				0.418
10_wild	20°C	109.27 ± 2.80def	***	127.64 ± 3.50bc ***	135.09 ± 2.85c	0.114153.73 ± 3.95ef	**	181.09 ± 8.64fg					
	28°C	144.36 ± 2.77ab	**	187.73 ± 3.08a ***	218.73 ± 2.63ab	***	230.27 ± 3.34ad *	*	260.64 ± 3.10e				
16_elite	20°C	115.82 ± 2.82cdef	**	126.18 ± 2.38bc *	132.73 ± 2.44c	0.069159.18 ± 4.25cef	***	182.64 ± 4.82fg					
	28°C	134.00 ± 3.45abc	0.214175.64 ± 6.56a	***	206.27 ± 5.43ab	**	219.45 ± 5.29a	0.098	236.64 ± 6.80ade				0.060
16_wild	20°C	103.27 ± 1.97f	***	110.55 ± 2.27b *	127.55 ± 4.01c	**	151.45 ± 4.79ef	**	175.64 ± 3.74fg				
	28°C	124.91 ± 2.63acde	**	168.36 ± 3.35a ***	196.73 ± 2.87ab	***	206.82 ± 3.29ab *	*	228.91 ± 4.62abd				
17_elite	20°C	107.91 ± 7.11ef	0.239118.55 ± 6.91bc	0.296140.73 ± 8.31c	0.054170.82 ± 9.94ce	*	195.36 ± 9.61cf	*	195.36 ± 9.61cf				0.091
	28°C	131.55 ± 7.82abc	*	174.00 ± 8.95a **	195.45 ± 9.60a	0.118206.36 ± 8.78ab	0.412235.45 ± 10.60ade	*	195.36 ± 9.61cf				
17_wild	20°C	115.00 ± 5.25cdef	0.096125.27 ± 4.66bc	0.159141.00 ± 6.74c	0.069171.27 ± 7.34ce	**	197.18 ± 7.09cf	*	197.18 ± 7.09cf				
	28°C	132.91 ± 5.00abc	*	175.82 ± 6.01a ***	207.64 ± 5.34ab	***	219.09 ± 3.88a	0.098	231.45 ± 5.04ade				0.066

† Different letters indicate significant differences at each time point (two-way ANOVA and Tukey's HSD test, $P < 0.05$).

* Significant increase of plant height compared to the previous time point (*, $P < 0.05$; **, $P < 0.01$; ***, $P < 0.001$); two-sided Student's t-test).

Table 10 Length and width of the first and second leaves (related to Fig. 5-3D).

Genotype Temp		Length or width (mm) \pm SEM ($n=5$) at 16 DAS			
Time		Length first leaf	Length second leaf	Width first leaf	Width second leaf
Bowman	20°C	105.30 \pm 1.40ab [†]	197.85 \pm 7.50abcd	8.98 \pm 0.16abcd	9.51 \pm 0.42acd
	28°C	95.45 \pm 7.92ab	205.25 \pm 3.65acd	7.88 \pm 0.47a	7.20 \pm 0.43fi
BW290	20°C	114.96 \pm 6.07b	211.44 \pm 9.19acd	8.55 \pm 0.45abd	9.27 \pm 0.42ade
	28°C	113.44 \pm 3.43ab	221.16 \pm 2.84a	8.28 \pm 0.20ab	7.31 \pm 0.28fi
10_elite	20°C	112.77 \pm 2.02ab	193.71 \pm 2.63abcd	9.16 \pm 0.12abcd	10.31 \pm 0.13abc
	28°C	109.38 \pm 1.49ab	216.81 \pm 3.63ac	8.04 \pm 0.25ab	8.23 \pm 0.18efgh
10_wild	20°C	115.44 \pm 1.35b	194.73 \pm 3.03abcd	9.02 \pm 0.18abcd	10.56 \pm 0.12bc
	28°C	105.63 \pm 6.69ab	213.36 \pm 11.41ac	8.11 \pm 0.40ab	7.87 \pm 0.28fghi
16_elite	20°C	103.82 \pm 2.24ab	181.93 \pm 4.34bd	9.32 \pm 0.32bcd	10.73 \pm 0.08b
	28°C	97.73 \pm 0.99ab	190.86 \pm 2.55bcd	8.48 \pm 0.31ab	8.51 \pm 0.15degh
16_wild	20°C	93.45 \pm 1.65a	174.94 \pm 3.54b	10.00 \pm 0.16c	10.33 \pm 0.13abc
	28°C	99.45 \pm 4.12ab	189.58 \pm 7.84bcd	9.87 \pm 0.23cd	8.96 \pm 0.16deg
17_elite	20°C	107.19 \pm 1.49ab	214.87 \pm 2.91ac	8.72 \pm 0.19abcd	9.14 \pm 0.17de
	28°C	100.00 \pm 6.18ab	198.82 \pm 9.87abcd	8.00 \pm 0.32ab	6.87 \pm 0.31i
17_wild	20°C	103.48 \pm 3.35ab	204.52 \pm 4.82abcd	8.44 \pm 0.09ab	9.59 \pm 0.17abcd
	28°C	102.25 \pm 2.89ab	213.67 \pm 3.76ac	8.58 \pm 0.15abd	7.55 \pm 0.12fhi

[†] Different letters indicate significant differences (two-way ANOVA and Tukey's HSD test, $P<0.05$).

Table 3 Plant height during barley growth and development (related to Fig. 5-5A).

Genotype	Temp	Plant height (mm) ± SEM (n=11)										
		8 DAS	11 DAS	14 DAS	16 DAS	18 DAS	21 DAS	24 DAS	49 DAS	52 DAS		
Bowman	20°C	36.82 ± 2.89a [†]	75.68 ± 3.77ab	97.09 ± 5.17d	144.36 ± 6.67a	163.91 ± 4.82a	235.64 ± 7.60ab	273.32 ± 5.78a				
	28°C	50.55 ± 2.34abc	72.64 ± 2.57ab	137.05 ± 4.36ab	172.32 ± 7.42abc	249.91 ± 4.43df	290.27 ± 6.93c	345.27 ± 5.88ef				
BW290	20°C	44.82 ± 2.92ab	92.68 ± 3.17bcd	127.82 ± 5.22ab	179.82 ± 4.93bcde	204.91 ± 4.47bc	283.50 ± 7.20c	325.41 ± 5.48de				
	28°C	84.27 ± 3.17f	118.23 ± 5.26e	192.32 ± 4.28e	266.59 ± 6.62g	287.00 ± 3.57e	332.27 ± 9.57e	370.00 ± 10.55f				
10_elite	20°C	52.59 ± 1.55abcd	83.82 ± 1.52abc	135.41 ± 3.54abc	154.73 ± 3.98ab	185.73 ± 7.71ab	232.95 ± 6.48ab	270.86 ± 3.12a				
	28°C	65.91 ± 2.47cdef	103.95 ± 3.51cde	152.05 ± 4.42acfg	202.86 ± 6.77def	226.09 ± 7.42cf	274.36 ± 6.27cd	309.91 ± 5.16cd				
10_wild	20°C	41.09 ± 2.21a	87.86 ± 3.59abcd	128.00 ± 3.14ab	156.14 ± 3.47ab	193.45 ± 3.82ab	246.41 ± 3.98bd	280.73 ± 5.57abc				
	28°C	78.09 ± 3.23ef	124.05 ± 3.24e	189.23 ± 2.92e	226.09 ± 5.04f	270.05 ± 6.64de	288.86 ± 4.60c	319.50 ± 7.63de				
16_elite	20°C	44.45 ± 2.92ab	82.86 ± 2.62abc	125.05 ± 4.26b	149.73 ± 2.55ab	188.50 ± 5.96ab	225.05 ± 4.61ab	278.86 ± 2.98abc				
	28°C	66.68 ± 4.24cdef	107.86 ± 5.39de	169.73 ± 5.04ef	195.18 ± 9.45def	237.59 ± 8.81f	285.36 ± 6.95c	326.91 ± 3.64de				
16_wild	20°C	35.86 ± 2.88a	69.59 ± 3.02a	120.18 ± 3.53bd	144.64 ± 2.45a	179.64 ± 2.23ab	210.86 ± 4.85a	272.95 ± 3.67a				
	28°C	62.59 ± 2.23bcde	108.45 ± 4.41de	162.68 ± 3.41fg	191.00 ± 5.38cde	230.64 ± 6.05cf	281.23 ± 3.49cd	325.55 ± 8.15de				
17_elite	20°C	42.00 ± 6.07a	74.50 ± 6.58ab	132.00 ± 10.13abc	155.45 ± 7.83ab	191.55 ± 9.05ab	231.09 ± 11.27ab	284.45 ± 8.97abc				
	28°C	62.14 ± 7.56bcde	107.91 ± 7.93de	156.27 ± 9.06cfg	200.82 ± 9.15def	237.18 ± 10.21f	280.91 ± 7.96cd	306.77 ± 10.86bcd				
17_wild	20°C	49.82 ± 5.34abc	80.14 ± 4.57ab	133.14 ± 6.03abc	162.91 ± 6.29abc	191.36 ± 6.81ab	232.50 ± 10.77ab	276.45 ± 5.70ab				
	28°C	69.55 ± 4.10def	107.95 ± 5.03de	155.95 ± 4.33cfg	206.32 ± 8.42df	233.14 ± 4.26cf	285.23 ± 5.13c	326.00 ± 7.91de				
Time	28 DAS	31 DAS	35 DAS	38 DAS	42 DAS	45 DAS	49 DAS	52 DAS				
Bowman	20°C	364.09 ± 6.63acdef	396.95 ± 5.54ac	435.55 ± 4.10bc	448.14 ± 7.43ac	527.32 ± 8.83d	578.91 ± 6.54e	629.32 ± 7.19bc	663.95 ± 6.22a			
	28°C	387.18 ± 7.43efg	410.86 ± 8.74ce	436.18 ± 8.77b	428.18 ± 7.65ab	448.95 ± 6.95ag	447.82 ± 6.81cg	447.86 ± 8.54ef	470.50 ± 15.28e			
BW290	20°C	399.14 ± 4.61eg	452.91 ± 6.96d	515.18 ± 11.85e	565.00 ± 8.96de	621.50 ± 12.02ef	693.55 ± 11.06f	768.68 ± 10.49d	764.55 ± 6.58d			
	28°C	418.50 ± 7.06g	468.45 ± 11.81d	543.45 ± 8.32e	552.86 ± 8.96e	592.64 ± 8.51f	586.50 ± 8.31e	584.82 ± 6.62ab	572.77 ± 8.29c			
10_elite	20°C	334.09 ± 8.98abc	381.41 ± 6.92abc	403.91 ± 8.69abcd	430.86 ± 9.29ab	481.18 ± 7.69abcd	491.95 ± 8.63abc	566.64 ± 13.19a	666.55 ± 12.77a			
	28°C	328.09 ± 6.08ab	344.82 ± 3.80b	378.82 ± 7.97a	375.64 ± 10.61f	424.77 ± 7.00g	449.91 ± 9.14cg	469.68 ± 6.46ef	504.55 ± 7.11e			
10_wild	20°C	359.23 ± 9.77abcdf	401.05 ± 4.31ac	421.00 ± 7.05bcd	480.45 ± 6.35c	596.27 ± 9.95f	670.82 ± 8.19f	761.82 ± 6.77d	802.64 ± 6.58d			
	28°C	356.55 ± 11.35abcdf	446.45 ± 9.52de	538.36 ± 7.77e	601.05 ± 12.70d	659.91 ± 8.41e	674.59 ± 9.94f	668.45 ± 9.08c	654.41 ± 8.90a			
16_elite	20°C	337.55 ± 7.66abcd	369.09 ± 6.25ab	378.64 ± 12.62a	437.55 ± 13.33abc	499.27 ± 15.20bcd	516.09 ± 12.82b	562.91 ± 9.88a	574.77 ± 8.95bc			
	28°C	369.05 ± 5.75cdef	370.86 ± 7.71ab	385.23 ± 7.60ad	393.36 ± 9.57bf	461.82 ± 11.18acg	471.95 ± 9.48ab	496.32 ± 12.82f	512.95 ± 14.44e			
16_wild	20°C	321.55 ± 3.94b	379.27 ± 7.57abc	417.27 ± 7.35abcd	464.91 ± 8.79ac	518.41 ± 7.40bd	562.41 ± 11.42de	592.55 ± 11.23ab	617.50 ± 7.45abc			
	28°C	371.95 ± 4.39def	379.86 ± 5.73abc	396.86 ± 5.07acd	401.05 ± 8.15bf	443.14 ± 6.00ag	457.36 ± 10.50acg	489.64 ± 8.75f	510.36 ± 9.39e			
17_elite	20°C	330.00 ± 11.14ab	379.59 ± 11.11abc	401.91 ± 7.23abcd	427.59 ± 9.57ab	478.59 ± 18.67abcd	496.86 ± 8.20ab	549.36 ± 9.07a	593.73 ± 17.52bc			
	28°C	341.68 ± 10.08abcd	350.18 ± 9.07b	389.95 ± 6.02ad	378.36 ± 6.80f	439.73 ± 8.42ag	440.23 ± 5.78g	474.73 ± 16.49ef	486.18 ± 15.78e			
17_wild	20°C	332.59 ± 5.66abc	363.45 ± 9.39ab	380.00 ± 5.22a	430.41 ± 8.99ab	477.27 ± 5.73abc	516.86 ± 7.92bd	592.95 ± 12.70ab	626.09 ± 7.73ab			
	28°C	353.45 ± 6.51abcdf	376.73 ± 6.06abc	382.27 ± 5.36ad	393.14 ± 9.27bf	417.82 ± 7.47g	434.55 ± 10.51g	439.27 ± 8.12e	490.45 ± 9.15e			

[†] Different letters indicate significant differences at each time point (two-way ANOVA and Tukey's HSD test, P<0.05).

Table 5 Top-view plant area during barley growth and development (related to Fig. 5-5B).

Genotype	Temp	Top-view plant area ($\times 10^3 \text{ mm}^2$) \pm SEM ($n=11$)														
		8 DAS	11 DAS	14 DAS	16 DAS	18 DAS	21 DAS	24 DAS	28 DAS	31 DAS	35 DAS	38 DAS	42 DAS	45 DAS	49 DAS	52 DAS
Bowman	20°C	0.02 \pm 0.01b [†]	0.04 \pm 0.01h	0.18 \pm 0.03f	0.47 \pm 0.07d	0.85 \pm 0.10e	2.67 \pm 0.23a	3.34 \pm 0.24g								
	28°C	0.05 \pm 0.01abc	0.08 \pm 0.01ah	0.27 \pm 0.03af	0.71 \pm 0.06ad	1.49 \pm 0.13abde	4.74 \pm 0.41def	5.16 \pm 0.27abf								
BW290	20°C	0.11 \pm 0.03abcdef	0.25 \pm 0.04bcdefg	0.37 \pm 0.06abdf	0.69 \pm 0.09ad	1.22 \pm 0.08de	2.84 \pm 0.21a	4.03 \pm 0.22fg								
	28°C	0.22 \pm 0.03f	0.35 \pm 0.06b	0.63 \pm 0.10bcdeg	1.56 \pm 0.19cfg	2.48 \pm 0.21cfg	4.50 \pm 0.22bcdef	6.70 \pm 0.58bcdei								
10_elite	20°C	0.10 \pm 0.02abcdef	0.20 \pm 0.03abcdefg	0.53 \pm 0.08abcde	1.11 \pm 0.09abc	1.98 \pm 0.12abc	3.21 \pm 0.28abcd	5.96 \pm 0.26abcde								
	28°C	0.12 \pm 0.01abcde	0.26 \pm 0.02bcdefg	0.85 \pm 0.09g	1.69 \pm 0.09efg	2.72 \pm 0.13fg	4.85 \pm 0.49ef	6.95 \pm 0.23cdehi								
10_wild	20°C	0.05 \pm 0.01abce	0.18 \pm 0.03acdegh	0.39 \pm 0.03abcdf	0.95 \pm 0.08abd	1.47 \pm 0.12abde	3.20 \pm 0.26abcd	5.50 \pm 0.26abcdf								
	28°C	0.20 \pm 0.04df	0.29 \pm 0.04bcfg	0.77 \pm 0.07eg	2.10 \pm 0.13e	3.10 \pm 0.10f	4.53 \pm 0.26bdef	8.54 \pm 0.27h								
16_elite	20°C	0.07 \pm 0.02abce	0.11 \pm 0.02aceh	0.37 \pm 0.05abdf	0.78 \pm 0.07abd	1.60 \pm 0.15abd	2.93 \pm 0.18ac	5.34 \pm 0.29abcdf								
	28°C	0.17 \pm 0.03def	0.30 \pm 0.03bfg	0.67 \pm 0.06cdeg	1.99 \pm 0.14eg	3.08 \pm 0.16f	4.63 \pm 0.44bdef	8.18 \pm 0.44hi								
16_wild	20°C	0.04 \pm 0.01ab	0.13 \pm 0.03acdeh	0.34 \pm 0.05abf	0.67 \pm 0.07ad	1.40 \pm 0.13ade	3.31 \pm 0.19abcde	4.92 \pm 0.20afg								
	28°C	0.16 \pm 0.03acdef	0.19 \pm 0.02acdefgh	0.52 \pm 0.06abcde	1.62 \pm 0.12cefg	2.70 \pm 0.14fg	5.05 \pm 0.37f	7.30 \pm 0.31ehi								
17_elite	20°C	0.08 \pm 0.02abcde	0.10 \pm 0.03ach	0.31 \pm 0.06af	0.65 \pm 0.11ad	1.18 \pm 0.19de	2.86 \pm 0.33a	3.96 \pm 0.44fg								
	28°C	0.11 \pm 0.03abcdef	0.27 \pm 0.04bcfg	0.50 \pm 0.08abcde	1.31 \pm 0.14bcf	2.16 \pm 0.19bcg	3.72 \pm 0.50abcde	6.45 \pm 0.59abcde								
17_wild	20°C	0.10 \pm 0.03abcdef	0.13 \pm 0.02acdeh	0.43 \pm 0.08abcdf	0.75 \pm 0.07ad	1.49 \pm 0.21abde	3.13 \pm 0.16abc	5.24 \pm 0.42abdf								
	28°C	0.17 \pm 0.03cdef	0.34 \pm 0.03bf	0.69 \pm 0.07ceg	1.64 \pm 0.12efg	2.52 \pm 0.11cfg	3.89 \pm 0.35abcdef	7.03 \pm 0.20cehi								
Time		28 DAS	31 DAS	35 DAS	38 DAS	42 DAS	45 DAS	49 DAS	52 DAS							
Bowman	20°C	6.46 \pm 0.34e	9.47 \pm 0.49f	16.49 \pm 0.72b	25.04 \pm 0.87ad	39.95 \pm 1.09abc	54.35 \pm 1.75acd	73.78 \pm 1.68ade	85.37 \pm 2.01abcd							
	28°C	10.52 \pm 0.50bcg	15.89 \pm 0.62abcdeg	26.21 \pm 1.03def	33.32 \pm 0.91bee	42.13 \pm 0.78abcd	47.95 \pm 0.83abce	53.08 \pm 1.19fg	55.62 \pm 1.65gh							
BW290	20°C	6.94 \pm 0.34de	11.15 \pm 0.42df	18.26 \pm 0.76b	26.76 \pm 0.89acd	33.63 \pm 1.46b	38.70 \pm 1.56e	42.02 \pm 1.74g	43.42 \pm 1.80fg							
	28°C	12.36 \pm 0.65cfg	17.08 \pm 1.00bcgeh	19.78 \pm 1.23ab	21.54 \pm 1.25d	20.93 \pm 1.39e	18.22 \pm 1.09f	11.86 \pm 0.94i	10.07 \pm 0.80i							
10_elite	20°C	10.05 \pm 0.29abc	15.00 \pm 0.53abcde	21.37 \pm 0.70abcd	28.25 \pm 1.09abc	39.94 \pm 1.35abc	50.11 \pm 1.97abc	70.18 \pm 2.15abcd	90.32 \pm 1.98abc							
	28°C	12.51 \pm 0.27cfg	16.95 \pm 0.45bcgeh	25.52 \pm 0.72cdef	34.03 \pm 0.93be	40.56 \pm 1.22abc	49.02 \pm 1.59abce	58.43 \pm 2.17cf	68.91 \pm 2.15eh							
10_wild	20°C	10.20 \pm 0.44abc	16.18 \pm 0.65abcdeg	24.64 \pm 0.84cdf	34.98 \pm 1.40e	48.10 \pm 1.72cd	56.88 \pm 2.31cd	72.37 \pm 2.82abde	81.46 \pm 3.40acde							
	28°C	14.17 \pm 0.35f	17.96 \pm 0.80eghi	21.01 \pm 0.91abcd	23.01 \pm 0.66ad	24.94 \pm 0.65e	24.74 \pm 0.79f	25.58 \pm 1.17h	29.70 \pm 0.76f							
16_elite	20°C	9.27 \pm 0.41abd	13.86 \pm 0.50abcd	20.38 \pm 0.69abc	25.33 \pm 0.81ad	36.64 \pm 1.65ab	43.35 \pm 1.90be	59.10 \pm 2.63bcf	75.38 \pm 2.67cde							
	28°C	14.41 \pm 0.70f	21.67 \pm 0.94i	33.26 \pm 1.16g	41.56 \pm 2.02f	50.43 \pm 2.41d	57.73 \pm 3.43cd	65.52 \pm 4.80abcdf	73.35 \pm 4.82de							
16_wild	20°C	9.18 \pm 0.47abd	13.57 \pm 0.55abd	20.00 \pm 0.99ab	25.90 \pm 1.04ad	36.35 \pm 1.54ab	45.32 \pm 2.29abe	63.39 \pm 2.53abcdf	81.26 \pm 3.27cde							
	28°C	13.09 \pm 0.50fg	19.61 \pm 0.70ghi	29.67 \pm 1.09efg	37.09 \pm 0.87ef	44.69 \pm 1.84acd	53.49 \pm 2.12abcd	61.22 \pm 1.58bcdf	71.34 \pm 1.83de							
17_elite	20°C	7.80 \pm 0.78ade	12.57 \pm 1.17adf	20.03 \pm 1.86ab	25.84 \pm 2.65ad	40.94 \pm 3.50abc	53.10 \pm 4.03abcd	76.34 \pm 5.16ae	96.46 \pm 5.76ab							
	28°C	11.28 \pm 0.93bcg	17.69 \pm 1.31cegh	26.97 \pm 1.84ef	37.46 \pm 2.06ef	46.52 \pm 2.13cd	54.93 \pm 2.86acd	65.33 \pm 3.72abcdf	73.24 \pm 4.29de							
17_wild	20°C	9.65 \pm 0.67ab	16.15 \pm 1.05abcdeg	25.03 \pm 0.76acdef	34.13 \pm 1.02be	50.10 \pm 1.63d	61.24 \pm 1.59d	84.15 \pm 2.85e	98.78 \pm 3.83b							
	28°C	13.07 \pm 0.61fg	20.19 \pm 0.75hi	30.09 \pm 0.74eg	37.44 \pm 1.08ef	47.29 \pm 1.42cd	54.05 \pm 1.83acd	65.65 \pm 2.79abcdf	73.35 \pm 2.97de							

[†] Different letters indicate significant differences at each time point (two-way ANOVA and Tukey's HSD test, $P < 0.05$).

Table 5 Side-view plant area during barley growth and development (related to Fig. 5-5C).

Genotype	Temp	Side-view plant area ($\times 10^3 \text{ mm}^2$) \pm SEM (n=11)														
		8 DAS	11 DAS	14 DAS	16 DAS	18 DAS	21 DAS	24 DAS	28 DAS	31 DAS	35 DAS	38 DAS	42 DAS	45 DAS	49 DAS	52 DAS
Bowman	20°C	0.09 \pm 0.01h [†]	0.20 \pm 0.02e	0.43 \pm 0.03g	0.63 \pm 0.05e	0.93 \pm 0.08d	1.82 \pm 0.16d	2.90 \pm 0.22d								
	28°C	0.10 \pm 0.01gh	0.23 \pm 0.03de	0.53 \pm 0.04eg	0.84 \pm 0.06abcde	1.44 \pm 0.09ab	2.66 \pm 0.15abc	4.35 \pm 0.21abc								
BW290	20°C	0.16 \pm 0.01acefgh	0.32 \pm 0.02bd	0.58 \pm 0.02efg	0.83 \pm 0.03ade	1.24 \pm 0.03ad	2.28 \pm 0.05ad	3.42 \pm 0.09bd								
	28°C	0.27 \pm 0.02d	0.50 \pm 0.03cg	1.00 \pm 0.06dh	1.46 \pm 0.08fg	1.91 \pm 0.13bcf	3.35 \pm 0.20bcf	4.65 \pm 0.28ac								
10_elite	20°C	0.21 \pm 0.00abcd	0.39 \pm 0.01abc	0.80 \pm 0.04abcd	1.07 \pm 0.04abc	1.59 \pm 0.07abc	2.84 \pm 0.10abc	4.53 \pm 0.16abc								
	28°C	0.23 \pm 0.01bcd	0.51 \pm 0.01cfg	0.93 \pm 0.03cd	1.43 \pm 0.04fg	2.15 \pm 0.06ef	3.80 \pm 0.08ef	5.80 \pm 0.19ef								
10_wild	20°C	0.15 \pm 0.01aefgh	0.36 \pm 0.01ab	0.66 \pm 0.03abef	0.90 \pm 0.02abcde	1.41 \pm 0.05a	2.66 \pm 0.07abc	4.30 \pm 0.13abc								
	28°C	0.27 \pm 0.01d	0.62 \pm 0.02f	1.15 \pm 0.03h	1.70 \pm 0.04f	2.56 \pm 0.06e	4.29 \pm 0.08e	6.42 \pm 0.19ef								
16_elite	20°C	0.17 \pm 0.01abcefg	0.35 \pm 0.02abd	0.66 \pm 0.04abef	0.97 \pm 0.05abd	1.45 \pm 0.07ab	2.76 \pm 0.10abc	4.40 \pm 0.17abc								
	28°C	0.21 \pm 0.01abcde	0.52 \pm 0.02fg	0.99 \pm 0.03dh	1.47 \pm 0.08fg	2.34 \pm 0.13ef	4.21 \pm 0.22e	6.89 \pm 0.24f								
16_wild	20°C	0.12 \pm 0.01fgh	0.30 \pm 0.02bde	0.60 \pm 0.03befg	0.85 \pm 0.05abcde	1.32 \pm 0.05ad	2.51 \pm 0.08ad	4.08 \pm 0.13ab								
	28°C	0.21 \pm 0.01abcd	0.47 \pm 0.03acg	0.92 \pm 0.04cd	1.38 \pm 0.07gh	2.20 \pm 0.10ef	4.08 \pm 0.18ef	6.71 \pm 0.22f								
17_elite	20°C	0.14 \pm 0.02efgh	0.29 \pm 0.03bde	0.58 \pm 0.06efg	0.76 \pm 0.08de	1.15 \pm 0.15ad	2.13 \pm 0.22ad	3.52 \pm 0.34abd								
	28°C	0.23 \pm 0.03bd	0.46 \pm 0.05acg	0.77 \pm 0.08abcf	1.13 \pm 0.10bch	1.90 \pm 0.16bcf	3.40 \pm 0.29cf	5.44 \pm 0.45ce								
17_wild	20°C	0.18 \pm 0.02abcef	0.35 \pm 0.03ab	0.69 \pm 0.05abef	0.96 \pm 0.07abd	1.47 \pm 0.10ab	2.59 \pm 0.17ab	4.18 \pm 0.25ab								
	28°C	0.23 \pm 0.01bd	0.49 \pm 0.03cg	0.82 \pm 0.03acd	1.27 \pm 0.04cgh	1.98 \pm 0.11cf	3.80 \pm 0.14ef	5.94 \pm 0.21ef								

[†] Different letters indicate significant differences at each time point (two-way ANOVA and Tukey's HSD test, $P < 0.05$).

Table 1 Plant volume during barley growth and development (related to Fig. 5-5D).

Genotype	Temp	8 DAS	11 DAS	14 DAS	16 DAS	18 DAS	21 DAS	24 DAS	49 DAS	52 DAS
		Plant volume ($\times 10^4 \text{ mm}^3$) \pm SEM ($n=11$)								
Bowman	20°C	0.02 \pm 0.01a [†]	0.10 \pm 0.03e	0.58 \pm 0.09f	1.38 \pm 0.21d	2.77 \pm 0.40d	9.37 \pm 1.06c	16.89 \pm 1.86e		
	28°C	0.07 \pm 0.02ab	0.21 \pm 0.04ae	0.87 \pm 0.09f	2.19 \pm 0.16ad	5.55 \pm 0.54ad	17.47 \pm 1.03abd	31.12 \pm 2.14abd		
BW290	20°C	0.14 \pm 0.03abcd	0.48 \pm 0.07abc	1.07 \pm 0.11bf	2.11 \pm 0.16ad	4.26 \pm 0.19ad	11.83 \pm 0.37bc	21.57 \pm 1.00de		
	28°C	0.39 \pm 0.05e	0.93 \pm 0.14fg	2.47 \pm 0.31deg	5.75 \pm 0.61fg	9.56 \pm 0.97cf	22.12 \pm 1.36defg	37.93 \pm 3.62bci		
10_elite	20°C	0.18 \pm 0.03abcd	0.55 \pm 0.04abcd	1.84 \pm 0.16abcde	3.49 \pm 0.22abc	7.03 \pm 0.49abc	15.86 \pm 1.01abcd	34.83 \pm 1.79abc		
	28°C	0.24 \pm 0.02cde	0.79 \pm 0.03bd [†] fg	2.64 \pm 0.14dg	5.74 \pm 0.27fg	11.05 \pm 0.47efg	25.77 \pm 1.61ef	48.08 \pm 2.15fhi		
10_wild	20°C	0.09 \pm 0.02abd	0.46 \pm 0.05abc	1.31 \pm 0.09abcf	2.73 \pm 0.13abd	5.40 \pm 0.40ad	14.80 \pm 0.78abc	31.67 \pm 1.54abcd		
	28°C	0.35 \pm 0.04e	1.02 \pm 0.07f	3.10 \pm 0.18g	7.65 \pm 0.31e	13.99 \pm 0.38e	28.33 \pm 0.97e	58.92 \pm 2.25fg		
16_elite	20°C	0.11 \pm 0.04abcd	0.34 \pm 0.04ace	1.27 \pm 0.15bcf	2.71 \pm 0.25abd	5.79 \pm 0.51abd	14.87 \pm 0.91abc	32.02 \pm 1.91abcd		
	28°C	0.26 \pm 0.03cde	0.90 \pm 0.07g	2.55 \pm 0.17deg	6.54 \pm 0.57eg	13.02 \pm 1.08eg	28.10 \pm 1.97e	61.91 \pm 3.76g		
16_wild	20°C	0.06 \pm 0.02ab	0.30 \pm 0.05ace	1.09 \pm 0.12bf	2.18 \pm 0.21ad	4.94 \pm 0.40ad	14.30 \pm 0.71abc	28.58 \pm 1.43abde		
	28°C	0.26 \pm 0.04cde	0.63 \pm 0.06bcdg	2.08 \pm 0.20acde	5.51 \pm 0.40fg	11.40 \pm 0.75efg	28.69 \pm 2.16e	56.93 \pm 2.66fgh		
17_elite	20°C	0.12 \pm 0.03abcd	0.28 \pm 0.07ae	1.04 \pm 0.17bf	1.98 \pm 0.32ad	4.13 \pm 0.71ad	11.58 \pm 1.46bc	22.86 \pm 3.01ade		
	28°C	0.23 \pm 0.06bcde	0.76 \pm 0.11bd [†] fg	1.75 \pm 0.27abce	4.13 \pm 0.50bcf	8.97 \pm 0.96bcf	19.02 \pm 2.69adfg	44.50 \pm 4.95chi		
17_wild	20°C	0.17 \pm 0.03abcd	0.40 \pm 0.06ace	1.41 \pm 0.19abcf	2.65 \pm 0.30abd	5.74 \pm 0.76ad	14.44 \pm 1.19abc	30.50 \pm 2.93abd		
	28°C	0.27 \pm 0.04ce	0.89 \pm 0.08dfg	2.13 \pm 0.16ade	5.13 \pm 0.32cfg	9.97 \pm 0.67cfg	23.10 \pm 1.23efg	49.28 \pm 2.10fghi		
Time		28 DAS	31 DAS	35 DAS	38 DAS	42 DAS	45 DAS	49 DAS	52 DAS	
Bowman	20°C	45.50 \pm 3.61f	81.06 \pm 5.33e	164.31 \pm 9.16ef	277.92 \pm 14.27cdg	497.75 \pm 21.10a	702.23 \pm 31.46abd	943.09 \pm 33.36ab	1109.30 \pm 40.36cd	
	28°C	80.84 \pm 5.02abc	140.52 \pm 7.00abc	258.45 \pm 10.77bcg	358.01 \pm 10.58abcef	536.17 \pm 12.88abc	650.08 \pm 13.51ab	710.01 \pm 18.15d	780.13 \pm 21.02g	
BW290	20°C	52.65 \pm 2.71ef	94.33 \pm 4.16de	167.69 \pm 7.86def	256.45 \pm 14.17dg	352.78 \pm 21.24e	405.27 \pm 22.31e	443.52 \pm 28.59e	477.56 \pm 31.94e	
	28°C	81.81 \pm 6.21abc	124.29 \pm 10.15acd	150.31 \pm 13.83f	159.05 \pm 15.28h	167.58 \pm 16.47f	152.75 \pm 14.71f	101.85 \pm 12.29f	81.74 \pm 9.68f	
10_elite	20°C	84.99 \pm 3.90abcd	143.18 \pm 5.41abc	224.48 \pm 9.10abc	332.93 \pm 14.19abcde	520.01 \pm 13.98ab	661.28 \pm 23.91ab	972.16 \pm 30.95ab	1345.74 \pm 31.89abc	
	28°C	104.86 \pm 4.01cdg	170.55 \pm 5.13bf	272.79 \pm 5.55cg	380.41 \pm 9.43abef	535.18 \pm 16.43abc	679.85 \pm 17.59ab	780.11 \pm 31.51bd	990.87 \pm 44.36d	
10_wild	20°C	83.06 \pm 3.73abc	154.20 \pm 6.35bcf	261.45 \pm 12.06bcg	408.56 \pm 17.55befi	638.72 \pm 26.78bcd	766.89 \pm 31.73abcd	974.34 \pm 42.81ab	1142.68 \pm 57.16cd	
	28°C	111.23 \pm 4.11dgh	165.92 \pm 7.63bcf	197.55 \pm 9.13adef	206.43 \pm 7.89gh	242.42 \pm 7.64ef	273.29 \pm 7.47ef	303.58 \pm 10e	328.01 \pm 10.99ef	
16_elite	20°C	79.04 \pm 3.46abce	138.09 \pm 5.86abc	215.62 \pm 10.31abde	319.30 \pm 14.06abcd	504.58 \pm 24.11a	608.22 \pm 26.75a	805.05 \pm 36.27bd	1077.21 \pm 40.87d	
	28°C	142.15 \pm 6.79i	247.81 \pm 10.69g	379.69 \pm 16.66i	542.91 \pm 30.63j	738.59 \pm 42.22d	855.51 \pm 58.37cd	933.45 \pm 64.58ab	1126.97 \pm 85.75cd	
16_wild	20°C	74.02 \pm 4.22abe	134.40 \pm 5.96abcd	221.95 \pm 6.34abcd	342.23 \pm 14.33abcdef	538.56 \pm 23.21abc	687.62 \pm 35.27ab	919.27 \pm 37.67ab	1236.57 \pm 46.31acd	
	28°C	134.02 \pm 5.96hi	234.62 \pm 8.56g	353.45 \pm 14.97hi	499.52 \pm 16.12ij	679.79 \pm 30.52d	807.52 \pm 38.29bcd	911.13 \pm 28.93abd	1123.46 \pm 31.23cd	
17_elite	20°C	59.11 \pm 7.47aef	110.85 \pm 12.73ade	195.63 \pm 16.40adef	307.89 \pm 33.11acd	516.39 \pm 49.57ab	730.73 \pm 56.56abcd	1069.9 \pm 75.25ac	1436.56 \pm 95.83ab	
	28°C	97.42 \pm 10.10bcdg	167.20 \pm 14.91bf	267.14 \pm 15.87bcg	416.28 \pm 31.10efi	607.51 \pm 36.87abcd	739.14 \pm 43.32abcd	878.68 \pm 51.56abd	1006.23 \pm 65.06dg	
17_wild	20°C	74.87 \pm 5.76abe	140.34 \pm 9.79abc	251.46 \pm 9.32abcbg	397.79 \pm 15.95abef	662.38 \pm 23.28cd	869.35 \pm 31.03c	1231.19 \pm 49.59c	1568.23 \pm 77.05b	
	28°C	113.93 \pm 4.81gh	191.72 \pm 8.84f	303.06 \pm 7.26gh	426.78 \pm 18.28fi	619.38 \pm 27.50abcd	736.65 \pm 32.00abcd	891.82 \pm 43.81abd	1053.76 \pm 49.13d	

[†] Different letters indicate significant differences at each time point (two-way ANOVA and Tukey's HSD test, $P < 0.05$).

Table 5 Top-view convex hull area during barley growth and development (related to Fig. 5-5E).

Genotype	Temp	Top-view convex hull area ($\times 10^5$ pixels ²) \pm SEM (n=11)															
		8 DAS	11 DAS	14 DAS	16 DAS	18 DAS	21 DAS	24 DAS	28 DAS	31 DAS	35 DAS	38 DAS	42 DAS	45 DAS	49 DAS	52 DAS	
Bowman	20°C	0.09 \pm 0.07a ^t	0.01 \pm 0.00a	0.01 \pm 0.00a	0.04 \pm 0.01a	0.21 \pm 0.07abc	0.29 \pm 0.04a	0.49 \pm 0.03a									
	28°C	0.05 \pm 0.03a	0.01 \pm 0.01a	0.02 \pm 0.00a	0.07 \pm 0.02abc	0.23 \pm 0.05abc	0.46 \pm 0.10ab	1.21 \pm 0.20bcde									
	20°C	0.00 \pm 0.00a	0.02 \pm 0.01a	0.02 \pm 0.01a	0.06 \pm 0.01ab	0.18 \pm 0.03ab	0.57 \pm 0.10abc	0.82 \pm 0.13abcd									
BW290	28°C	0.05 \pm 0.03a	0.07 \pm 0.03a	0.13 \pm 0.06a	0.32 \pm 0.10e	0.43 \pm 0.07abc	0.77 \pm 0.09bce	1.54 \pm 0.17ef									
	20°C	0.08 \pm 0.04a	0.01 \pm 0.00a	0.04 \pm 0.01a	0.10 \pm 0.02abcd	0.28 \pm 0.09abc	0.51 \pm 0.05abc	0.84 \pm 0.05abcd									
	28°C	0.01 \pm 0.00a	0.02 \pm 0.01a	0.16 \pm 0.10a	0.23 \pm 0.04bcde	0.41 \pm 0.06abc	0.68 \pm 0.06abce	1.47 \pm 0.17def									
10_wild	20°C	0.01 \pm 0.01a	0.00 \pm 0.00a	0.02 \pm 0.00a	0.08 \pm 0.02abc	0.15 \pm 0.03ab	0.65 \pm 0.13abcde	0.82 \pm 0.07abcd									
	28°C	0.04 \pm 0.02a	0.02 \pm 0.01a	0.15 \pm 0.07a	0.27 \pm 0.03de	0.44 \pm 0.03abc	1.31 \pm 0.18d	1.89 \pm 0.19f									
	20°C	0.11 \pm 0.09a	0.03 \pm 0.01a	0.01 \pm 0.00a	0.06 \pm 0.01abc	0.23 \pm 0.06abc	0.44 \pm 0.05ab	0.66 \pm 0.07abc									
16_elite	28°C	0.07 \pm 0.04a	0.03 \pm 0.01a	0.06 \pm 0.01a	0.29 \pm 0.04e	0.55 \pm 0.10c	0.98 \pm 0.07cde	1.31 \pm 0.11cdef									
	20°C	0.03 \pm 0.02a	0.05 \pm 0.04a	0.03 \pm 0.01a	0.05 \pm 0.01a	0.17 \pm 0.02ab	0.48 \pm 0.10ab	0.62 \pm 0.02ab									
	28°C	0.02 \pm 0.01a	0.05 \pm 0.02a	0.04 \pm 0.01a	0.21 \pm 0.02abcde	0.56 \pm 0.12c	1.06 \pm 0.19de	1.17 \pm 0.15bcde									
17_elite	20°C	0.02 \pm 0.02a	0.02 \pm 0.01a	0.02 \pm 0.00a	0.05 \pm 0.01a	0.10 \pm 0.02b	0.33 \pm 0.04ab	0.51 \pm 0.08a									
	28°C	0.02 \pm 0.01a	0.04 \pm 0.03a	0.04 \pm 0.01a	0.17 \pm 0.03abcde	0.50 \pm 0.16ac	0.49 \pm 0.05ab	1.12 \pm 0.22abcde									
	20°C	0.01 \pm 0.01a	0.01 \pm 0.00a	0.03 \pm 0.01a	0.07 \pm 0.02abc	0.18 \pm 0.04ab	0.46 \pm 0.05ab	0.92 \pm 0.16abcde									
17_wild	28°C	0.02 \pm 0.01a	0.03 \pm 0.01a	0.05 \pm 0.01a	0.23 \pm 0.05cde	0.32 \pm 0.03abc	0.79 \pm 0.05bce	1.06 \pm 0.07abcde									
	20°C	1.15 \pm 0.10a	2.31 \pm 0.28abc	3.76 \pm 0.25a	5.03 \pm 0.32ab	6.88 \pm 0.32bd	7.67 \pm 0.29f	9.99 \pm 0.66f									
	28°C	2.05 \pm 0.14bcde	3.04 \pm 0.17abc	4.16 \pm 0.32a	4.23 \pm 0.21ab	4.91 \pm 0.47ace	4.14 \pm 0.17beg	4.68 \pm 0.21dg									
BW290	20°C	1.24 \pm 0.13a	2.97 \pm 0.55abc	3.81 \pm 0.24a	5.55 \pm 0.25b	7.20 \pm 0.42d	7.26 \pm 0.30df	7.86 \pm 0.29bce									
	28°C	2.73 \pm 0.18d	3.48 \pm 0.22c	4.25 \pm 0.50a	4.63 \pm 0.54ab	4.26 \pm 0.51ae	3.47 \pm 0.29g	2.54 \pm 0.23h									
	20°C	1.46 \pm 0.14ab	2.35 \pm 0.20abc	3.31 \pm 0.26a	4.82 \pm 0.47ab	5.88 \pm 0.46abcd	5.74 \pm 0.38abcd	6.77 \pm 0.37abc									
10_elite	28°C	2.28 \pm 0.18cde	2.90 \pm 0.19abc	3.73 \pm 0.27a	4.33 \pm 0.27ab	4.10 \pm 0.17ae	5.04 \pm 0.28bceg	4.87 \pm 0.24adg									
	20°C	1.42 \pm 0.13ab	2.80 \pm 0.27abc	3.66 \pm 0.28a	4.95 \pm 0.37ab	6.58 \pm 0.24bcd	7.11 \pm 0.32adf	9.38 \pm 0.58ef									
	28°C	2.55 \pm 0.14cd	3.25 \pm 0.20ac	3.59 \pm 0.20a	4.84 \pm 0.44ab	5.10 \pm 0.36abce	4.57 \pm 0.29bceg	5.43 \pm 0.26adg									
16_elite	20°C	1.22 \pm 0.13a	1.93 \pm 0.23b	3.17 \pm 0.24a	3.56 \pm 0.24ab	6.02 \pm 0.46abcd	5.81 \pm 0.40abcd	7.71 \pm 0.58bce									
	28°C	2.34 \pm 0.20cde	3.16 \pm 0.29abc	4.02 \pm 0.30a	5.45 \pm 0.68b	4.27 \pm 0.22ae	5.34 \pm 0.43bce	5.03 \pm 0.35adg									
	20°C	1.45 \pm 0.24ab	2.07 \pm 0.22ab	2.83 \pm 0.18a	3.25 \pm 0.22a	5.14 \pm 0.32abce	6.13 \pm 0.54acdf	8.33 \pm 0.65cef									
16_wild	28°C	1.77 \pm 0.09abe	2.65 \pm 0.22abc	3.94 \pm 0.38a	4.75 \pm 0.73ab	4.49 \pm 0.35ae	4.62 \pm 0.42bceg	5.23 \pm 0.33adg									
	20°C	1.16 \pm 0.14a	1.98 \pm 0.23ab	3.61 \pm 0.43a	3.79 \pm 0.42ab	5.21 \pm 0.41abce	5.76 \pm 0.40abcd	6.78 \pm 0.31abc									
	28°C	1.87 \pm 0.19abc	2.88 \pm 0.29abc	4.03 \pm 0.34a	4.71 \pm 0.27ab	4.55 \pm 0.42ae	4.61 \pm 0.42bceg	4.65 \pm 0.39dg									
17_wild	20°C	1.50 \pm 0.12ab	2.46 \pm 0.22abc	4.05 \pm 0.44a	4.15 \pm 0.28ab	6.02 \pm 0.66abcd	5.45 \pm 0.32abce	6.28 \pm 0.28abd									
	28°C	2.34 \pm 0.16cde	2.64 \pm 0.16abc	3.38 \pm 0.24a	4.21 \pm 0.38ab	3.72 \pm 0.23e	3.90 \pm 0.27eg	4.26 \pm 0.35gh									

^t Different letters indicate significant differences at each time point (two-way ANOVA and Tukey's HSD test, $P < 0.05$).

Table 6 Side-view convex hull area during barley growth and development (related to Fig. 5-5F).

Genotype	Temp	Side-view convex hull area ($\times 10^5$ pixels ²) \pm SEM (n=11)													
		8 DAS	11 DAS	14 DAS	16 DAS	18 DAS	21 DAS	24 DAS	28 DAS	31 DAS	35 DAS	42 DAS	45 DAS	49 DAS	52 DAS
Bowman	20°C	0.02 \pm 0.01a ^t	0.03 \pm 0.01b	0.15 \pm 0.03a	0.18 \pm 0.02a	0.36 \pm 0.05c	1.06 \pm 0.10a	1.71 \pm 0.09a							
	28°C	0.03 \pm 0.01a	0.05 \pm 0.01abc	0.15 \pm 0.03a	0.28 \pm 0.02a	0.65 \pm 0.06ac	1.43 \pm 0.10ab	2.48 \pm 0.14bcd							
BW290	20°C	0.03 \pm 0.01a	0.06 \pm 0.01abcde	0.23 \pm 0.03abc	0.28 \pm 0.02a	0.66 \pm 0.05ac	1.46 \pm 0.08ab	2.16 \pm 0.10abcd							
	28°C	0.06 \pm 0.02a	0.13 \pm 0.02f	0.39 \pm 0.03d	0.73 \pm 0.07bc	1.32 \pm 0.12d	2.33 \pm 0.13de	3.33 \pm 0.18e							
10_elite	20°C	0.02 \pm 0.00a	0.06 \pm 0.01abcde	0.19 \pm 0.02ab	0.38 \pm 0.03a	0.68 \pm 0.04ab	1.48 \pm 0.07abc	2.03 \pm 0.05abc							
	28°C	0.05 \pm 0.02a	0.10 \pm 0.01def	0.28 \pm 0.02abcd	0.62 \pm 0.03bc	0.98 \pm 0.04be	1.95 \pm 0.12ce	2.82 \pm 0.11ef							
10_wild	20°C	0.02 \pm 0.01a	0.05 \pm 0.00bc	0.17 \pm 0.02a	0.32 \pm 0.02a	0.58 \pm 0.04ac	1.37 \pm 0.03a	2.08 \pm 0.07abcd							
	28°C	0.05 \pm 0.01a	0.13 \pm 0.01f	0.36 \pm 0.02cd	0.82 \pm 0.04b	1.32 \pm 0.05d	2.47 \pm 0.06d	3.33 \pm 0.12e							
16_elite	20°C	0.03 \pm 0.01a	0.04 \pm 0.00b	0.18 \pm 0.03a	0.29 \pm 0.03a	0.53 \pm 0.04ac	1.36 \pm 0.07a	1.94 \pm 0.08ab							
	28°C	0.03 \pm 0.00a	0.10 \pm 0.01def	0.33 \pm 0.02bcd	0.68 \pm 0.05bc	1.24 \pm 0.06de	2.35 \pm 0.11de	3.06 \pm 0.08ef							
16_wild	20°C	0.03 \pm 0.01a	0.05 \pm 0.01abc	0.21 \pm 0.03ab	0.25 \pm 0.02a	0.53 \pm 0.03ac	1.16 \pm 0.04a	1.77 \pm 0.07a							
	28°C	0.03 \pm 0.01a	0.09 \pm 0.01acdef	0.28 \pm 0.03abcd	0.63 \pm 0.04bc	1.17 \pm 0.05de	2.14 \pm 0.09de	2.84 \pm 0.12ef							
17_elite	20°C	0.03 \pm 0.01a	0.06 \pm 0.01abcde	0.19 \pm 0.02ab	0.21 \pm 0.03a	0.46 \pm 0.07ac	1.20 \pm 0.13a	1.60 \pm 0.16a							
	28°C	0.05 \pm 0.02a	0.10 \pm 0.02ef	0.25 \pm 0.05abcd	0.60 \pm 0.07c	0.99 \pm 0.09e	1.87 \pm 0.14bce	2.63 \pm 0.23cdf							
17_wild	20°C	0.03 \pm 0.01a	0.05 \pm 0.01abcd	0.28 \pm 0.04abcd	0.29 \pm 0.03a	0.64 \pm 0.07ac	1.40 \pm 0.11ab	2.08 \pm 0.15abcd							
	28°C	0.06 \pm 0.02a	0.10 \pm 0.01def	0.28 \pm 0.03abcd	0.66 \pm 0.06bc	1.10 \pm 0.08de	2.08 \pm 0.10de	2.64 \pm 0.07df							
Bowman	20°C	3.05 \pm 0.12ab	4.24 \pm 0.17a	6.41 \pm 0.17abc	6.26 \pm 0.20ab	9.20 \pm 0.24ae	9.96 \pm 0.20ae	10.50 \pm 0.27bc	11.51 \pm 0.20a						
	28°C	4.32 \pm 0.16eg	5.48 \pm 0.12cd	6.95 \pm 0.21bcd	6.11 \pm 0.22ab	7.26 \pm 0.30cdg	6.92 \pm 0.14g	6.32 \pm 0.17de	6.90 \pm 0.36d						
BW290	20°C	3.34 \pm 0.16abcd	4.45 \pm 0.21ab	7.17 \pm 0.10cde	7.74 \pm 0.15de	10.55 \pm 0.12f	10.52 \pm 0.22ef	10.69 \pm 0.22c	10.86 \pm 0.25a						
	28°C	5.23 \pm 0.16f	6.25 \pm 0.24d	8.23 \pm 0.37e	7.71 \pm 0.46cde	8.76 \pm 0.36ab	7.18 \pm 0.32dg	5.68 \pm 0.29e	5.37 \pm 0.24e						
10_elite	20°C	3.41 \pm 0.12abcd	4.62 \pm 0.13abc	5.95 \pm 0.20ab	6.30 \pm 0.27ab	8.82 \pm 0.25ab	8.84 \pm 0.33ab	9.04 \pm 0.25a	11.10 \pm 0.34a						
	28°C	3.89 \pm 0.10cdeg	4.52 \pm 0.07ab	5.70 \pm 0.20a	5.56 \pm 0.17a	6.91 \pm 0.17g	7.55 \pm 0.19bcdg	7.26 \pm 0.19d	8.03 \pm 0.18cd						
10_wild	20°C	3.63 \pm 0.10abcdg	4.91 \pm 0.13abc	6.61 \pm 0.11abc	7.23 \pm 0.20bce	10.60 \pm 0.25f	11.57 \pm 0.32f	12.67 \pm 0.34f	13.57 \pm 0.35f						
	28°C	4.51 \pm 0.15ef	6.14 \pm 0.26d	8.04 \pm 0.34de	8.49 \pm 0.31d	10.48 \pm 0.24ef	9.94 \pm 0.26ae	9.08 \pm 0.20a	9.24 \pm 0.22bc						
16_elite	20°C	3.27 \pm 0.10abc	4.15 \pm 0.09a	5.78 \pm 0.17a	5.98 \pm 0.27a	9.16 \pm 0.40ae	8.79 \pm 0.41abc	9.15 \pm 0.32ab	10.42 \pm 0.32ab						
	28°C	4.36 \pm 0.13eg	5.15 \pm 0.15bc	6.35 \pm 0.29abc	5.68 \pm 0.26a	7.64 \pm 0.34bcdg	7.72 \pm 0.35bcdg	7.28 \pm 0.34d	7.65 \pm 0.40d						
16_wild	20°C	3.06 \pm 0.12ab	4.15 \pm 0.09a	6.18 \pm 0.19abc	6.06 \pm 0.14ab	8.90 \pm 0.35ab	9.39 \pm 0.40ae	9.69 \pm 0.41abc	11.13 \pm 0.43a						
	28°C	4.04 \pm 0.10deg	4.88 \pm 0.08abc	5.94 \pm 0.16ab	5.52 \pm 0.12a	7.16 \pm 0.19dg	7.36 \pm 0.28cdg	7.44 \pm 0.30d	7.83 \pm 0.28cd						
17_elite	20°C	2.98 \pm 0.23a	4.07 \pm 0.31a	6.06 \pm 0.38abc	5.95 \pm 0.39a	8.27 \pm 0.35abcd	8.53 \pm 0.40abcd	9.39 \pm 0.31abc	10.77 \pm 0.34a						
	28°C	3.78 \pm 0.27bcdg	4.46 \pm 0.28ab	6.11 \pm 0.27abc	5.95 \pm 0.24a	7.37 \pm 0.24cdg	7.21 \pm 0.23dg	7.18 \pm 0.29d	7.20 \pm 0.30d						
17_wild	20°C	3.51 \pm 0.18abcd	4.60 \pm 0.18abc	6.10 \pm 0.26abc	6.51 \pm 0.16abc	8.56 \pm 0.18abc	8.66 \pm 0.18abc	9.47 \pm 0.24abc	10.82 \pm 0.30a						
	28°C	4.07 \pm 0.12deg	5.23 \pm 0.13bc	6.08 \pm 0.17abc	5.69 \pm 0.15a	6.81 \pm 0.22g	6.55 \pm 0.25g	6.42 \pm 0.26de	7.25 \pm 0.26d						

^t Different letters indicate significant differences at each time point (two-way ANOVA and Tukey's HSD test, $P < 0.05$).

Table 1 Total tiller number during barley growth and development (related to Fig. 5-6).

GenotypeTemp	Total tiller number \pm SEM (<i>n</i> =11)												
	14 DAS	16 DAS	18 DAS	21 DAS	24 DAS	28 DAS	31 DAS	35 DAS	38 DAS	42 DAS	45 DAS	49 DAS	52 DAS
Bowman	20°C	0.64 \pm 0.20abcde [†]	1.64 \pm 0.15ab	1.82 \pm 0.18abd	2.64 \pm 0.34bc	4.45 \pm 0.25ad							6.00 \pm 0.49d
	28°C	0.00 \pm 0.00e	0.82 \pm 0.12c	1.09 \pm 0.09d	2.09 \pm 0.09c	3.00 \pm 0.23e							5.91 \pm 0.16d
BW290	20°C	0.91 \pm 0.21cd	1.73 \pm 0.14ab	2.45 \pm 0.21bc	3.09 \pm 0.31abc	4.73 \pm 0.38abd							6.09 \pm 0.37d
	28°C	0.18 \pm 0.12abe	1.36 \pm 0.20bc	1.64 \pm 0.24ad	3.09 \pm 0.21abc	3.91 \pm 0.25de							5.91 \pm 0.28d
10_elite	20°C	0.55 \pm 0.16abcde	2.00 \pm 0.00ab	2.00 \pm 0.00abc	3.64 \pm 0.24ab	5.36 \pm 0.20abc							9.00 \pm 0.45ab
	28°C	0.00 \pm 0.00e	1.36 \pm 0.15bc	2.00 \pm 0.00abc	3.00 \pm 0.23abc	5.09 \pm 0.09abd							8.36 \pm 0.28abc
10_wild	20°C	0.82 \pm 0.12acd	1.91 \pm 0.09ab	2.00 \pm 0.00abc	3.45 \pm 0.16ab	5.36 \pm 0.20abc							8.82 \pm 0.23ab
	28°C	0.00 \pm 0.00e	1.55 \pm 0.16abc	2.18 \pm 0.12abc	3.45 \pm 0.16ab	5.09 \pm 0.16abd							6.55 \pm 0.28cd
16_elite	20°C	1.09 \pm 0.09d	2.00 \pm 0.19ab	2.18 \pm 0.12abc	4.00 \pm 0.13a	5.82 \pm 0.38abc							10.18 \pm 0.46b
	28°C	0.27 \pm 0.14abce	1.36 \pm 0.15bc	2.27 \pm 0.14abc	3.82 \pm 0.18a	6.00 \pm 0.30bc							10.09 \pm 0.28ab
16_wild	20°C	0.91 \pm 0.21cd	2.27 \pm 0.14a	2.36 \pm 0.15abc	3.82 \pm 0.18a	5.73 \pm 0.33abc							9.36 \pm 0.31ab
	28°C	0.09 \pm 0.09be	1.36 \pm 0.15bc	2.09 \pm 0.09abc	4.00 \pm 0.27a	5.73 \pm 0.19abc							10.00 \pm 0.30ab
17_elite	20°C	0.73 \pm 0.14abcd	1.55 \pm 0.25abc	1.73 \pm 0.19abd	3.18 \pm 0.30abc	4.55 \pm 0.34ad							8.18 \pm 0.67ac
	28°C	0.27 \pm 0.14abce	1.36 \pm 0.24bc	1.82 \pm 0.23abd	3.18 \pm 0.30abc	5.36 \pm 0.39abc							8.18 \pm 0.62ac
17_wild	20°C	0.91 \pm 0.09cd	1.82 \pm 0.12ab	2.18 \pm 0.12abc	3.73 \pm 0.27ab	5.55 \pm 0.21abc							8.64 \pm 0.34ab
	28°C	0.55 \pm 0.16abcde	1.64 \pm 0.20ab	2.64 \pm 0.15c	3.73 \pm 0.19ab	6.64 \pm 0.39c							9.55 \pm 0.34ab
Bowman	20°C	8.82 \pm 0.50de	10.27 \pm 0.65gh	12.00 \pm 0.62fg	15.45 \pm 0.59df	18.55 \pm 0.96eh	21.73 \pm 0.99cef	23.73 \pm 0.70bef					
	28°C	6.45 \pm 0.21f	9.91 \pm 0.56gh	13.36 \pm 0.53fg	19.64 \pm 0.91acd	24.64 \pm 0.75abcde	29.09 \pm 0.87abodgh	34.82 \pm 1.26cdg					
BW290	20°C	7.27 \pm 0.38ef	8.55 \pm 0.34g	10.00 \pm 0.27f	12.91 \pm 0.56f	15.09 \pm 0.89h	18.64 \pm 0.72f	20.55 \pm 0.90ef					
	28°C	7.09 \pm 0.48ef	9.91 \pm 0.68gh	11.55 \pm 0.55fg	15.82 \pm 0.78df	19.55 \pm 0.62aeh	20.09 \pm 1.02ef	20.45 \pm 0.84f					
10_elite	20°C	11.55 \pm 0.39abc	16.00 \pm 0.56abcd	19.82 \pm 0.54abcd	22.82 \pm 0.71ab	25.55 \pm 0.61abcd	27.27 \pm 0.92abcd	28.91 \pm 1.16abc					
	28°C	9.82 \pm 0.40ad	14.73 \pm 0.41abcf	18.45 \pm 0.62ab	24.09 \pm 0.91abe	28.91 \pm 0.80bdfg	32.55 \pm 0.71dgh	35.18 \pm 0.92cdg					
10_wild	20°C	10.55 \pm 0.21abd	12.00 \pm 0.33efh	14.09 \pm 0.46eg	17.36 \pm 0.54cdf	20.73 \pm 0.89aceh	25.27 \pm 0.81abcef	27.36 \pm 0.74abef					
	28°C	6.82 \pm 0.23ef	10.91 \pm 0.25egh	14.64 \pm 0.58deg	20.09 \pm 1.16acd	23.18 \pm 0.62abce	25.45 \pm 0.67abcef	26.64 \pm 0.61abef					
16_elite	20°C	12.73 \pm 0.76bc	17.45 \pm 0.96cd	21.45 \pm 0.87bc	26.73 \pm 1.54be	32.09 \pm 1.99fg	34.55 \pm 2.00gh	36.36 \pm 1.54dg					
	28°C	12.45 \pm 0.37bc	16.64 \pm 0.51bcd	20.27 \pm 0.71abc	25.73 \pm 1.29be	27.00 \pm 1.00bcdfg	29.73 \pm 1.44abodgh	31.55 \pm 1.83acd					
16_wild	20°C	12.10 \pm 0.43abc	16.27 \pm 0.27abcd	20.00 \pm 0.70abc	23.64 \pm 0.80ab	25.64 \pm 1.09abcd	27.82 \pm 0.87abcdg	27.64 \pm 0.83abe					
	28°C	13.45 \pm 0.49c	18.00 \pm 0.59d	22.27 \pm 0.89c	29.27 \pm 1.27e	32.27 \pm 1.66g	35.27 \pm 1.77h	37.64 \pm 1.81g					
17_elite	20°C	9.82 \pm 0.63ad	13.82 \pm 1.08abef	18.27 \pm 1.11abd	22.36 \pm 1.65abc	24.36 \pm 1.86abcde	26.82 \pm 2.07abcde	29.36 \pm 2.25abcd					
	28°C	9.82 \pm 0.75ad	13.82 \pm 0.91abef	17.45 \pm 1.35ade	22.36 \pm 1.40abc	26.91 \pm 1.83bcd	30.55 \pm 2.37adgh	32.27 \pm 2.15acd					
17_wild	20°C	10.91 \pm 0.28abd	13.45 \pm 0.62aef	17.64 \pm 0.62ade	19.64 \pm 0.97acd	21.91 \pm 1.50ace	23.45 \pm 1.45bcef	25.18 \pm 1.85abef					
	28°C	11.73 \pm 0.49abc	15.82 \pm 0.42abcd	19.18 \pm 1.00abc	24.91 \pm 1.34abe	30.18 \pm 2.25dfg	35.00 \pm 1.84h	36.45 \pm 1.95dg					

[†] Different letters indicate significant differences at each time point (two-way ANOVA and Tukey's HSD test, *P*<0.05).

Table 18 Chlorophyll content in the second leaf during barley growth and development (related to Fig. 5-8).

Genotype Temp		SPAD readings \pm SEM (n=11)					
Time		16 DAS	23 DAS	30 DAS	37 DAS	44 DAS	52 DAS
Bowman	20°C	41.45 \pm 0.91 ^{adef†}	45.02 \pm 0.64 ^{bcd}	44.96 \pm 0.44 ^{cde}	46.88 \pm 0.81 ^{ab}	45.64 \pm 0.59 ^a	42.68 \pm 2.06 ^{bc}
	28°C	39.27 \pm 1.13 ^f	39.97 \pm 0.48 ^{ef}	41.42 \pm 0.44 ^{ef}	42.15 \pm 0.52 ^{cd}	37.44 \pm 3.88 ^{ab}	0.85 \pm 0.85 ^f
BW290	20°C	39.55 \pm 1.21 ^f	40.55 \pm 0.91 ^{efg}	39.99 \pm 0.40 ^{fg}	40.85 \pm 0.41 ^{cde}	42.55 \pm 0.47 ^{ab}	43.27 \pm 0.51 ^c
	28°C	38.53 \pm 0.50 ^f	37.90 \pm 0.61 ^f	37.48 \pm 0.51 ^g	36.99 \pm 0.50 ^e	33.90 \pm 3.46 ^{abc}	0.00 \pm 0.00 ^f
10_elite	20°C	44.48 \pm 1.07 ^{abcde}	47.97 \pm 0.60 ^{abc}	46.61 \pm 1.02 ^{abc}	47.52 \pm 1.15 ^{ab}	47.55 \pm 0.99 ^a	29.57 \pm 4.96 ^{abc}
	28°C	42.58 \pm 0.75 ^{adef}	42.83 \pm 0.61 ^{deg}	44.38 \pm 0.66 ^{cde}	44.87 \pm 0.60 ^{bc}	43.61 \pm 0.60 ^{ab}	7.95 \pm 4.03 ^{def}
10_wild	20°C	39.94 \pm 1.02 ^{ef}	43.79 \pm 1.19 ^{deg}	42.54 \pm 0.80 ^{def}	42.45 \pm 0.62 ^{cd}	44.15 \pm 0.75 ^{ab}	42.65 \pm 1.66 ^{bc}
	28°C	38.69 \pm 0.77 ^f	40.27 \pm 0.44 ^{ef}	39.26 \pm 0.55 ^{fg}	40.35 \pm 0.87 ^{de}	42.05 \pm 0.66 ^{ab}	23.06 \pm 5.38 ^{ad}
16_elite	20°C	45.75 \pm 0.74 ^{bcd}	48.75 \pm 1.28 ^{ab}	45.42 \pm 1.21 ^{bcd}	45.20 \pm 0.78 ^{abc}	45.63 \pm 0.55 ^a	19.18 \pm 5.05 ^{ade}
	28°C	43.18 \pm 0.97 ^{abdef}	44.16 \pm 0.52 ^{cdg}	41.91 \pm 0.44 ^{def}	41.25 \pm 0.61 ^{cde}	10.82 \pm 5.00 ^d	0.16 \pm 0.16 ^f
16_wild	20°C	45.04 \pm 0.68 ^{abcd}	45.41 \pm 0.64 ^{bcd}	45.20 \pm 0.93 ^{bcd}	44.99 \pm 0.92 ^{bc}	42.62 \pm 0.83 ^{ab}	24.01 \pm 4.00 ^{ad}
	28°C	41.01 \pm 0.40 ^{aef}	41.74 \pm 0.32 ^{defg}	40.04 \pm 0.46 ^{fg}	37.33 \pm 1.78 ^e	13.80 \pm 5.20 ^d	4.97 \pm 3.73 ^{ef}
17_elite	20°C	47.50 \pm 1.41 ^{bc}	49.77 \pm 1.13 ^a	49.62 \pm 1.02 ^a	49.50 \pm 0.87 ^a	47.55 \pm 0.90 ^a	25.19 \pm 4.38 ^{ad}
	28°C	45.75 \pm 1.31 ^{bcd}	45.36 \pm 0.76 ^{bcd}	45.49 \pm 0.60 ^{bcd}	47.76 \pm 1.17 ^{ab}	21.13 \pm 6.40 ^{cd}	3.37 \pm 3.37 ^{ef}
17_wild	20°C	48.93 \pm 0.79 ^c	49.85 \pm 0.81 ^a	48.78 \pm 1.06 ^{ab}	48.99 \pm 0.86 ^{ab}	43.02 \pm 1.22 ^{ab}	25.75 \pm 5.26 ^{ab}
	28°C	44.32 \pm 0.90 ^{abcde}	43.71 \pm 0.83 ^{deg}	44.11 \pm 0.60 ^{cde}	42.35 \pm 0.76 ^{cd}	30.27 \pm 4.79 ^{bc}	3.34 \pm 2.86 ^{ef}

† Different letters indicate significant differences at each time point (two-way ANOVA and Tukey's HSD test, $P < 0.05$).

Table 19 Transcript levels of barley flowering genes during growth and development (related to Fig. 5-10B).

Time		12 DAS	19 DAS	27 DAS	33 DAS	40 DAS
Genotype Temp		<i>Ppd-H1</i> relative expression \pm SEM (n=3)				
10_elite	20°C	0.5953 \pm 0.0771a [†]	1.0878 \pm 0.1463a	1.4070 \pm 0.0896a	0.9001 \pm 0.1029a	0.9610 \pm 0.1550ab
	28°C	0.4858 \pm 0.0818a	0.6202 \pm 0.0438b	0.4941 \pm 0.0558b	0.4351 \pm 0.1101a	0.4889 \pm 0.0468c
10_wild	20°C	0.9827 \pm 0.1660a	0.6969 \pm 0.0813ab	1.4690 \pm 0.0070a	1.1348 \pm 0.1484a	1.0965 \pm 0.1195b
	28°C	0.9601 \pm 0.3120a	0.4276 \pm 0.0235b	1.3214 \pm 0.2059a	1.1150 \pm 0.3222a	0.5234 \pm 0.0231ac
		<i>FT1</i> relative expression \pm SEM (n=3)				
10_elite	20°C	0.0039 \pm 0.0010ab	0.1057 \pm 0.0515a	0.3694 \pm 0.0952ab	1.0975 \pm 0.1111ab	0.5810 \pm 0.0959a
	28°C	0.0012 \pm 0.0004a	0.0366 \pm 0.0049a	0.0907 \pm 0.0114a	0.3794 \pm 0.0981b	0.3756 \pm 0.1634a
10_wild	20°C	0.0149 \pm 0.0035b	0.1366 \pm 0.0212a	0.5773 \pm 0.0895b	1.3145 \pm 0.4021ab	1.7149 \pm 0.1277b
	28°C	0.0112 \pm 0.0043ab	0.0994 \pm 0.0211a	0.3241 \pm 0.0911ab	2.2500 \pm 0.6589a	0.6048 \pm 0.1410a
		<i>VRN1</i> relative expression \pm SEM (n=3)				
10_elite	20°C	0.8940 \pm 0.1655a	4.1969 \pm 0.9151a	6.5418 \pm 1.2402a	8.3500 \pm 0.6266a	6.7857 \pm 1.5543a
	28°C	0.6817 \pm 0.0982a	2.5177 \pm 0.0956a	0.1257 \pm 0.2178b	5.8349 \pm 1.3113a	4.6895 \pm 0.6559a
10_wild	20°C	1.0197 \pm 0.0964a	1.8994 \pm 0.0371a	7.1400 \pm 0.8869a	6.4362 \pm 0.6593a	5.3958 \pm 0.4752a
	28°C	0.9393 \pm 0.2899a	2.9647 \pm 0.8071a	8.0983 \pm 0.3481a	5.9167 \pm 1.1447a	3.1167 \pm 0.5153a
		<i>BM3</i> relative expression \pm SEM (n=3)				
10_elite	20°C	2.5E-05 \pm 2.5E-05a	0.0003 \pm 0.0001a	0.0388 \pm 0.0179a	0.2197 \pm 0.0106ab	0.3027 \pm 0.0326a
	28°C	3.1E-06 \pm 2.4E-06a	0.0003 \pm 0.0002a	0.0063 \pm 0.0014a	0.1010 \pm 0.0397b	0.3052 \pm 0.0625a
10_wild	20°C	5.6E-05 \pm 2.7E-05a	0.0014 \pm 0.0002a	0.1192 \pm 0.0111ab	0.3416 \pm 0.0169a	0.3058 \pm 0.0255a
	28°C	2.6E-05 \pm 1.6E-05a	0.0180 \pm 0.0002b	0.2793 \pm 0.0933b	0.3157 \pm 0.0330a	0.1904 \pm 0.0135a
		<i>BM8</i> relative expression \pm SEM (n=3)				
10_elite	20°C	0.0005 \pm 2.9E-04a	0.0016 \pm 6.5E-04a	0.0097 \pm 0.0041a	0.1119 \pm 0.0111a	0.2633 \pm 0.0129a
	28°C	0.0004 \pm 1.3E-04a	0.0005 \pm 2.6E-05a	0.0025 \pm 0.0005a	0.1331 \pm 0.0456a	0.4696 \pm 0.1616ab
10_wild	20°C	0.0003 \pm 5.4E-05a	0.0007 \pm 1.4E-04a	0.0525 \pm 0.0098a	0.1961 \pm 0.0511a	0.7725 \pm 0.0194b
	28°C	0.0002 \pm 4.5E-05a	0.0102 \pm 9.1E-04b	0.1879 \pm 0.0373b	0.5960 \pm 0.0811b	0.6754 \pm 0.0479b
		<i>ELF3</i> relative expression \pm SEM (n=3)				
10_elite	20°C	0.9134 \pm 0.1589a	0.3463 \pm 0.0968a	0.9213 \pm 0.0614ab	0.4026 \pm 0.0220a	0.7685 \pm 0.1112a
	28°C	1.2925 \pm 0.0467a	0.3143 \pm 0.0160a	0.6066 \pm 0.1113a	0.3339 \pm 0.0433a	0.6138 \pm 0.0253a
10_wild	20°C	1.0100 \pm 0.2786a	0.4938 \pm 0.0248a	1.2601 \pm 0.0985b	0.5108 \pm 0.0562a	1.3877 \pm 0.0381b
	28°C	0.5650 \pm 0.1950a	0.3073 \pm 0.0390a	0.7655 \pm 0.0431a	0.3744 \pm 0.0381a	0.5744 \pm 0.0845a

[†] Different letters indicate significant differences at each time point (two-way ANOVA and Tukey's HSD test, $P < 0.05$).

Acknowledgments

First of all, I would like to thank my supervisor Professor Dr. Marcel Quint for giving me the opportunity to work in his group and guiding me throughout my PhD. I will always be very grateful for his constant encouragement and inspirational advice, as well as for giving me great freedom to work on diverse scientific projects. These are necessary for me to complete this thesis. In addition, this thesis would not have been possible without the funding support of the European Social Fund (ESF).

Then, I wish to gratefully appreciate Dr. Carolin Delker and Dr. Usman Muhammad Anwer for their encouragement, enlightening discussions, and suggestions during our scientific meetings. I would like to thank Professor Dr. Klaus Pillen, Dr. Andreas Maurer, and Tanja Zahn for the great collaboration in our barley project.

Many results presented in this thesis are inseparable from the contributions of my colleagues. I would like to thank Jana Trenner for her help with the phylogenetic analysis and microscopy, as well as Dr. Steve Babben and Finn Esche for their assistance in barley phenotyping and sequencing. I would like to thank Kathrin Denk, Annette Pahlich, Matthias Reimers, and Lara Grüttner for their help in the experiments. I also greatly appreciate the efforts of Dr. Albrecht Serfling in the barley yield component experiment.

I am also thankful to all members of the Quint lab for their understanding and support. I thank the AGRIPOLY Graduate School 'Determinants of Plant Performance' for providing a great international research environment in Halle. Special thanks to PD Dr. Carsten Milkowski for organizing all meetings, lectures, and excursions.

Last but not least, I would like to thank my friends and family for their unconditional and endless support during my PhD.

Curriculum Vitae

Personal data

Name Zihao Zhu
Date of birth 12 November 1992
Place of birth Shanghai, China
Nationality Chinese

Education

Since Dec 2017 **PhD student Crop Physiology** Martin-Luther-University Halle-Wittenberg, Germany

Sep 2015 – Sep 2017 **MSc Plant Sciences** Wageningen University & Research, the Netherlands

Sep 2011 – July 2015 **BSc Plant Biotechnology** Shanghai Jiao Tong University, China

List of publications

- Zhu Z**, Quint M, Anwer MU. 2022. Arabidopsis EARLY FLOWERING 3 controls temperature responsiveness of the circadian clock independently of the evening complex. *Journal of Experimental Botany* 73, 1049-1061.
- Zahn T, **Zhu Z**, Ritoff N, Krapf J, Junker A, Altmann T, Schmutzer T, Tueting C, Kastiris PL, Quint M, Pillen K, Maurer A. 2022. Exotic alleles of EARLY FLOWERING 3 determine plant development and grain yield in barley. *bioRxiv*, 2022.07.15.500212. [Preprint]
- Zhu Z**, Esche F, Babben S, Trenner J, Serfling A, Pillen K, Maurer A, Quint M. 2023. An exotic allele of barley EARLY FLOWERING 3 contributes to developmental plasticity at elevated temperatures. *Journal of Experimental Botany*, doi: 10.1093/jxb/erac470.

Declaration under Oath

Eidesstattliche Erklärung / *Declaration under Oath*

Ich erkläre an Eides statt, dass ich die Arbeit selbstständig und ohne fremde Hilfe verfasst, keine anderen als die von mir angegebenen Quellen und Hilfsmittel benutzt und die den benutzten Werken wörtlich oder inhaltlich entnommenen Stellen als solche kenntlich gemacht habe.

I declare under penalty of perjury that this thesis is my own work entirely and has been written without any help from other people. I used only the sources mentioned and included all the citations correctly both in word or content.

Datum / *Date*

Unterschrift des Antragstellers / *Signature of the applicant*